The University of Sheffield

Electromagnetic Performance of Novel Stator Wound Field and Switched Flux Machines

Yanjian Zhou

Department of Electronic and Electrical Engineering

The University of Sheffield

Mappin Street, Sheffield, S1 3JD, UK

April 2015

ABSTRACT

This thesis investigates the electromagnetic performance of novel stator wound field (WF) machines and switched flux permanent magnet (SFPM) machines for high performance and low-cost applications. The analyses are validated by finite element (FE) calculations and experiments.

The SFPM machine exhibits the advantages of high torque density, robust rotor structure and easy thermal management. Among all SFPM machines, the sandwiched SFPM machine shows relatively high torque density. In this thesis, the torque density of the sandwiched SFPM machine is improved further by employing V-shaped magnets. Additionally, the usage of PMs in the V-shaped sandwiched SFPM machine is reduced. Thus, compared with the conventional SFPM machines, the PM material usage efficiency of this machine is much higher.

In cost sensitive applications, the material price of SFPM machine using rare-earth PMs is high. Thus, DC coils can replace high-cost rare-earth PMs in stator-PM machines to significantly reduce the material cost. In this thesis, several new stator-WF machine topologies derived from existing stator-PM machines are proposed. The investigations of the stator-WF machines are mainly focused on a WF switched flux (WFSF) machine and a non-overlapping stator-WF synchronous (NSWFS) machine. It is found that the proposed WFSF machine shows lower material cost, higher torque density and better material usage efficiency compared with the conventional WFSF machine. The proposed NSWFS machine employing non-overlapping winding and salient-pole rotor exhibits higher torque density and lower torque ripple than the segmented rotor NSWFS machine.

Compared with three-phase stator-WF machines, the single-phase stator-WF machine has simpler control circuit, and consequently, even lower cost can be achieved. Some novel single-phase stator-WF machines are proposed in this thesis. Compared with the conventional single-phase stator-WF machines, these machines have the merits of lower material costs, better material usage efficiencies and lower iron losses.

ACKNOWLEDGEMENTS

Foremost, I would like to express my sincere gratitude to my supervisor Professor Zi-Qiang Zhu for his continuous support during my Ph.D. study. Without his instruction and encouragement, hardly can I complete this thesis.

I thank all my fellows of the Electrical Machines and Drives Group at the University of Sheffield for the inspired discussions and struggling nights we had together in last three years. My sincere thanks also go to Mr John Wilkinson and Mr Lawrence Obodo for their assistances in the building of the prototype machines.

I warmly thank my parents for their financial supports and encouragements, which make me brave enough to face the challenges during my Ph.D. study. Finally, I thank my wife for her support and understanding.

Contents

NOMECLATURE

B_m	Amplitude of flux density (T)
D_{ri}	Rotor inner diameter (mm)
D_{ro}	Rotor outer diameter (mm)
D_{sf}	Shaft diameter (mm)
D_{si}	Stator inner diameter (mm)
D_{so}	Stator outer diameter (mm)
f	Operation frequency (Hz)
h	Slot depth (mm)
I_a	RMS phase current (A)
I_d	d-axis current (A)
I_f	Field current (A)
I_q	q-axis current (A)
J_{PM}	Eddy current density of permanent magnet (A/mm^2)
k_{pf}	Winding packing factor (effective copper area/slot area)
k_w	Winding factor
k_e	Excessive loss coefficient
k_h	Hysteresis loss coefficient
k_c	Eddy-current loss coefficient
L	Machine axial length (mm)
L_{end}	Phase end-winding length (mm)
n	Harmonic order
N_a	Number of turns per phase
N_{at}	Total number of turns per armature coil
N_{ft}	Total number of turns per field coil
p	Pole number of a machine
P_{Cu}	Copper loss (W)
P_{iron}	Iron loss (W)
P_{PM}	Permanent magnet loss (W)
R_a	Phase resistance (Ω)
R_{at}	Total armature winding resistance (Ω)
R_{ft}	Total field winding resistance (Ω)

R_r	Rotor outer radius (Ω)
R_s	Stator inner radius (Ω)
S	Area of one stator slot (mm^2)
S_a	Phase slot area (mm^2)
T	Electromagnetic torque (Nm)
T_r	Torque ripple ($\%$)
T_{max}	Maximum torque (Nm)
T_{min}	Minimum torque (Nm)
T_{avg}	Average torque (Nm)
U_a	Phase terminal voltage (V)
U_d	d-axis voltage (V)
U_q	q-axis voltage (V)
W_{pm}	PM thickness (mm)
W_s	Slot width (mm)
W_{sd}	Sandwiching pole thickness (mm)
W_t	Tooth width (mm)
W_y	Yoke thickness (mm)
ρ_{Cu}	Electrical resistivity of copper ($\Omega \cdot mm$)
ρ_{PM}	Electrical resistivity of permanent magnet ($\Omega \cdot mm$)
Ψ_d	d-axis flux-linkage (Wb)
Ψ_{pm}	PM excited flux-linkage (Wb)
Ψ_q	q-axis flux-linkage (Wb)
φ_c	Current angle (^{o})
ω	Electrical angular velocity (Rad/s)

CHAPTER I. GENERAL INTRODUCTION

Permanent magnet (PM) machines are of high torque density and high efficiency, and now widely used in automotive, aerospace and wind power applications etc. However, since >80% rare-earth magnet raw materials are in China, there is a major concern on its resources and prices, as well as its availability. Hence, it is important to investigate novel machine topologies using less/no rare-earth permanent magnet materials.

With the development over a hundred years, numerous of electrical machine topologies have been proposed and investigated. Among them, brushless PM machine has the advantages of high torque density, higher efficiency and high power factor. Moreover, this type of machine shows long service life and high reliability without brushes/slip rings. However, since PMs are mounted on the rotors, the thermal capability and rotor integrity of conventional rotor-PM machines are relatively poor. Therefore, if the machine is applied for high-speed appliance such as a compressor, protecting sleeve of high strength has to be employed. This may lead to the increase in material and manufacture costs. Moreover, poor thermal capability will limit the maximum output power of the conventional PM machine.

To overcome these drawbacks, several types of stator-PM machines have been proposed. In general, there are three categories of machines having permanent magnets on stator, namely, doubly-salient PM (DSPM) machine, flux-reversal PM (FRPM) machine and switched flux PM (SFPM) machine [ZHU11]. All of these machines employ salient-pole stators and rotors. It is notable that their windings are all non-overlapping and concentrated.

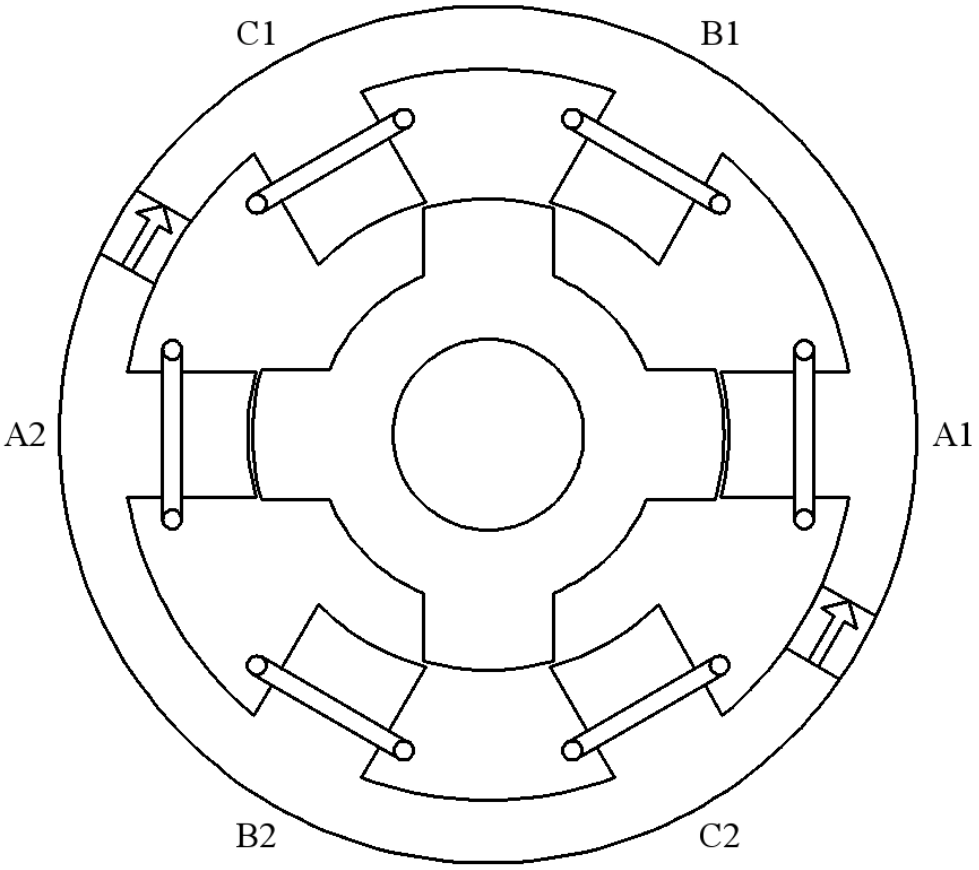

Fig. 1.1. Topology of a DSPM machine

The PMs of a DSPM machine are mounted in the stator back-iron [SAR94] [LIA95], as shown in Fig. 1.1. Besides the advantages of easy thermal management and robust rotor structure, this machine also shows relatively low PM usage compared with other stator-PM machines. However, 3-phase back-EMFs of this machine are unbalanced, non-sinusoidal, and asymmetric. Moreover, its flux-linkage is unipolar. In general, a bipolar flux linkage can result in better utilisation of the magnetic circuit. For a unipolar flux linkage machine, in order to achieve similar performance to the bipolar flux linkage machine, the peak value needs to be very high and consequently the magnetic saturation of a unipolar machine is likely to be severer than that of a bipolar machine. This means the torque capability of the unipolar machine is limited. These disadvantages will result in high torque ripple and low torque density in a DSPM machine.

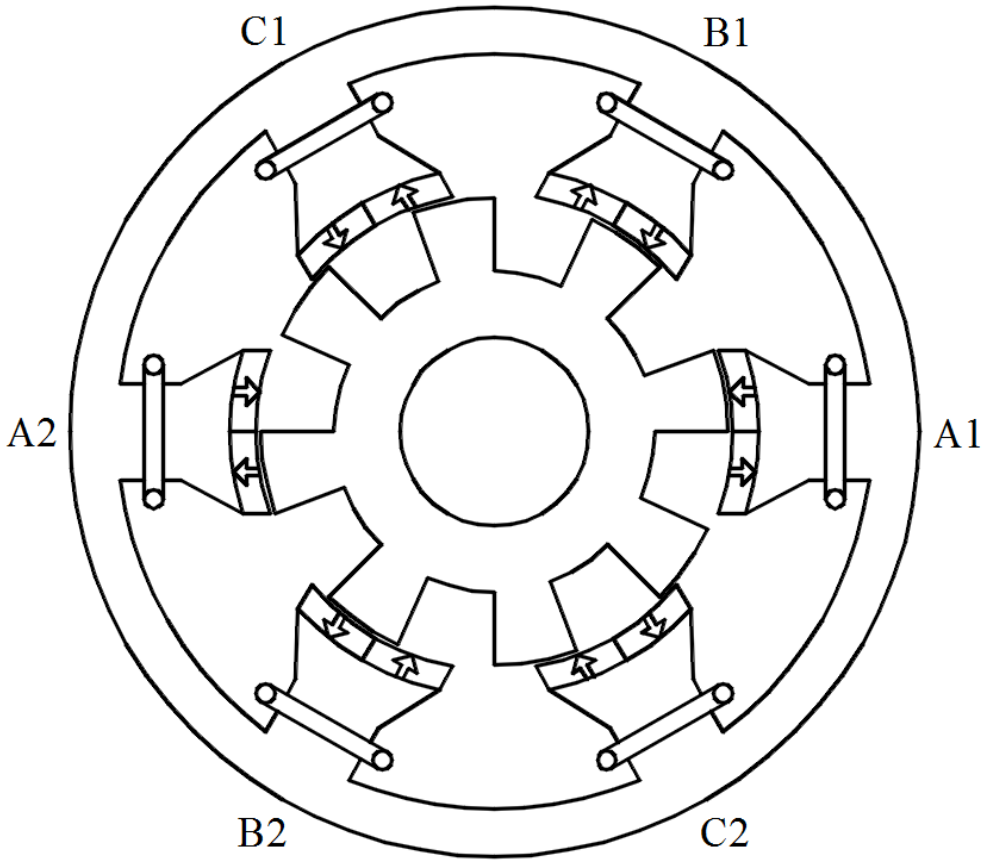

Fig. 1.2. Topology of a FRPM machine

The PMs of a FRPM machine are mounted on the surface of stator teeth [DEO97] [WAN99], as shown in Fig. 1.2. This machine exhibits relatively high torque density due to its bipolar flux-linkage. Compared with the DSPM machine, this machine shows lower torque ripple due to symmetrical and balanced 3-phase back-EMFs. However, the disadvantages of this machine are obvious, such as potential irreversible demagnetisation and large radial magnetic force on PMs.

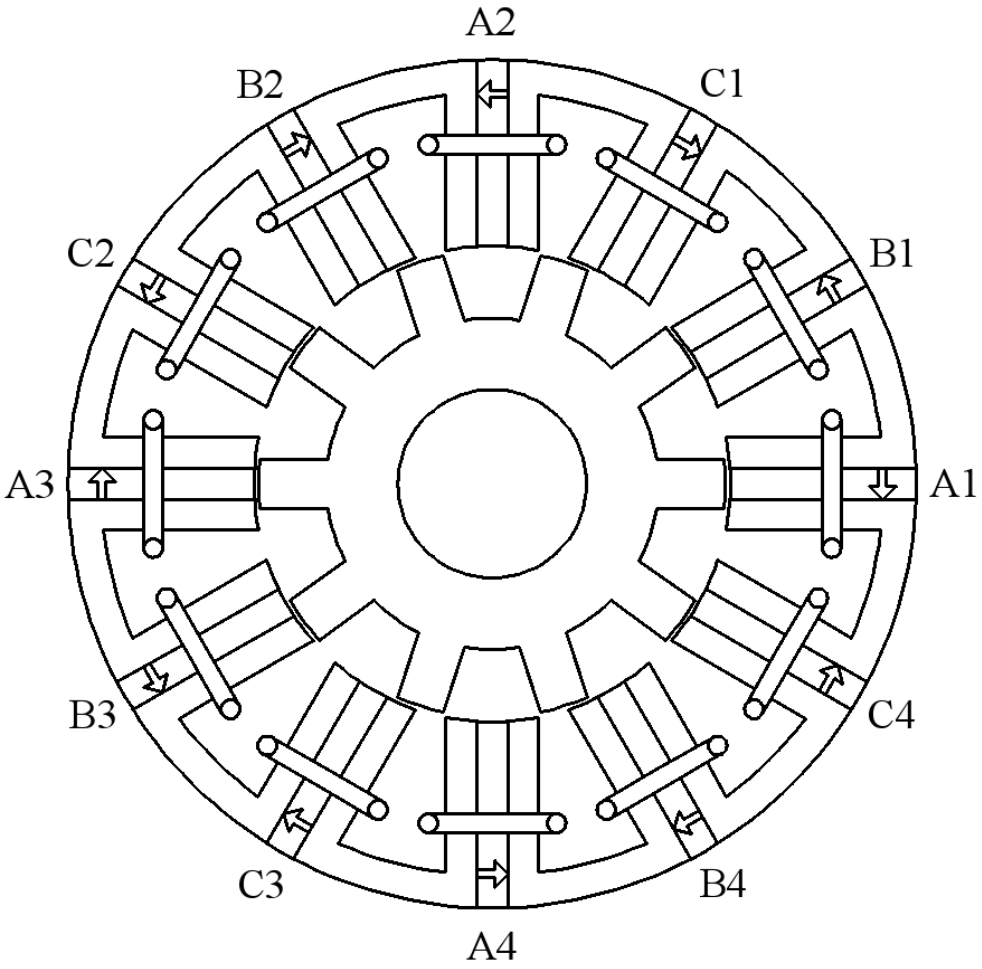

Fig. 1.3. Topology of a SFPM machine

The PMs of a SFPM machine are sandwiched in the stator teeth, as shown in Fig. 1.3. Compared with the DSPM and FRPM machines, this machine shows the advantages of higher torque density and lower torque ripple. The SFPM machines will be reviewed in following sections.

1.1.Switched flux permanent magnet machine

The operation principle of SFPM machines, i.e., switched flux principle, was firstly introduced in 1955 [RAU55]. Fig. 1.4 shows the topology of the first stator-PM machine which was proposed as a single-phase power generator in [RAU55]. Due to the limitation of the PM material in 1950s, this machine can hardly meet the requirements in practical applications.

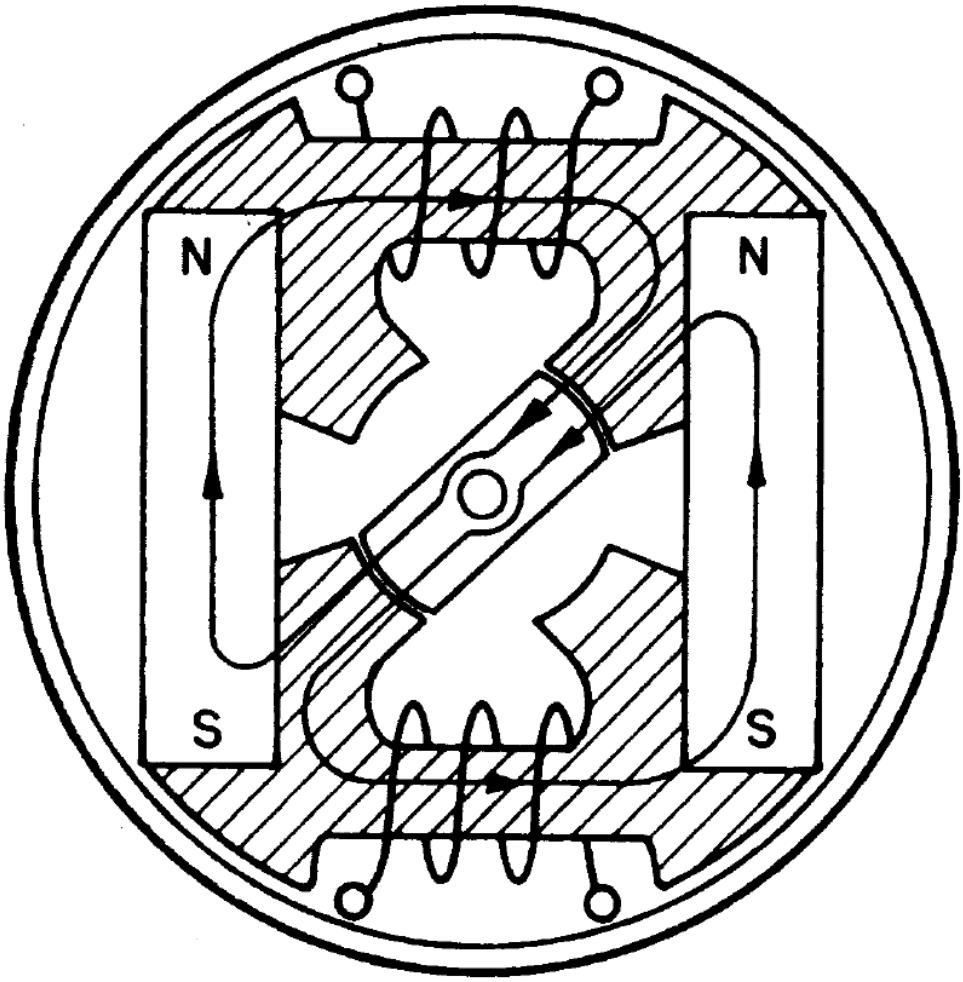

Fig. 1.4. Topology of the first SFPM machine [RAU55].

With the development of the rare-earth magnet material, power device and control theory, many SFPM machines are proposed and investigated within last 30 years. Based on different stator lamination profiles, three-phase radial-field rotary SFPM machines can be classified as:

- Conventional SFPM machine [HOA97], Fig. 1.3, Fig. 1.5;
- Multi-PM sandwiched SFPM machines [FEI06][LU11], Fig. 1.6;
- Multi-tooth SFPM machine [ZHU08][CHE08], Fig. 1.7;
- E-core SFPM machine [CHE11], Fig. 1.8;
- C-core SFPM machine [CHE11b], Fig. 1.9;
- Segmented rotor SFPM machine [ZUL12], Fig. 1.10.

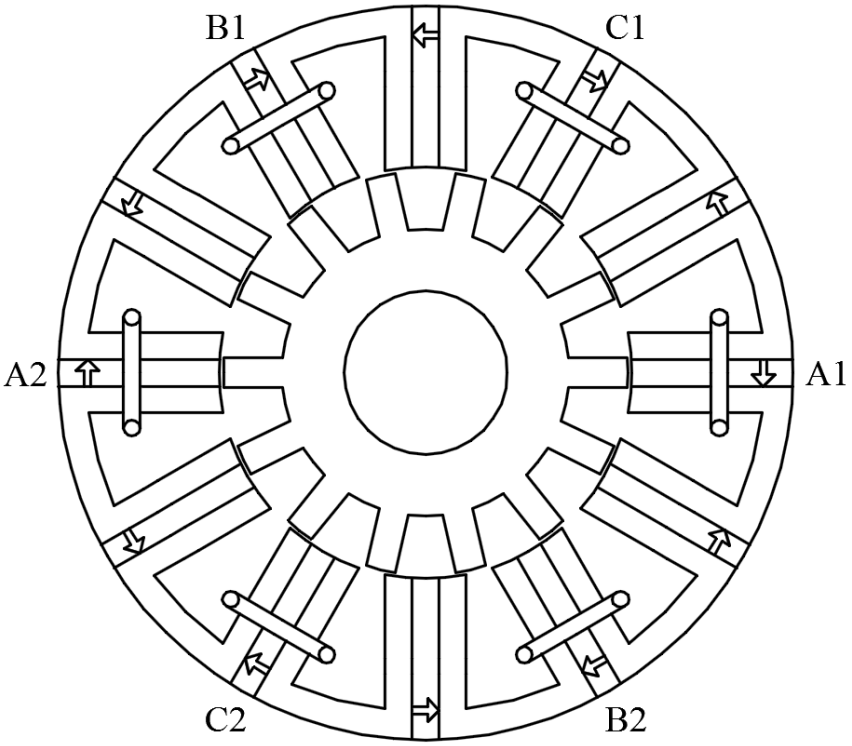

Fig. 1.5. Topology of alternate poles wound SFPM machine.

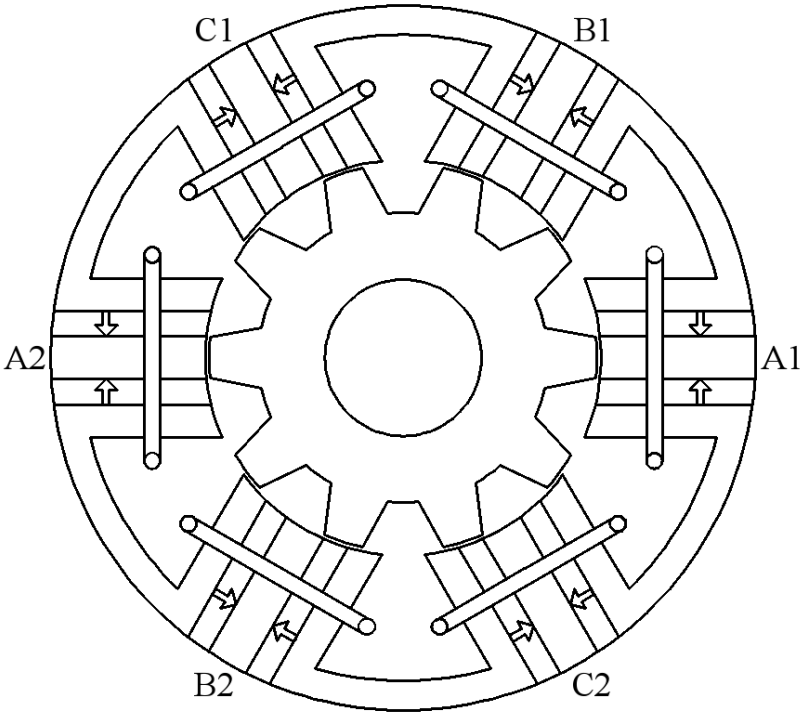

Fig. 1.6. Topology of multi-PM sandwiched SFPM machine.

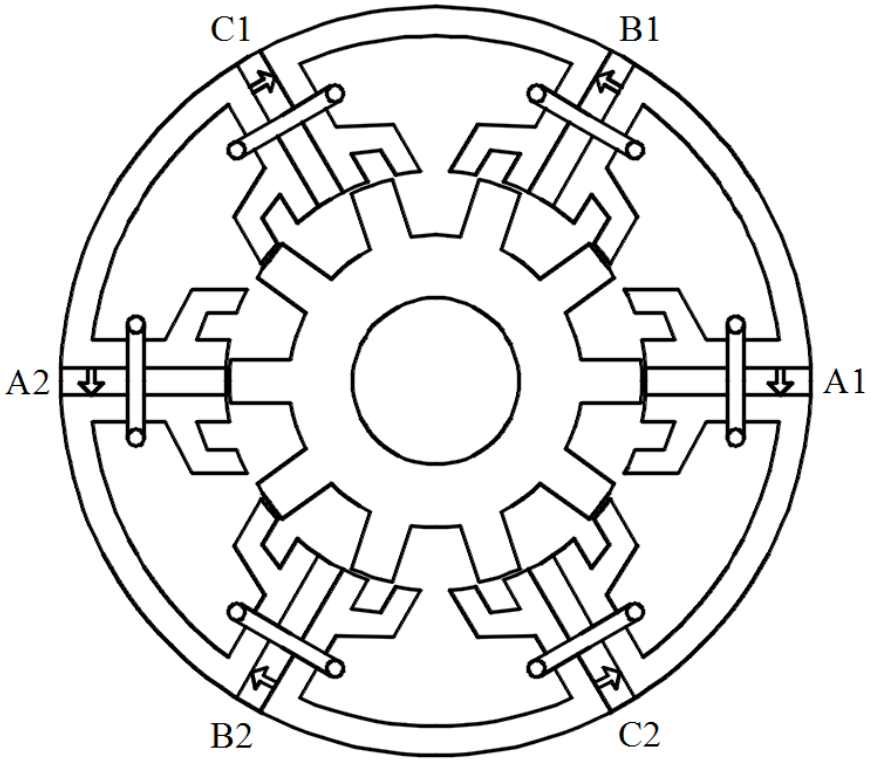

Fig. 1.7. Topology of multi-tooth SFPM machine.

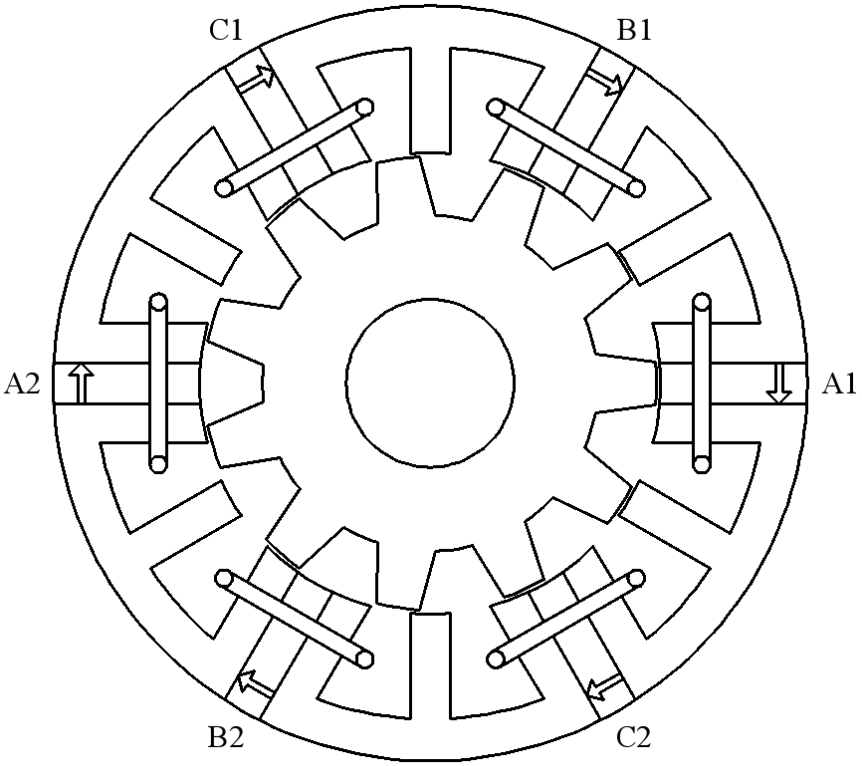

Fig. 1.8. Topology of E-core SFPM machine.

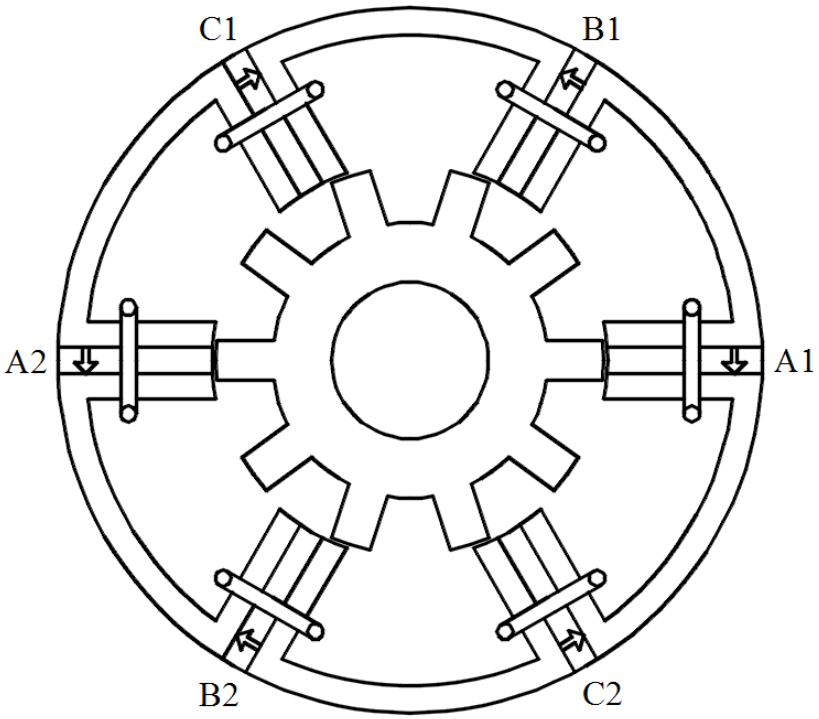

Fig. 1.9. Topology of C-core SFPM machine.

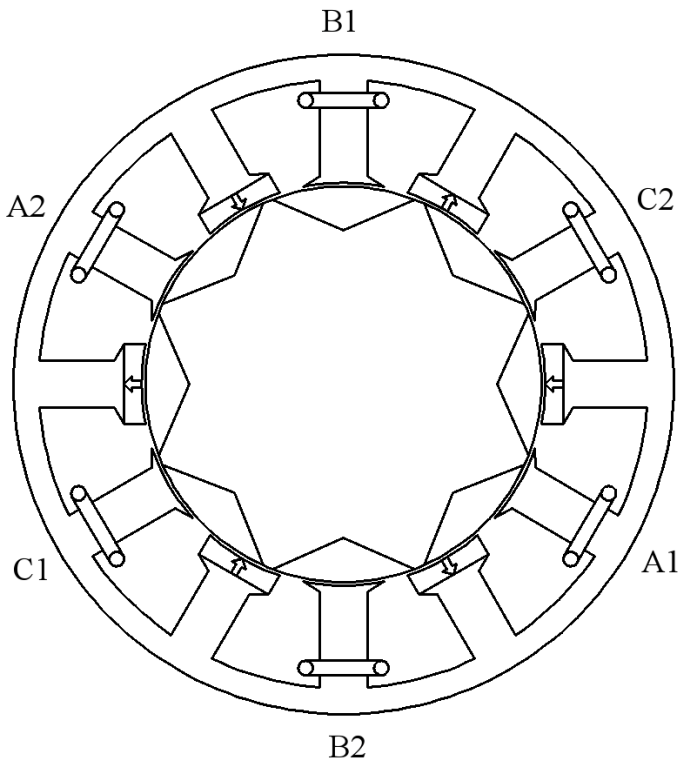

Fig. 1.10. Topology of segmented rotor SFPM machine.

Although in segmented rotor SFPM machine, PMs are not sandwiched in stator teeth, this machine can be classified as a SFPM machine according to its operation principle. Compared with the conventional SFPM machine having all and alternate poles wound, the multi-tooth, E-core and C-core SFPM machines shows less PM usages and higher torque densities under low electric loadings [ZHU11]. The sandwiched SFPM machine also shows higher torque density than the conventional SFPM machine [ZHO13]. The torque density can be increased and PM usage can be reduced in sandwiched SFPM machine by employing improved PM placement, and this will be carried out in this thesis.

The competitiveness of rare-earth SFPM machine is limited in cost sensitive applications in terms of material cost. By replacing rare-earth PMs with ferrite PMs, the material cost of SFPM machine can be significantly reduced. However, the performances, such as torque density and demagnetization withstand capability, of the SFPM machine employing ferrite PMs are worse than the SFPM machine employing rare-earth PMs [FAS14].

High cost rare-earth magnets in SFPM machines can always be replaced by DC coils, resulting in wound field switched flux (WFSF) machines. Compared with the PM machines, this machine shows the merits of low material cost and no demagnetization of PMs. In following section, stator wound field machines will be reviewed.

1.2.Stator wound field machines

Wound field (WF) machines are emerged in various applications, such as domestic application [POL99], [POL03], [POL03b], [POL06], electric vehicles [ROS06], [FRI10], [SUL11], [POL06b], aerospace applications [GRI12], [LUO09], [LIU12], wind turbine generators [RIB07], [POL06], [LI08], [QU13], and high temperature superconducting applications, [SCH08], [LUO09], [QU13], [HWA14]. Therefore, many investigations on WF machines have been carried out [BAS11], [BAS12], [MI09], [DOR11], [TRA12], [YAM11], [GAU12], [GAU13].

Basically, rotary WF machines can be classified as rotor-WF machines and stator-WF machines. No brushes/slip rings are required in the stator-WF machines. Thus, the rotor robustness and reliability of stator-WF machine have potential to be better and the maintenance cost has potential to be lower compared with the rotor-WF machines. Moreover, since all excitation sources are mounted on the stator in a stator-WF machine, better thermal capacity and higher power density can be achieved compared with the rotor-WF machines.

In a conventional SFPM machine, DC coils having lamination steel cores in the middle of them can replace PMs, as shown in Fig. 1.11 (b). Obviously, the DC field conductors at the outer stator will not produce the main flux. Therefore, these conductors can be removed to enlarge the slots having DC field conductors at the inner stator and result in a typical WFSF machine, as shown in Fig. 1.11 (c).

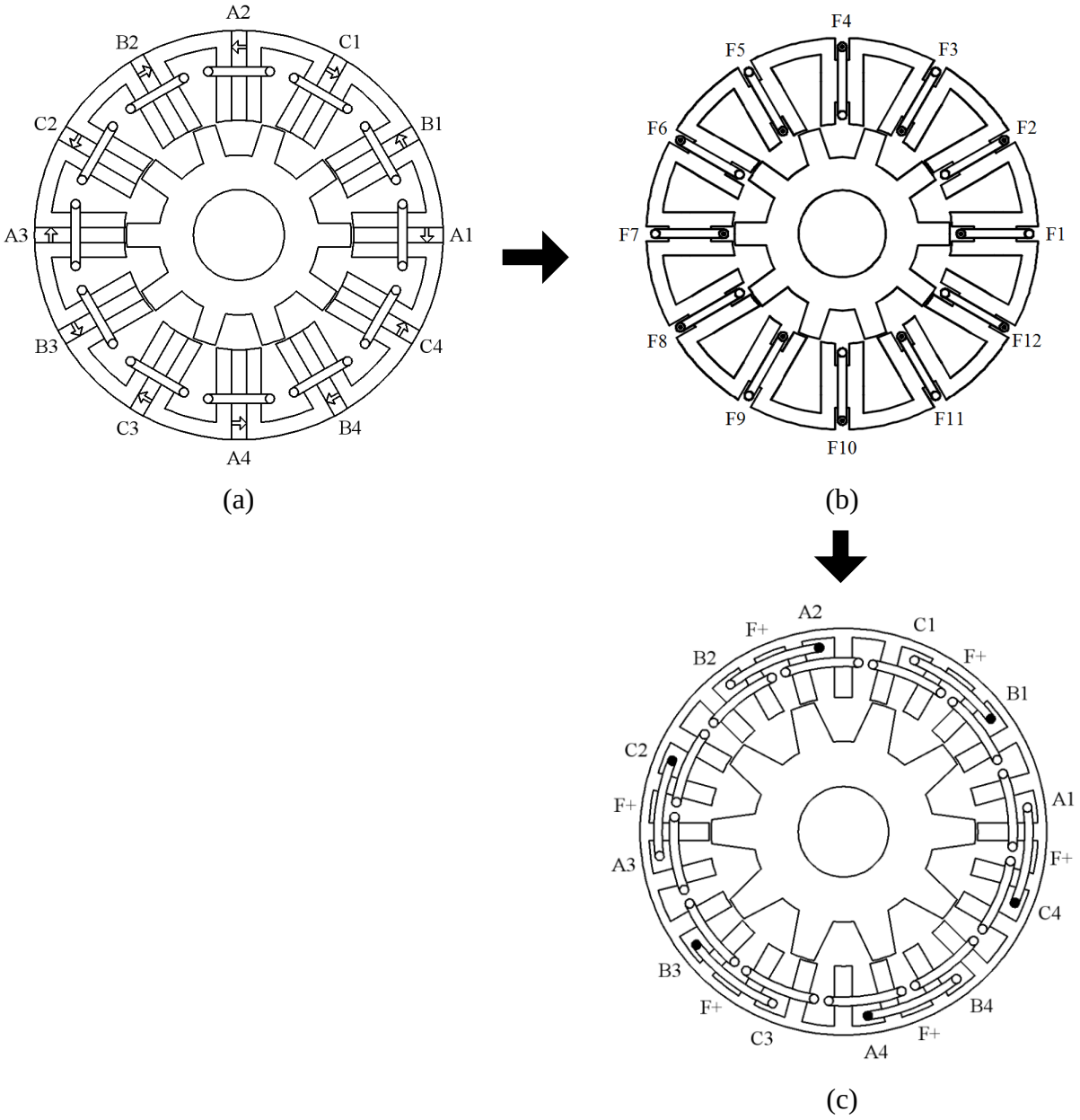

Fig. 1.11. Topologies of conventional SFPM machine and WFSF machines. (a) Conventional 12-slot/10-pole SFPM machine. (b) 12-slot/10-pole WFSF machine (for clarity, armature windings are not shown). (c) 24-slot/10-pole WFSF machine (Field coil pitch=2 slot-pitches, armature coil pitch=2 slot-pitches).

Based on aforementioned PM replacing principle of the conventional SFPM machine, many WFSF machine topologies can be derived from existing SFPM machines.

A WFSF machine with DC field and AC armature windings having 1 and 3 slot-pitches, respectively, is derived from a sandwiched SFPM machine, as shown in Fig. 1.12. Compared with aforementioned 24-slot/10-pole WFSF machine, this machine shows higher torque density and shorter end-winding [ZHO14] [ZHO14b], and will be investigated in this thesis.

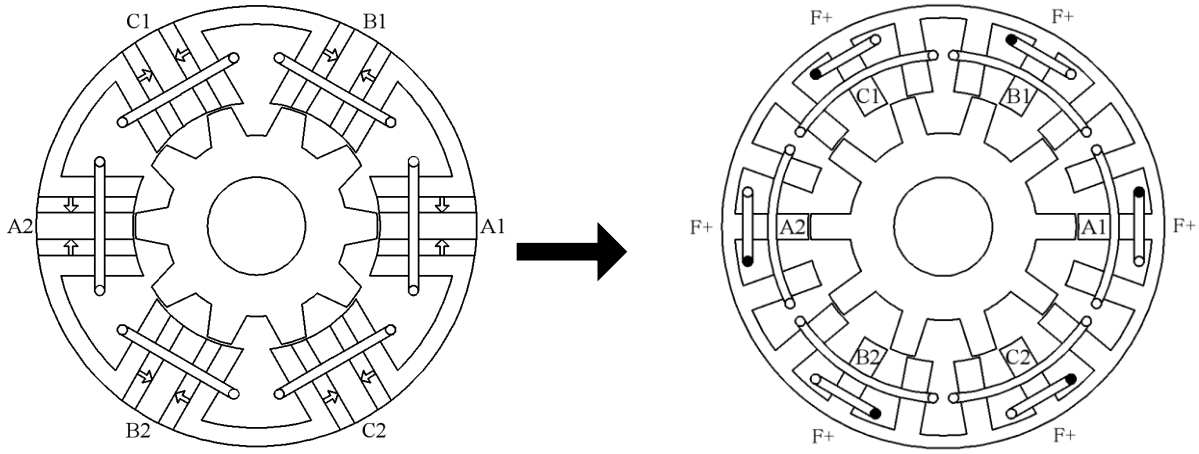

(a) (b)

Fig. 1.12. Topologies of machines. (a) Sandwiched SFPM machine. (b) WFSF machine (Field coil pitch=1 slot-pitch, armature coil pitch=3 slot-pitches).

Based on different armature winding arrangements, there exist two types of E-core SFPM machines. In the typical E-core SFPM machine, armature coils are wound on the stator teeth having PMs, as shown in Fig. 1.13 (a). For the E-core SFPM machine type II, armature coils are wound on the stator teeth without PMs, as shown in Fig. 1.14 (a). When the DC coils replace the PMs in these two types of SFPM machines, two WFSF machines having the same field coil pitch of 3 slot-pitches and the different armature coil pitches of 2 and 1 slot-pitches/pitch are obtained, as shown in Fig. 1.13 (b) and Fig. 1.14 (b), respectively.

The WFSF machine having armature/field windings of 2/3 coil-pitches has long end-windings, and this can be a huge disadvantage in cost-sensitive applications due to the increased copper usage. Similar to the E-core SFPM machine type II, the torque density in the WFSF machine having armature/field windings of 1/3 coil-pitch/pitches is low due to the saturation and flux leakage in the stator. Therefore, two WFSF machines shown in Fig. 1.13 (b) and Fig. 1.14 (b) will not be investigated systematically in this thesis.

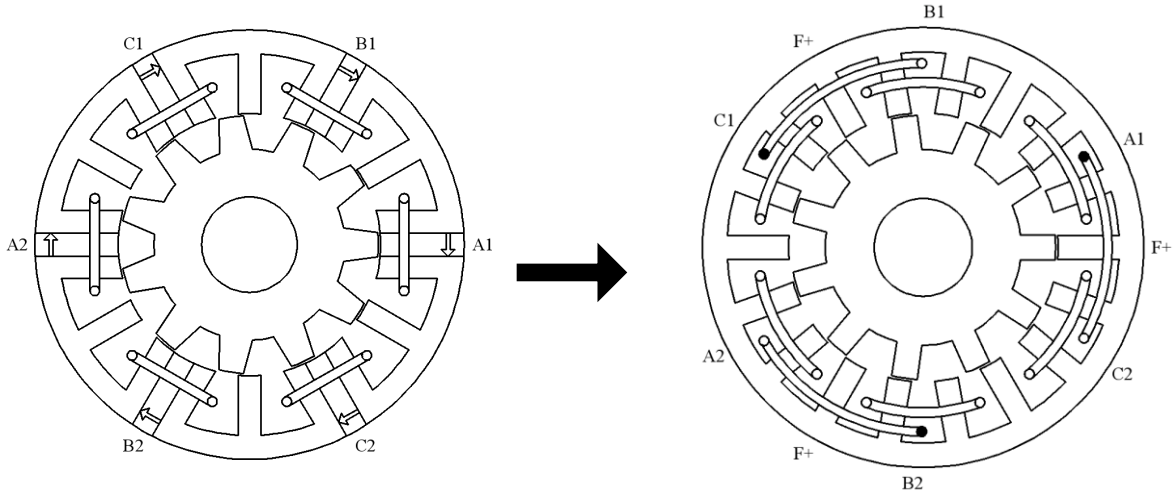

(a) (b)

Fig. 1.13. Topologies of machines. (a) E-core SFPM machine (Type I). (b) WFSF machine (Field coil pitch=3 slot-pitches, armature coil pitch=2 slot-pitches).

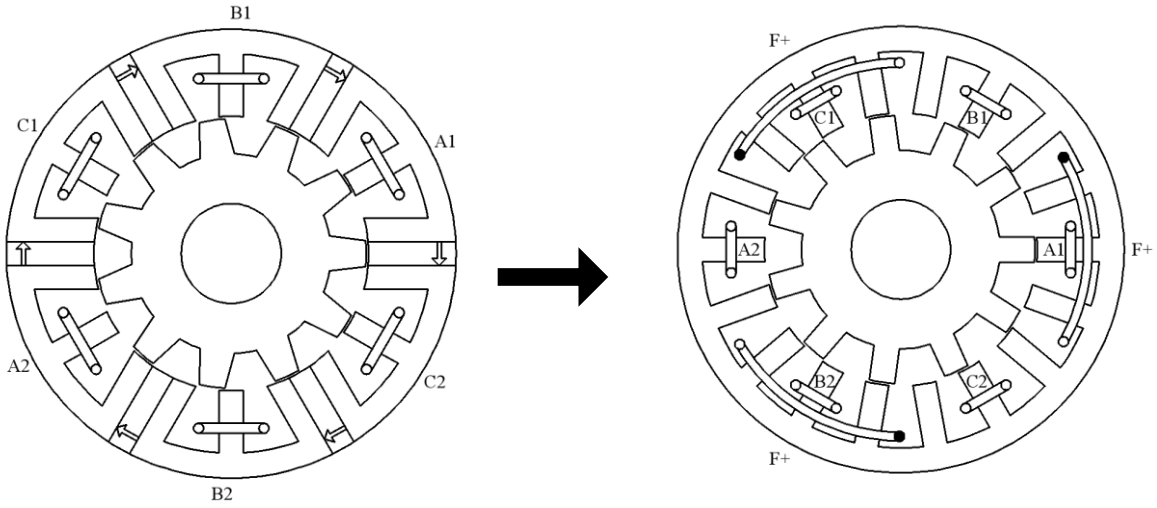

(a) (b)

Fig. 1.14. Topologies of machines. (a) E-core SFPM machine (Type II). (b) WFSF machine (Field coil pitch=3 slot-pitches, armature coil pitch=1 slot-pitch).

Unlike the sandwiched SFPM and E-core SFPM machines, the segmented rotor WFSF machine was proposed ahead of the segmented rotor SFPM machine [ZUL10] [ZUL12]. However, the segmented rotor WFSF machine, as shown in Fig. 1.15 (b), can still be regarded as a machine derived from the segmented rotor SFPM machine. As can be seen, the segmented rotor WFSF machine employs short-pitched field and armature coils. This can be an advantage in the cost-sensitive applications. In this thesis, segmented rotor WFSF machines will be investigated.

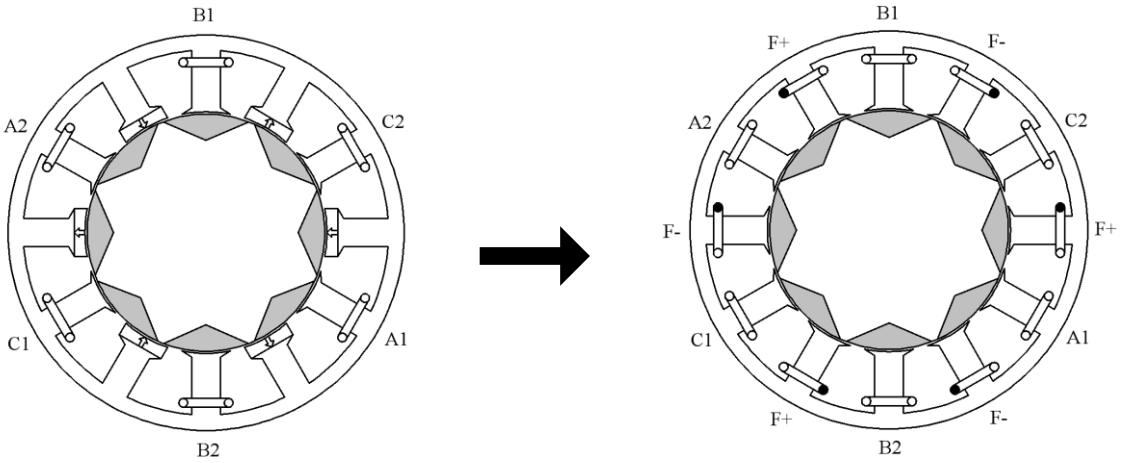

(a) (b)

Fig. 1.15. Topologies of machines. (a) Segmented rotor SFPM machine. (b) WFSF machine (Field coil pitch=1 slot-pitch, armature coil pitch=1 slot-pitch).

Similar to the SFPM machines, the DC coils can replace the PMs in other stator-PM machines. As shown in Fig. 1.16, a stator-WF machine having armature/field windings of 1/3 coil-pitch/pitches can be derived from the conventional short-pitched DSPM machine. This stator-WF machine is mainly used in generator applications [CHE08b] [ZHA12]. Full-pitched DSPM machine is proposed as a single-phase generator [ZHA09] [ZHA11]. Correspondingly, three-phase stator-WF machine employing full-pitched field and armature coils can be derived by replacing PMs with DC coils, as shown in Fig. 1.17 (b). However, the full-pitched stator-WF machine shows significantly increased end-winding length and will not be investigated systematically in this thesis.

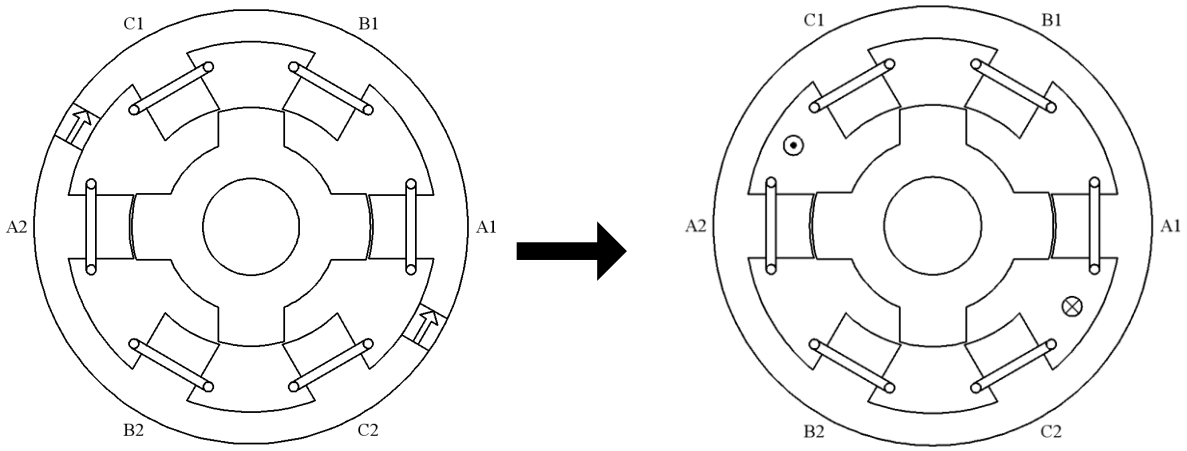

(a) (b)

Fig. 1.16. Topologies of machines. (a) short-pitched DSPM machine. (b) Stator-WF machine (Field coil pitch=3 slot-pitches, armature coil pitch=1 slot-pitch).

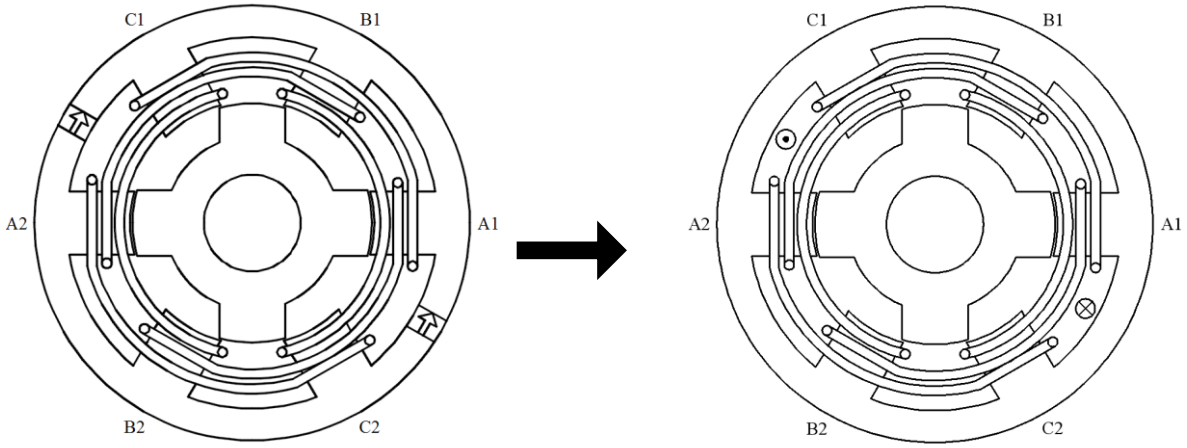

(a) (b)

Fig. 1.17. Topologies of machines. (a) full-pitched DSPM machine. (b) Stator-WF machine (Field coil pitch=3 slot-pitches, armature coil pitch=3 slot-pitches).

The price of copper is much higher than the other materials in a stator-WF machine. Therefore, short-pitched stator-WF machines are competitive in cost-sensitive applications due to low copper usage. Besides of the segmented rotor WFSF machine, variable flux reluctance (VFR) machine is also a stator-WF machine employing short-pitched field and armature coils [FUK12] [LIU13], as shown in Fig. 1.18 (a). Compared with the segmented rotor WFSF machine, VFR machine shows higher torque density and lower torque ripple. However, the over-lapping windings of this machine lead to reduced slot filling factor and complicated winding configuration. Moreover, the manufacture cost is high if segmented stator is employed in this machine. In order to overcome these disadvantages, a non-overlapping stator-WF synchronous machine will be investigated in this thesis, as shown in Fig. 1.18 (b).

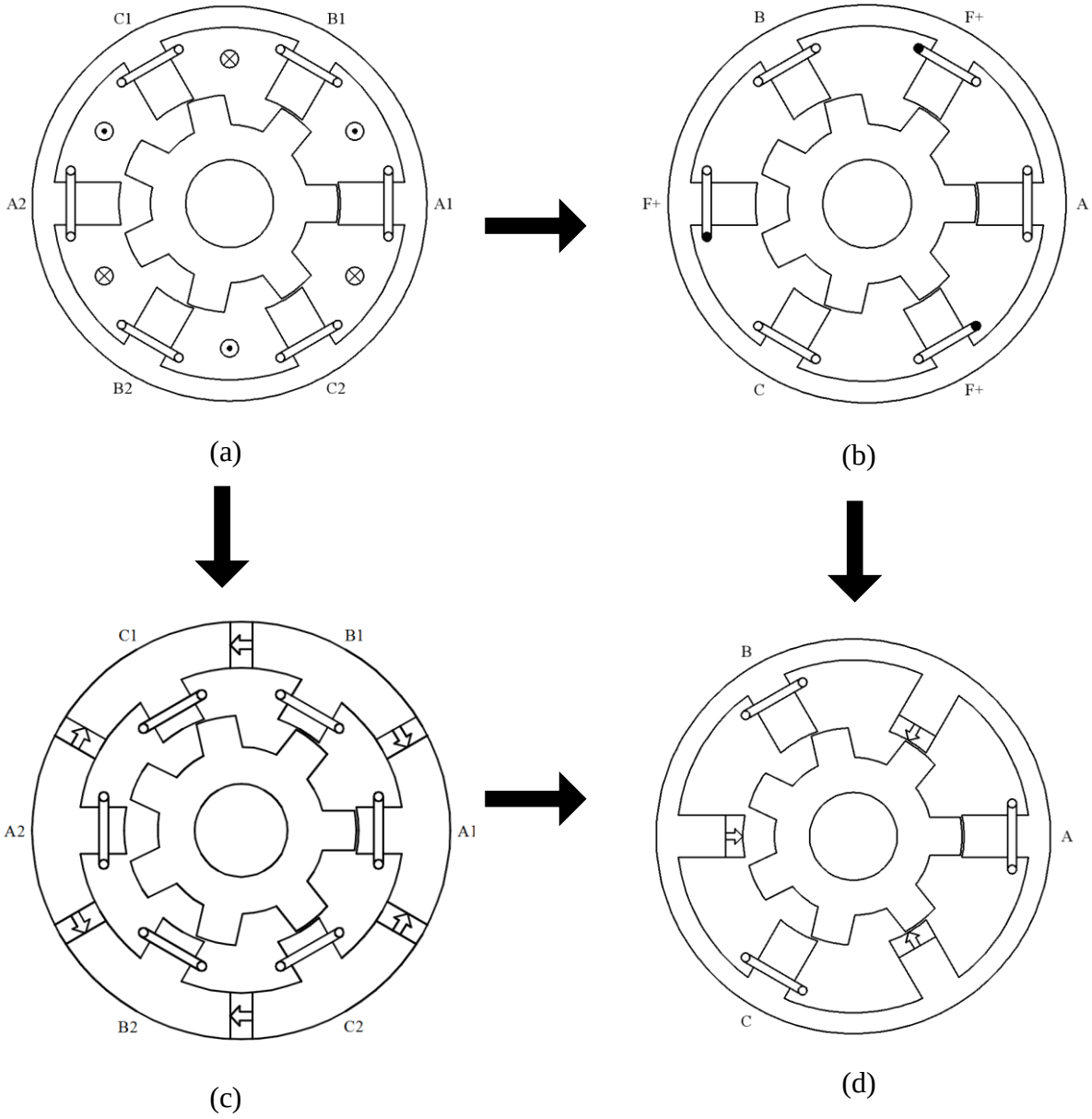

Fig. 1.18. Topologies of machines. (a) Stator-WF machine (Field coil pitch=1 slot-pitch, armature coil pitch=1 slot-pitch, overlapping). (b) Stator-WF machine (Field coil pitch=1 slot-pitch, armature coil pitch=1 slot-pitch, non-overlapping). (c) Synchronous machine with PMs in stator yoke. (d) Synchronous machine having PMs in stator poles.

Obviously, PMs can also replace the DC coils in machines. As can be seen in Fig. 1.18 (c) and (d), by replacing the DC coils with PMs in aforementioned two short-pitched stator-WF synchronous machines, two novel synchronous machines having PMs in stator yoke and pole were proposed in [WU14] and [SHI14], respectively.

In Table 1.1, all three-phase stator-WF machines mentioned in this section are organized in the matrix by the coil pitches of armature and field windings. To easily differentiate the

machines, these stator-WF machines are named after their field and armature winding pitches (for instance, the stator-WF machine with 3/2-field/armature coil pitches will be named and organized as F3A2 machine).

As can be seen in Table 1.1, an F1A2 machine is introduced by filling the empty cells in the matrix. However, if the polarities of two armature coils in one phase are the same, essentially, this machine can be regarded as a F1A1 machine. Meanwhile, if the polarities of two armature coils in one phase are not the same, the main flux-linkages will be cancelled in coils, and this will lead to poor performance. Thus, the investigation of this machine will not be carried out in this thesis. At this moment, for the "F2" stator-WF machines, only F2A2 machine is feasible. For the F2A1 and F2A3 machines, it is hard to find out the topologies with reasonable winding arrangements.

A possible method to discover new topologies of stator-WF and stator-PM machines is summarized in this thesis based on above contents, as shown in Fig. 1.19. Overall, for the machines having excitation sources on the stators, new machine topologies can be obtained by replacing the PMs and DC coils with each other.

Table 1.1. Matrix of stator-WF machines

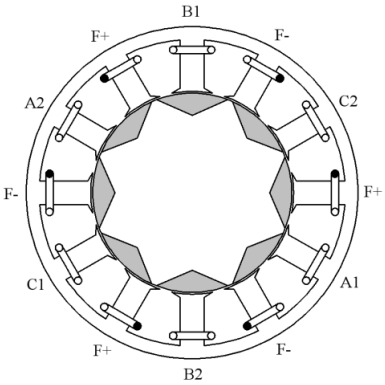

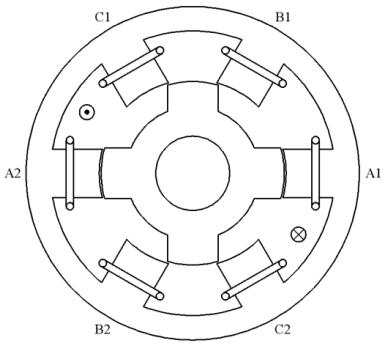

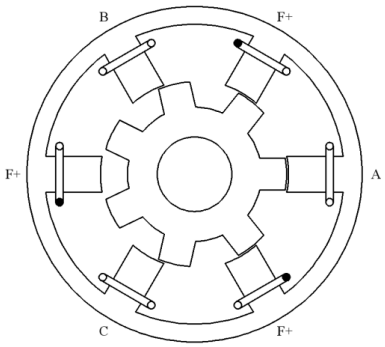

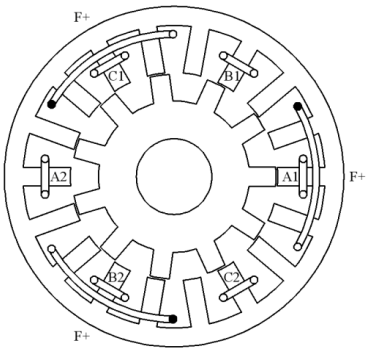

F1A1 **F2A1** **F3A1**

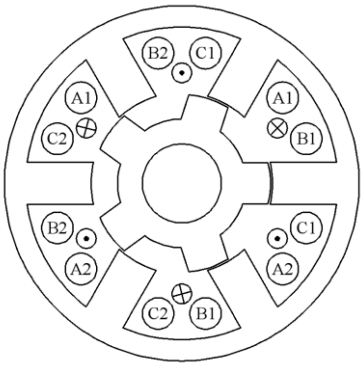

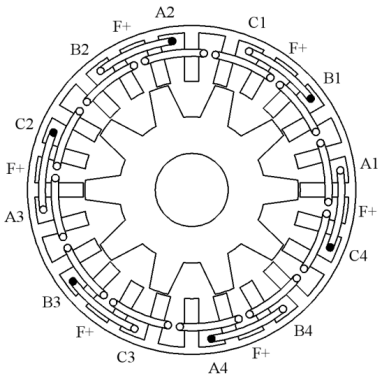

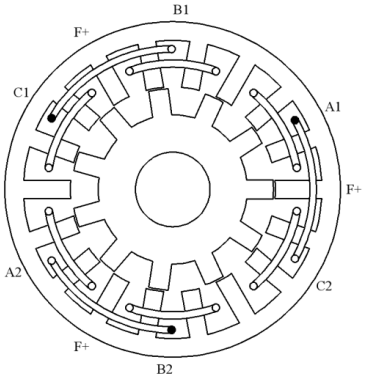

F1A2 **F2A2** **F3A2**

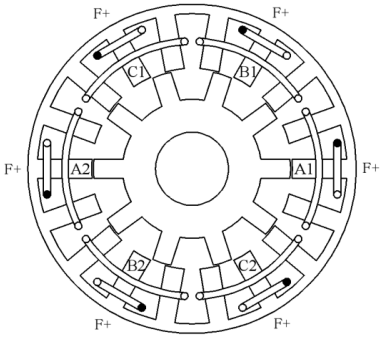

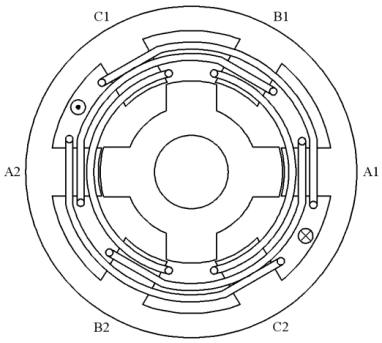

F1A3 **F2A3** **F3A3**

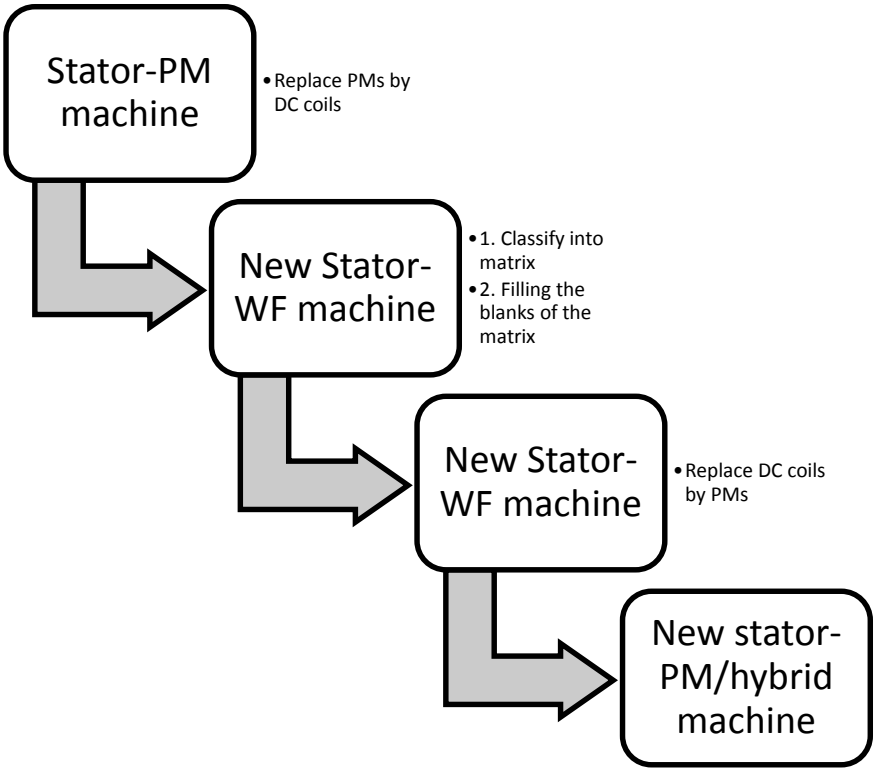

Fig. 1.19. A possible method to discover new topologies of stator-WF and stator-PM machines.

In cost-sensitive applications, the single-phase stator-WF machines have larger advantage in terms of the power device costs compared with the multi-phase stator-WF machines. A single-phase 8-slot/4-pole WFSF machine has been successfully commercialized for more than 10 years [POL03], as shown in Fig. 1.20. Compared with an induction machine, this machine exhibits higher efficiency and power factor. However, the performance of this machine can be improved further. In this thesis, single-phase WFSF machines employing "F1A3" or "F2A2" stator topologies are compared. It is found that the F1A3 WFSF machine shows reduced end-winding length and iron loss compared with the F2A2 WFSF machine of the same size and slot/pole combination.

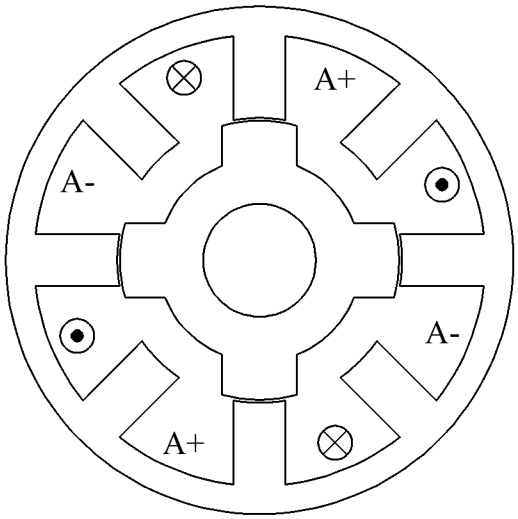

Fig. 1.20. Topologies of a single-phase F2A2 WFSF machine.

It is worth noticing that in a stator-PM/WF machine of which coil flux-linkage is bipolar, the coil has the positive or negative maximum flux-linkage when the D-axis aligns with the coil, as shown in Fig. 1.21. Meanwhile, for the stator-PM/WF machine having unipolar coil flux-linkage, the coil has the maximum or minimum flux-linkage when the D-axis aligns with the coil, as shown in Fig. 1.22.

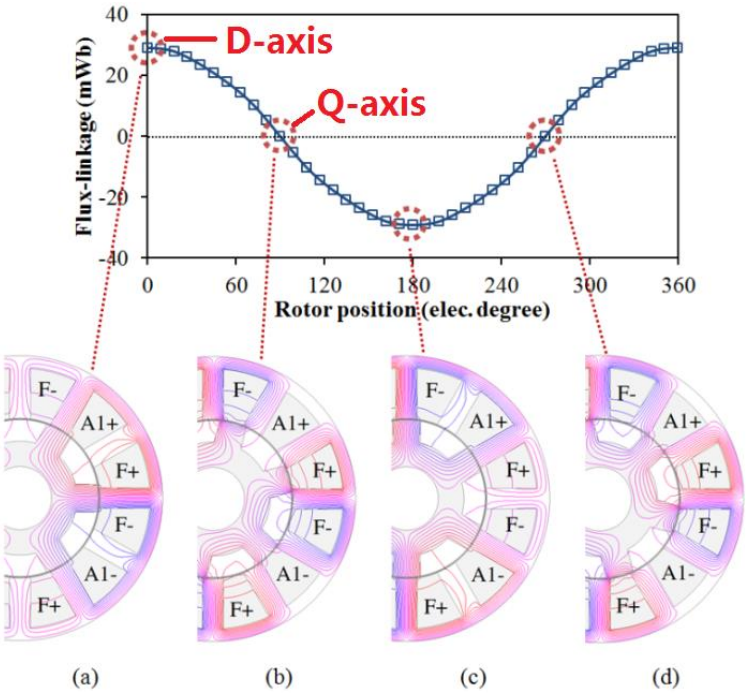

Fig. 1.21. Open-circuit field distributions and typical flux-linkage waveform of single bipolar coil in a F1A3 stator-WF machine.

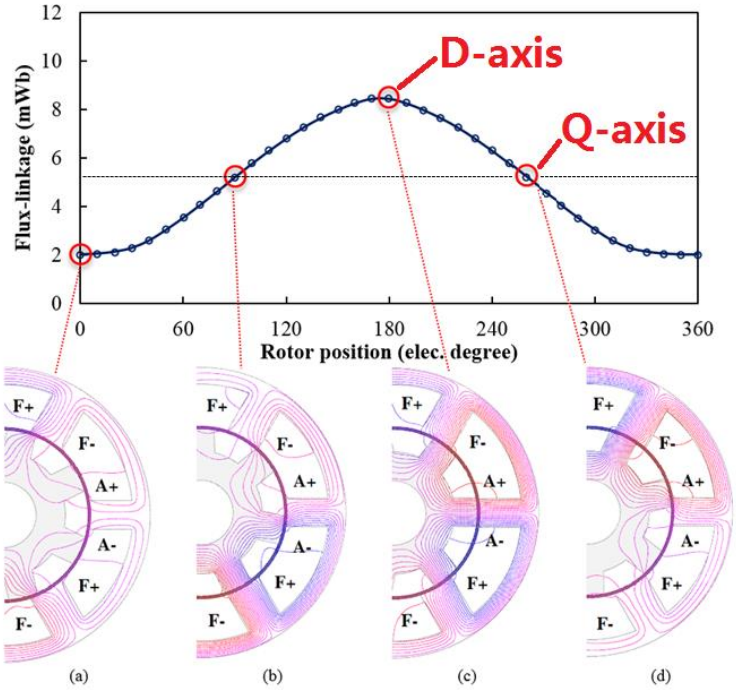

Fig. 1.22. Open-circuit field distributions and typical flux-linkage waveform of single unipolar coil in a F1A1 stator-WF machine.

In this thesis, the split ratio of machine is defined as the ratio of rotor outer diameter to stator outer diameter. The packing factor of machine is defined as effective copper area/slot area.

1.3.Scope of research and contributions of the thesis

The topologies of the machines with excitation sources on the stators have been reviewed in Chapter I. Particular attentions have been paid to the stator-WF machines. In this thesis, some novel stator-WF machine topologies have been obtained by replacing the PMs with DC coils in the stator-PM machines. In addition, based on the field and armature coil pitches, the radial-field rotary stator-WF machines have been classified in a matrix. The following chapters are summarized below:

Chapter II:

A sandwiched SFPM machine using V-shaped magnets is proposed in this chapter, compared with the conventional SFPM and the conventional sandwiched SFPM machine.

This machine shows less magnet usage and higher torque density under the same current density.

Further, 2-step rotor skewing is employed in the sandwiched SFPM machine using V-shaped magnets to reduce the torque ripple.

Chapter III:

An F1A3-5-pole WFSF machine is proposed in this chapter. Compared with the conventional F2A2-5-pole WFSF machine and the segmented rotor F1A1-8-pole WFSF machine, this machine shows higher torque density under the same copper loss.

Additionally, it is found that halving the numbers of stator slots and rotor poles can be an effective method to increase the torque densities for the WFSF machines.

Chapter IV:

Unequal slots can be employed in segmented rotor F1A1, conventional F2A2 and F1A3 WFSF machines to increase the torque densities. Compared with the SFPM machine using low-cost ferrite PMs, the WFSF machines employing unequal slots show higher material usage efficiencies (average torque/material usage) and higher torque densities when the electric loading is high.

Toyota Prius 2010 interior permanent magnet (IPM) machine is a successfully commercialized machine. The torque density of a WFSF machine of the same size can reach to ~80% as much as that of this IPM machine under the same current density. Besides it is found that the material usage efficiencies of the WFSF machines are much higher than that of the Prius IPM machine.

Chapter V:

Based on the topology and operation principle of the F2A2-4 pole single-phase WFSF machine, an F2A2-6 pole single-phase WFSF machine is proposed in this chapter. This machine shows similar torque density but better material usage efficiency compared with the F2A2-4 pole machine under the same copper loss.

An F1A3-6 pole machine is proposed in this chapter as well. This single-phase WFSF machine, which can share the same stator topology with the F2A2-6 pole machine, has shorter end-windings and smaller iron loss than the F2A2-6 pole machine.

The slot number and pole number of F1A3-6 pole machine can be halved and result in a F1A3-3 pole machine. Compared with the F2A2-4 pole machine, this machine shows significantly reduced iron loss.

Chapter VI:

The segmented rotor in the non-overlapping segmented rotor F1A1 machine is not easy for fabrication. Therefore, a non-overlapping F1A1 stator-WF machine employing salient-pole rotor is proposed in this chapter. The slot/pole combinations of this machine are investigated as well. It is found that the salient-pole rotor F1A1 machine can achieve much higher torque density and much lower torque ripple than the segmented rotor F1A1 machine.

Chapter VII:

This chapter contains the general conclusions of this thesis as well as the potential future work.

Appendix A:

It contains the testing and calculation methods of torque, and the calculation methods of iron loss and torque speed curve.

Appendix B:

It contains some performances of the aforementioned F3A1 stator-WF machine.

Appendix C:

It lists the photos and mechanical drawings of all prototypes.

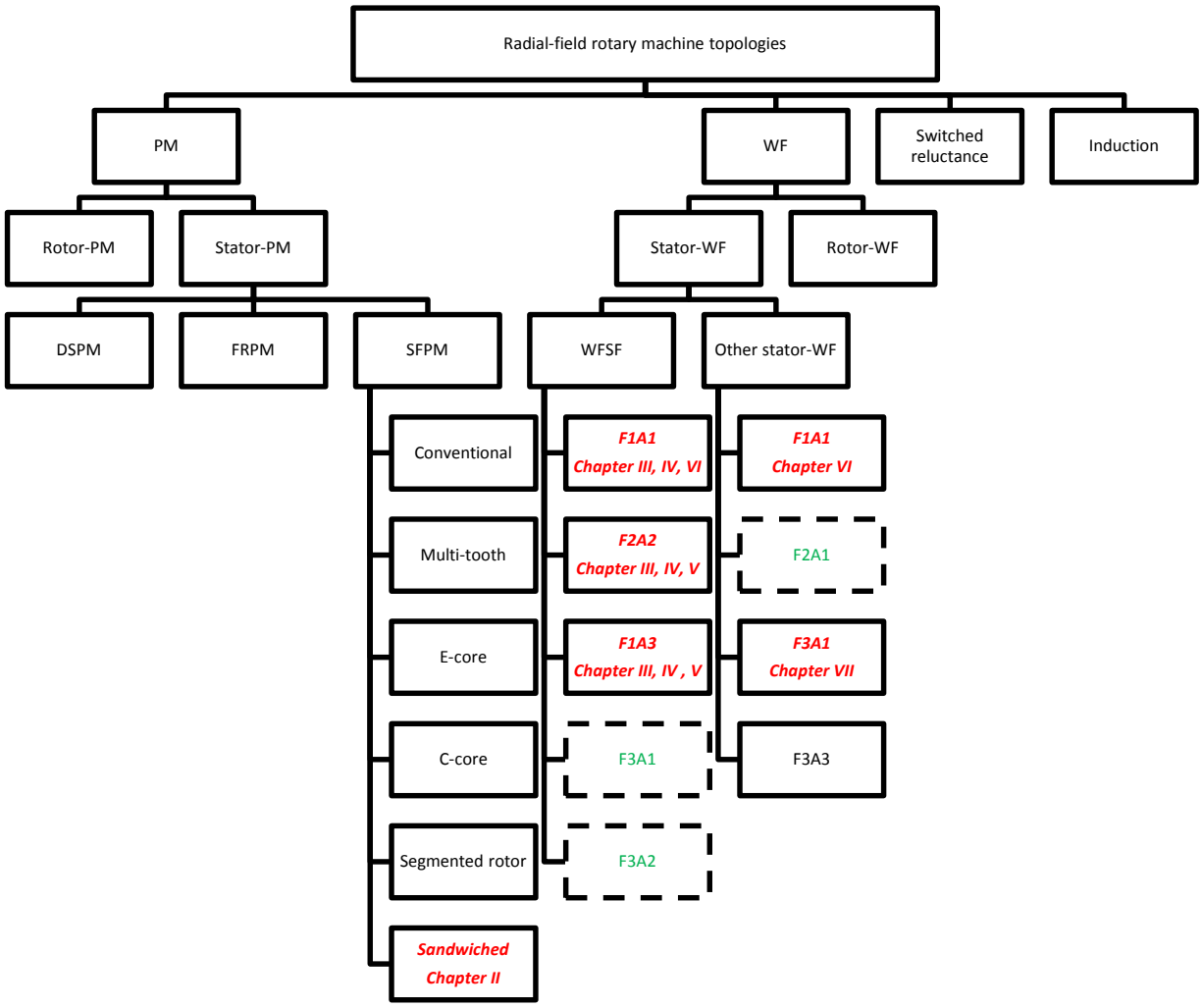

Fig. 1.23. Hierarchy of radial-field rotary machine topologies.

1.4. Major Contributions of Thesis

The major contributions of this thesis are highlighted as follows.

(a) Improved machine topology of sandwiched SFPM machine.

(b) Novel three-phase WFSF machine topologies.

(c) Novel low-cost single-phase WFSF machine topologies.

(d) Novel three-phase non-overlapping stator-WF machine topologies.

CHAPTER II. TORQUE DENSITY AND MAGNET USAGE EFFICIENCY ENHANCEMENT OF SANDWICHED SWITCHED FLUX PERMANENT MAGNET MACHINES USING V-SHAPED MAGNETS

A novel sandwiched switched flux permanent magnet (SSFPM) machine using V-shaped magnets for maximizing output torque and improving magnet usage efficiency is proposed in this chapter. The operation principle of conventional 6/10-stator/rotor-pole SSFPM machine is firstly described. Such SSFPM machine and a novel one with V-shaped magnets are optimized and then compared with the conventional 12/10-stator/rotor-pole switched flux permanent magnet (SFPM) machine by two-dimensional (2-D) finite element analysis (FEA). It is found that the SSFPM machine with V-shaped magnets exhibits higher torque density and higher magnet usage efficiency under the constraint of the same copper loss. In addition, the influence of step-skew angle on the torque ripple suppression is investigated in the SSFPM machine with V-shaped magnets. The FEA predicted back-EMF, cogging torque, torque-current characteristic are validated by experiments on the prototype machines.

2.1.Introduction

The SFPM machines have gained wide application from aerospace to automobile industries since they offer several key advantages, such as simple and robust rotor, short end-winding, high torque density, high efficiency, excellent flux-weakening capability, etc. Various SFPM machine topologies have been emerged since its operation principle was firstly introduced [RAU55], [ZHU10], and [ZHU11].

One of the typical SFPM machine topologies which are often investigated is the 12/10-stator/rotor-pole SFPM machine where one permanent magnet (PM) piece is located in each stator pole, as shown in Fig. 2.1. However, the torque density is still limited due to reduced space for windings. Therefore, a SSFPM machine, in which two PM pieces are sandwiched in one stator pole, is proposed and the electromagnetic performance is investigated by FEA [FEI06], as shown in Fig. 2.2. A single-phase hybrid switched flux machine with sandwiched magnets is investigated by FEA and experiment [LU11].

A novel SSFPM machine with V-shaped magnets will be investigated in this chapter. Compared with the conventional SSFPM machine, the average torque is increased since the

slot area is increased, whilst the PM volume can be reduced due to flux-concentrating, resulting in high magnet usage efficiency. Moreover, the influence of step-skew angle on the torque ripple suppression is investigated in the V-shaped magnet SSFPM machine with 2-step skew rotor. The FEA predicted back-EMF, cogging torque, torque-current characteristic are validated by experiments on the prototype machines.

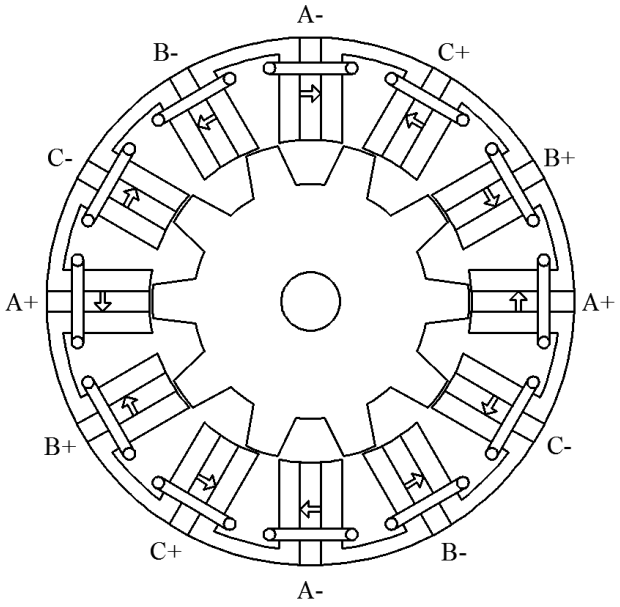

Fig. 2.1. Conventional 12/10-stator/rotor-pole SFPM machine.

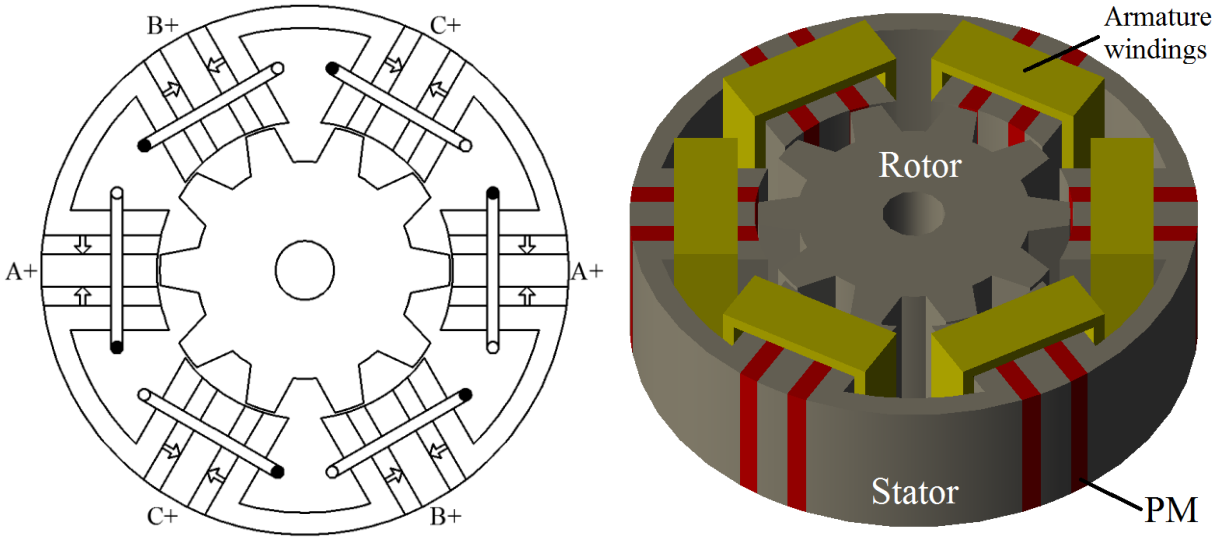

(a) (b)

Fig. 2.2. Conventional SSFPM machine. (a) Cross-section. (b) 3D model.

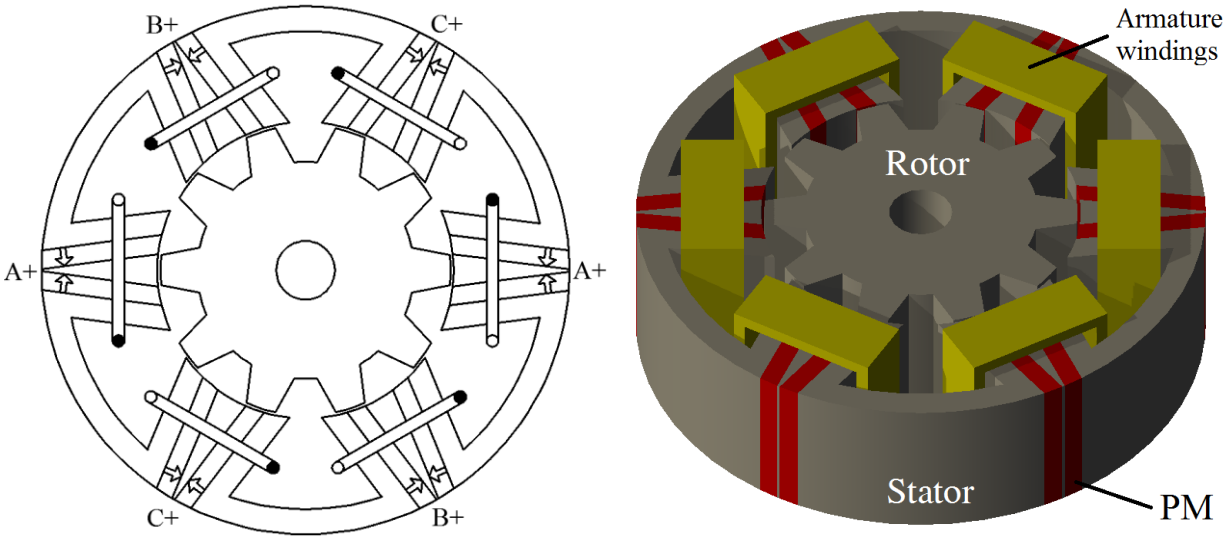

(a) (b)

Fig. 2.3. V-shaped magnets SSFPM machine. (a) Cross-section. (b) 3D model.

Before further investigations, it is worthwhile to compare the aforementioned three 10-rotor-pole machines with E-core and C-core SFPM machines, which are known as high torque density SFPM machines, as shown in Fig. 2.4 and Fig. 2.5, respectively. According to the investigations in [CHE11] and [CHE11b], the 11-rotor-pole E-core machine and the 13-rotor-pole C-core machine exhibit the highest torque densities among the 6-stator-pole E-core and C-core SFPM machines, respectively. Therefore, a 6/11-stator/rotor-pole E-core SFPM, a 6/13-stator/rotor-pole C-core SFPM and aforementioned three 10-rotor-pole machines have been optimized to achieve the maximum average output torque under the constraint of the same copper loss (33.33W) before the comparison (for the these five machines, stator outer radius=45mm, axial length=25mm, air-gap length=0.5mm).

The average torque-copper loss curves of these machines are shown in Fig. 2.6. As can be seen, the torques of the E-core and C-core SFPM machines are smaller compared with two SSFPM machines. Additionally, unbalanced magnetic forces will be detected in the E-core and C-core SFPM machines due to odd-number-pole rotors. Thus, two SSFPM machines and the conventional 12/10-stator/rotor-pole SFPM will be compared and investigated in following parts.

It is worth mentioning that the comparison of these machines based on the constraint of the same copper loss may not be comprehensive enough. For instance, each slot of the 6-slot C-core machine is much larger than those of the other investigated machines. This means even under the same copper loss and slot filling factor, the thermal condition at the centre of the coil in C-core machine can be much severer than those of the other machines.

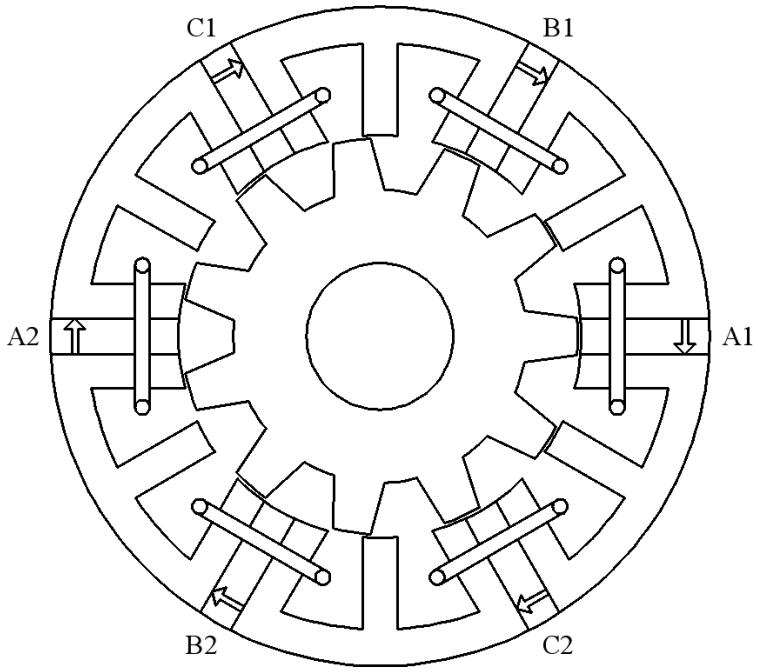

Fig. 2.4. Topology of 6/11-stator/rotor-pole E-core SFPM machine.

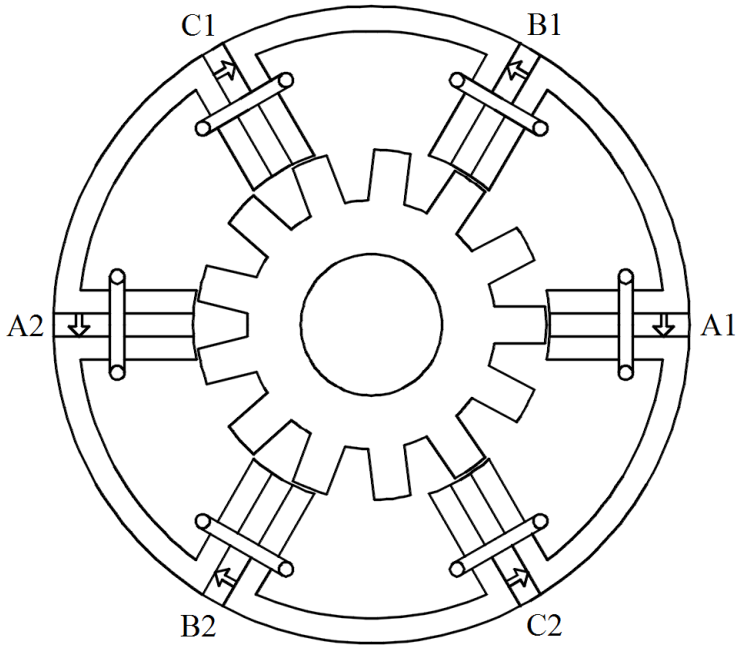

Fig. 2.5. Topology of 6/13-stator/rotor-pole C-core SFPM machine.

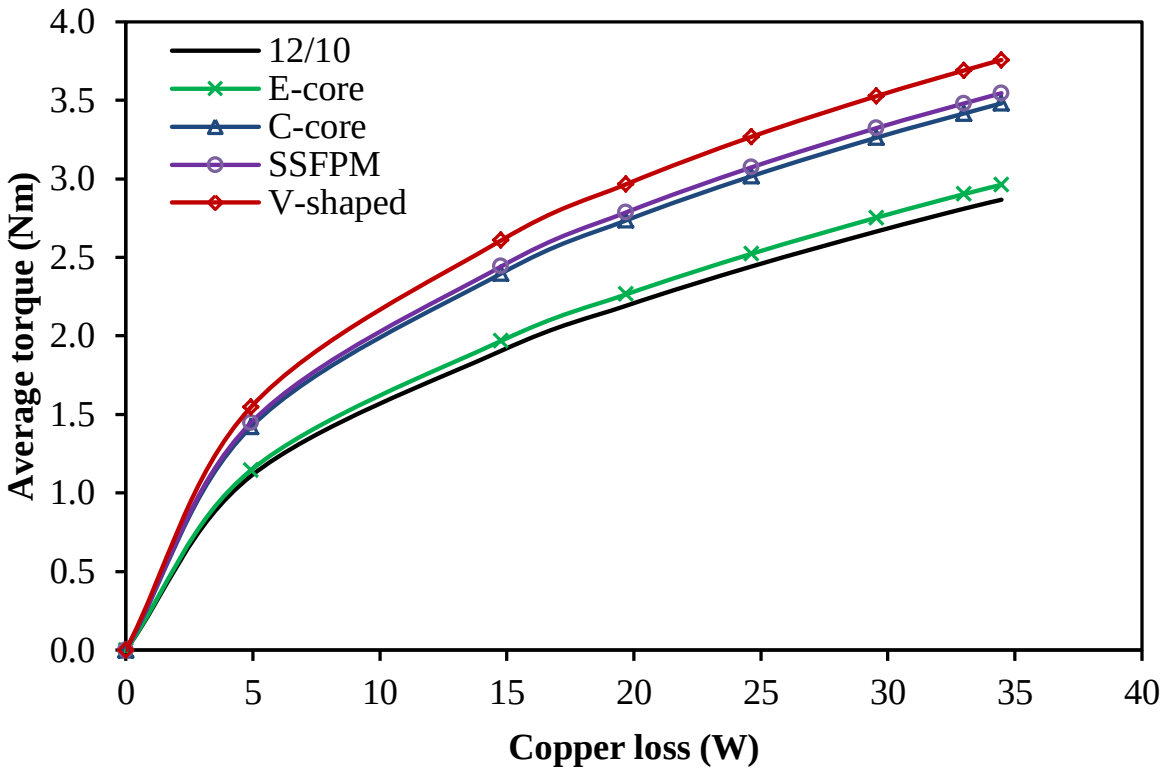

Fig. 2.6. Comparison of average torque-copper loss curves.

2.2.Machine topology and operation principle

The conventional SSFPM machine as shown in Fig. 2.2 has 12 circumferentially opposite magnetized PMs and 6 U-shaped laminated segments on its stator. The lamination segment sandwiched between two PMs in a stator tooth is defined as “sandwiching pole”. Its operation principle is similar to that of a conventional SFPM machine, as shown in Fig. 2.7 (a) and (b). It can be seen from Fig. 2.7 (a) when the rotor pole aligns with a sandwiching pole, the flux-linkage in coil A1 move from stator side to rotor side, while in Fig. 2.7 (b), when the rotor pole aligns with a stator tooth, the direction of flux-linkage is reversed. The periodical variation of flux-linkage with rotor position will induce back-EMF in the coils. However, as shown in Fig. 2.8 (b), the flux density of a conventional SSFPM machine in some parts of sandwiching poles are far below the saturation knee-point of steel B-H curve (steel grade: M330-35A), which means the material has not be used efficiently. Therefore, the V-shaped magnet SSFPM machine, Fig. 2.8 (c), is proposed to shrink low flux density part in lamination and consequently increase the slot area. The position of two PM pieces in one stator pole close to the rotor is the same as the conventional one, but the PM position at outer stator is moved closer, resulting in V-shaped PM structure. Additionally, due to the waste of

material in conventional design, the thickness of a PM piece at outer stator can be reduced without sacrificing the average torque.

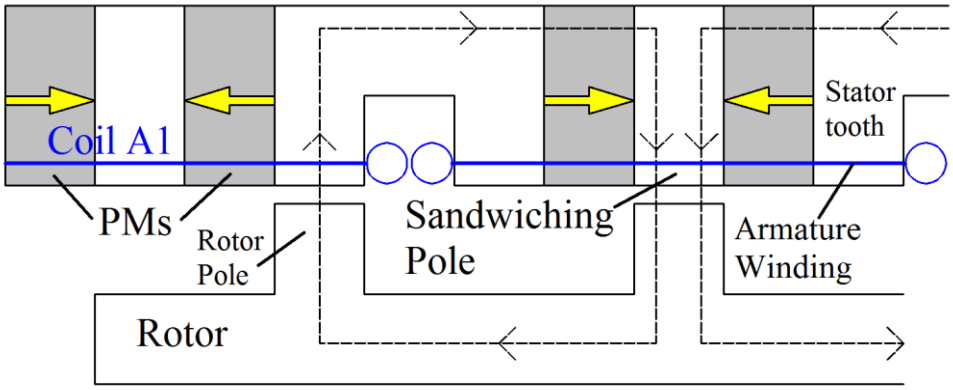

(a)

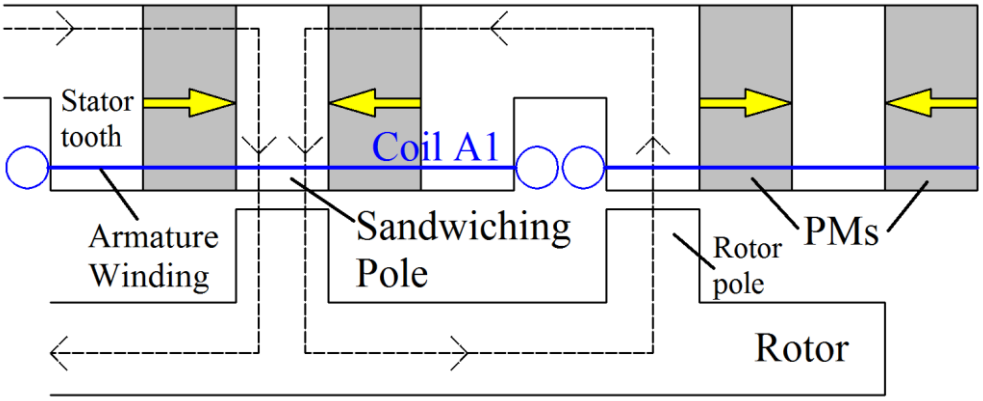

(b)

Fig. 2.7. Operation principle of SSFPM machines.

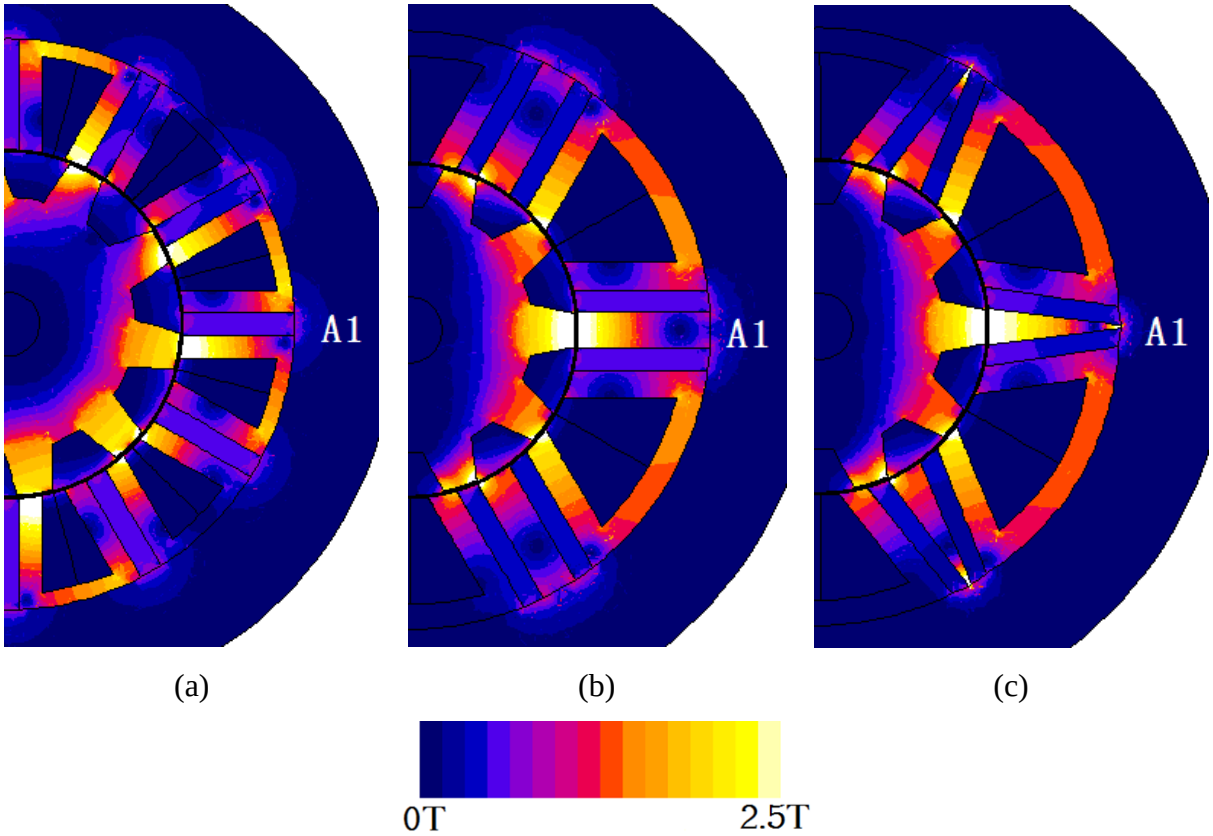

Fig. 2.8. Open-circuit flux density. (a) 12/10 SFPM machine. (b) Conventional SSFPM. (c) V-shaped SSFPM.

2.3.Parameter optimization

For comparison, all the stator and rotor parameters in the conventional 12/10-stator/rotor-pole SFPM machine, the conventional SSFPM machine and SSFPM machine with V-shaped magnets have been optimized to achieve the maximum average output torque under the constraint of same copper loss (33.33W). When the end-winding is ignored, the copper loss P_{Cu} of a conventional SFPM machine can be expressed as:

$$P_{Cu} = 3I_a^2 R_a = \frac{6I_a^2 N_a^2 \rho_{Cu} L}{S_a k_{pf}} \tag{2.1}$$

where I_a is the RMS phase current, R_a is the phase resistance, N_a is the number of turns per phase, ρ_{Cu} is the electrical resistivity of copper, L is the axial length, S_a is the phase slot area, k_{pf} is the winding packing factor.

The optimized parameters of the investigated machines are given in Table 2.1. It can be seen that the slot area of the V-shaped SSFPM machine has been increased by >15% compared with the conventional SSFPM machine. Hence, the phase current can be increased for the same copper loss according to (2.1). On the other hand, the magnet usage of a V-

shaped SSFPM machine is reduced by 4%, compared with that of the conventional one. It is worth noticing that although the copper slot area is increased in V-shaped machine, the packing factor is not increased. The reason for this is that the corner of a slot is sharper than that of the conventional SSFPM machine, and consequently, the slot area is not effectively utilized.

Table 2.1. Main parameters of machines

Items	**12/10**	**SSFPM**	**V-shaped SSFPM**
Rated speed (rpm)	400	400	400
Stator outer radius (mm)	45	45	45
Axial length (mm)	25	25	25
Split ratio	0.6	0.55	0.55
Stator slot number	12	6	6
Rotor pole number	10	10	10
Air-gap length (mm)	0.5	0.5	0.5
Sandwiching pole arc (degree)	--	12.5	12.5
Stator pole arc (degree)	7.5	10	10
Stator slot arc (degree)	7.5	12.5	12.5
Rotor pole arc (degree)	12	12	12
Total stator slot area (mm^2)	1361	1356	1560
Number of turns per coil	18	36	36
Packing factor	0.5	0.5	0.5
Magnet material	NdFeB	NdFeB	NdFeB
Remanence of PMs (T)	1.2	1.2	1.2
Total magnet volume (mm^3)	18870	19440	18660
Rated phase current (A)	16.7	16.6	19.1

2.4.Comparison with conventional switched flux permanent magnet

The performance of aforementioned three optimized SFPM machines are compared in this section. It should be noticed that the end effects are ignored in 2-D FEA.

2.4.1. Flux distribution

Fig. 2.9 shows the open-circuit flux distributions of three SFPM machines when the d-axis is aligned with phase A. It can be seen that from Fig. 2.9 (b) and (c), in V-shaped machine, not only the low flux density parts in sandwiching pole is shrunken, but also the flux leakage at outer stator is reduced, compared with the conventional one. Therefore, even the PM volume in V-shaped SSFPM machine is reduced, its air-gap flux density (radial and

tangential components) for both SSFPM machines remain the same, as shown in Fig. 2.10, which has the potential to maintain the same phase back-EMFs.

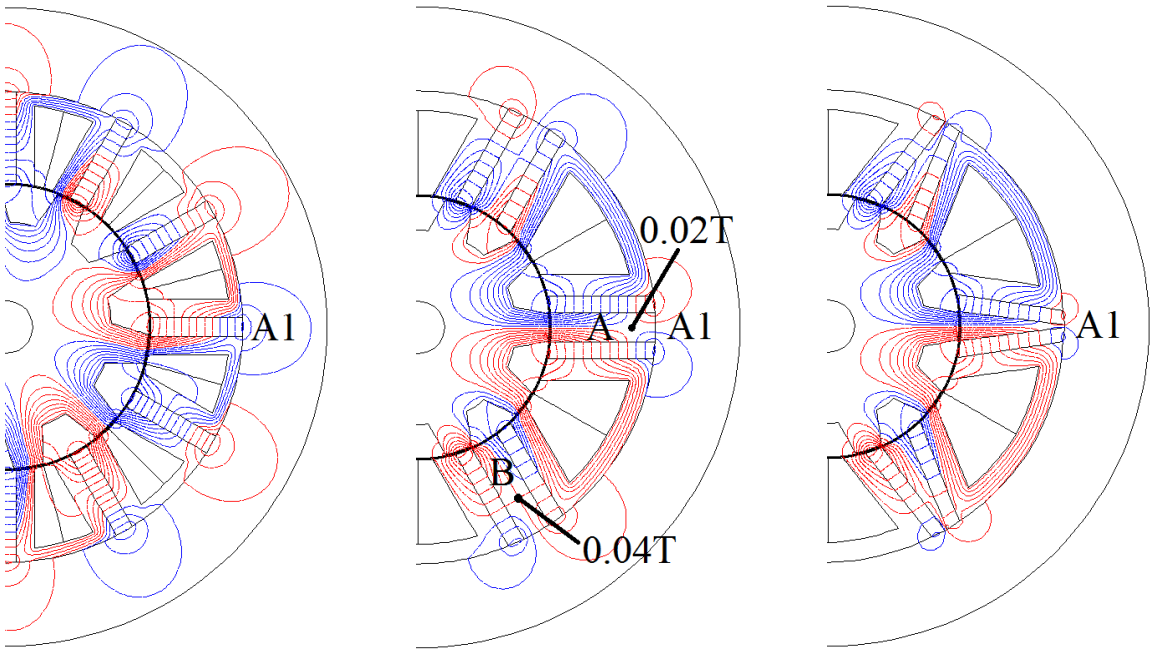

(a) (b) (c)

Fig. 2.9. Open-circuit field distributions. (a) 12/10 SFPM machine. (b) Conventional SSFPM. (c) V-shaped SSFPM.

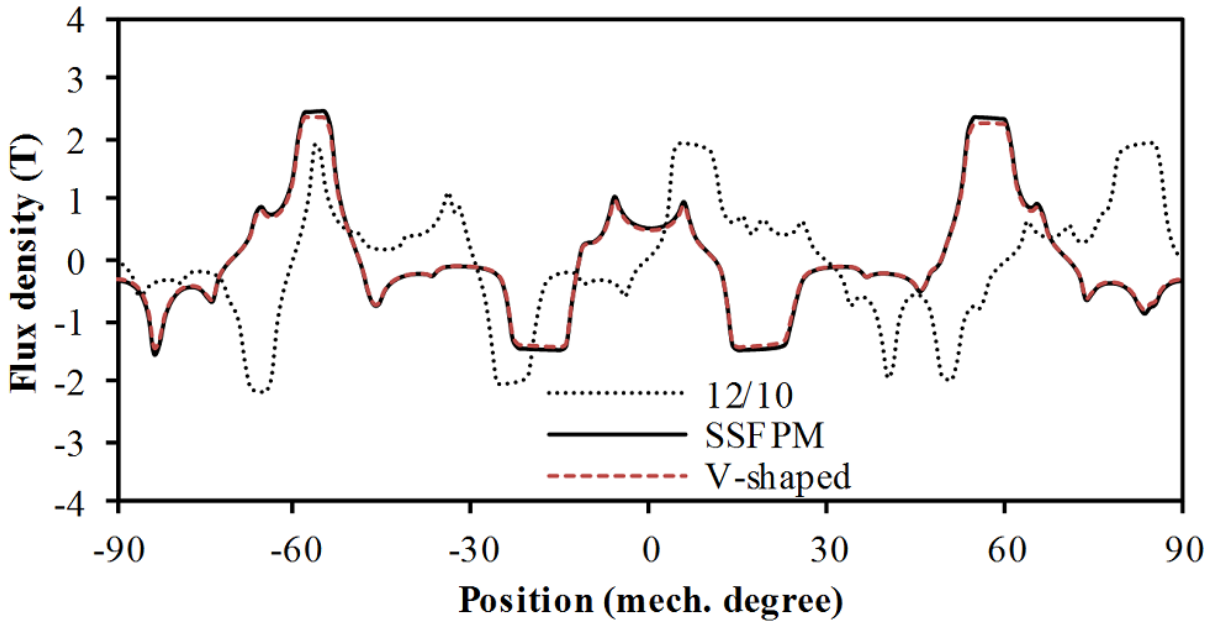

(a)

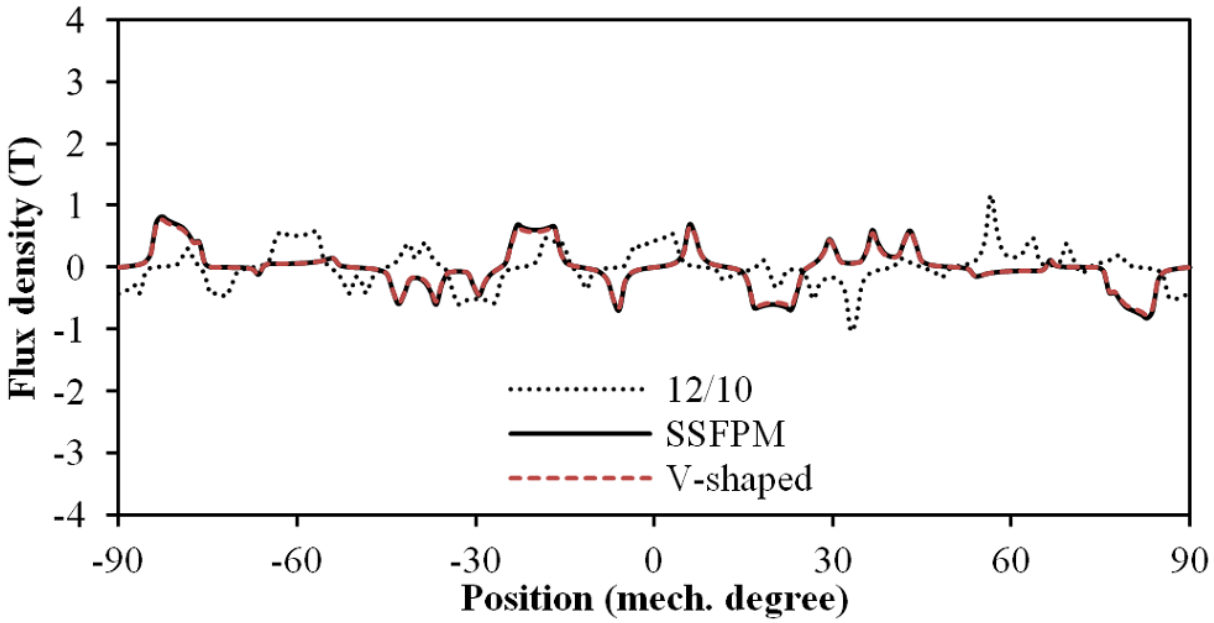

(b)

Fig. 2.10. Comparison of air-gap field distributions. (a) Radial component. (b) Tangential component.

2.4.2. Back-EMF

The variation of back-EMF with rotor position and harmonics in those three SFPM machines are compared in Fig. 2.11. As can be seen, the back-EMFs in SSFPM machines have been significantly improved compared with the conventional 12/10 machine. The back-EMF of V-shaped SSFPM is slightly reduced compared with the conventional SSFPM machine due to the reduced PM volume. The 12/10 machine has sinusoidal back-EMF, which makes it suitable for brushless AC (BLAC) operation. However, the back-EMFs in SSFPM machines are slightly asymmetric due to the asymmetry in the magnetic circuit and even order EMF harmonics exhibits. For one rotor pole in a SSFPM machine, two magnets are connected to the magnetic circuit at the rotor position shown in Fig. 2.7 (a). On the other hand, only one magnet is connected to the magnetic circuit at the rotor position shown in Fig. 2.7 (b).

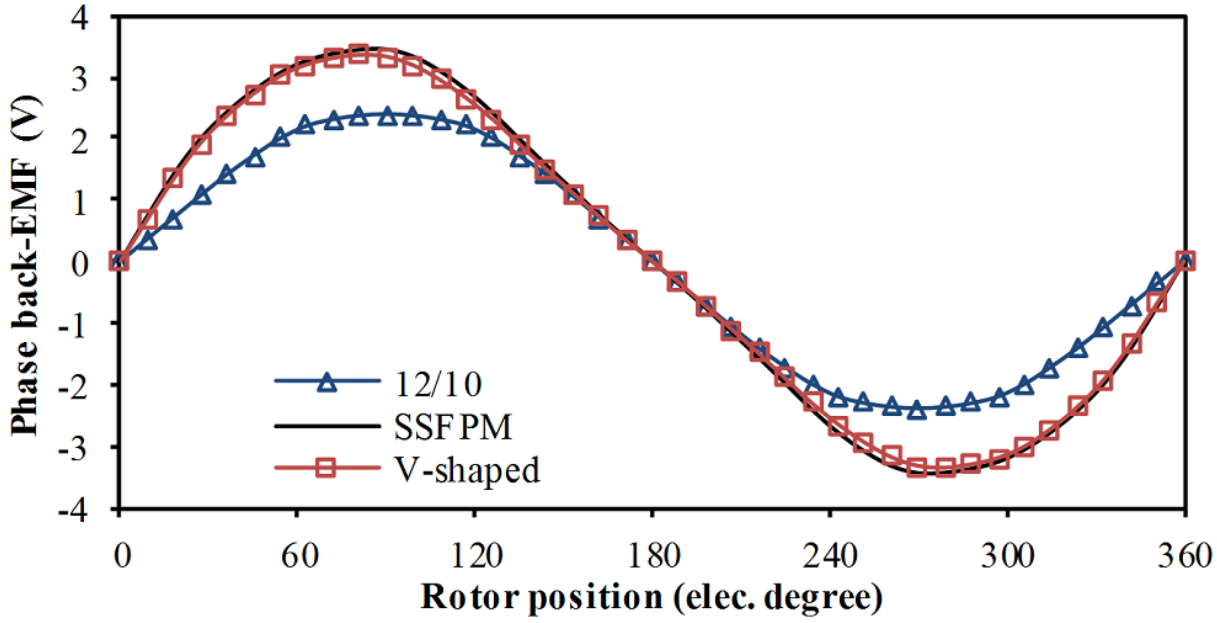

(a)

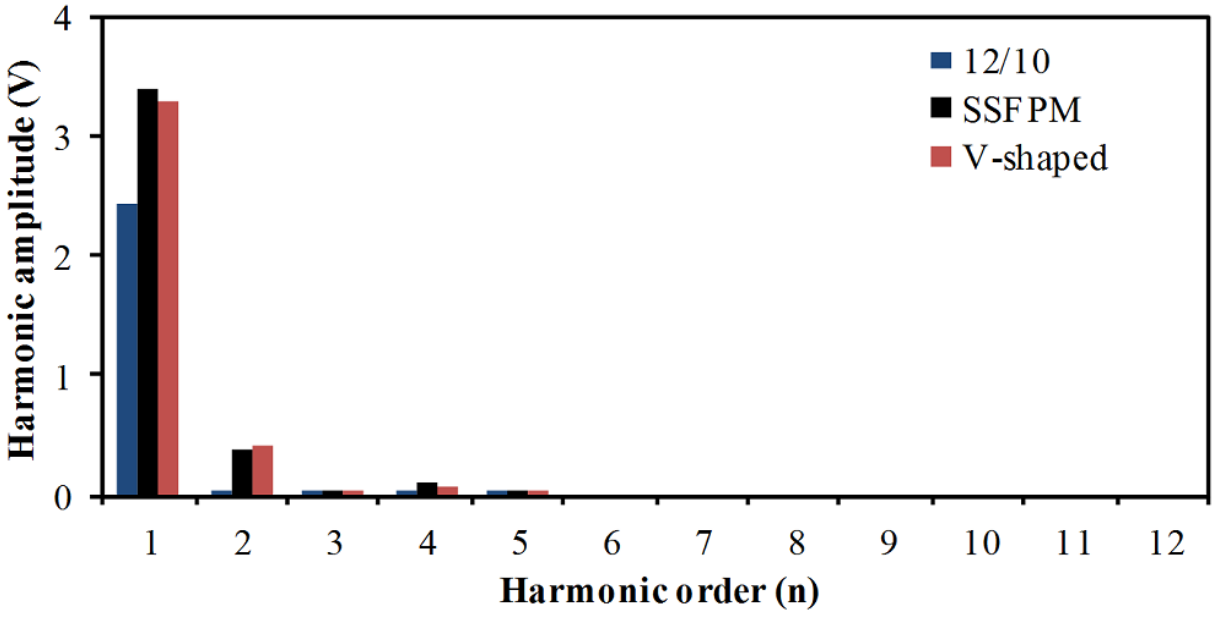

(b)

Fig. 2.11. Comparison of back-EMF, 400rpm. (a) Waveforms. (b) Harmonics.

2.4.3. Cogging torque

In terms of cogging torque waveforms, the peak to peak values of the SSFPM machines are large and the frequencies are halved compared with that of the 12/10 machine. The reason for this is that the stator pole number of a SSFPM machine is halved and this leads to half of the least common multiple between stator and rotor pole numbers [BIA02], Fig. 2.12.

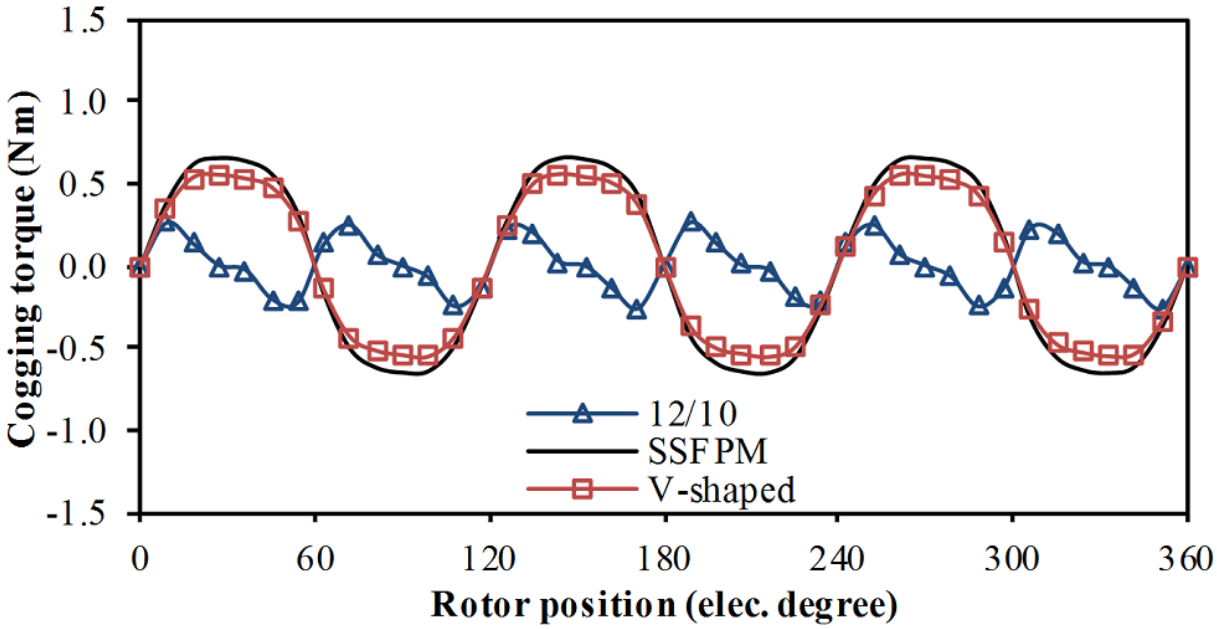

Fig. 2.12. Cogging torque in SFPM machines.

2.4.4. Torque Characteristics

Fig. 2.13 shows the variations of torque with current angle when current density is fixed to 10.6A/mm^2 (for the conventional SSFPM machine, copper loss = 33.33W). The current density in this thesis is defined as the current (unit: A) per unit effective copper area (unit: mm^2). The current angle between the d-axis and the current vector can be expressed as:

$$\varphi_c = \tan^{-1}\frac{I_d}{I_q} \tag{2.2}$$

where I_d and I_q are the d- and q-axis currents, respectively.

It can be seen form this figure that the maximum torque of the V-shaped machine is the highest one among all the investigated machines mainly due to the significant increase of slot area, as shown in Table 2.1. In addition, the maximum torque is achieved when the current angle is almost equal to 0. Therefore, the reluctance torque is negligible and the d-axis current of each phase will be set to 0 in further analysis. Under such a current density, the air-cooled systems can be employed to improve the reliability of those machines.

Fig. 2.14 shows the torque waveforms when the current densities are fixed to 10.6A/mm^2. The average torque of the 12/10 machine, the conventional and V-shaped SSFPM machines are 2.82Nm, 3.48Nm and 3.96Nm, respectively. Therefore, the ratio of torque to PM volume of those machines are 1.49×10^{-4} Nm/mm^3, 1.79×10^{-4} Nm/mm^3 and 2.12×10^{-4} Nm/mm^3, respectively. This means the V-shaped machine has much better magnet usage efficiency

than others. However, due to the high even order harmonics in back-EMF waveform and the large peak to peak cogging torque, the torque ripple is large in a SSFPM machine, compared with that in a 12/10 machine. Therefore, the rotor skewing is employed to reduce the torque ripple in a V-shaped machine. It is worth mentioning that the torque ripples of the 12/10 machine, the conventional and V-shaped SSFPM machines are 17.6%, 57.1%, and 56.7%, respectively. The torque ripple is given by:

$$T_r = \frac{T_{max} - T_{min}}{T_{avg}} \times 100\% \tag{2.3}$$

where T_{max}, T_{min}, and T_{avg} are the maximum torque, the minimum torque, and the average torque of one electric cycle, respectively.

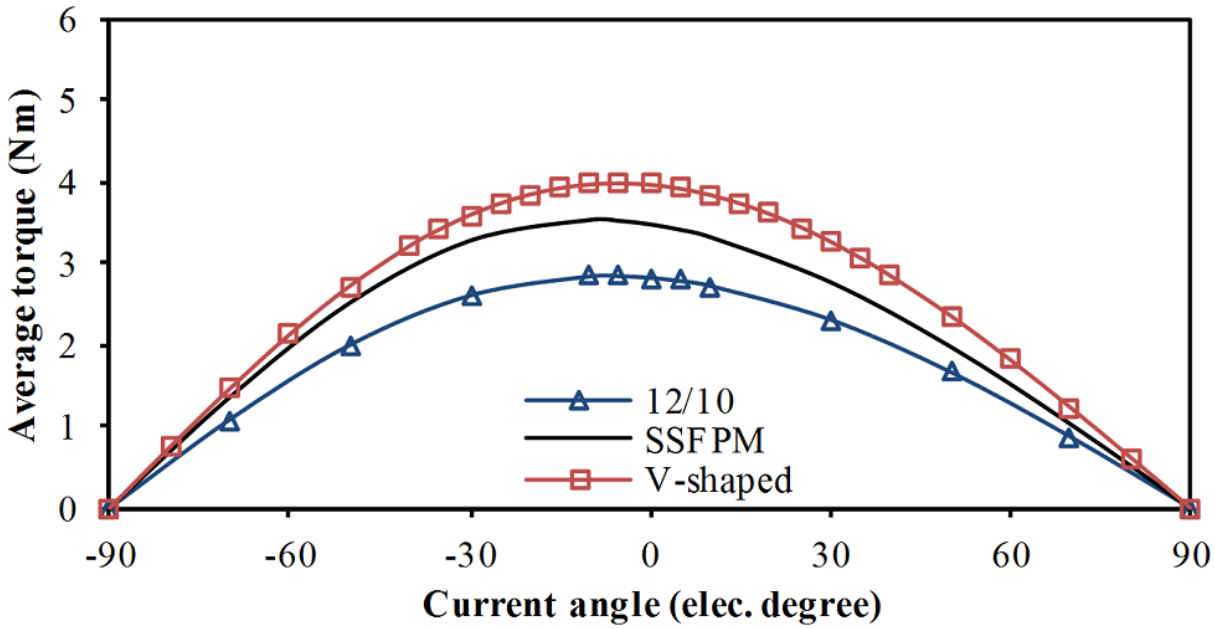

Fig. 2.13. Torque-current angle curve of V-shaped machine, current density = 10.6A/mm^2.

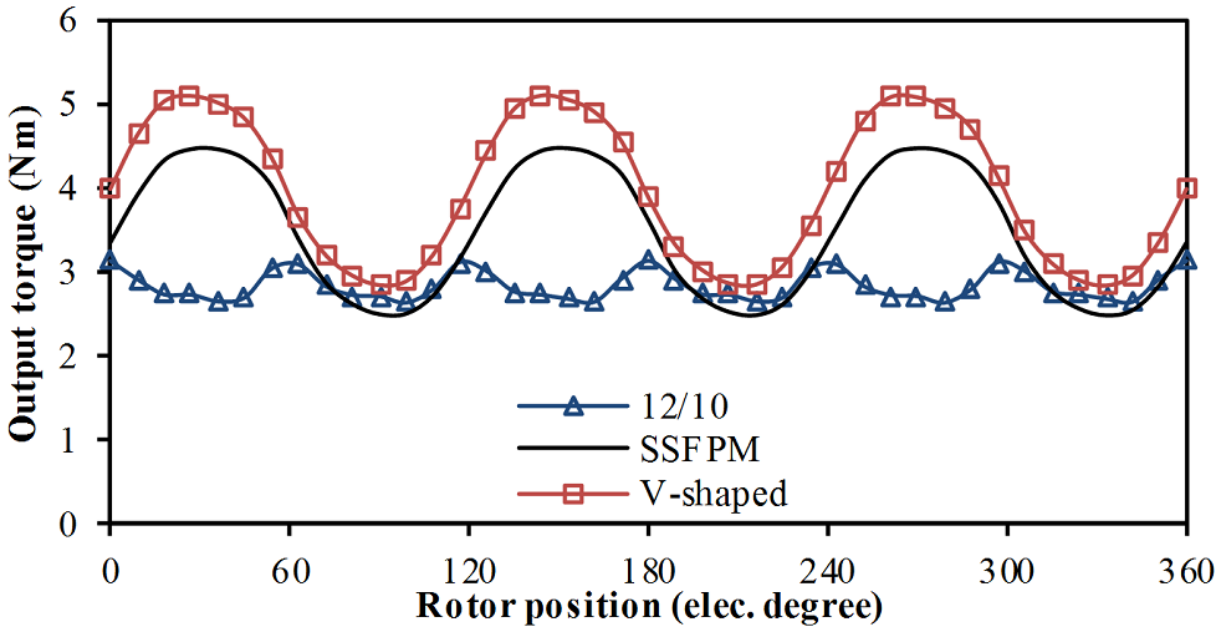

Fig. 2.14. Torque waveforms, current density = 10.6A/mm^2, I_d = 0.

2.5.Rotor skewing

The rotor skewing can be employed in SFPM machines to reduce the torque ripple and EMF harmonics. Unlike the continuous rotor skewing that was investigated in [FEI06], the rotor with two-stepped skewing is employed for the V-shaped SSFPM machine to ease manufacture, as shown in Fig. 2.15. It is worth noting that the selection of the rotor step-skewing angle is not decided by the optimization of cogging torque and back-EMF, as described in [FEI06], but is aimed to reduce the torque ripple to minimum in this chapter. For 2-D FEA, the electromagnetic torque of a two-step skewed machine can be regarded as the sum of the torques of two half axial-length machines having corresponding positive/negative angles. For instance, the two torque waveforms from two 12.5mm axial-length SFPM machines having initial rotor positions of positive and negative 3.5 mechanical degrees (under the same current density/current angle) can be added together to obtain the torque waveform of a SFPM machine of 25mm axial length employing a rotor with 7-degree two-stepped skewing. Obviously, this is a simple method but with the limitation of ignoring the interaction between the rotor parts and end-effects.

When the current densities are fixed to 10.6A/mm^2, the 7-degree rotor step-skewed V-shaped machine has the smallest torque ripple, as shown in Fig. 2.16, although according to [FEI12], 3-degree two-stepped rotor skewing is appropriate for torque ripple suppression in the 12/10 machines. Compared with this machine, the 7-degree rotor step-skewed V-shaped

one has a 20.3% enhancement in the average torque, but only a 4.6% increase in the torque ripple, as shown in Fig. 2.17.

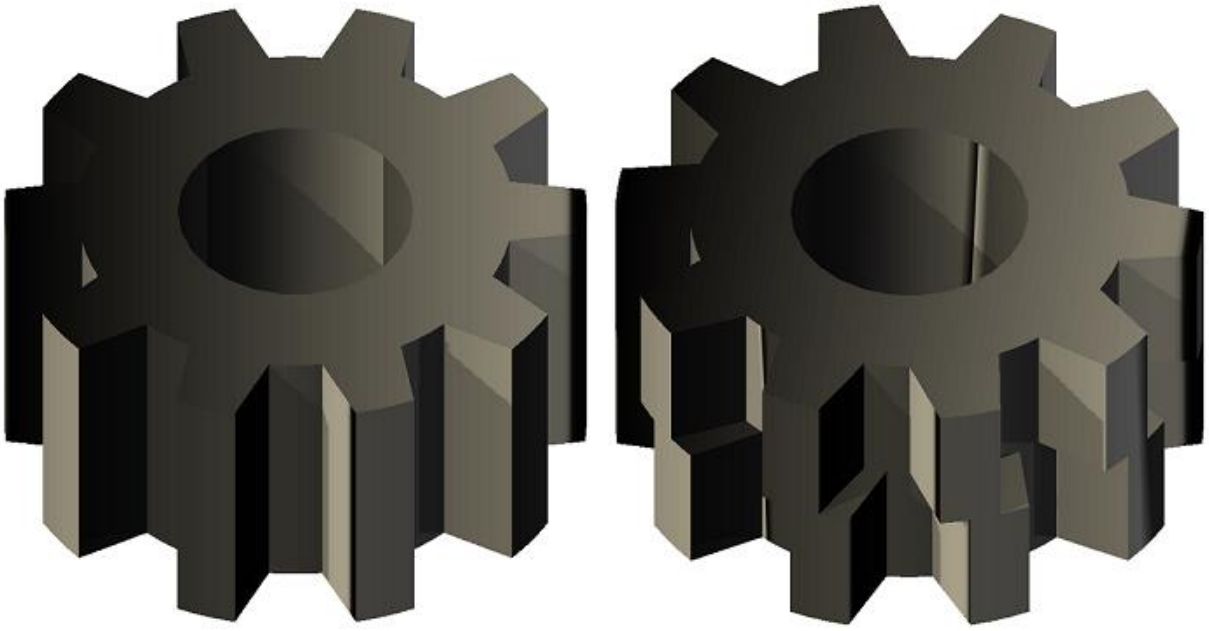

(a) (b)

Fig. 2.15. Schematics of rotors. (a) Unskewed rotor. (b) Rotor with 7-degree two-stepped skewing.

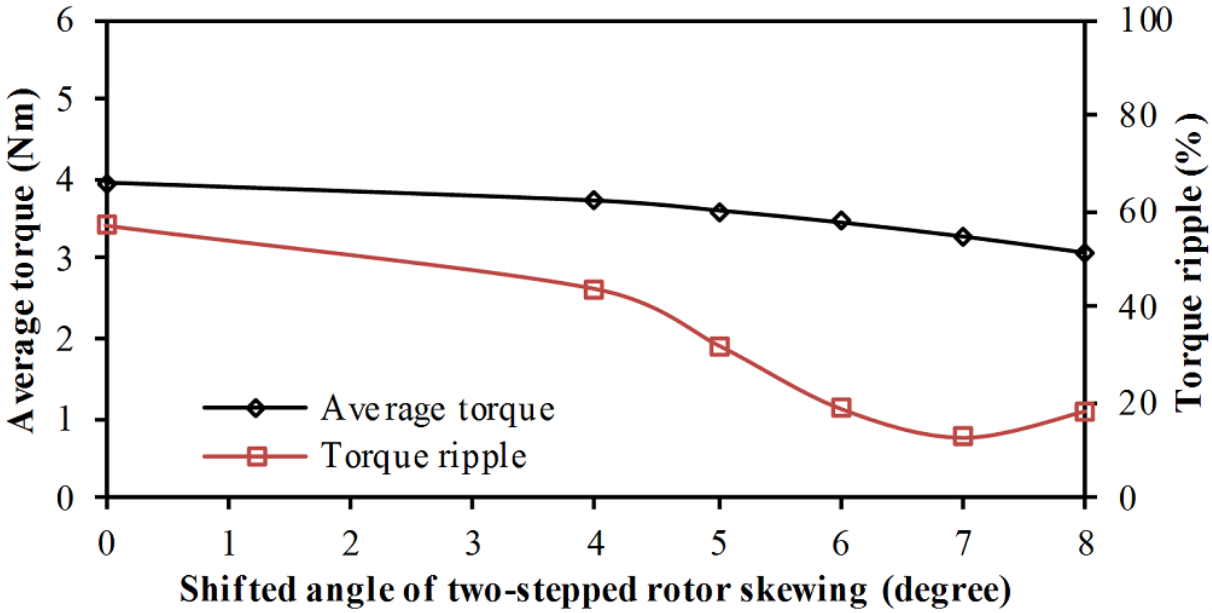

Fig. 2.16. Variation of average torque and torque ripple with rotor skewing angle of V-shaped machine, current density = 10.6A/mm^2.

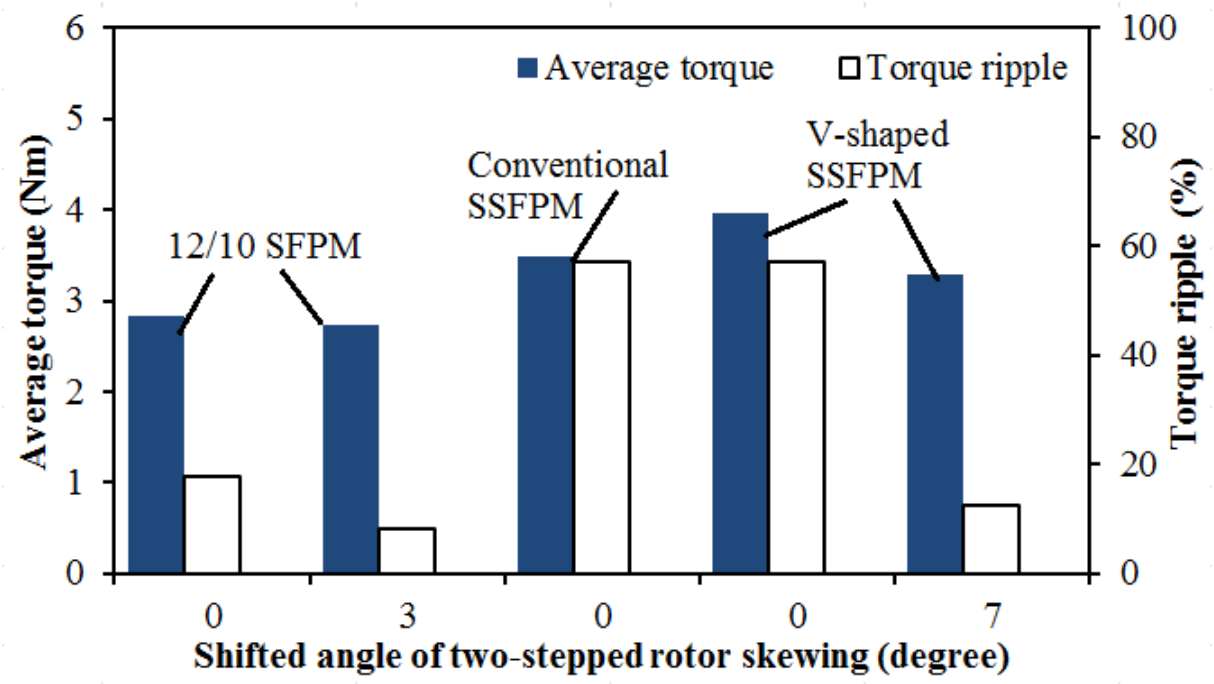

Fig. 2.17. Comparison of average torque and torque ripple, current density = 10.6A/mm^2.

2.6.Experimental validations

A stator and two different rotors of V-shaped machine have been prototyped and tested to validate the FEA, as shown in Fig. 2.18. Load tests are carried out under forced air-cooling. It can be noticed for Fig. 2.19 (a) that the measured cogging torque waveforms are slightly different from the prediction due to the mechanical tolerance. To ease manufacture, the sharp corners and arcs of PMs in the original design have been eliminated and result in a reduction of total PM volume. For this reason and also due to the ignoring of end-effects [ZHU05], the peak to peak values of measured EMF waveforms are smaller than those from 2-D FEAs, as shown in Fig. 2.19 (b). In Fig. 2.19 (c) each point represents the maximum positive torque corresponding to different current value. Due to the reduced PM volume and end effects, the measured results are lower than the prediction. But overall, good agreement has been achieved. It should be noticed that the cogging torques and the maximum positive torques are measured based on the method shown in Appendix A. Although there is no relative displacement between the bearings and the rotor during the measurement, the static friction between them may lead to inaccuracy of the measuring results. Forced air-cooling in this measuring system may also lead to inaccuracy due to the disturbance on the scale. Fortunately, forced air-cooling is not necessary at low electric loadings, and the disturbance

from the forced air-cooling on the measured results are negligible when the electric loading is high.

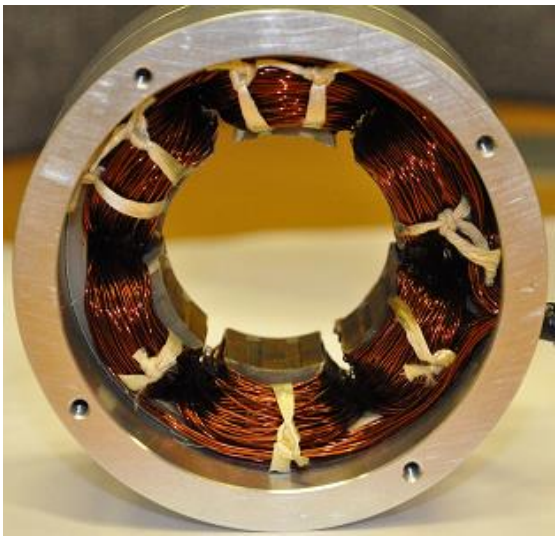

(a)

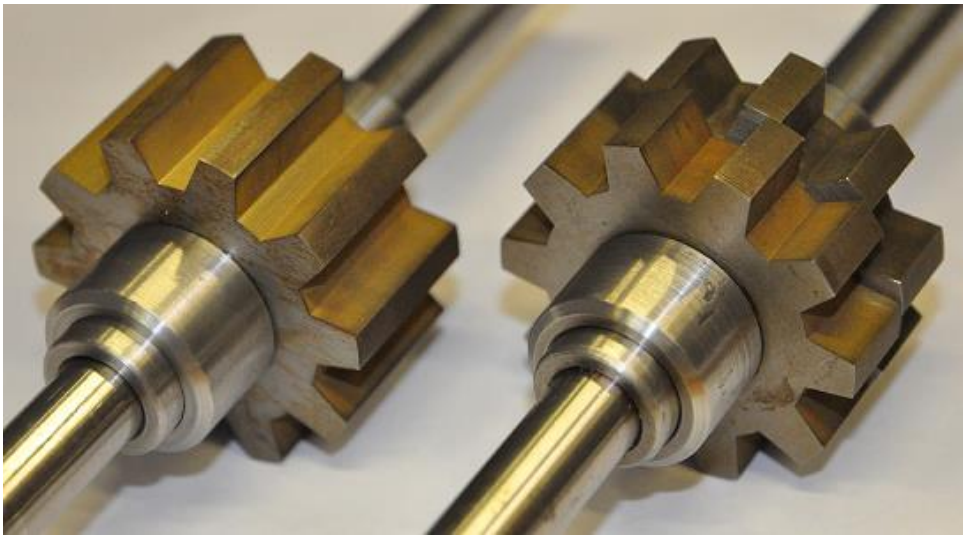

(b)

Fig. 2.18. Prototypes of V-shaped SSFPM machine. (a) Stator. (b) Rotor without skewing and the rotor with 7^{o} two-stepped skewing.

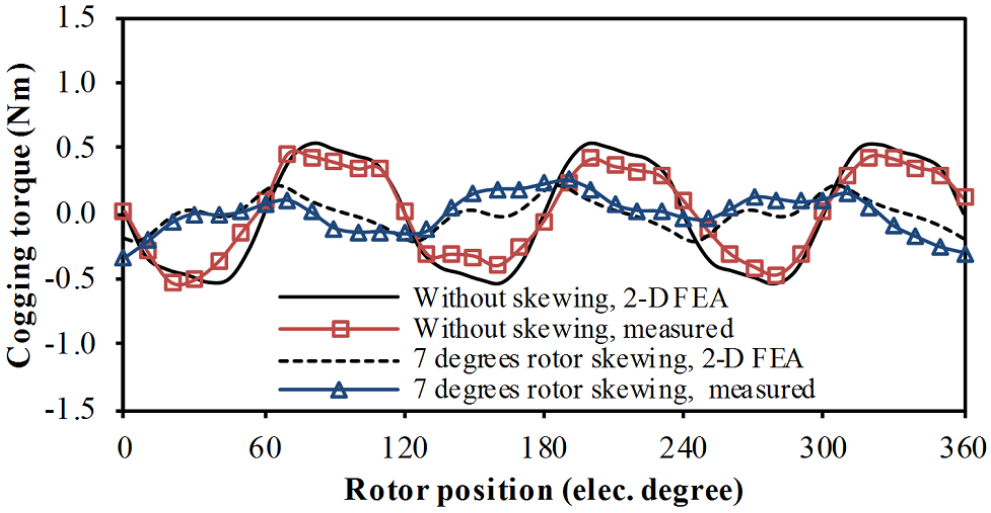

(a)

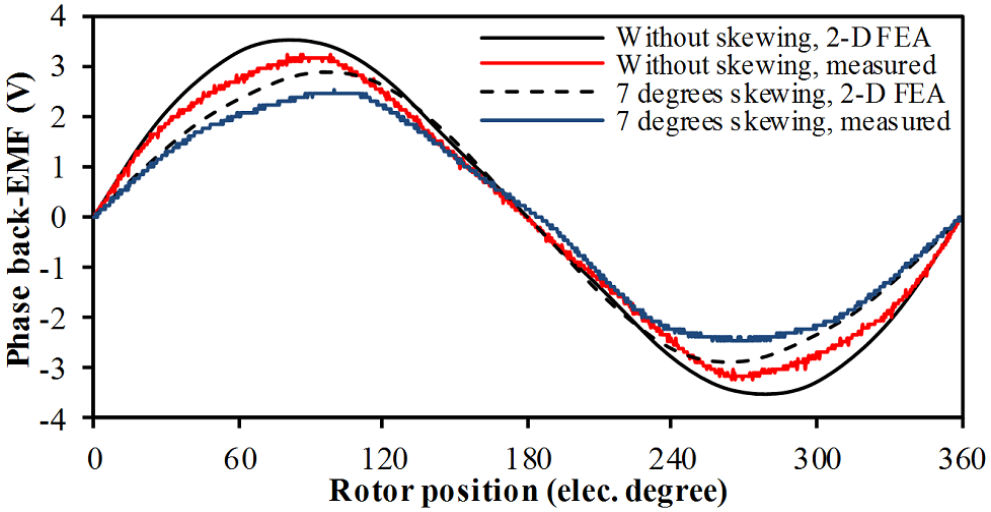

(b)

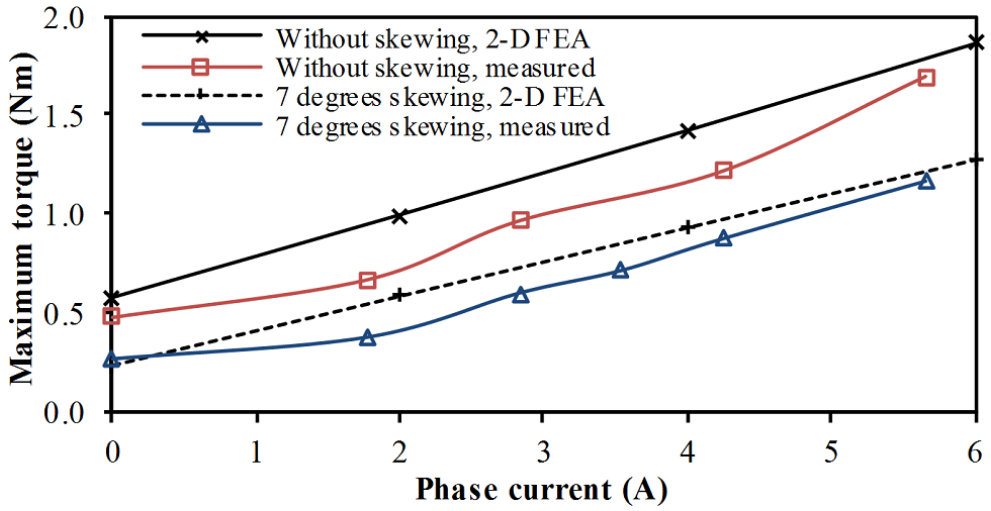

(c)

Fig. 2.19. Comparison of predicted and measured results. (a) Cogging torque. (b) Back-EMF waveforms, 400rpm. (c) Maximum torque-current characteristics.

2.7.Summary

A novel SSFPM machine with V-shaped magnets has been investigated in this chapter. According to the 2-D FEA, compared with the conventional SSFPM machine under the same copper loss, the average torque is increased by 13.8% since the slot area is increased by 15%. Meanwhile, the PM volume is reduced by 4% due to flux-focusing, resulting in an 18.5% increase of the magnet usage efficiency. Moreover, two-stepped rotor skewing is easily employed to reduce the torque ripple from 57.0% to 12.6% in the V-shaped machine. The FEA predicted cogging torque, back-EMF, torque-current curve are validated by experiments on the prototype machines.

CHAPTER III. THREE-PHASE WOUND FIELD SWITCHED FLUX MACHINES HAVING VARIOUS ARMATURE AND FIELD COIL PITCHES

A three-phase wound field switched flux (WFSF) machine derived from the sandwiched SFPM machine mentioned in the last chapter is proposed in this chapter. It is found that this machine has much higher average torque compared with the conventional 12-slot/8-pole machine with segmented rotor and 12-slot/5-pole WFSF machine under the constraint of same copper loss. All of those machines have been optimized to achieve the maximum torque for comparison. The performance, including back-EMF, cogging torque, and static torque, of four machines are analysed and compared by two-dimensional (2-D) finite element analysis (FEA) and validated by experiments on the prototype machines.

3.1.Introduction

The quest for low-cost high-performance machines has never ceased. Since the switched flux (SF) principle was firstly introduced in 1955, numerous SF machine topologies have emerged and been investigated [RAU55], [HOA97], [ZHU10], [ZHU11], [OWE10], [CHE10], [FEI12b], [OJE12], [THO12], and [ZUL12]. The switched flux permanent magnet (SFPM) machine, which is designed for high-performance applications, has two prominent advantages: simple temperature management and robust rotor structure, as the stator contains all excitation sources. Due to the increase in permanent magnet (PM) cost, the demand for PM-usage-reduced or non-PM machines has risen sharply. For SFPM machine, PMs can always be replaced by field windings, and some wound field switched flux (WFSF) machines have been proposed for low-cost applications [ZUL10], [POL99], [POL03], [POL03b], [POL06], [POL06b], [CHE10], [SUL11], [SUL12], [WAN12], and [GAU12]. The WFSF machine also possesses other merits such as high power density and easy flux weakening operation. However, compared with SFPM machine, the WFSF machine shows much lower torque density and this demerit restricts the popularization of existing WFSF machines. For this reason, it is desirable to increase the torque density of existing WFSF machines or seek new WFSF topologies for high torque density applications.

A 12-slot/8-pole segmented rotor WFSF machine was proposed in [ZUL10], as shown in Fig. 3.1. Both DC field and AC armature windings are concentrated windings and this is

advantageous to ease manufacture. However, as described in [ZUL10], this machine suffers from low torque density due to its special structure. A single-phase WFSF, whose DC field and AC armature windings are both fully pitched, was proposed and investigated in [POL99], [POL03], [POL03b], and [POL06]. This machine shows higher efficiency than a series universal machine of similar size [POL03]. Based on the operation principle of this single-phase WFSF machine, a three-phase 24-slot/10-pole WFSF machine has been studied in [CHE10], [SUL11], [SUL12], [WAN12], and [GAU12]. Its torque density can be over 60% as much as that of an interior PM machine used for electric vehicle applications [SUL11]. For further improvement in the torque density of a 24-slot/10-pole WFSF machine, a machine, whose number of slots and poles are both halved, is used in the comparison in this chapter, i.e. 12-slot/5-pole WFSF machine, as shown in Fig. 3.2. 7-pole rotor can be also equipped in this machine, and it is found that the 12-slot/7-pole machine shows higher torque density and lower torque ripple than the 12-slot/5-pole machine when the copper loss is fixed. As shown in Fig. 3.3, a WFSF machine having 1 slot-pitch DC field windings and 3 slot-pitch AC armature windings is firstly proposed in this chapter. This 9-slot/5-pole machine also shows higher torque density than the 12-slot/5-pole machine when the copper loss is fixed. The FEA predicted back-EMFs, cogging torques, static torques of the 12-slot/5-pole, 12-slot/7-pole, and 9-slot/5-pole WFSF machines are validated by experiments.

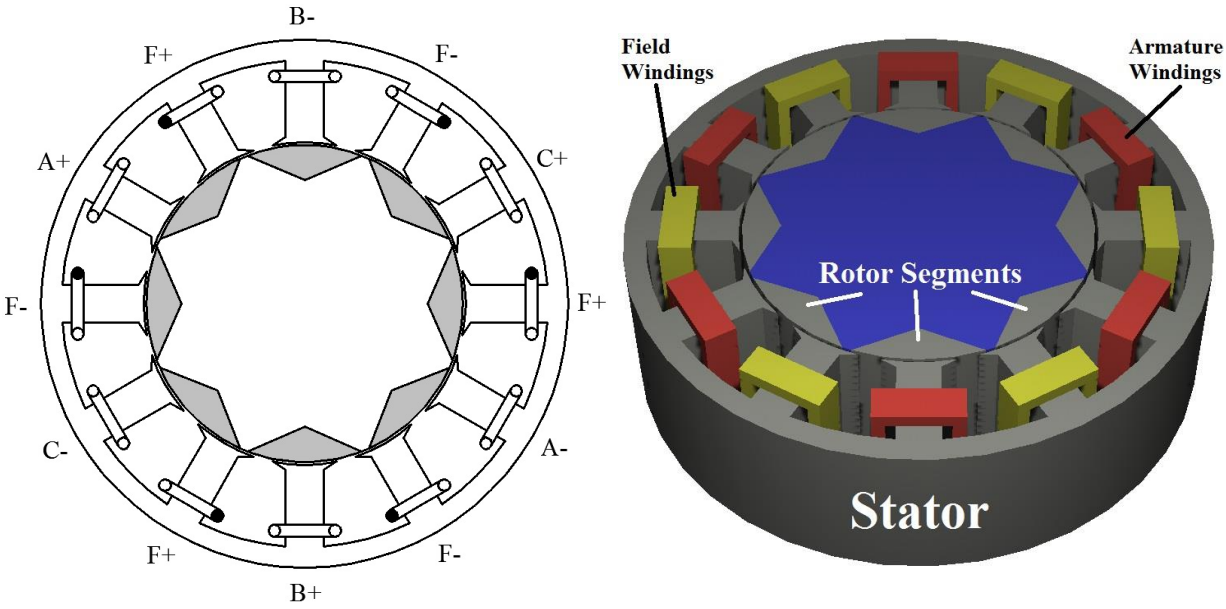

(a) (b)

Fig. 3.1. 12-slot/8-pole machine. (a) Cross-section. (b) 3D model.

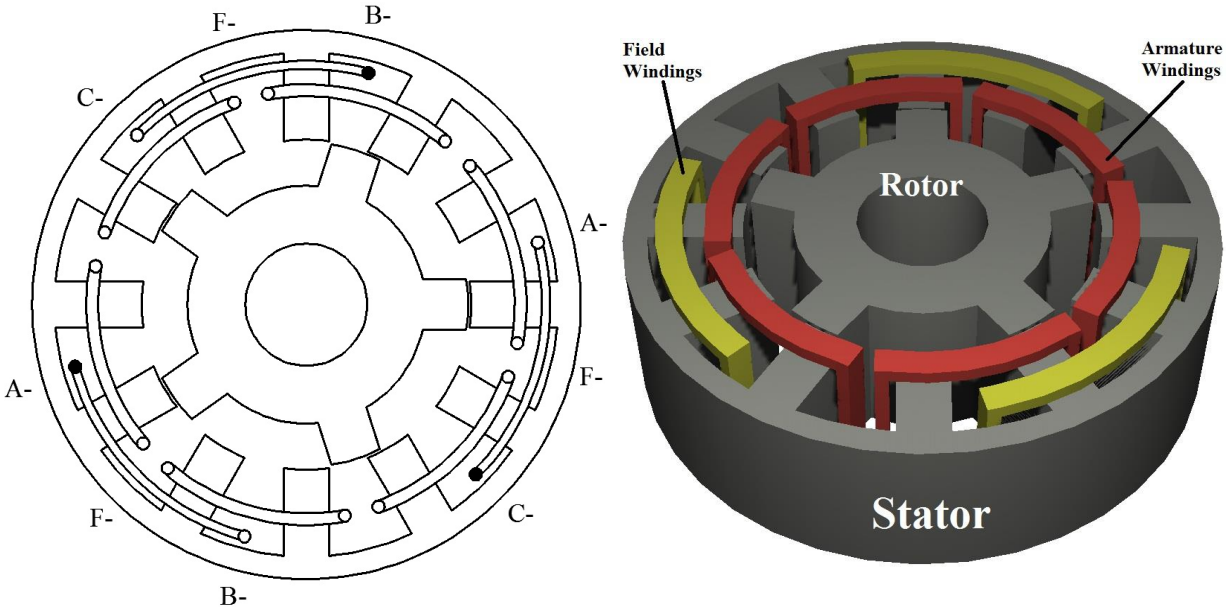

(a) (b)

Fig. 3.2. 12-slot/5-pole machine. (a) Cross-section. (b) 3D model.

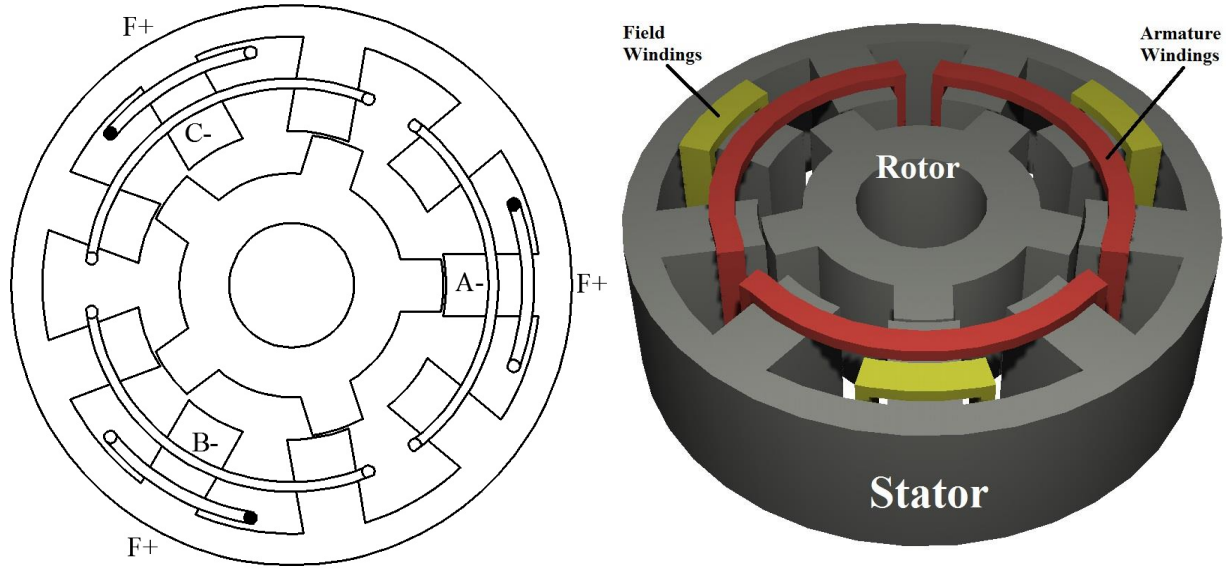

(a) (b)

Fig. 3.3. 9-slot/5-pole machine. (a) Cross-section. (b) 3D model.

3.2.Stator and rotor pole combination

Among 12-stator-slot segmented rotor machines having different rotor pole numbers, the 8-pole-rotor one can produce the highest average torque and lowest torque ripple [ZUL10]. It can be seen from Fig. 3.1 that the 12-slot/8-pole machine is equipped with a salient-pole

stator and segmented rotor. Its DC field windings and AC armature windings have the same short coil pitch of 1 slot. Correspondingly, 6 field and 6 armature coils are arranged on the stator alternately. For the machine shown in Fig. 3.2, both 5- and 7-rotor-pole machines have the largest winding factor (0.866) among the feasible rotor pole numbers. It can be seen that this machine is equipped with a salient-pole stator and rotor. The coil pitches of field and armature windings are both 2 slots. Accordingly, there are 6 armature coils and 6 (or 3, for consequent pole windings) field coils on the stator. In terms of the proposed 9-stator-slot machine, any rotor pole number from 1 to 10 can be employed except 3, 6 and 9. When the copper loss is fixed at 60 W, the average torques and torque ripples of 4-, 5- and 7-pole-rotor machines are compared in Table 3.1. Although 4-pole-rotor and 5-pole-rotor machines have the same winding factor, the 5-pole-rotor one shows acceptable performance due to its operation principle. As shown in Fig. 3.3, salient-pole stator and rotor are employed in the 9-slot/5-pole machine. 3 short pitched field coils having 1 slot-pitch and 3 long pitched field coils having 3 slot-pitches are arranged on the stator.

Table 3.1. Torque comparison of 9-stator-slot machines

Items	9-slot/4-pole	9-slot/5-pole	9-slot/7-pole
Average torque (Nm)	1.21	1.43	0.54
Torque ripple (%)	31	22	127

When the RMS current densities of all slots are 10 A/mm^2, the flux distribution of aforementioned 12-slot/5-pole and 24-slot/10-pole machines are shown in Fig. 3.4 (a) and (b) respectively. Compared with the 12-slot/5-pole machine, the conventional 24-slot/10-pole machine shows significantly increased flux leakage (Note: The number of divisions of flux lines is the same in Fig. 3.4.), and consequently, a 30.9% decrease of the average torque, when the current density is 20 A/mm^2, as shown in Fig. 3.5. For the proposed 9-slot/5-pole machine, the number of stator slots, rotor pole and coils can be doubled, thus an 18-slot/10-pole machine has the same operation principle. Compared with the 9-slot/5-pole machine, the 18-slot/10-pole machine also shows increased flux leakage, as shown in Fig. 3.4 (c) and (d), and consequently, a 20.7% decrease of the average torque, when the current density is 20 A/mm^2, as shown in Fig. 3.5. With respect to torque density, two 5-pole machines will be chosen for further comparison and investigation.

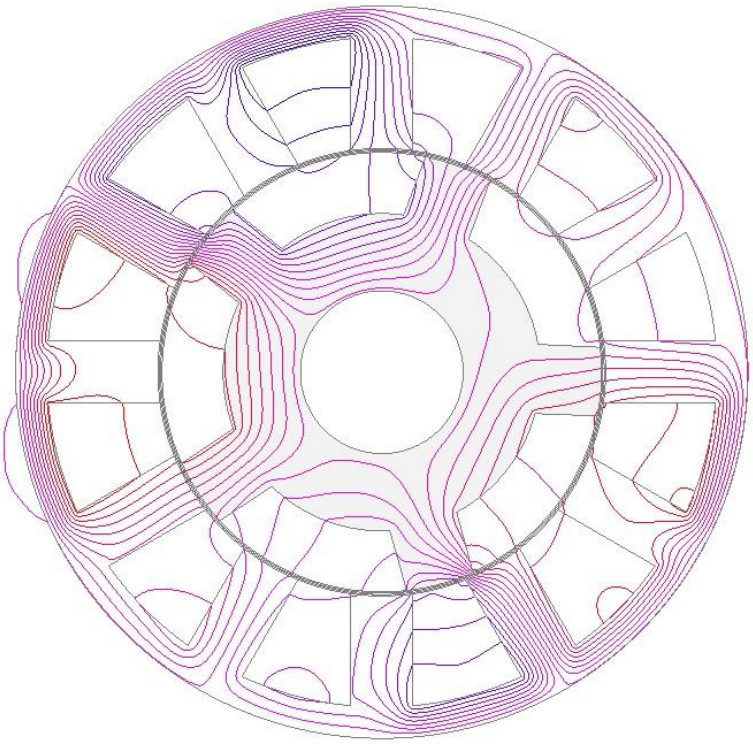

(a)

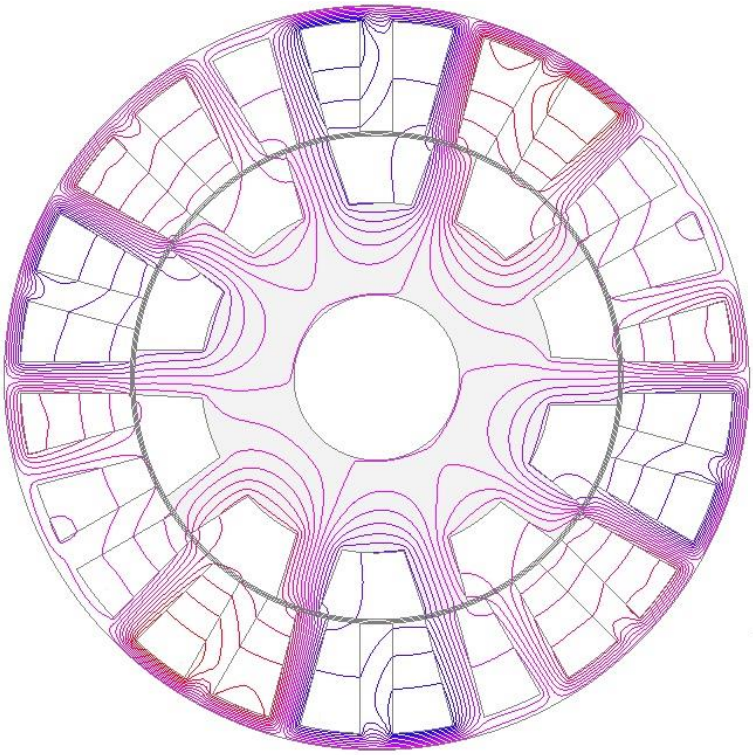

(b)

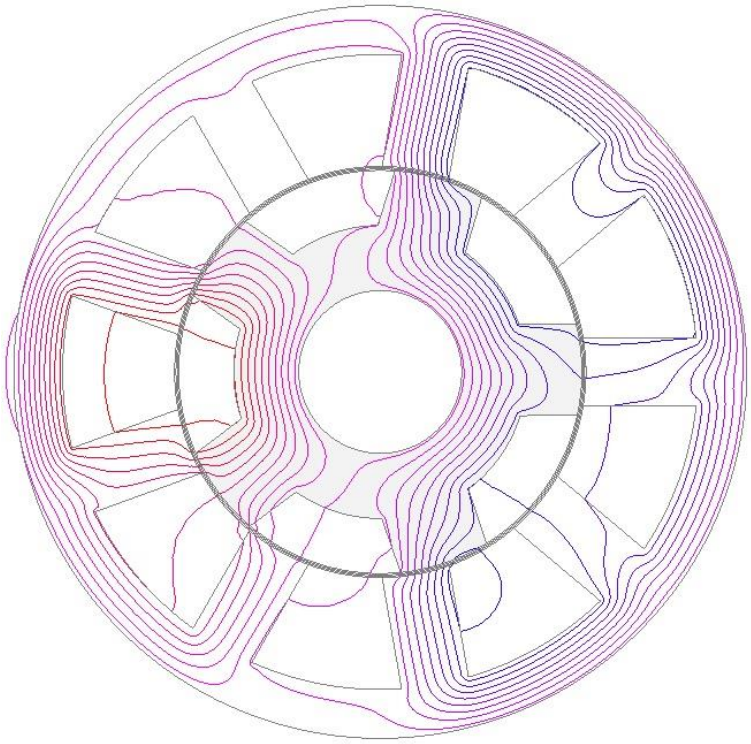

(c)

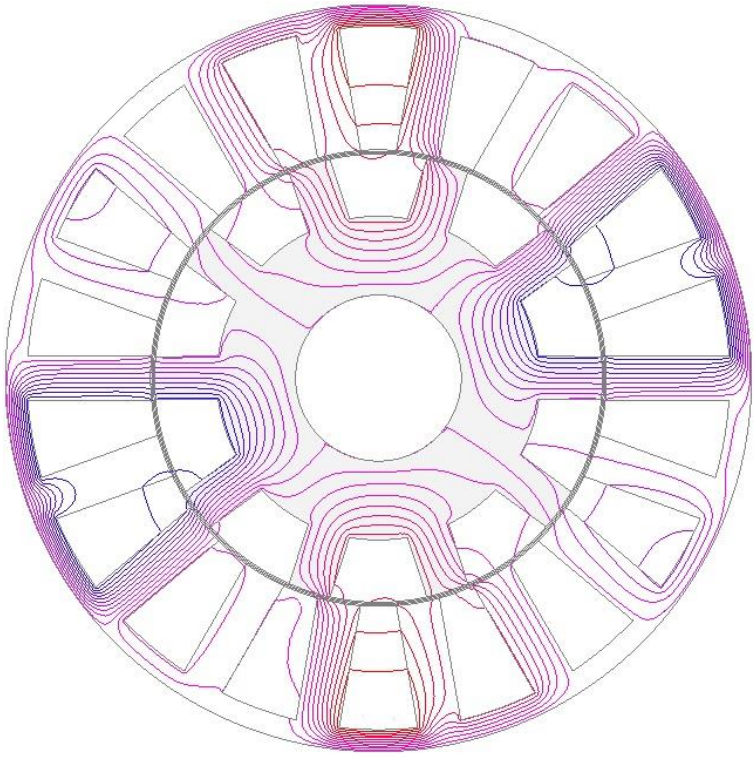

(d)

Fig. 3.4. Flux distributions, both field and armature slot current density =10 A/mm^2. (a) 12-slot/5-pole. (b) 24-slot/10-pole. (c) 9-slot/5-pole. (d) 18-slot/10-pole.

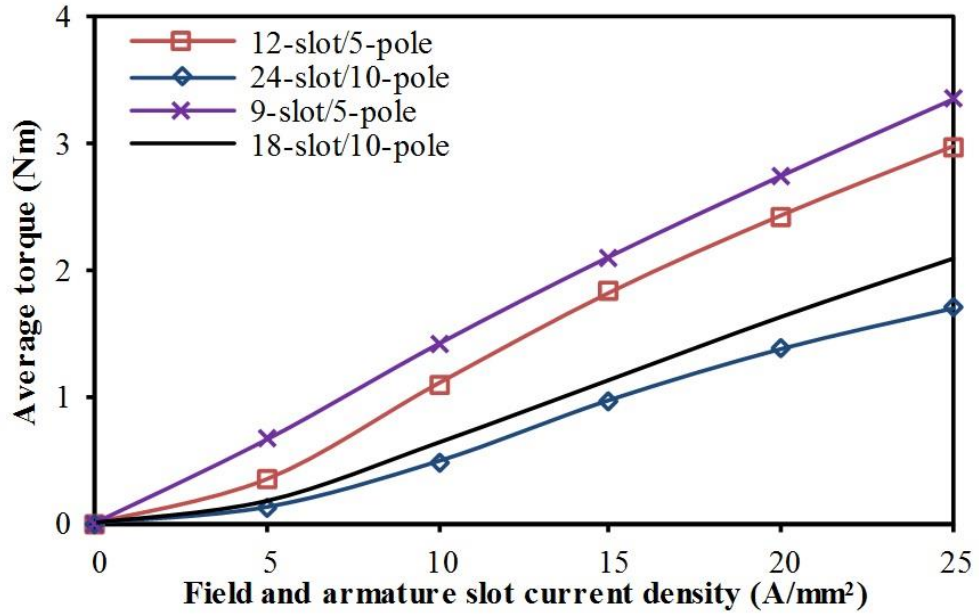

Fig. 3.5. Comparison of torque-current density curves.

3.3.Operation principle

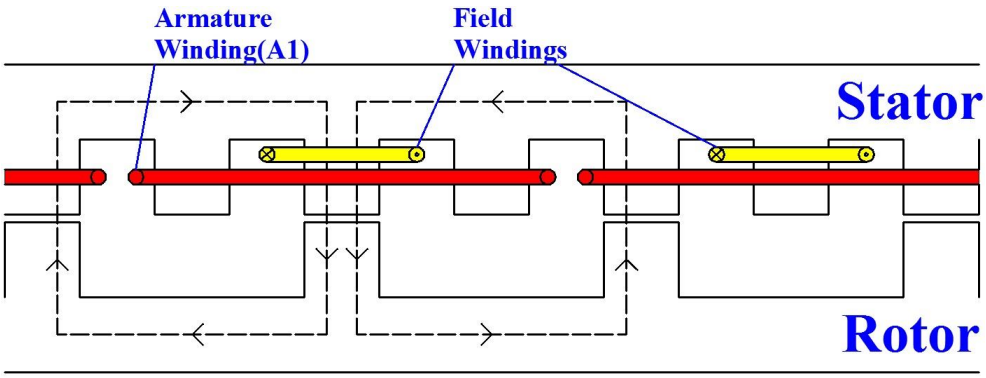

(a)

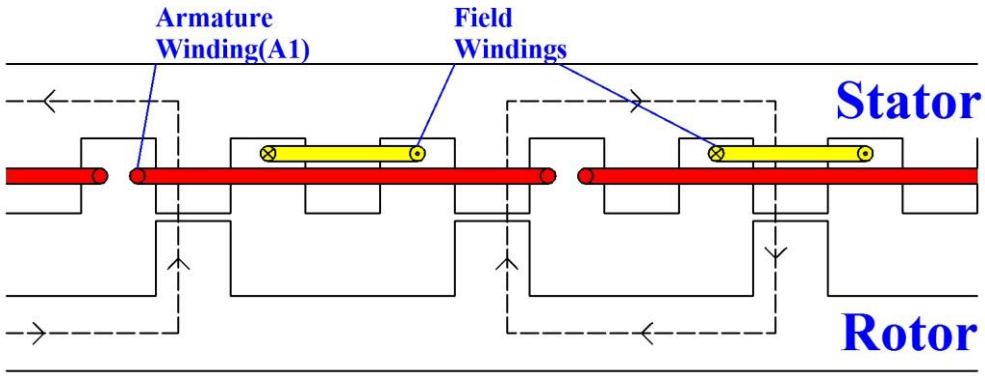

(b)

Fig. 3.6. Operation principle of 9-slot/5-pole machine. (a) Rotor pole aligned with stator field winding pole. (b) Rotor pole unaligned with stator field winding pole.

Fig. 3.6 (a) and (b) show the principle of operation of the proposed 9-slot/5-pole machine. When the rotor pole aligns with the centre of a field coil, the flux-linkage in coil A1 goes from the stator side to the rotor side, as shown in Fig. 3.6 (a). When the rotor pole aligns with the centre of another field coil, the direction of flux-linkage in coil A1 is reversed, as shown in Fig. 3.6 (b). The periodic variation of flux-linkage with rotor position will induce back-EMF in the coils.

3.4.Parameter optimization

For comparison, all the stator and rotor parameters in the aforementioned machines have been optimized. Similar to the SFPM machines, the rotor pole width, stator pole width, stator slot opening and stator back-iron thickness are initially set to be the same in each machine before optimization [HOA97], [ZHU10], and [ZHU11]. With respect to torque density, the optimization objective is to achieve the maximum average torque under the constraint of the same copper loss. It is worth mentioning that the average torque of each machine is obtained from one electrical cycle. The individually optimized parameters of four WFSF machines under different copper losses are shown in Table 3.2 (for the 12-slot/8-pole machine, the width of stator pole and the depth of the rotor segment are also optimized). The "Optimetrics-parametric" function of Ansoft Maxwell (Version 15.0) has been employed during the optimization. The sequence of the optimized parameters follows the first column in this table (from top to bottom). The winding resistance changes with the split ratio, the ratio of field to armature slot current density, and stator parameters. These have been taken into consideration during the optimization. The iron losses are neglected, and this means the optimized parameters may be not suitable for the machines operated at high speeds. Although the fixed copper loss is the constraint during the optimization, the thermal conditions of the machines can be different due to the different topologies and parameters, which is a limitation of this optimization. Nevertheless, for the maximum torque capability at low speed, the iron loss is negligible while the copper loss is dominant.

As can be seen from Table 3.2, according to the optimized ratio of field to armature current, the maximum average torque will be achieved when the ratio of field to armature slot current density is approximately 1 for all the WFSF machines under different copper losses.

In a WFSF machine the reluctance torque is not the major component of the output torque [ZHO14a]. The electromagnetic torque of a WFSF machine can be expressed as:

$$\mathrm{T} = \frac{3}{2} p \Psi_f I_q \tag{3.1}$$

where p is the rotor pole number of a machine, Ψ_f is the wound field excited flux-linkage in the WFSF machine. I_q is the q-axis current. With respect of (3.1), theoretically, the maximum torque can be achieved when $I_q = I_f$, due to the fact that Ψ_f is proportional to I_f.

Table 3.2. Optimization variables of machines

Items	12-slot/8-pole			12-slot/5-pole			12-slot/7-pole			9-slot/5-pole		
	30W	60W	120W	30W	60W	120W	30W	60W	120W	30W	60W	120W
Split ratio	0.54	0.58	0.63	0.55	0.62	0.65	0.55	0.6	0.65	0.54	0.55	0.58
Ratio of field to armature slot current density	1	1	0.95	0.9	0.9	0.9	1	1.05	1.05	0.9	0.9	0.9
Stator pole arc (degree)	25	23	23	16	15	14	15	15	15	18	19	19
Stator back-iron thickness (mm)	3.2	4	4.5	3.5	4.1	4.5	3.6	4.3	4.7	5.5	6.1	6.7
Rotor pole/segment arc (degree)	39	40	40	19	17	17	19	17	17	28	26	26

Since the machines are designed for low-power applications, the optimized parameters for 30 W copper losses will be employed in further investigations. The copper loss P_{Cu} of a WFSF machine can be expressed as:

$$P_{Cu} = I_a^2 R_{at} + I_f^2 R_{ft} \tag{3.2}$$

where I_a is the RMS armature current, R_{at} is the total armature winding resistance, I_f is the field current, R_{ft} is the total field winding resistance. The end-winding resistance changes with the stator parameters during the optimization and this has been taken into consideration in the optimization.

The total armature winding resistance R_{at1} of a 12-slot/8-, 5- or 7-pole WFSF machine is given in (3.3) and their field winding resistances R_{ft1} is given in (3.4). The armature winding resistance R_{at2} and field winding resistance R_{ft2} of a 9-slot/5-pole machine are given in (3.5) and (3.6), respectively.

$$R_{at1} = \frac{2N_{at1}^2 \rho_{Cu}(12L_1 + L_{end\_a1})}{S_1 k_{pf1}} \tag{3.3}$$

$$R_{ft1} = \frac{2N_{ft1}^2 \rho_{Cu}(12L_1 + L_{end\_f1})}{S_1 k_{pf1}} \tag{3.4}$$

$$R_{at2} = \frac{2N_{at2}^2 \rho_{Cu}(6L_2 + L_{end\_a2})}{S_2 k_{pf2}} \tag{3.5}$$

$$R_{ft2} = \frac{N_{ft2}^2 \rho_{Cu}(6L_2 + L_{end\_f2})}{S_2 k_{pf2}} \tag{3.6}$$

where N_{at} and N_{ft} are the total number of turns per armature coil and field coil, respectively. ρ_{Cu} is the electrical resistivity of copper, L is the machine depth, L_{end_a} and L_{end_f} are the total armature and field end-winding length, respectively, S is the area of one stator slot, k_{pf} is the winding packing factor.

Fig. 3.7 shows the idealized disposition of the coil-sides of four WFSF machines. To simplify the calculation, it can be assumed that the end-turns are semi-circular [ZHU00].

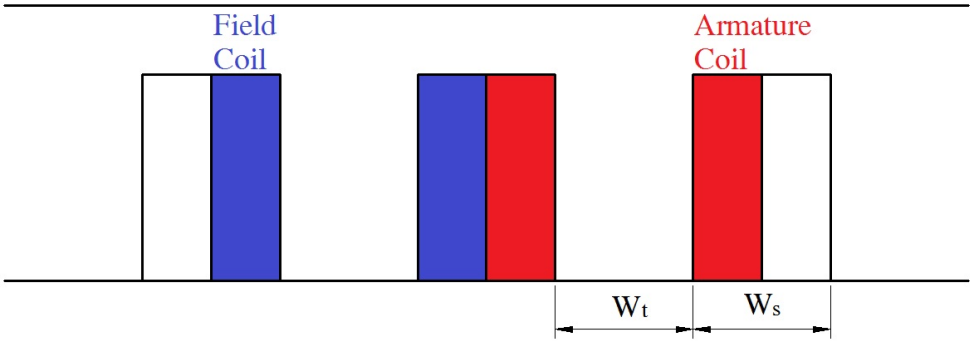

(a)

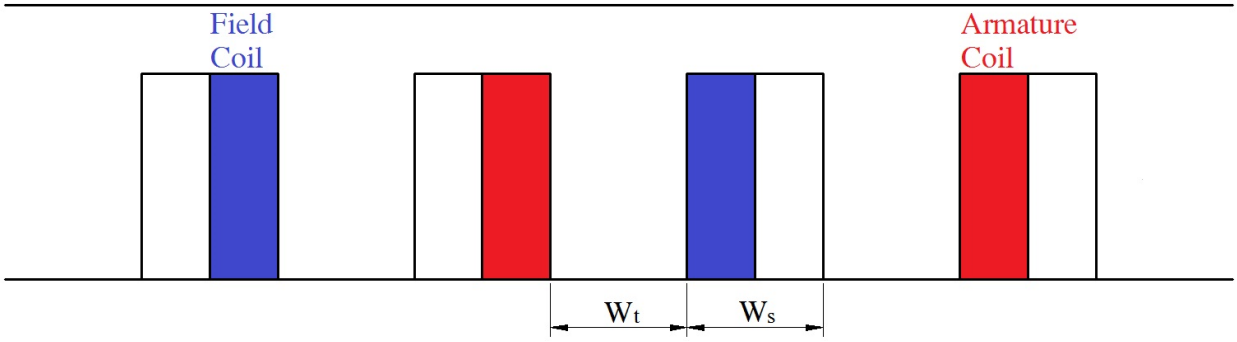

(b)

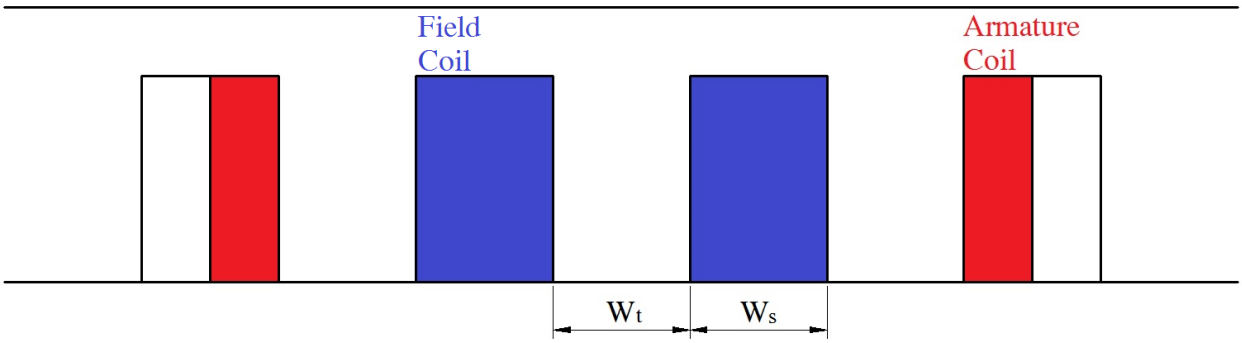

(c)

Fig. 3.7. Idealized coils dispositions. (a) 12-slot/8-pole. (b) 12-slot/5- and 7-pole. (c) 9-slot/5-pole.

Then, the total armature and field end-winding lengths, L_{end_a1} and L_{end_f1}, of a 12-slot/8-pole WFSF machine can be expressed as:

$$L_{end\_a1} = L_{end\_f1} = 6\pi(W_s/2 + W_t) \tag{3.7}$$

where W_s is the stator slot width, W_t is the stator tooth width.

The total armature and field end-winding lengths, L_{end_a2} and L_{end_f2}, of a 12-slot/5 or 7-pole WFSF machine can be expressed as:

$$L_{end\_a2} = L_{end\_f2} = 6\pi(3W_s/2 + 2W_t) \tag{3.8}$$

The total armature and field end-winding lengths, L_{end_a3} and L_{end_f3}, of a 9-slot/5-pole WFSF machine can be expressed as (3.9) and (3.10), respectively.

$$L_{end\_a3} = 3\pi(5\,W_s/2 + 3W_t) \tag{3.9}$$

$$L_{end\_f3} = 3\pi(W_s + W_t) \tag{3.10}$$

The optimized parameters of 12-slot/8-pole, 12-slot/5-pole, 12-slot/7-pole and 9-slot/5-pole WFSF machines are given in Table 3.3. It can be noticed that the stator parameters of 12-slot/5-pole and 12-slot/7-pole machines are nearly the same which means in actual fabrication, the common stator can be employed.

Table 3.3. Main parameters of machines

Items	12slot/8pole	12slot/5pole	12slot/7pole	9slot/5pole
Rated speed (r/min)	400	400	400	400
Stator outer radius (mm)	45	45	45	45
Axial length (mm)	25	25	25	25
Split ratio	0.54	0.55	0.55	0.54
Stator slot number	12	12	12	9
Rotor pole number	8	5	7	5
Air-gap length (mm)	0.5	0.5	0.5	0.5
Stator pole arc (degree)	25	16	15	18
Rotor pole/segment arc (degree)	39	19	19	28
Total armature slot area (mm^2)	1205	1016	1050	647
Total field slot area (mm^2)	1205	1016	1050	1294
Total number of turns of armature windings	72	72	72	72
Total number of turns of field windings	72	72	72	72
Packing factor (effective copper area/slot area)	0.4	0.4	0.4	0.4
Copper usages (g)	396	479	500	421

In order to share the same stator lamination between 12-slot/5-pole and 12-slot/7-pole for the prototypes and also for easy operation, the ratio of field and armature current can be adjusted by changing the field and armature currents directly rather than by changing the field and armature slot areas. The highest average torque of a 12-slot/8-pole machine is achieved when the armature slot current density is equal to the field slot current density, as shown in Table 3.2. Both 12-slot/5-pole and 9-slot/5-pole machines have the largest average torque when the field slot current density is 0.9 times as the armature slot current density. For the 12-slot/7-pole machine, this ratio is 1.05.

3.5.Stability of field currents

Fig. 3.8 shows the field currents of four optimized WFSF machines under various sinusoidal armature currents when the rotor speed is 400 r/min. It can be seen that the FEA predicted field current ripples of WFSF machines are no more than 3.1%. Overall, the field current in WFSF machine shows good stability under voltage source. Since the fluctuations in the field current are negligible, constant field currents are engaged in further analysis.

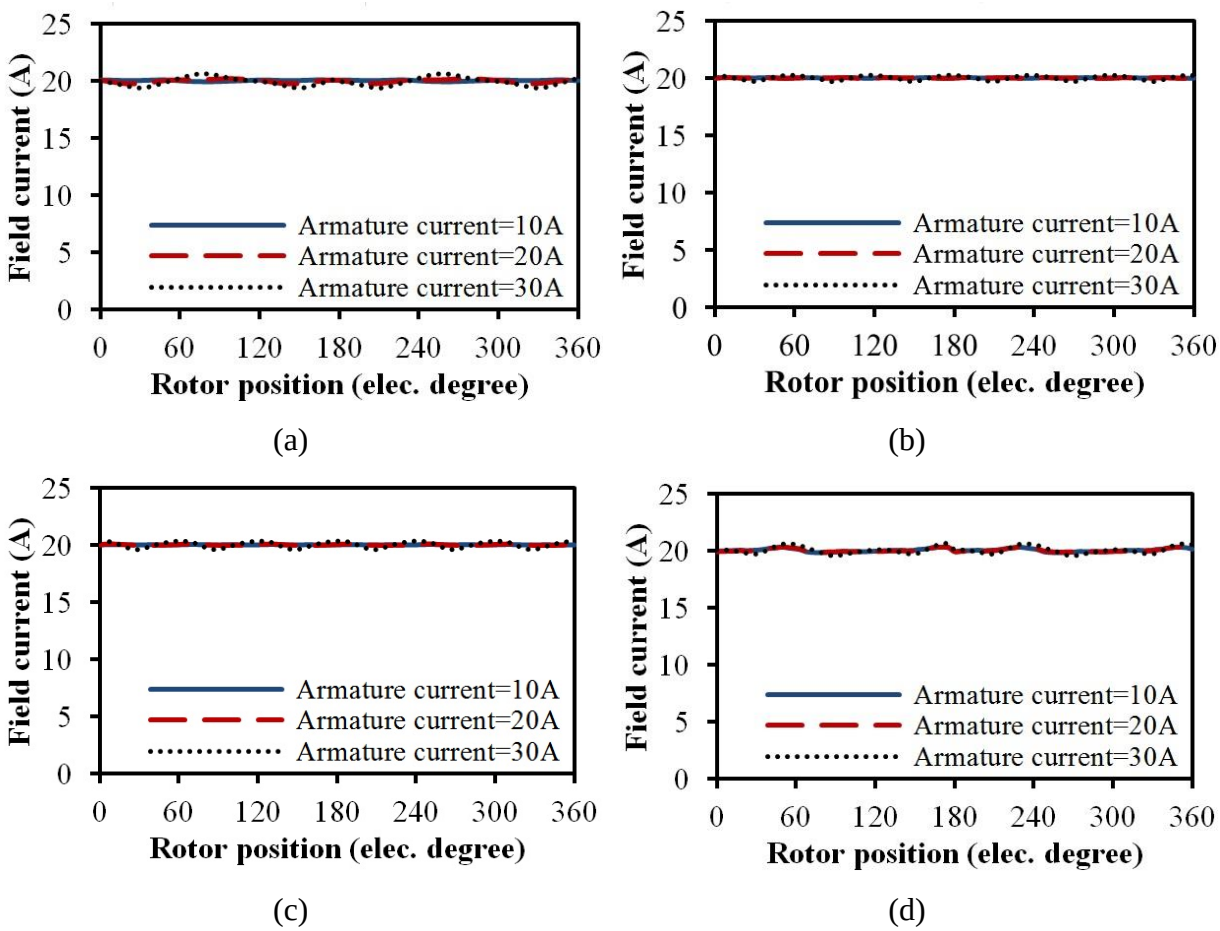

Fig. 3.8. Field current waveforms under 12 V terminal voltage and different armature current, 400 r/min. (a) 12-slot/8-pole. (b) 12-slot/5-pole. (c) 12-slot/7-pole. (d) 9-slot/5-pole.

When the rotor speed increases to 4000 r/min, the field currents of all WFSF machines show large current ripples, as shown in Fig. 3.9. In order to maintain the constant field current, current close-loop control has to be engaged. This means that operating the WFSF machines at high rotor speed may lead to a significantly increase in the cost since current sensors and more power devices are required.

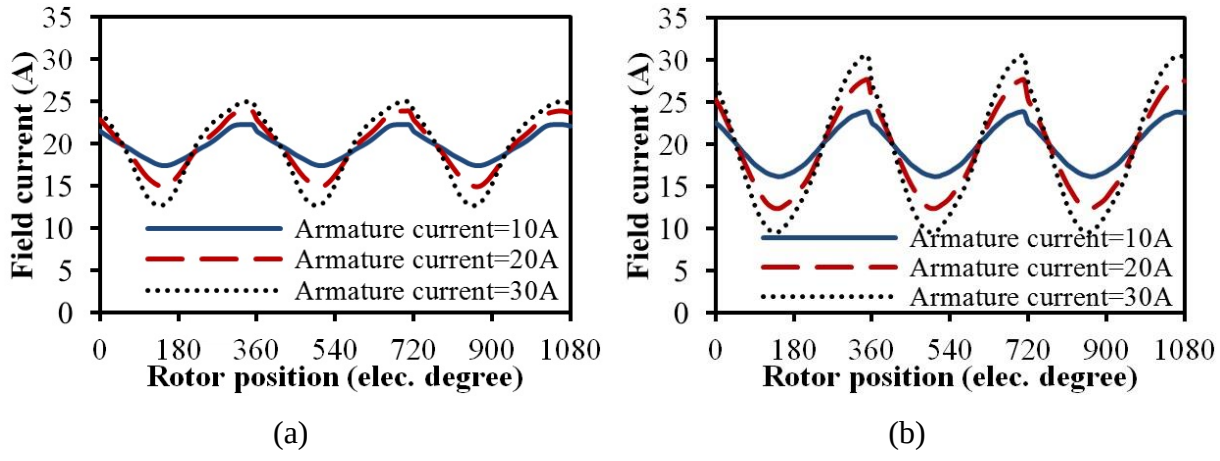

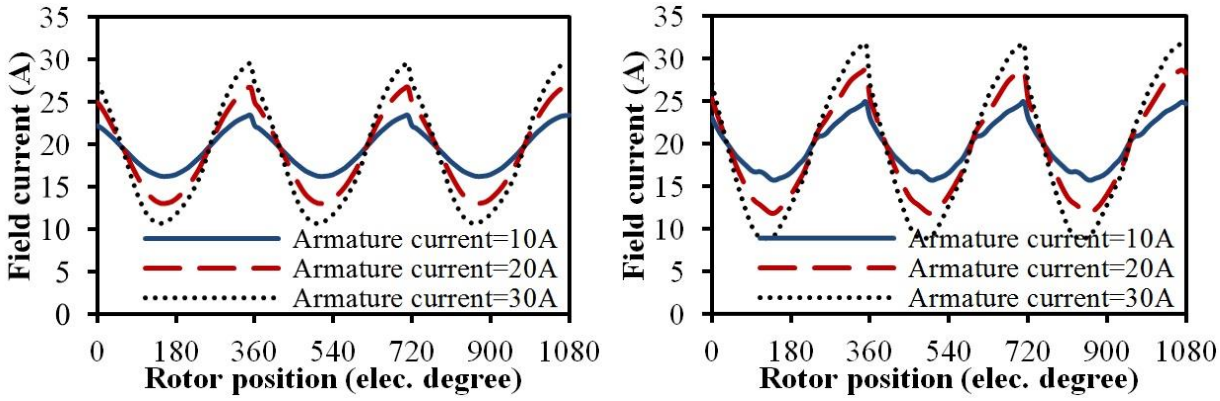

(c) (d)

Fig. 3.9. Field current waveforms under 12 V terminal voltage and different armature current, 4000 r/min. (a) 12-slot/8-pole. (b) 12-slot/5-pole. (c) 12-slot/7-pole. (d) 9-slot/5-pole.

3.6.Comparison of machines

The performance of above mentioned 12-slot/8-pole, 12-slot/5-pole, 12-slot/7-pole and 9-slot/5-pole machines are compared in this section.

3.6.1. Open-circuit field distribution

When the coil A1 has the maximum flux-linkage and DC field current is 30 A, the open-circuit field distributions of four WFSF machines are shown in Fig. 3.10. It can be seen from the figure that compared with 12-slot/5-pole or 12-slot/7-pole machine, the proposed 9-slot/5-pole machine shows smaller flux leakage. Consequently, its back-EMF has the potential to be high.

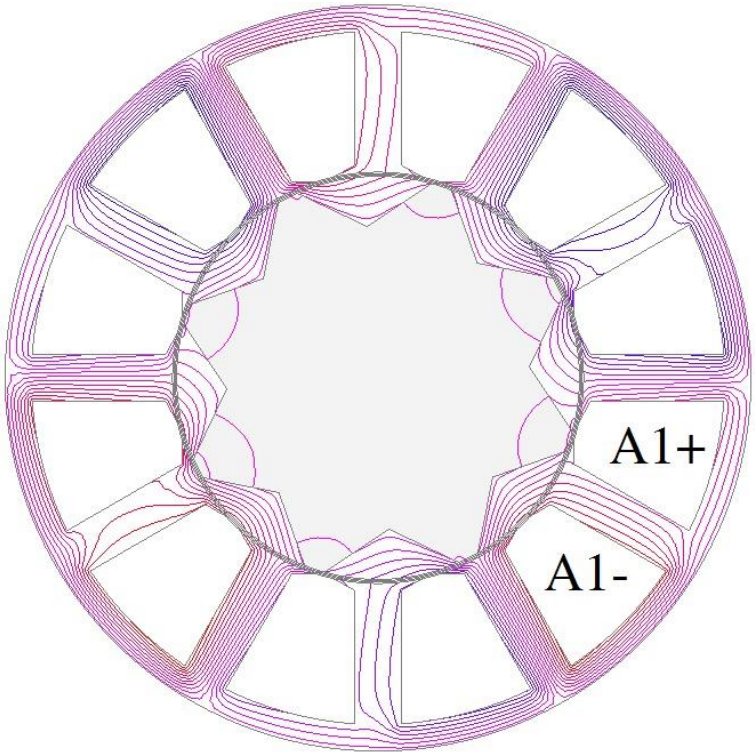

(a)

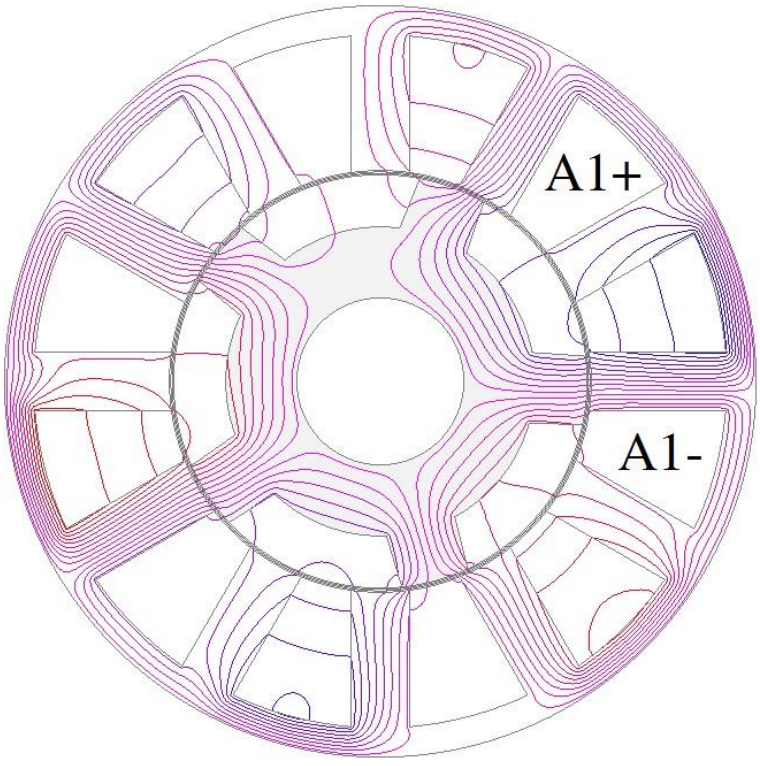

(b)

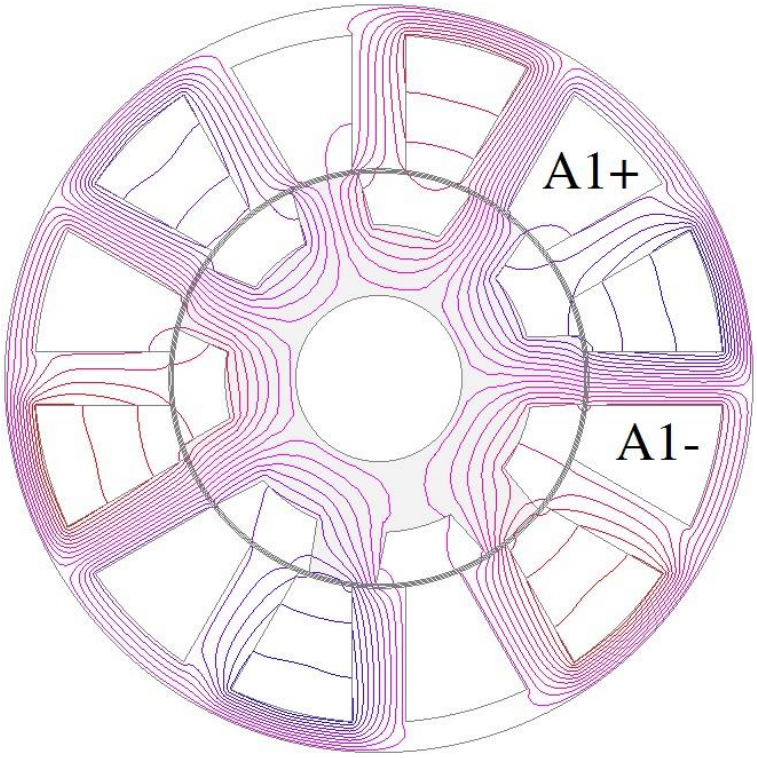

(c)

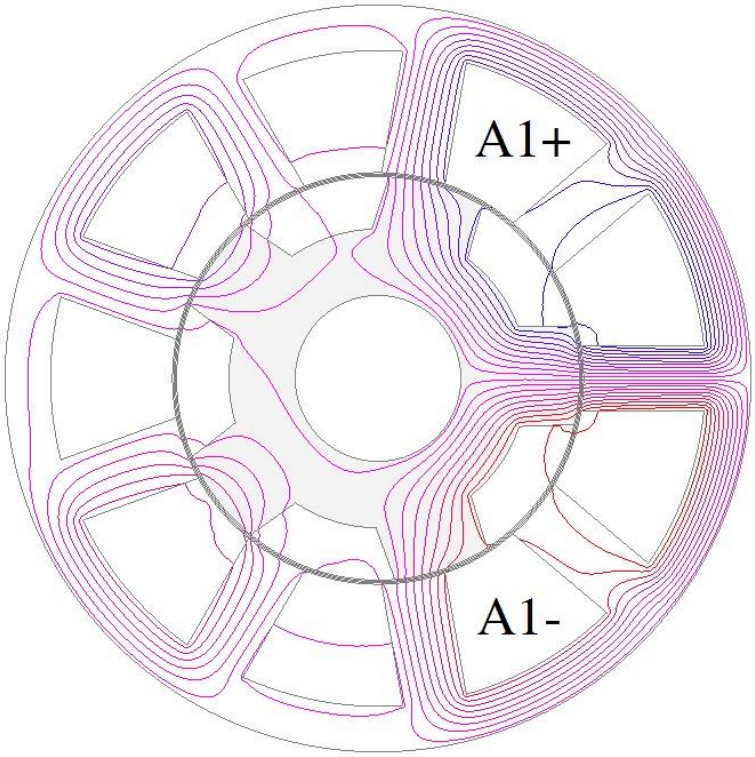

(d)

Fig. 3.10. Flux distributions with field excitation only, maximum flux-linkage with coil A1 (field current=30 A). (a) 12-slot/8-pole. (b) 12-slot/5-pole. (c) 12-slot/7-pole. (d) 9-slot/5-pole.

3.6.2. Back-EMF

Fig. 3.11 illustrates the 2-D FEA predicted back-EMF of four WFSF machines with various DC field currents and different rotor positions at a fixed rotor speed (400 r/min). As can be seen, all of those machines have nearly sinusoidal back-EMF waveforms, which make them suitable for Brushless AC (BLAC) operation. Fig. 3.12 compares the back-EMF waveform harmonics of four WFSF machines with 30 A field current at 400 r/min. As predicted before, the proposed 9-slot/5-pole shows higher fundamental harmonic than other machines. For this reason, the average torque of a 9-slot/5-pole machine is expected to be higher.

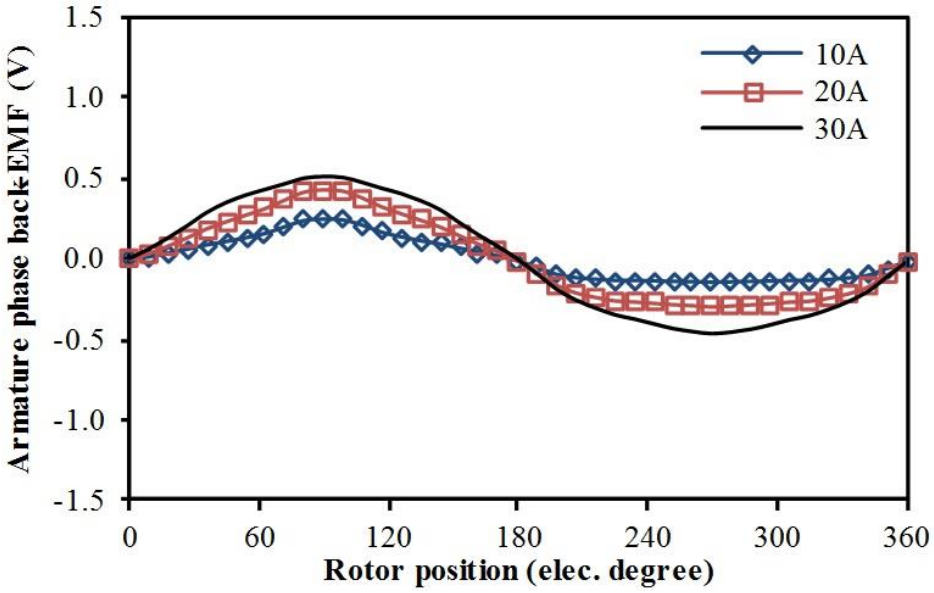

(a)

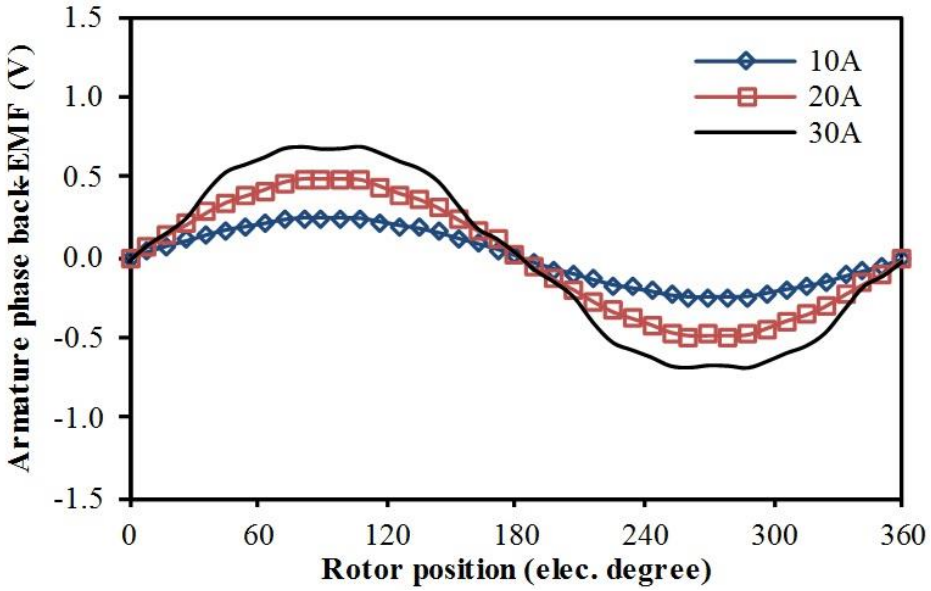

(b)

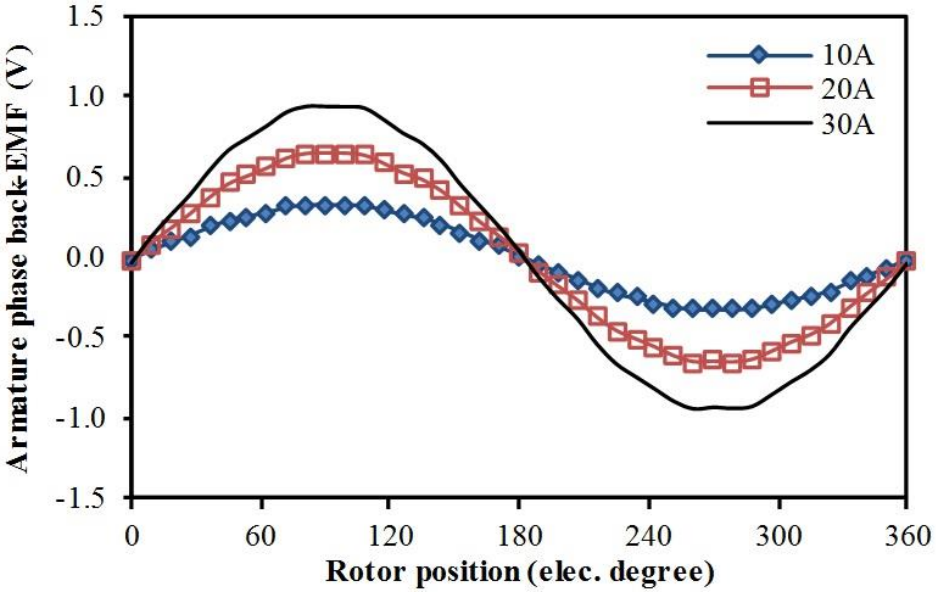

(c)

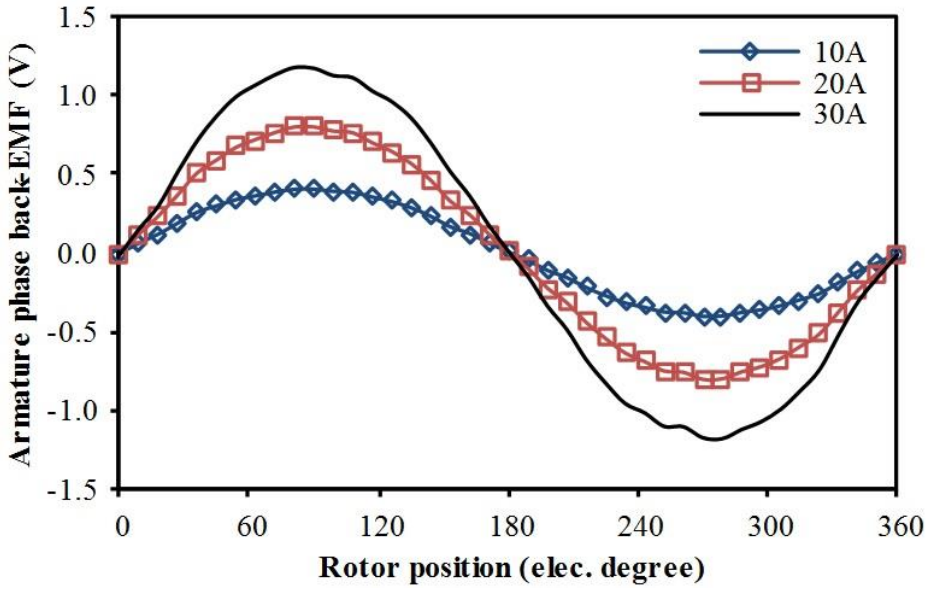

(d)

Fig. 3.11. Armature phase back-EMF waveforms at various field excitations, 400 r/min. (a) 12-slot/8-pole. (b) 12-slot/5-pole. (c) 12-slot/7-pole. (d) 9-slot/5-pole.

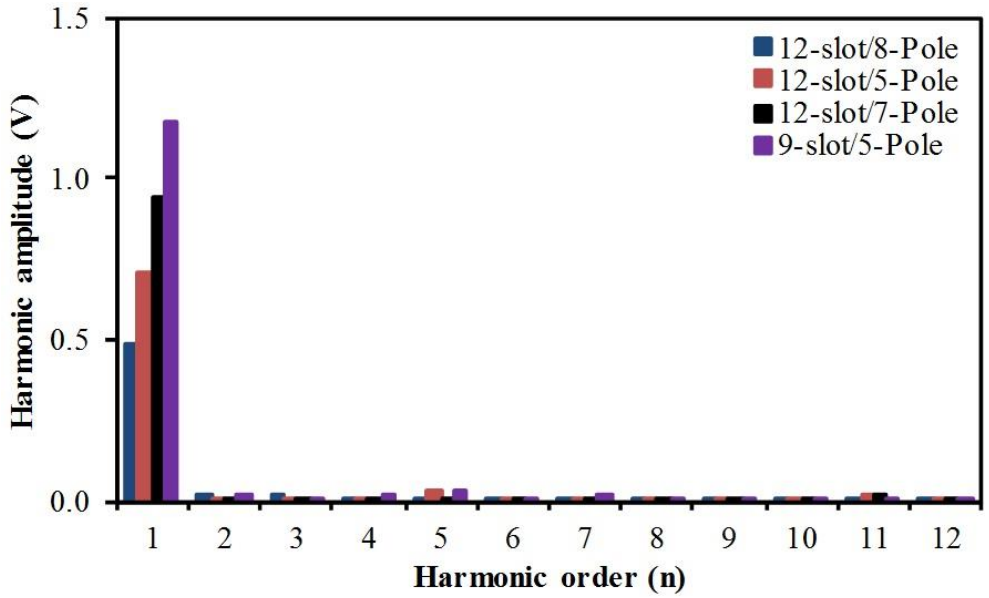

Fig. 3.12. Comparison of back-EMF harmonics, field current=30 A, 400 r/min.

3.6.3. Torque characteristics

In order to achieve the maximum average torque, it is necessary to determine the current angle of four WFSF machines before any further comparisons and investigations. As can be seen from Fig. 3.13, for three WFSF machines having normal salient-pole rotors, the maximum average torques are achieved when the current angles are about 10 electrical degrees due to the slight saliency effects caused by the differences between *d*- and *q*- axis magnetic paths. Meanwhile, for 12-slot/8-pole segmented rotor machine, the maximum average torque is achieved when the current angle is almost 0, since its saliency effect is negligible due to the special topology. It is worth noticing that this comparison is made under the same copper loss (30 W), and the ratio of field to armature slot current density of each machine follows the previous investigation shown in Table 3.3. In further comparison, current angle will be taken into consideration to achieve the maximum average torque.

The average torques of four WFSF machines at various field excitations and armature currents are shown in Fig. 3.14. The 12-slot/8-pole segmented rotor machine shows the lowest average torque due to its lowest fundamental back-EMF component. Meanwhile, the proposed 9-slot/5-pole machine shows much higher average torque than the 12-slot/5-pole machine under the same field and armature current as expected before, but lower average torque than the 12-slot/7-pole machine in the high field and armature current region since its stator is easily saturated. It is worth mentioning that the 9-slot/5-pole machine has the highest average torque when the electrical loading is low.

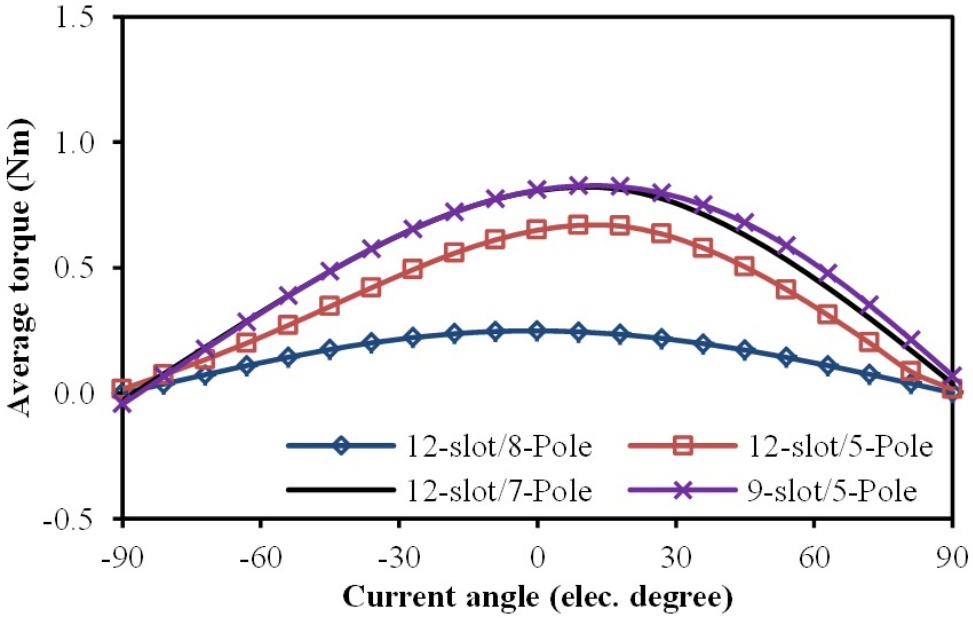

Fig. 3.13. Comparison of torque-current angle curves, copper loss=30 W, BLAC operation.

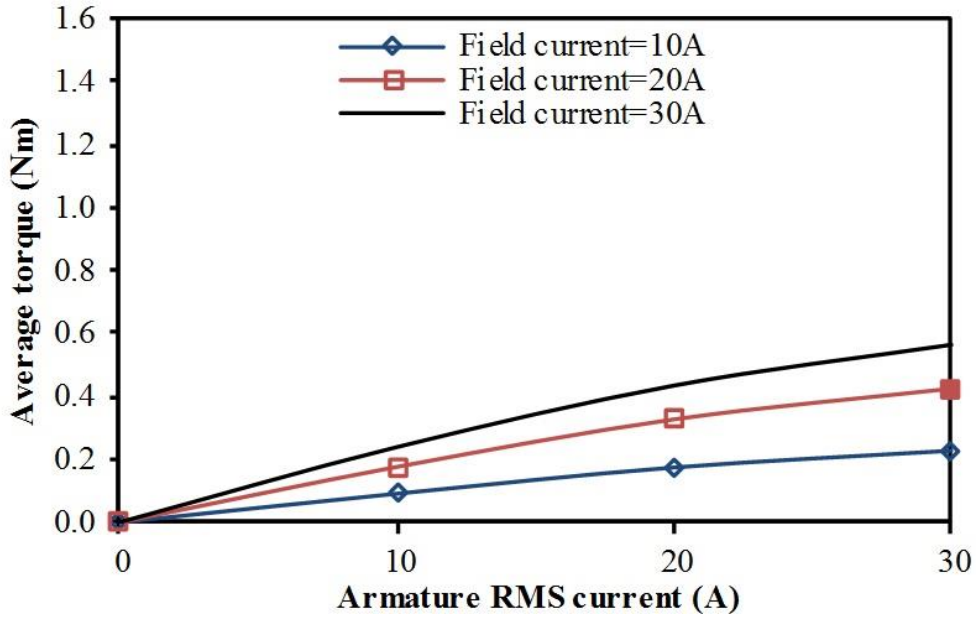

(a)

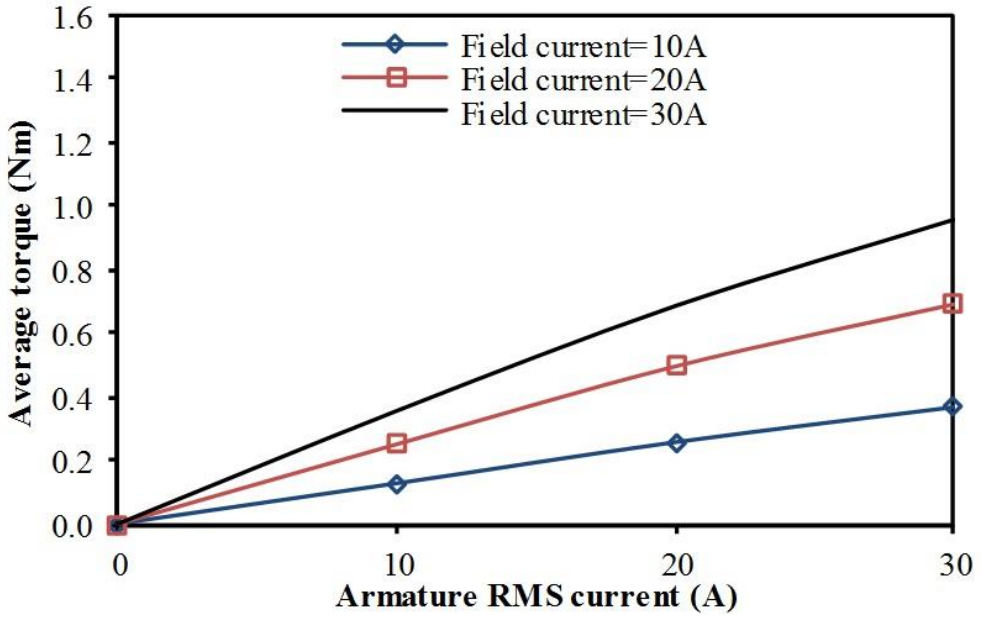
Field current=10A
Field current=20A
Field current=30A
Average torque (Nm)
1.6
1.4
1.2
1.0
0.8
0.6
0.4
0.2
0.0
0
10
20
30
Armature RMS current (A)

(b)

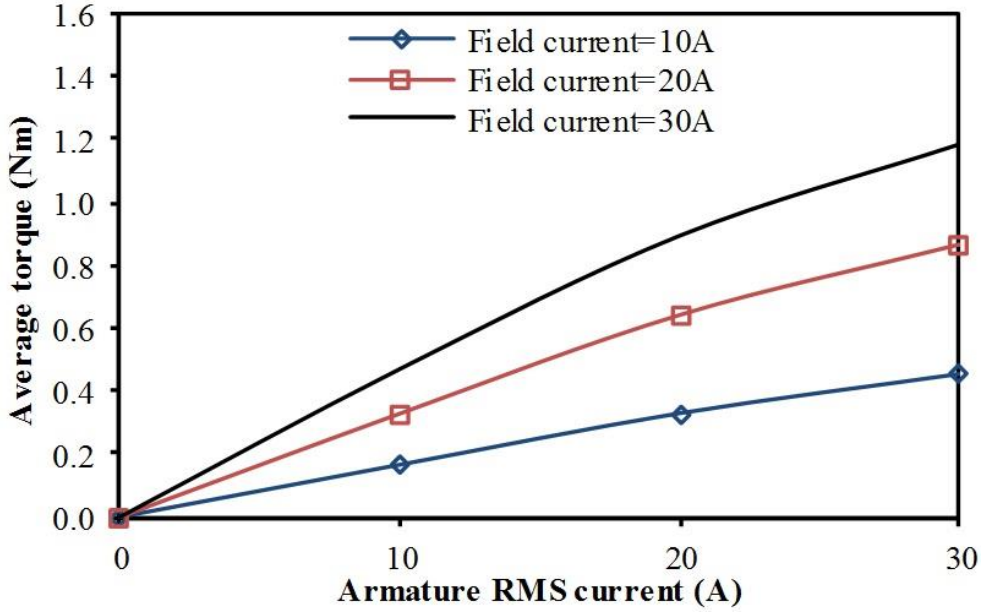
Field current=10A
Field current=20A
Field current=30A
Average torque (Nm)
1.6
1.4
1.2
1.0
0.8
0.6
0.4
0.2
0.0
0
10
20
30
Armature RMS current (A)

(c)

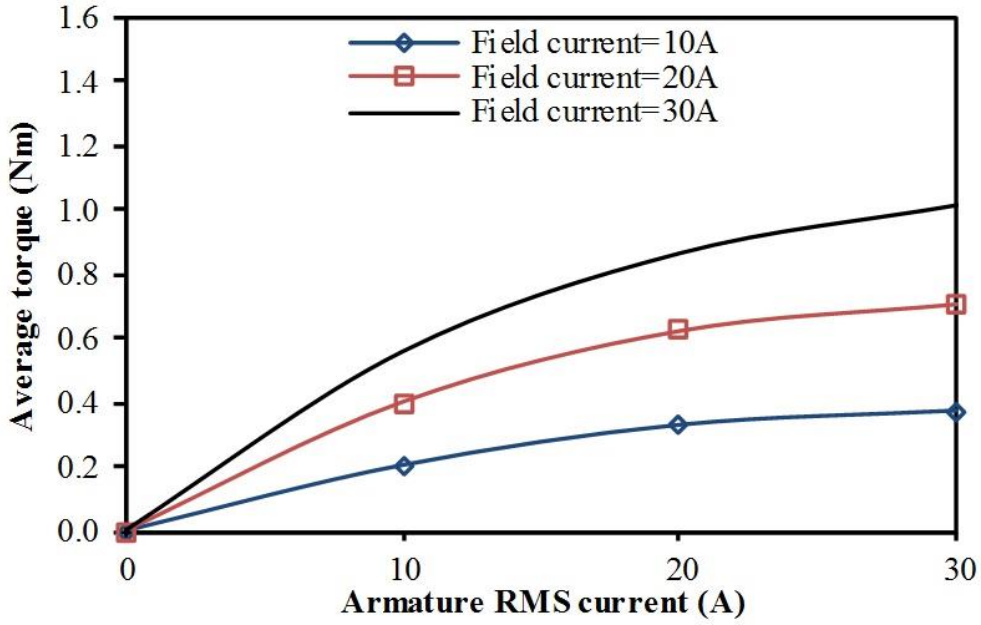

(d)

Fig. 3.14. Torque-current curves for different armature currents with different field current, BLAC operation. (a) 12-slot/8-pole. (b) 12-slot/5-pole. (c) 12-slot/7-pole. (d) 9-slot/5-pole.

Fig. 3.15 shows the torque waveforms of four WFSF machines when the armature currents are 0 A and the field currents are 30 A. Obviously, those curves represent the cogging torques in those machines. The least common multiple between stator and rotor pole number of the 12-slot/8-pole or 9-slot/5-pole machine is much smaller than that of 12-slot/5- or 7-pole machine. Therefore, as can be seen from the figure, the peak to peak cogging torques of the 12-slot/8-pole and 9-slot/5-pole machines are higher than that of the 12-slot/5-pole and 12-slot/7-pole machines, and their cogging torque frequencies are smaller [ZHU07]. Although none of four WFSF machines has very high harmonic components, the torque ripples in 12-slot/8-pole and 9-slot/5-pole machines are likely to be high due to their high peak to peak cogging torques.

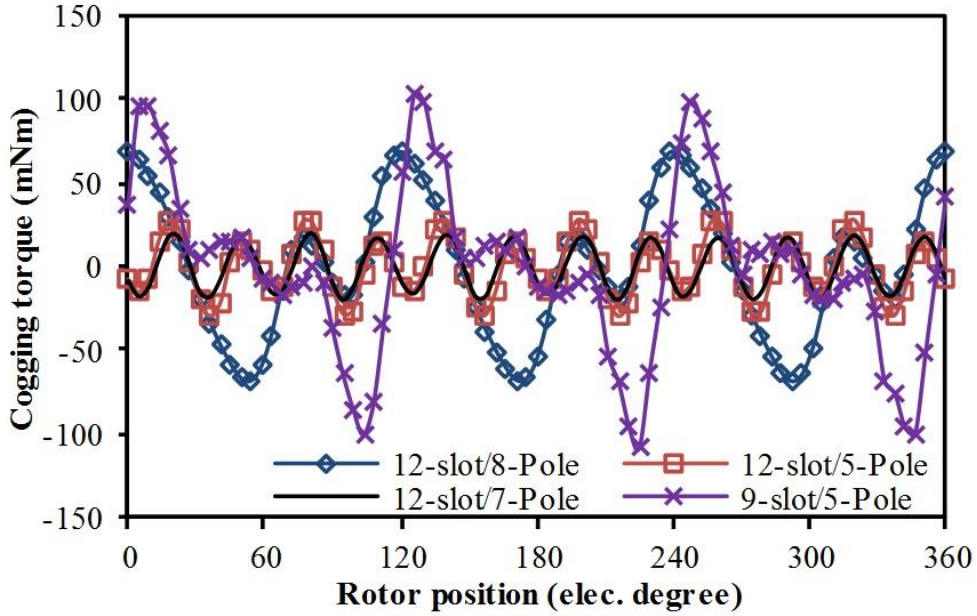

Fig. 3.15. Comparison of cogging torques, field current=30 A.

Fig. 3.16 shows the torque waveforms of four WFSF machines when their copper losses are fixed to 30 W. The ratio of field to armature slot density of each machine follows the previous optimization for maximum average torque shown in Table 3.2. The average torque of 12-slot/8-pole machine, 12-slot/5-pole machine, 12-slot/7-pole machine and 9-slot/5-pole machine are 0.25 Nm, 0.68 Nm, 0.84 Nm and 0.84 Nm, respectively. As predicted before, 12-slot/8-pole and 9-slot/5-pole machines show high torque ripples which are 33% and 20%. Meanwhile, the torque ripples in 12-slot/5-pole and 12-slot/7-pole machines are only 11% and 6%. The comparison of torque-copper loss curves of four WFSF machines is shown in Fig. 3.17. When the machines are optimized under the copper loss constraint of 30 W, the 9-slot/5-pole machine shows similar average torque compared with the 12-slot/7-pole machine, but larger average torque compared with the 12-slot/5-pole machine, as shown in Fig. 3.17 (a). In order to compare the WFSF machines under higher average torque, the machines have been re-optimized under the copper loss constraint of 120 W, as can be seen from Fig. 3.17 (b), the 9-slot/5-pole and 12-slot/7-pole machines still show higher average torques than that of the 12-slot/5-pole machine. However, the 9-slot/5-pole machine shows lower average torque compared with the 12-slot/7-pole machine under higher electric loading, since the stator poles with field coils in the 9-slot/5-pole machine can be more saturated when the flux goes from the stator side to the rotor side.

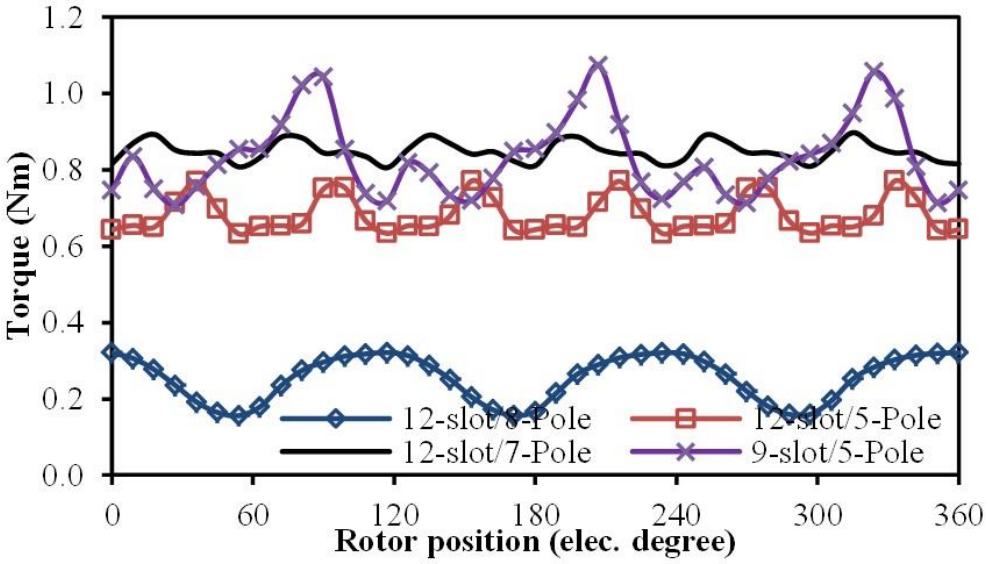

Fig. 3.16. Torque waveforms, copper loss=30W, BLAC operation.

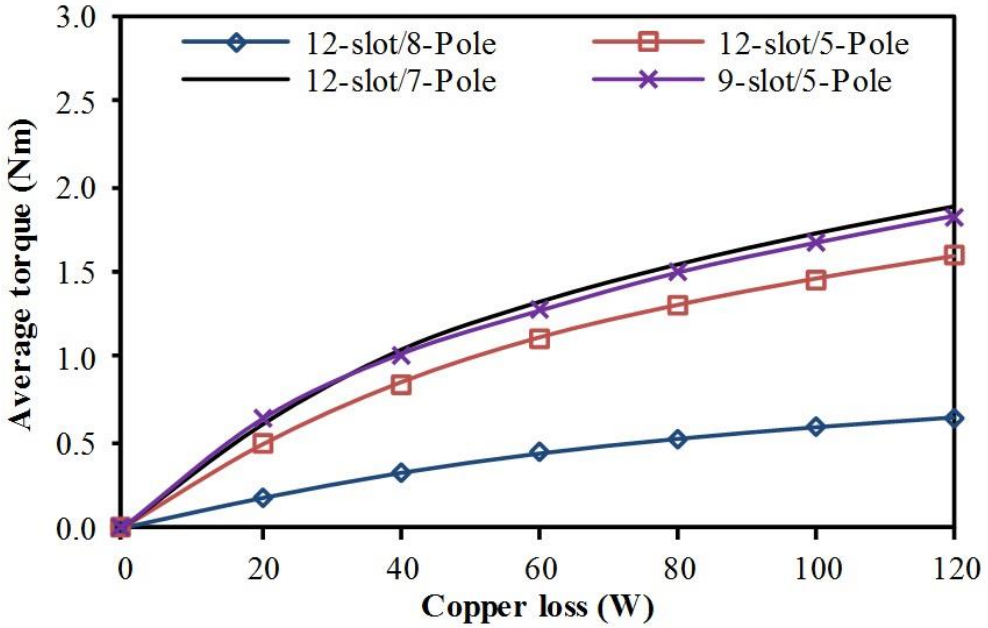

(a)

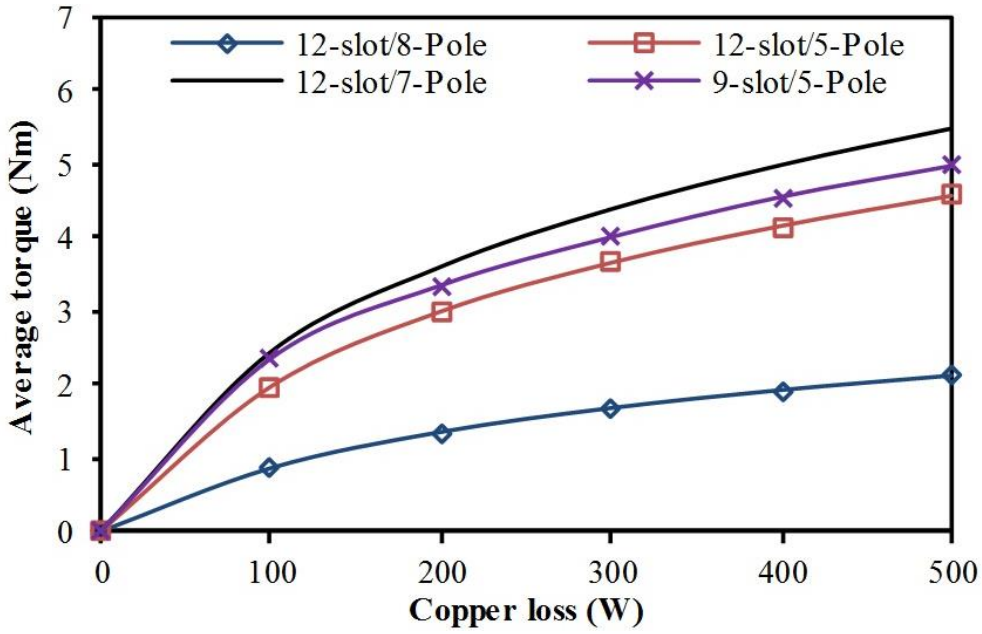

(b)

Fig. 3.17. Comparison of torque-copper loss curves, BLAC operation. (a) Machines are optimized when the copper loss=30 W. (b) Machines are optimized when the copper loss=120 W.

3.6.4. Copper Usage

In WFSF machines, the copper is much more expensive than other materials. Therefore, the copper usage is an important factor affecting the total cost. As can be seen from Table 3.3, the 12-slot/8-pole machine shows the smallest copper usage due to its short-pitched coils. Unlike the 12-slot/5- or 7-pole machine, whose coils are all fully-pitched, 2/3 of stator slots in the 9-slot/5-pole machine contain short-pitched coils. Therefore, the copper usage of the 9-slot/5-pole machine is much less than that of the 12-slot/5- or 7-pole machine.

The copper usage efficiencies (ratio of average torque to copper usage) of four WFSF machines are compared in Fig. 3.18. As can be seen, the 9-slot/5-pole machine shows much larger copper usage efficiency than other WFSF machines.

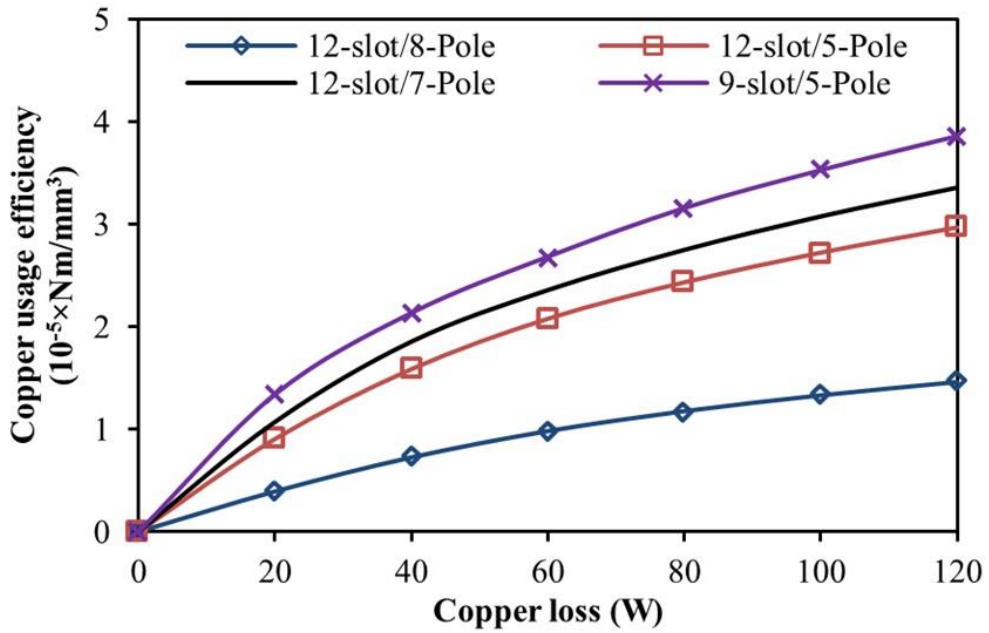

Fig. 3.18. Comparison of copper usage efficiencies with different copper loss, BLAC operation.

3.6.5. Unbalanced magnetic force

Unbalanced magnetic force (UMF) results from the odd pole number rotor, odd slot number stator, or even odd number field/armature coils. UMF may compromise the bearing life and result in excessive acoustic noise and vibration due to the rippled force imposed on the rotor and bearing [ZHU07b]. Fig. 3.19 shows the UMFs of the WFSF machines. No UMF is detected in the 12-slot/8-pole machine due to its symmetric topology. During an electric cycle, 6 UMF ripples exist in two 12-slot machines having 6 field/armature coils. In terms of the 9-slot machine having 3 field/armature coils, 3 UMF ripples are existed in one electric cycle. For the 9-slot machine, the UMF is larger and changes more rapidly than the other machines, which may lead to increased vibration.

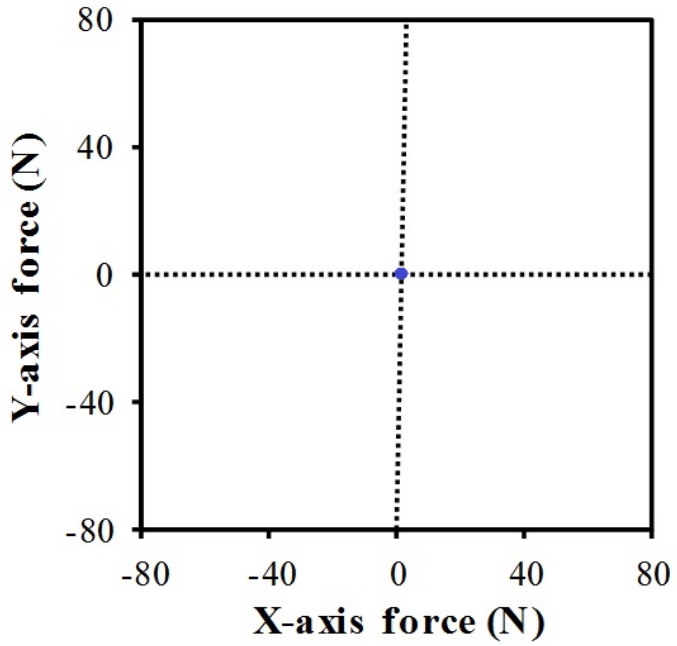
80
40
0
-40
-80
Y-axis force (N)
-80
-40
0
40
80
X-axis force (N)

(a)

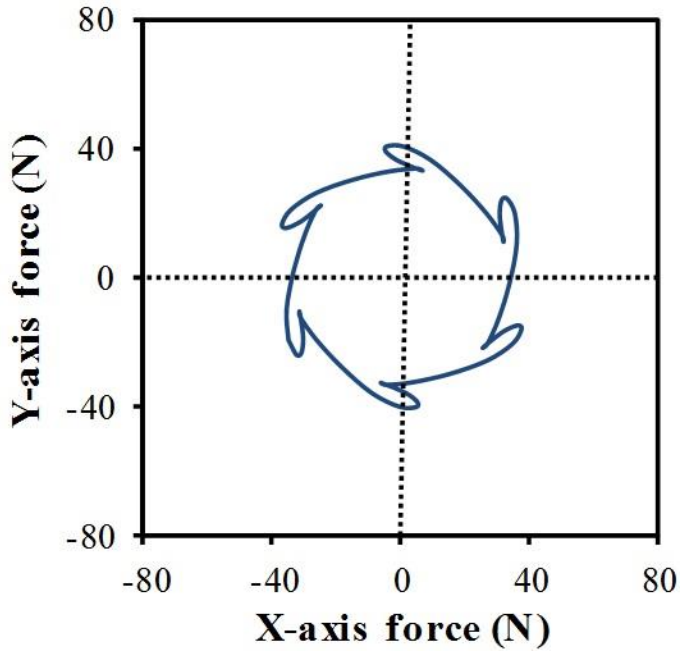
80
40
0
-40
-80
Y-axis force (N)
-80
-40
0
40
80
X-axis force (N)

(b)

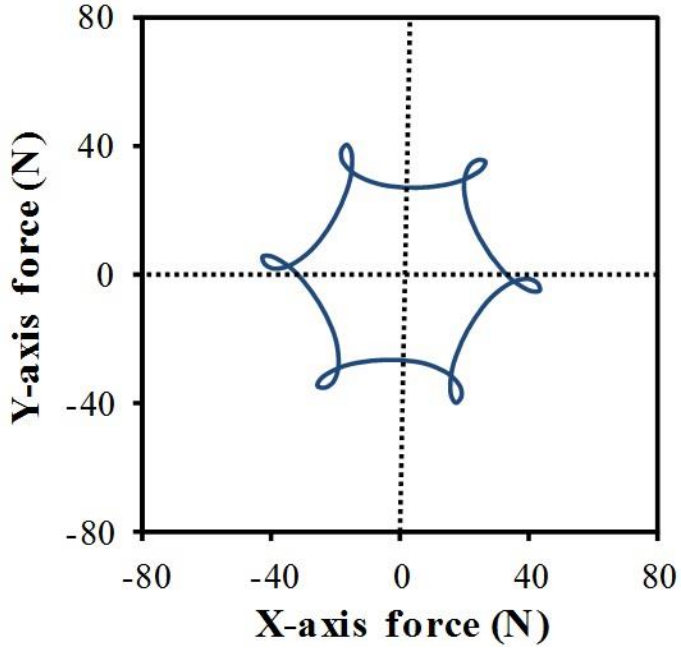

(c)

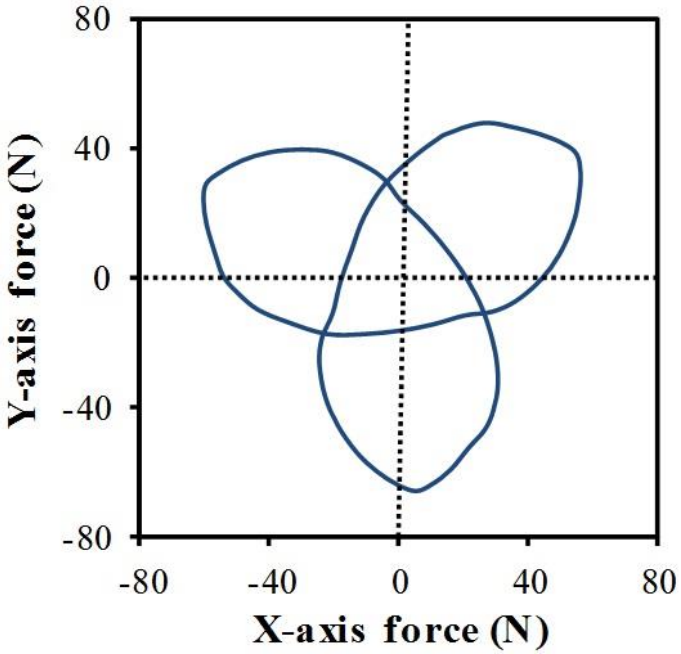

(d)

Fig. 3.19. Comparison of UMFs, copper loss=30 W, BLAC operation. (a) 12-slot/8-pole. (b) 12-slot/5-pole. (c) 12-slot/7-pole. (d) 9-slot/5-pole.

3.6.6. Summary and Prospect

The 12-slot/7-pole WFSF machine shows the highest average torque among aforementioned four WFSF machines. However, as mentioned before, the 9-slot/5-pole

machine has the best copper usage efficiency among four WFSF machines. Furthermore, the difference of the average torques between 9-slot/5-pole and 12-slot/7-pole machines is not large, and the average torque of the 9-slot/5-pole machine is slightly higher than that of the 12-slot/7-pole machine under low copper loss.

Ferrite magnets can be used in the SFPM machine to reduce the material cost. This machine also has a simple and robust rotor structure and shows low material cost like WFSF machines. However, the stator of the SFPM machine is segmented, which has to be assembled carefully, and this may lead to an increase in manufacturing costs. The switched reluctance machine (SRM) can be a superior option in low-cost applications due to its low material cost and robust structure. Nevertheless, it suffers from some defects, such as high torque ripple, vibration and acoustic noise. The induction motor (IM), which has mature manufacturing techniques and is relatively low-cost, has the largest share in most motor applications. However, for a typical IM, all coils are overlapping and long pitched and its rotor copper loss is relatively large. Hence, compared with other machines having relatively short axial length, the average torque of an IM is likely to be lower under the same copper loss.

When the machines are operating at high rotor speed, the iron losses are no longer negligible. Besides, as mentioned before, for the WFSF machines, if low-cost voltage sources are equipped in the field winding circuits, very high field current ripples are detected at high rotor speed. Therefore, the foregoing comparison and analysis based on relatively low rotor speed may not be valid any more. In order to operate the WFSF machine at high rotor speed, the field current is needed to be regulated by means of converter.

3.7.Experimental validation

In order to validate the FEA predictions, the aforementioned 12-slot/5-pole, 12-slot/7-pole and 9-slot/5-pole machines have been prototyped, as shown in Fig. 3.20. It can be noticed that the 12-slot/5-pole and 12-slot/7-pole machines share the same stator. The experimental validation of the WFSF machines is restricted to static performance and the dynamic performance needs to be done in the future. The back-EMFs, cogging torques, and static torques of those machines have been measured in this section. Since the FEA has shown that the field current in the WFSF machine has a good stability with sinusoidal armature current at low rotor speed. The field currents were excited from a DC power supply in the experiment.

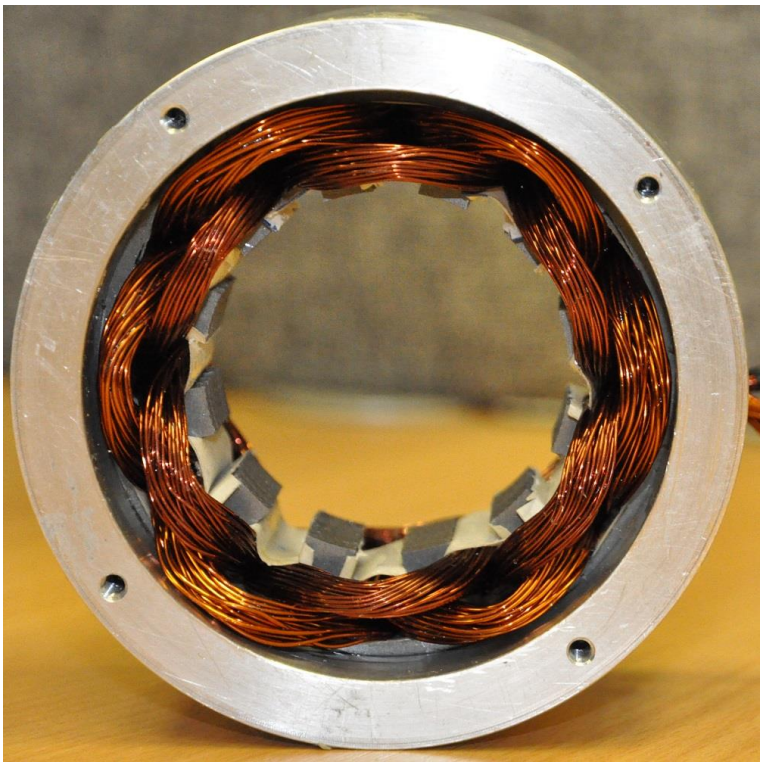

(a)

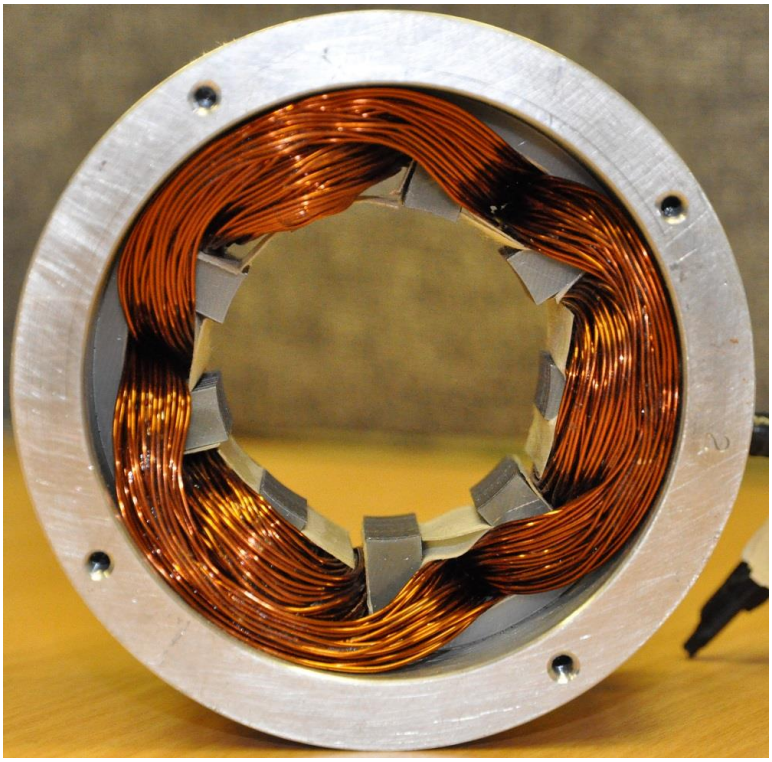

(b)

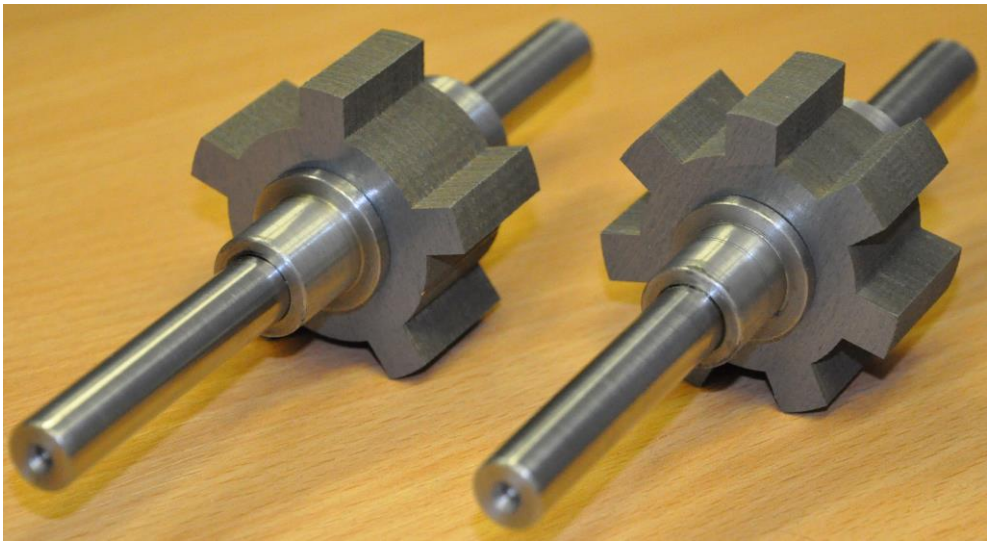

(c)

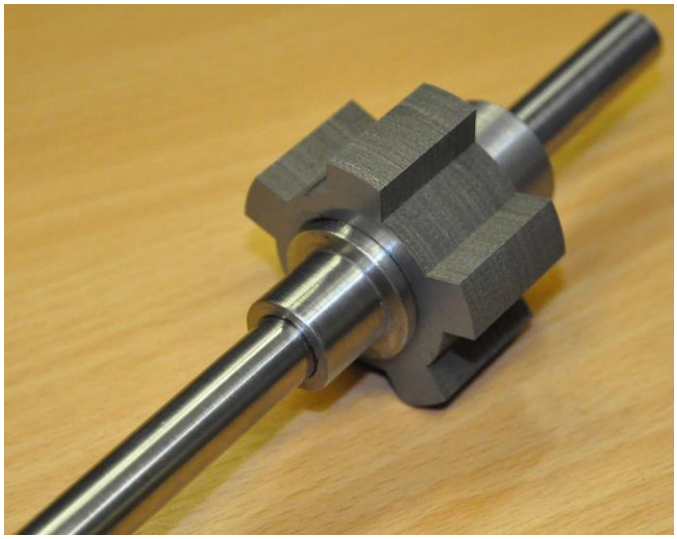

(d)

Fig. 3.20. Prototypes of WFSF machines. (a) Common stator of 12-slot/5- and 7-pole machines. (b) Stator of 9-slot/5-pole machine. (c) Rotors of 12-slot/5-pole and 7-pole machines. (d) Rotor of 9-slot/5-pole machine.

Under two different DC field excitations (10 A and 20 A), the predicted and measured armature back-EMF waveforms of three WFSF machines are shown in Fig. 3.21. Overall, there is good agreement between predicted and measured results except that the measured back-EMF peak value is slightly smaller than the predicted value. Such differences can be observed at different field excitations and ignoring the end-effects is mainly responsible for this [ZHU07].

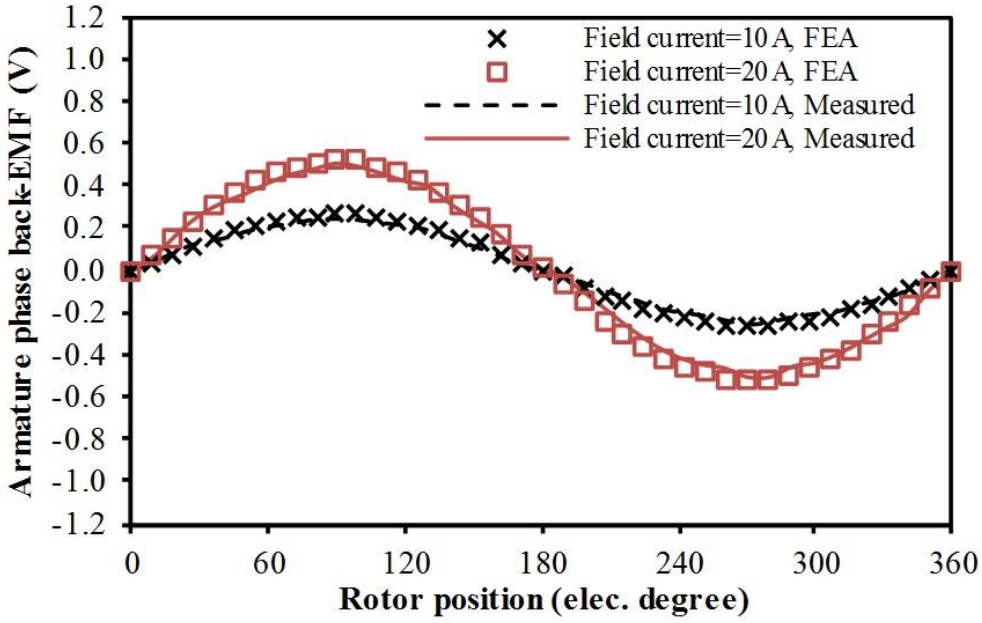
Armature phase back-EMF (V)
1.2
1.0
0.8
0.6
0.4
0.2
0.0
-0.2
-0.4
-0.6
-0.8
-1.0
-1.2
0
60
120
180
240
300
360
Rotor position (elec. degree)
Field current=10 A, FEA
Field current=20 A, FEA
Field current=10 A, Measured
Field current=20 A, Measured

(a)

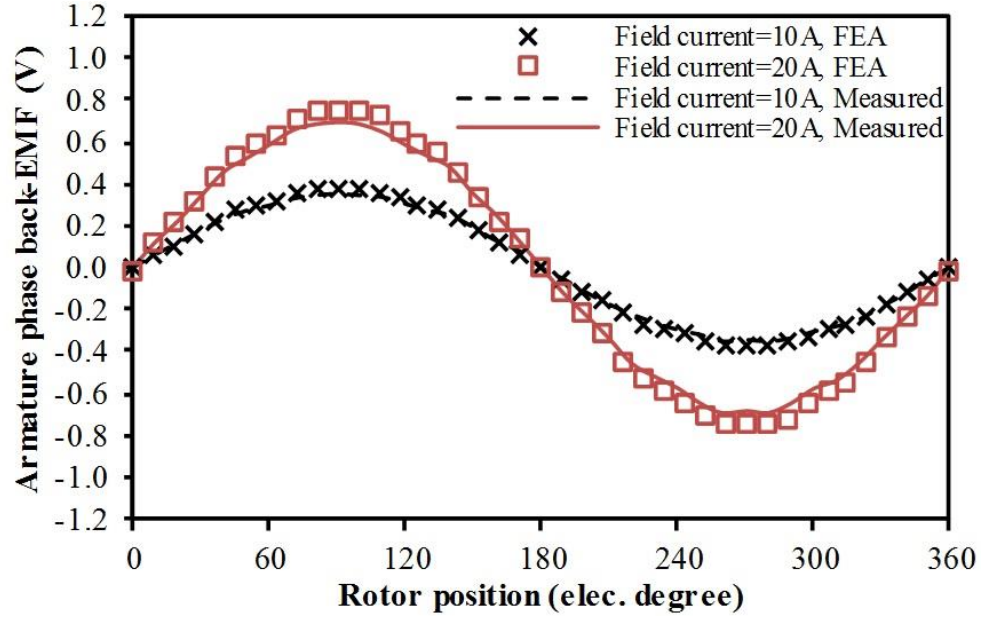
Armature phase back-EMF (V)
1.2
1.0
0.8
0.6
0.4
0.2
0.0
-0.2
-0.4
-0.6
-0.8
-1.0
-1.2
0
60
120
180
240
300
360
Rotor position (elec. degree)
Field current=10 A, FEA
Field current=20 A, FEA
Field current=10 A, Measured
Field current=20 A, Measured

(b)

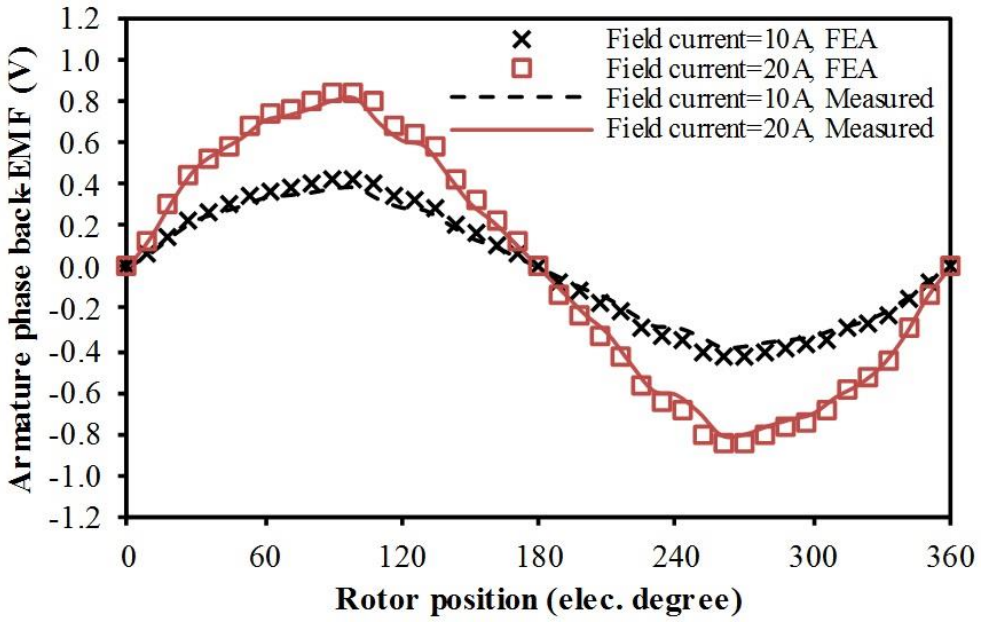

(c)

Fig. 3.21. Back-EMF waveforms, 400 r/min. (a) 12-slot/5-pole. (b) 12-slot/7-pole. (c) 9-slot/5-pole.

When the armature current is 0 A, the cogging torque waveforms under different field currents are measured and have been compared with the FEA predictions. As can be seen in Fig. 3.22, when the field current is 20 A, the predicted cogging torques of 12-slot/5-pole and 12-slot/7-pole machines are negligible. However, the measured peak-to-peak cogging torques are higher than those of FEA predictions in these machines due to assembly and mechanical tolerances. For the 9-slot/5-pole machine, a good agreement between measured and predicted cogging torque waveforms has been achieved.

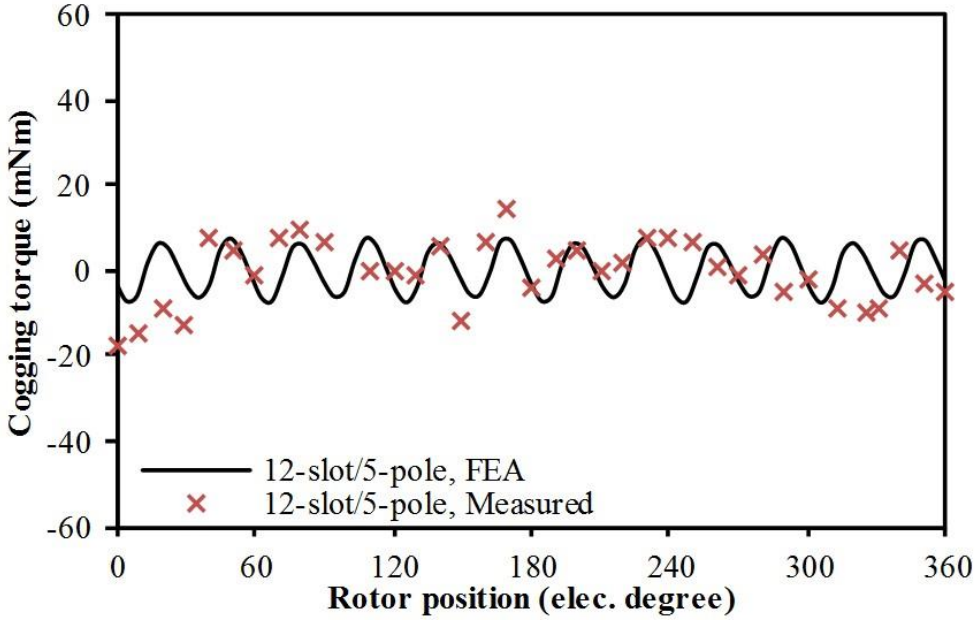
Cogging torque (mNm)
60
40
20
0
-20
-40
-60
0
60
120
180
240
300
360
Rotor position (elec. degree)
12-slot/5-pole, FEA
12-slot/5-pole, Measured

(a)

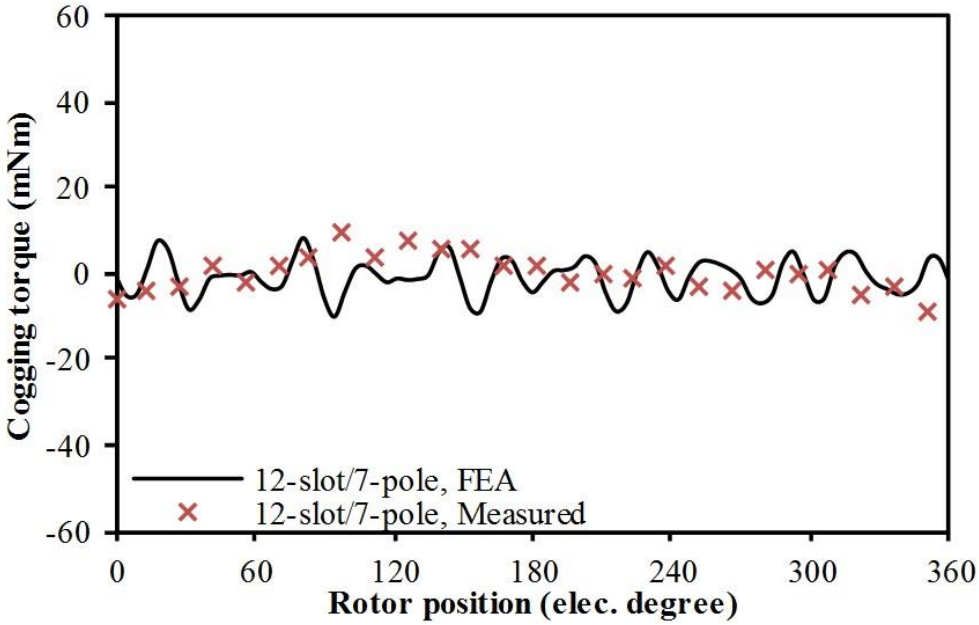
Cogging torque (mNm)
60
40
20
0
-20
-40
-60
0
60
120
180
240
300
360
Rotor position (elec. degree)
12-slot/7-pole, FEA
12-slot/7-pole, Measured

(b)

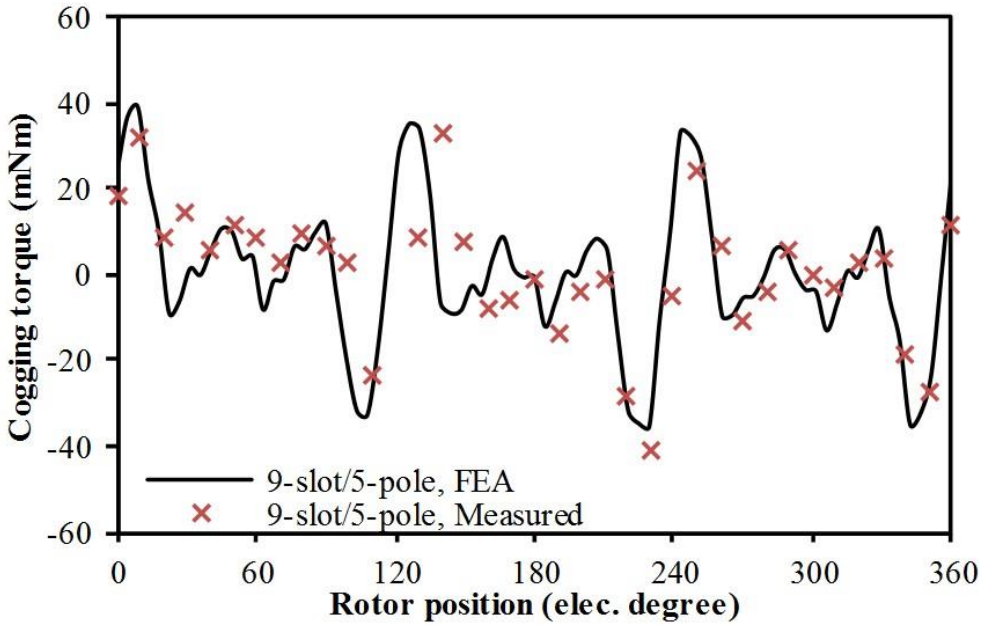

(c)

Fig. 3.22. Cogging torque, field current=20 A. (a) 12-slot/5-pole. (b) 12-slot/7-pole. (c) 9-slot/5-pole.

The static torque waveforms with various field current and armature current of one phase (other two phases are open-circuit) are shown in Fig. 3.23. It can be seen that, under the same field and armature currents, the 9-slot/5-pole machine shows the highest peak-to-peak torque. The measured results show generally good agreement with the predicted results.

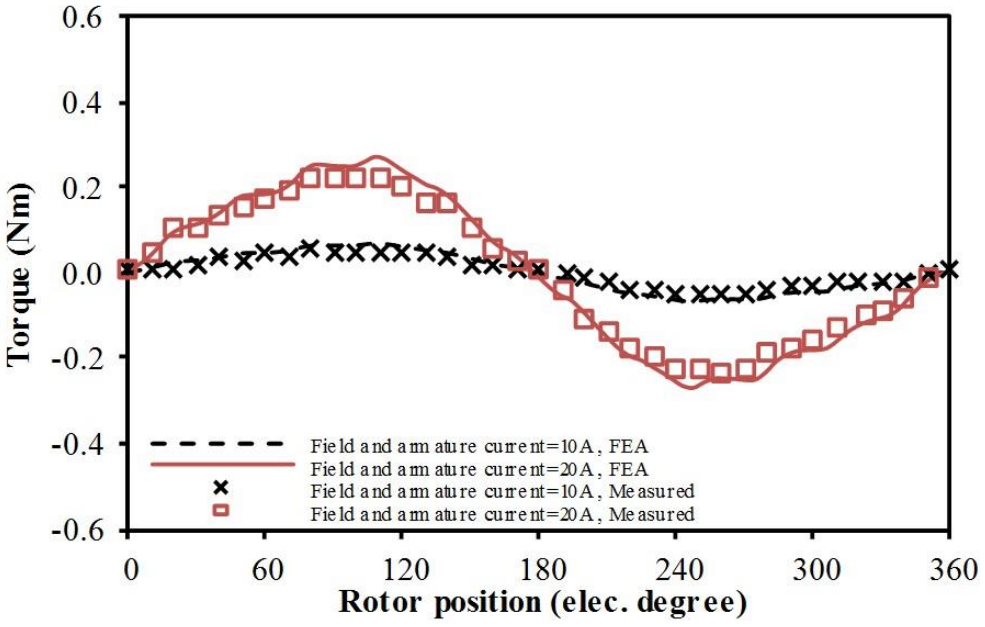

(a)

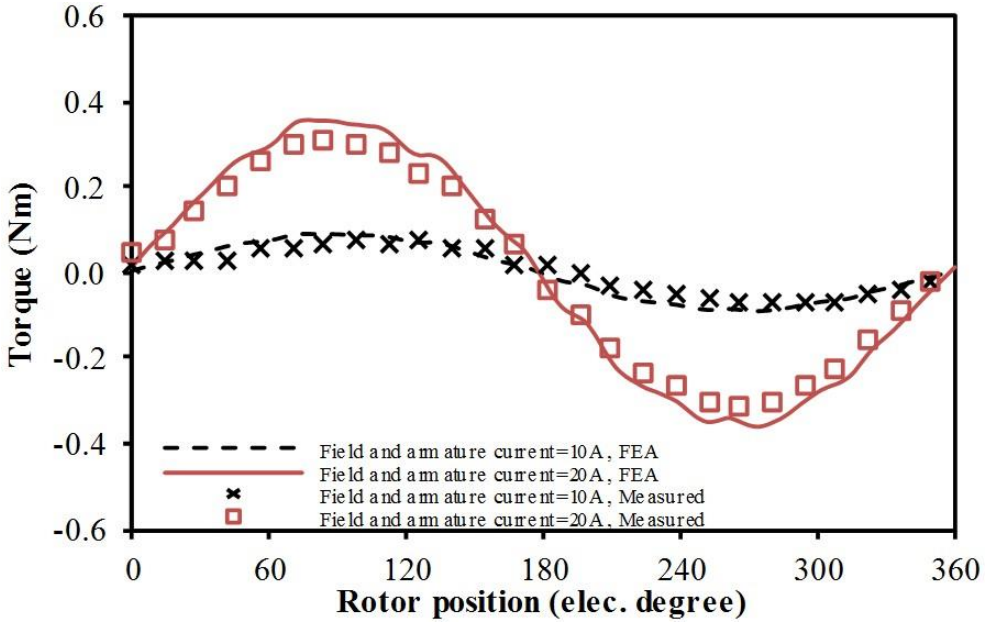

(b)

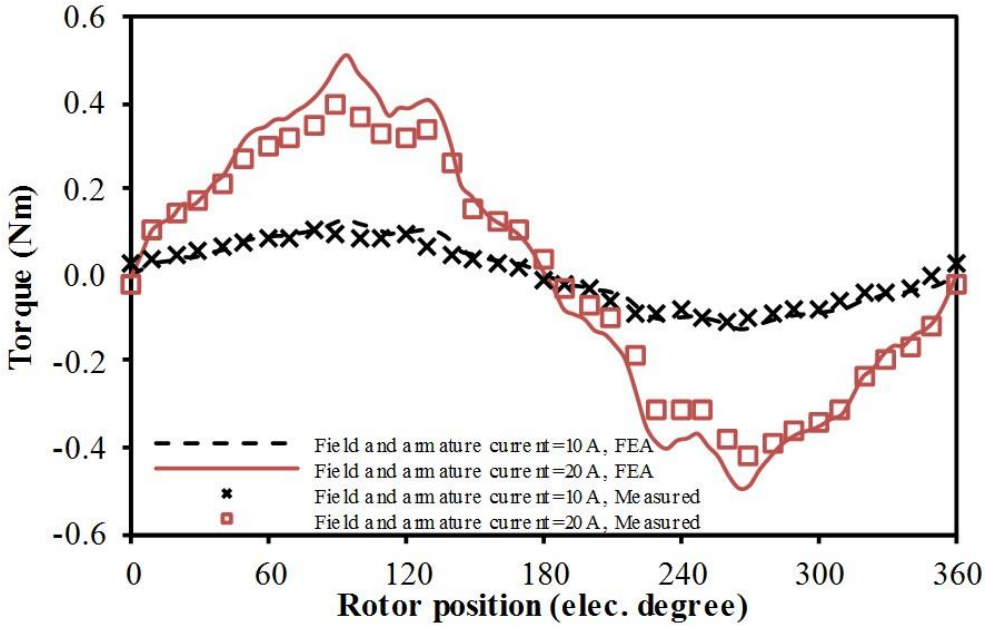

(c)

Fig. 3.23. Static torque waveforms with various field current and armature current. (a) 12-slot/5-pole. (b) 12-slot/7-pole. (c) 9-slot/5-pole.

3.8.Summary

Three types of low-cost wound field switched flux machines with DC field and AC armature windings having the same coil-pitch of 1 slot (12-slot/8-pole machine), 2 slots (12-

slot/5-pole machine and 12-slot/7-pole machine) and having different coil-pitches of 1 and 3 slots (9-slot/5-pole machine), respectively, are compared in this chapter.

It is found that halving the number of stator slots and rotor poles can be an effective method to increase the torque density for the WFSF machines having the same coil-pitch of 2 slots and having different coil-pitches of 1 slot-pitch and 3 slot-pitches. According to the 2-D FEA, the proposed 9-slot/5-pole machine shows a higher torque density than the conventional 12-slot/8-pole segmented rotor machine and 12-slot/5-pole machine. For the 12-slot/5-pole machine, its rotor can be replaced by a 7-pole rotor, and it is found that the 12-slot/7-pole machine has even higher torque density and lower torque ripple than the 12-slot/5-pole machine.

CHAPTER IV. COMPARISON OF THREE-PHASE WOUND FIELD SWITCHED FLUX MACHINES AND SWITCHED FLUX PERMANENT MAGNET MACHINES

Three types of wound field switched flux (WFSF) machines, namely, a 24-slot/14-pole WFSF machine, a 12-slot/8-pole segmented rotor WFSF machine and an 18-slot/10-pole WFSF machine, are compared in terms of torque density, with Toyota Prius 2010 interior permanent magnet (IPM) machine as well as the conventional switched flux PM machine in this chapter. According to two-dimensional (2-D) finite element analysis (FEA), it is found that the torque density of a WFSF machine can be increased further by employing unequal slots, and it can achieve ~80% as much as that of the IPM machine under the same current density. The material costs and efficiency maps of machines are also compared in this chapter.

4.1.Introduction

Rare-earth permanent magnet (PM) excited machines are widely employed for numerous applications due to high efficiency and torque density. However, the price of rare-earth PMs is high, and there exists a tendency to reduce/avoid the usage of PMs in the cost-sensitive applications, such as electric vehicle (EV), hybrid EV (HEV) and domestic appliances. Switched flux permanent magnet (SFPM) machine, whose principle was firstly introduced in 1955 [RAU55], shows the merits of high torque density, simple temperature management and robust rotor structure [HOA97], [ZHU10], and [ZHU11]. Fig. 4.1 (a) and (b) show the typical topologies of SFPM machines. In order to reduce the material cost of SFPM machines, low-cost ferrite magnets may be used in a SFPM machine.

PMs can be replaced by field windings in SFPM machines. Wound field switched flux (WFSF) machine, which is developed from SFPM machine, can be a superior choice in cost-sensitive applications. This PM-free machine inherits most advantages of SFPM machine, besides, its flux weakening capability can be better than that of the PM machines due to its adjustable field current. Some WFSF machine topologies have emerged since 1999 [ZHU11], [POL99], [POL06], [POL06b], [CHE06], [ZUL10], [SUL11], [SUL12], [TAN13], [GAU13], [ZHO14], and [ZHO14a]. The DC field and AC armature windings of a conventional WFSF machine are fully pitched, as shown in Fig. 4.1 (d). This machine suffers from some disadvantages, such as relatively long end-windings, large copper usage, high iron loss and

low efficiency [ZHU11], [POL99], [POL06], [CHE06], and [ZHO14a]. Segmented rotor WFSF machine, whose DC field and AC armature windings are both short pitched, has very short end-windings, and consequently, much less copper usage, Fig. 4.1 (e). However, the torque density of this machine is much lower than the conventional WFSF machine [ZUL10], [ZHO14b]. Fig. 4.1 (f) shows an improved 18-slot/10-pole WFSF machine. As can be seen, 2/3 of its slots contain short pitched coils, and this means that the end-winding of the 18-slot/10-pole WFSF machine is much shorter than that of the conventional WFSF machine. The aforementioned WFSF machines can be differentiated by and named after their field coil pitches, armature coil pitches and rotor pole number. Therefore, the 18-slot/10-pole WFSF machine, whose field winding pitch, armature winding pitch and rotor pole number are 1, 3 and 10, respectively, can be designated as "F1A3-10 pole". In this chapter, it is found that the torque density can be increased by employing unequal slots in WFSF machines.

Toyota Prius 2010 IPM machine, which has been successfully commercialized, shows good performance in many aspects and has been widely investigated. Therefore, this machine can be an excellent benchmark for comparison. However, as mentioned before, the material cost of this machine is high due the usage of rear-earth PMs. The material costs of aforementioned three WFSF machines, the Prius IPM machine and the SFPM machines have been compared in this chapter. The F1A3-10 pole machine shows the highest material usage efficiency (average torque/material usage) among those machines at relatively high current density. The efficiency maps of WFSF machines are investigated and compared in this chapter as well.

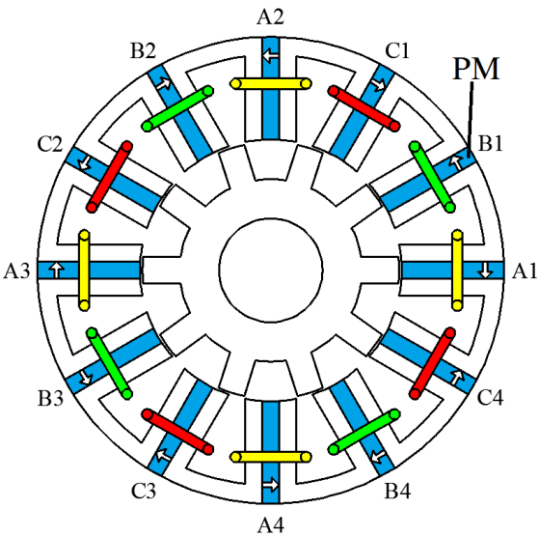

(a)

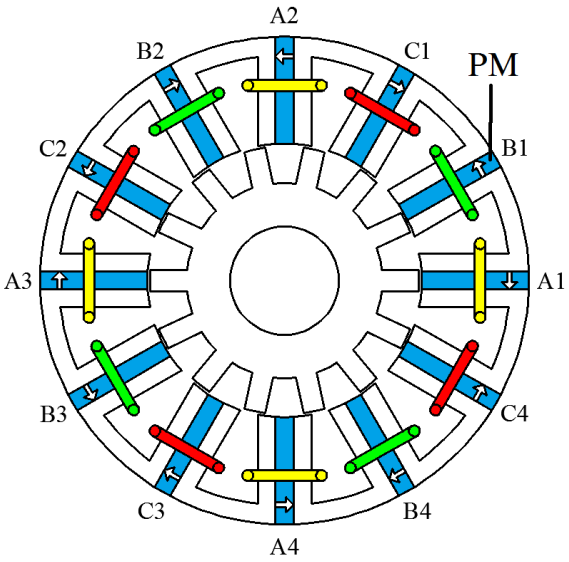
A2
B2
C1
PM
C2
B1
A3
A1
B3
C4
C3
B4
A4

(b)

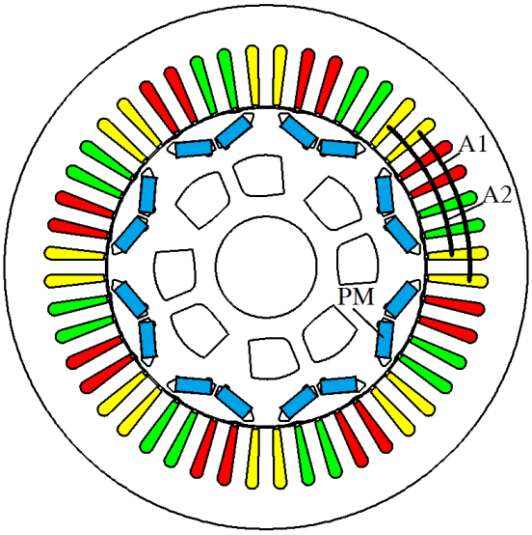
A1
A2
PM

(c)

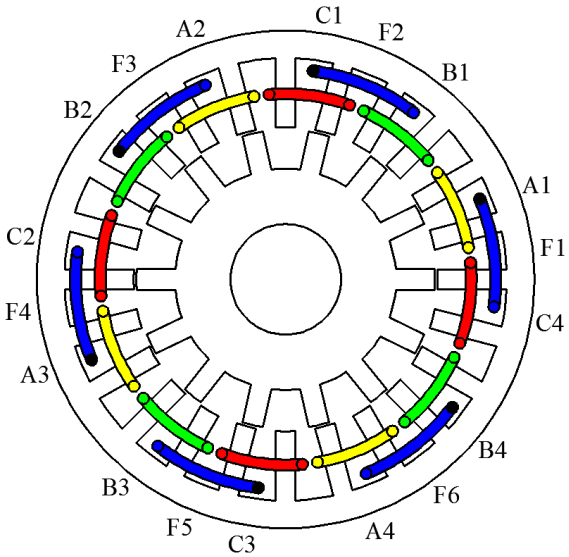
A2
C1
F2
F3
B1
B2
A1
C2
F1
F4
C4
A3
B4
B3
F6
F5
A4
C3

(d)

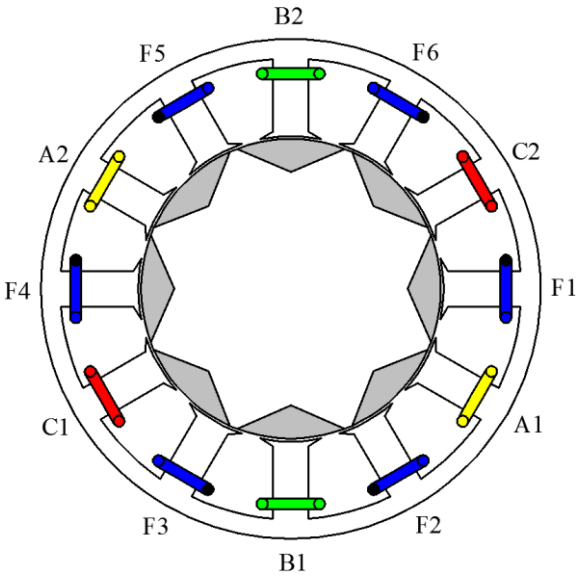

(e)

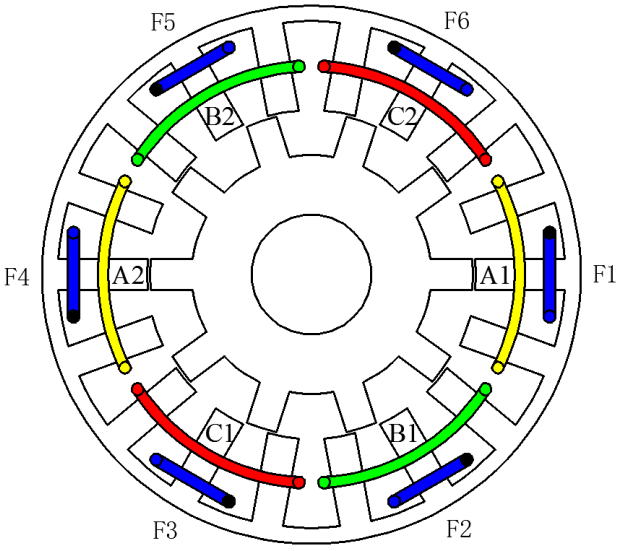

(f)

Fig. 4.1. Cross-sections of (a) 12-slot/10-pole SFPM machine. (b) 12-slot/14-pole SFPM machine. (c) Toyota Prius IPM machine. (d) Conventional WFSF machine. (e) Segmented rotor WFSF machine. (f) 18-slot/10-pole WFSF machine.

4.2.Design of WFSF machines

All the stator and rotor parameters in aforementioned WFSF machines have been globally optimized for comparison by Ansoft Maxwell (Version 16.0). The genetic algorithm, as a common method for the global optimization of machine, is employed to avoid inaccuracy due to the interactions between parameters during the individual optimization.

It has been reported that the WFSF machine suffers from relatively low torque density due to high saturation in the stator [CHE10]. Therefore, the only aim of the optimization is to achieve the maximum average torque under the same current density (26.8A/mm^2) with the Toyota Prius IPM machine.

For the F2A2-24-stator-slot WFSF machine, the 14-rotor-pole one shows the highest average torque and relatively low torque ripple [CHE10]. Therefore, the F2A2-14 pole machine will be chosen for further comparison. F1A1-8 pole machine shows the highest average torque and lowest torque ripple among all feasible rotor-pole numbers [ZUL10]. It has been reported that this machine shows similar torque density with the switched reluctance machine of the same size.

For the F1A3-18-stator-slot machine, which is firstly proposed in this chapter, 8-rotor-pole and 10-rotor-pole machines have the largest winding factor (0.866) among the feasible rotor pole numbers. As can be seen from Fig. 4.2, these two machines show much higher average torque than the F1A1 machine. Among other feasible rotor pole numbers, the 11-rotor-pole machine also shows higher average torque than the F1A1 machine. Besides, the F1A3-11 pole machine shows much lower torque ripple than that of the F1A1-8 pole machine when the current density is 26.8A/mm^2, Fig. 4.2 (b). The low torque ripple of the F1A3-11 pole machine is benefited from its low cogging torque since its least common multiple between stator and rotor pole number is very large [ZHU00]. With respect to torque density, F1A3-10 pole machine is chosen in further investigations.

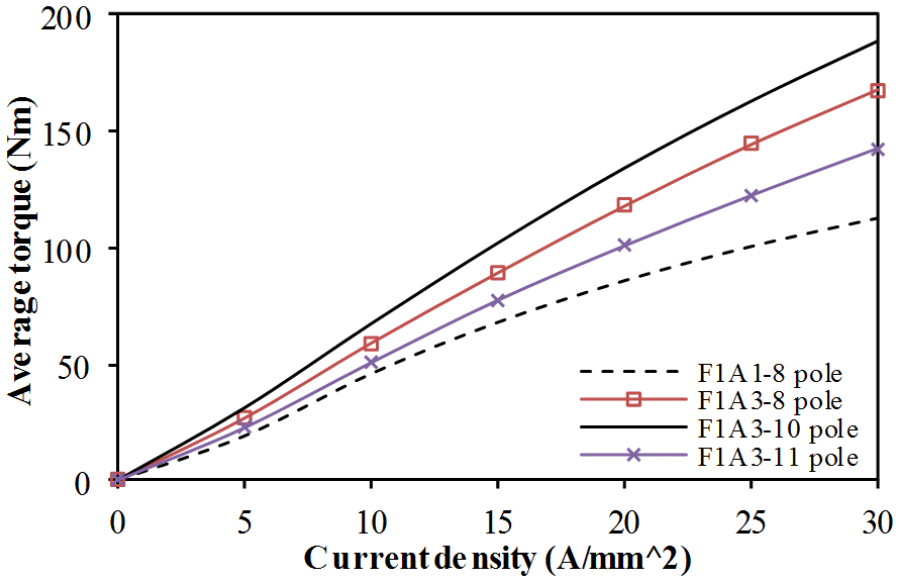

(a)

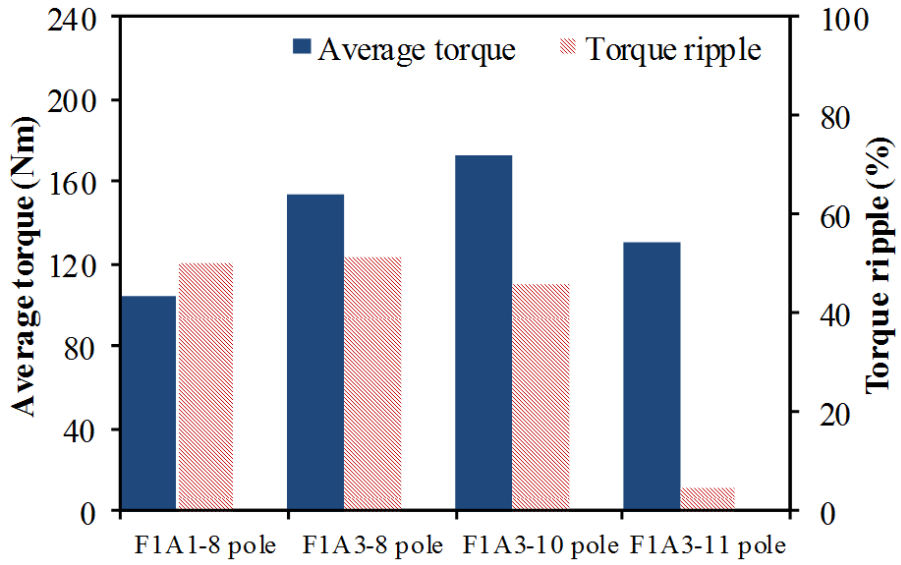

(b)

Fig. 4.2. Comparison of torque in F1A3 machines. (a) Average torque-current density curves. (b) Average torque and torque ripple, current density= 26.8A/mm^2.

4.2.1. Influence of air-gap length

In order to increase the air-gap flux density, the PM free machines usually need shorter air-gap lengths than the PM machines. For aforementioned F2A2-14 pole, F1A1-8 pole and F1A3-10 pole WFSF machines the air-gap lengths were 0.73mm which is the same with Prius IPM machine. When the air-gap is 0.3mm, these WFSF machines are re-optimized to achieve the highest average torque under the current density of 26.8A/mm^2. As can been seen from Fig. 4.3 that by reducing the air-gap lengths from 0.73mm to 0.3mm, the increases in the average torque of WFSF machines are less than 10% when the current density is higher than 20A/mm^2. The explanation is that the machines are saturated under high current density and reducing the air-gap length will not significantly increase the air-gap flux density in WFSF machines. Moreover, reducing the air-gap length will increase the machine manufacturing costs. For this reason, 0.73mm air-gap is selected during the comparison of WFSF machines.

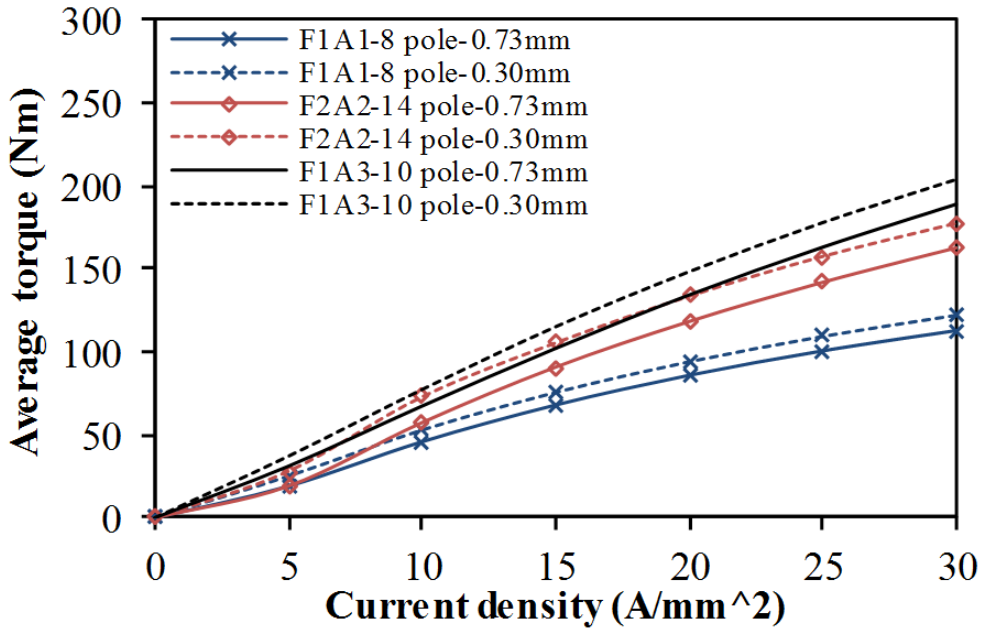

Fig. 4.3. Comparison of average torque with various current densities and air-gap lengths.

4.2.2. Unequal slot

In [ZHO14a], equal slot/tooth/back-iron is employed in each WFSF machine. However, as can be seen from Fig. 4.4 (a) and (b), for the F2A2-14 pole machine, the top part of a stator tooth is less saturated than the bottom part of a stator tooth. In terms of the F1A3-10 pole machine, the flux density differences exist in both stator teeth and stator back-irons, Fig. 4.4 (e) and (f). Therefore, the average torques of these machines have the potential to be increased by employing unequal slot and unequal stator tooth/back-iron to reduce the saturation. For the F1A1-8 pole machine, the flux densities in most part of a stator tooth are similar, Fig. 4.4 (c) and (d).

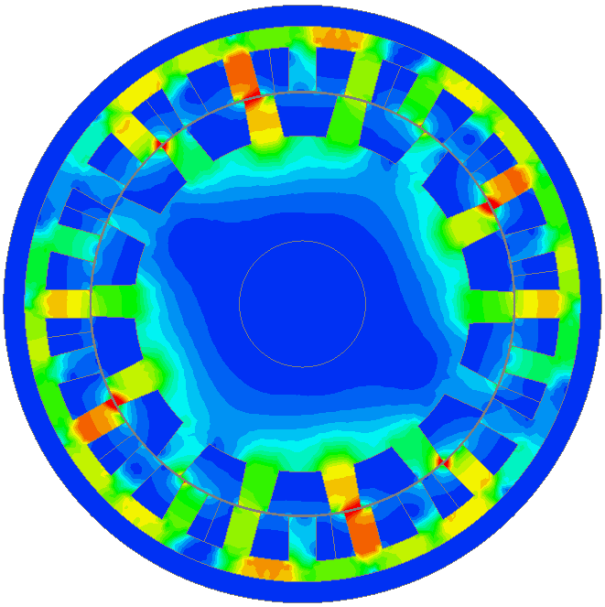

(a)

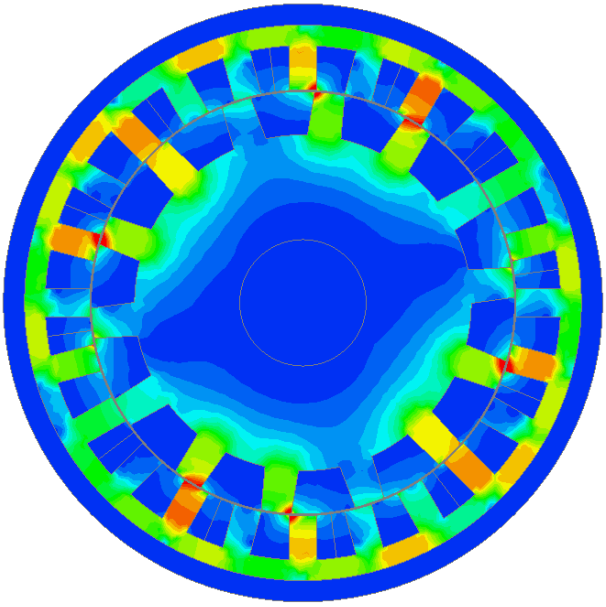

(b)

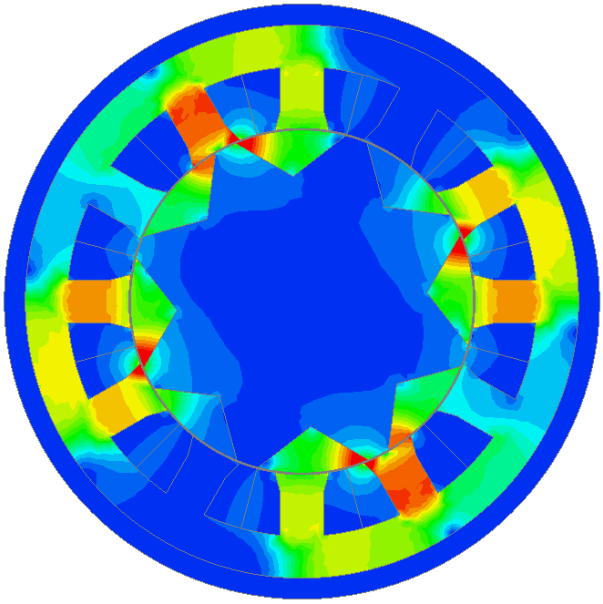

(c)

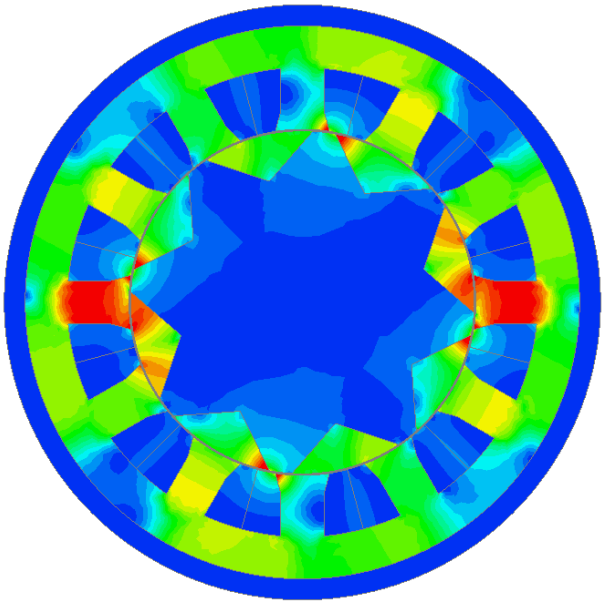

(d)

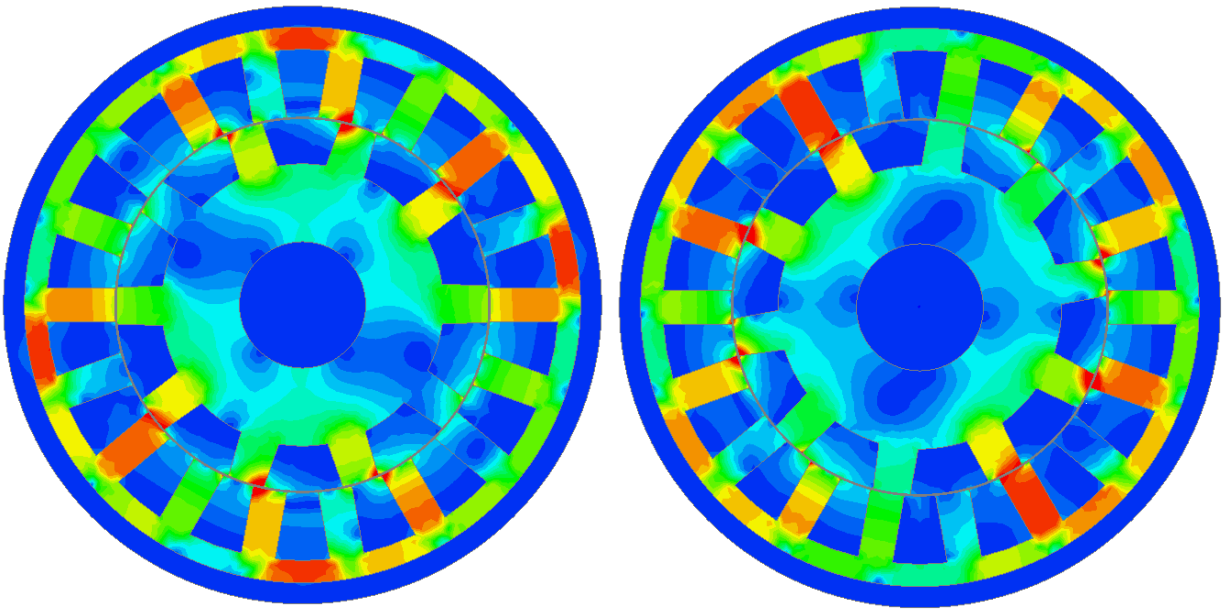

(e) (f)

Fig. 4.4. Flux densities of WFSF machines, current density=26.8A/mm^2. (a) F2A2-14 pole, 0 elec. degree. (b) F2A2-14 pole, 90 elec. degrees. (c) F1A1-8 pole, 0 elec. degree. (d) F1A1-8 pole, 90 elec. degrees. (e) F1A3-10 pole, 0 elec. degree. (f) F1A3-10 pole, 90 elec. degrees.

Fig. 4.5 shows the optimized stator parameters of aforementioned three WFSF machines. In order to achieve the maximum average torque when the current density is 26.8A/mm^2, all the stator and rotor parameters have been globally optimized, and the optimized parameter are shown in Table 4.1. As can be seen, for the unequal slot F2A2-14 pole machine, the stator tooth width at the bottom is larger than that at the top. Hence, the saturation at the stator tooth bottom becomes less severe. Since the stator back-iron of the field slot is less saturation, the optimized stator back-iron thickness of the field slot is smaller than that of the armature slot. Further, it can be seen that the ratio of the field slot area to the armature slot area is 1.09, which is similar to the conclusion in [ZHO14a] that for the F2A2 machine having equal slot the ratio of the field to armature current density is 1.1. As mentioned before, the flux density in the tooth of the F1A1-8 pole machine is similar; the widths of the stator tooth at the top and at the bottom are similar. In terms of the F1A3-10 pole machine, the flux in the stator tooth having field winding is almost as twice as that in the stator tooth having armature winding. Therefore, according to the optimization, the stator tooth having field winding is wider than the stator tooth having armature winding (the width of the stator tooth having armature winding, W_4=13.4mm). For the stator tooth having field winding, the width at the bottom is wider than that at the top. According to the special operation principle of the F1A3

machine [ZHO14a], the back-iron of the field slot contains the flux produced by a whole slot (half coil of the field winding); meanwhile, the back-iron of the armature slot contains the flux produced by only half slot (half coil of one phase) during the operation. For this reason, the global optimization result shows that the back-iron of the field slot is wider than the back-iron of the armature slot.

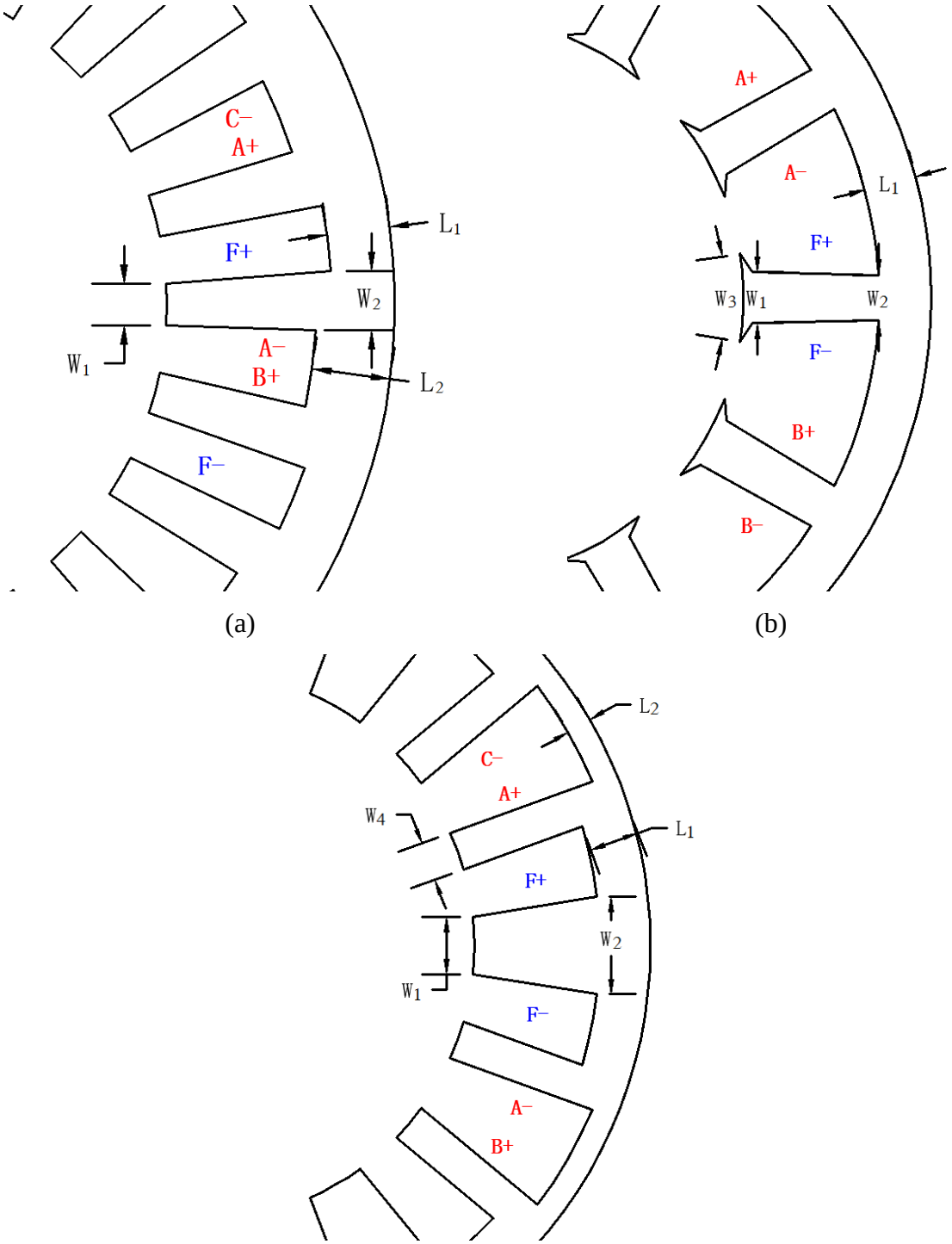

Fig. 4.5. Stator parameters of WFSF machines. (a) F2A2. (b) F1A1. (c) F1A3.

Table 4.1. Main parameters of machines

Items	IPM	SFPM 12s/10p B=1.2T	SFPM 12s/14p B=1.2T	SFPM 12s/10p B=0.4T	SFPM 12s/14p B=0.4T	WFSF F2A2-14 pole	WFSF F1A1-8 pole	WFSF F1A3-10 pole
Stator outer radius (mm)	132	132	132	132	132	132	132	132
Axial length (mm)	50.8	50.8	50.8	50.8	50.8	50.8	50.8	50.8
Air-gap length (mm)	0.73	0.73	0.73	0.73	0.73	0.73	0.73	0.73
Split ratio	0.61	0.69	0.71	0.70	0.73	0.72	0.59	0.67
Stator tooth width at the top, W_1 (mm)	7.3	11.6	11.1	11.2	11.2	11.5	21.2	18.6
Stator tooth width at the bottom, W_2 (mm)	7.3	11.6	11.1	11.2	11.2	16.9	18.2	24.8
Stator back-iron thickness of field slot, L_1 (mm)	--	--	--	--	--	8.6	20	12.2
Stator back-iron thickness of armature slot, L_2 (mm)	20.2	10.2	9.1	11.2	9.8	9	20	8.6
Rotor pole arc (degree)	--	11.6	8.8	8.5	7.7	8.5	36.5	12.5
Stator slot number	48	12	12	12	12	24	12	18
Total armature slot area (mm^2)	7156.8	6999.1	7118.9	5773.0	5368.3	4549.0	5928.7	4870.8
Total field slot area (mm^2)	--	--	--	--	--	4960.8	5928.7	6943.2
Total number of turns of armature windings	528	528	528	432	408	336	444	372
Total number of turns of field windings	--	--	--	--	--	372	444	528
Packing factor (effective copper area/slot area)	0.47	0.47	0.47	0.47	0.47	0.47	0.47	0.47
Magnet material	NdFeB	NdFeB	NdFeB	Ferrite	Ferrite	--	--	--
Number of PM pieces	16	12	12	12	12	--	--	--
PM thickness (mm)	7.2	13.1	13.7	15.9	16.9	--	--	--
PM length (mm)	17.9	40.3	37.6	39.0	35.0	--	--	--

Fig. 4.6 compares the average torque-current density curves of the aforementioned three WFSF machine with or without unequal slot. As can be seen, by using unequal slot, the average torques of the F2A2, the F1A1 and the F1A3 WFSF machine are increased by 10.3%, 2.5% and 9.9%, respectively, when the current density=26.8A/mm^2. With respect to the maximum average torque, these unequal slot machines are chosen for further investigation.

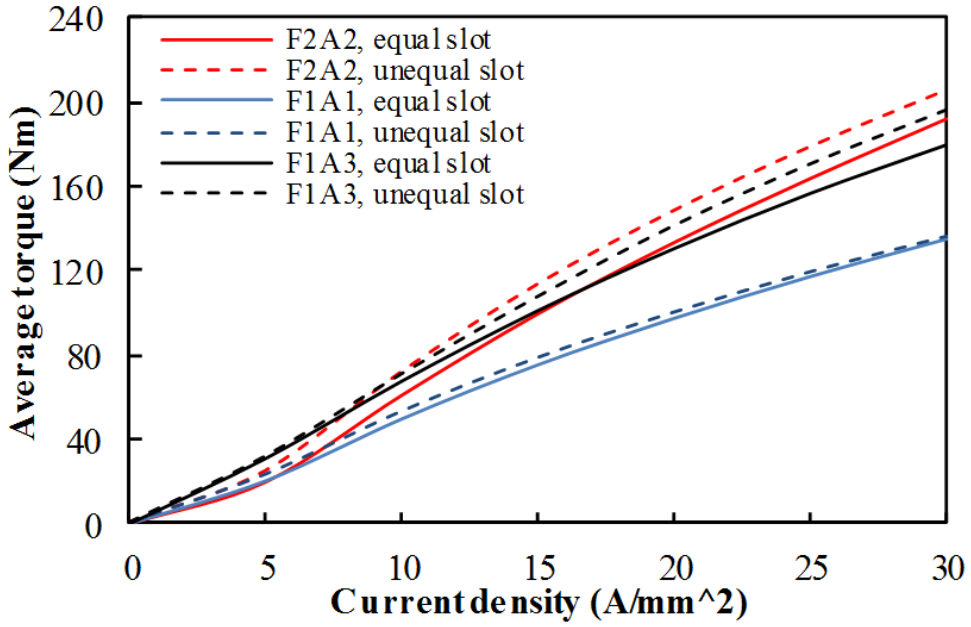

Fig. 4.6. Comparison of average torque-current density curves.

Based on the same stator outer radius and air-gap length of Prius IPM machine, the 12-slot/10-pole and 12-slot/14-pole SFPM machines using rare-earth and ferrite magnets are globally optimized to achieve the maximum average torque when the current density is 26.8A/mm^2. The optimized parameters of machines are shown in Table 4.1. The numbers of turns of armature and field windings of all machines have been determined to ensure that the armature and field currents are approximately 167Arms when the current densities are 26.8A/mm^2.

4.3. Comparison of electromagnetic performance of alternate machines

The performances of alternate machines in Table 4.1 are compared in this section. The end-windings have been taken into consideration during the material usage calculations.

Fig. 4.7 compares the average torques of all PM machines in Table 4.1. Among these machines, the SFPM machine using rare-earth magnets shows the highest average torque. Based on the purchase prices of materials in late 2013, the material usages and costs of PM machines are compared in Table 4.2. As can be seen, the usage of NdFeB magnets in SFPM machine is much larger than that in Prius IPM machine, and the NdFeB magnets SFPM machine seems hard to be popular in cost-sensitive applications due to its high material cost. NdFeB magnets can be replaced by cheap ferrite magnets in SFPM machines. According to [FAS14], the cheap ferrite magnets are more suitable for the SFPM machine than the IPM machine and the surface-mounted permanent magnet (SPM) machine due to the best demagnetization behaviour. It can be seen from Fig. 4.7 that there is a significant average torque decrease in SFPM machine after equipped with ferrite magnets. Between two SFPM machines using ferrite magnets, the 12-slot/14-pole one will be chosen in further comparison in term of the torque density.

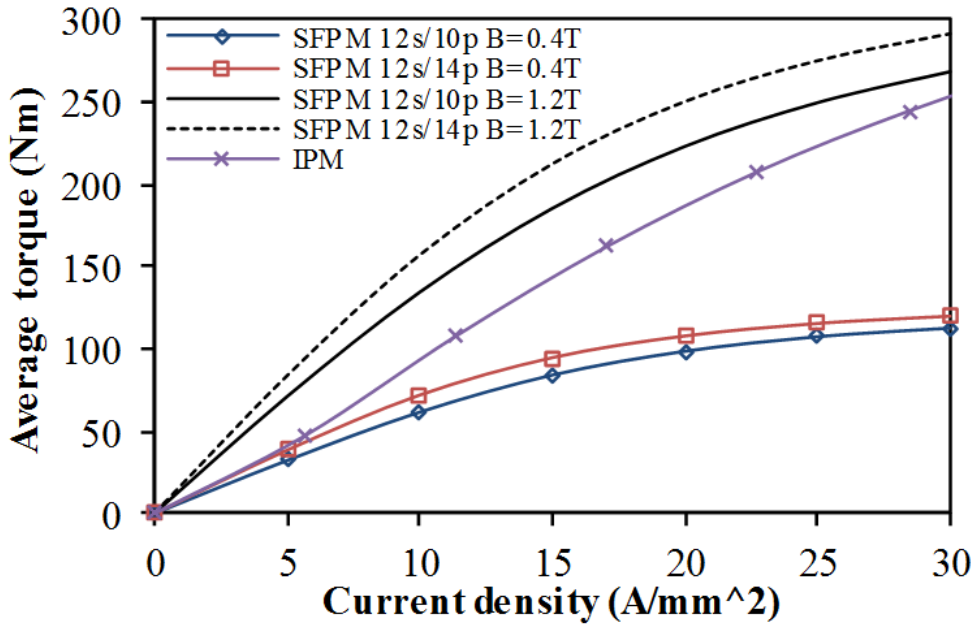

Fig. 4.7. Comparison of average torque with various current densities in PM machines, BLAC operation.

Table 4.2. Comparison of material costs

	IPM	SFPM 12s/14p B=1.2T	SFPM 12s/14p B=0.4T	WFSF 24s/14p	WFSF 12s/8p	WFSF 18s/10p
Copper usage (kg)	4.93	2.98	2.27	5.55	3.34	4.98
Copper cost (£)	34.5	20.9	15.9	38.9	23.4	34.9
Lamination usage (kg)	15.99	12.40	12.31	14.06	10.96	13.21
Lamination cost (£)	32.0	24.8	24.6	28.1	21.9	26.4
PM usage (kg)	0.77	2.31	1.80	--	--	--
PM cost (£)	77.0	231.0	14.4	--	--	--
Total cost (£)	143.5	276.7	54.9	67.0	45.3	61.3

Fig. 4.8 compares the air-gap flux densities of machines. As can be seen, when the field current density is 26.8A/mm^2, the air-gap flux density peak to peak values of WFSF machines are higher than that of the PM machines.

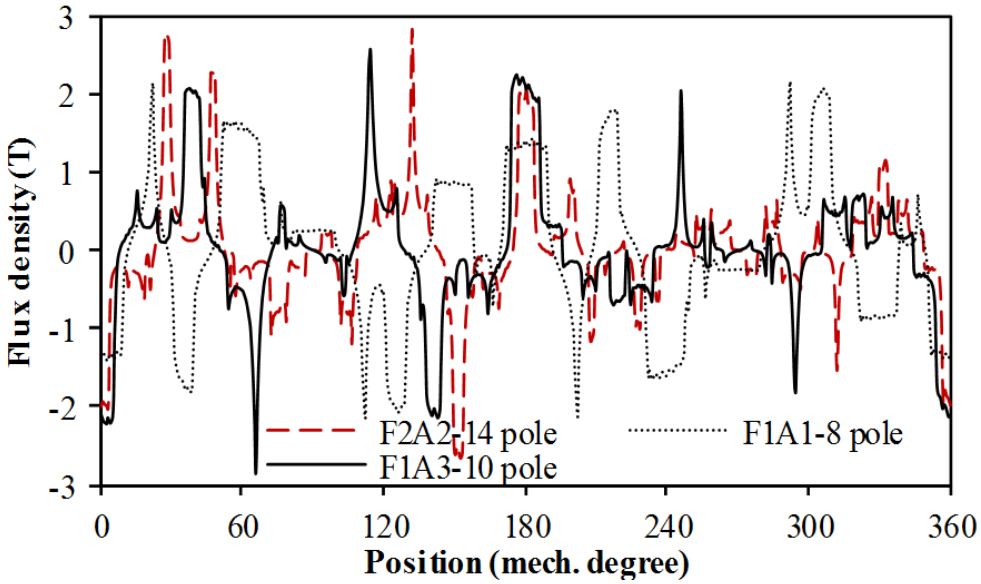

(a)

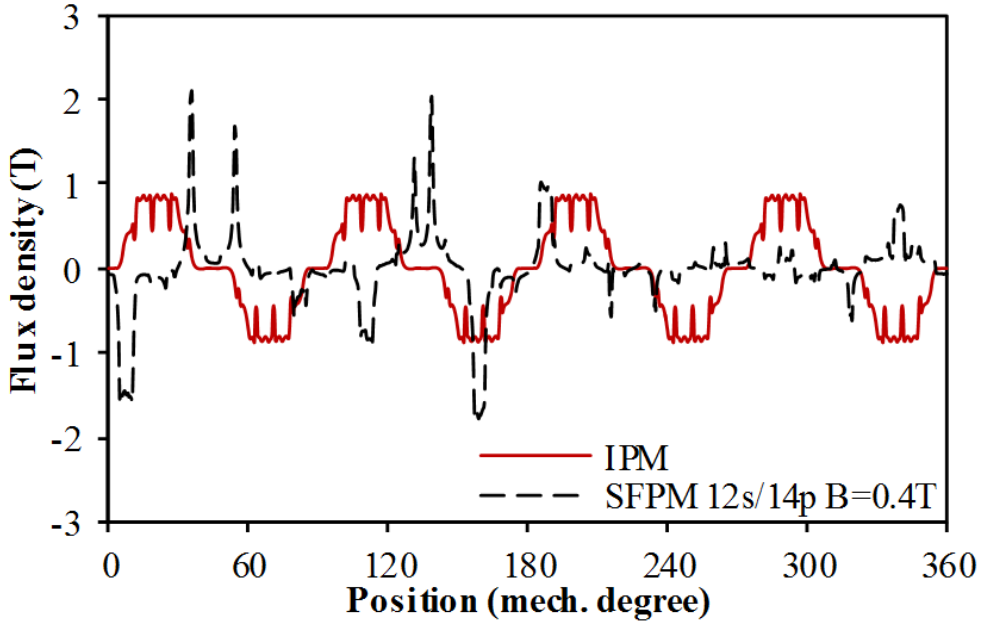

(b)

Fig. 4.8. Comparison of air-gap flux distributions. (a) WFSF machines, field current density=26.8A/mm^2. (b) PM machines.

The back-EMF waveforms at a fixed rotor speed (1000rpm) of the 12-slot/14-pole ferrite magnet SFPM machine, Prius IPM machine and three WFSF machines are compared in Fig. 4.9. As can be seen, all of these machines have nearly sinusoidal back-EMF waveforms, which make them suitable for brushless AC (BLAC) operation. F2A2-14 pole and F1A3-10 pole machines have the highest back-EMF fundamental components. For this reason, the average torques of F2A2 and F1A3 machines are expected to be higher.

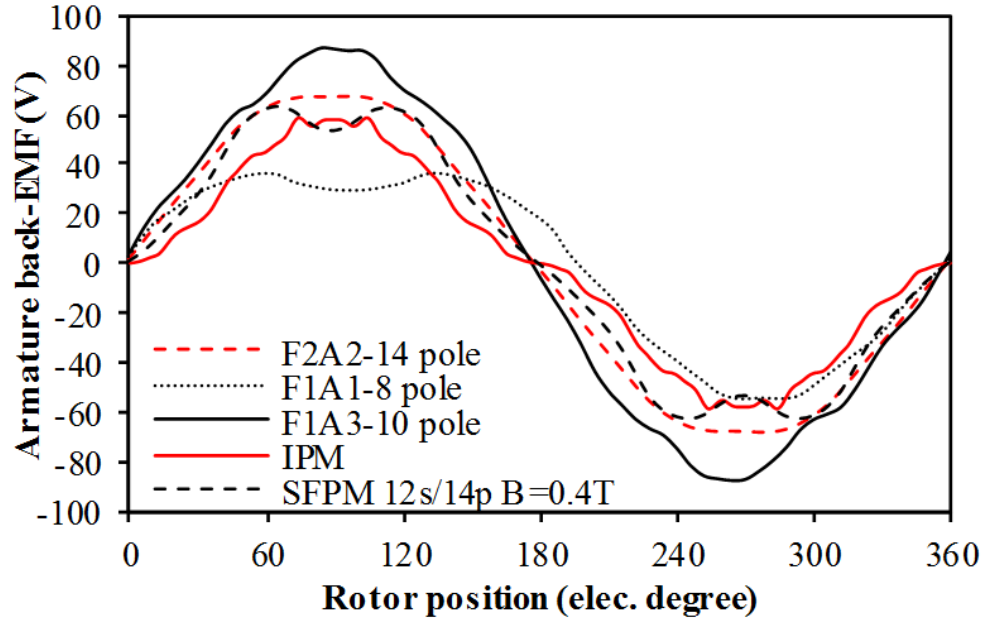

(a)

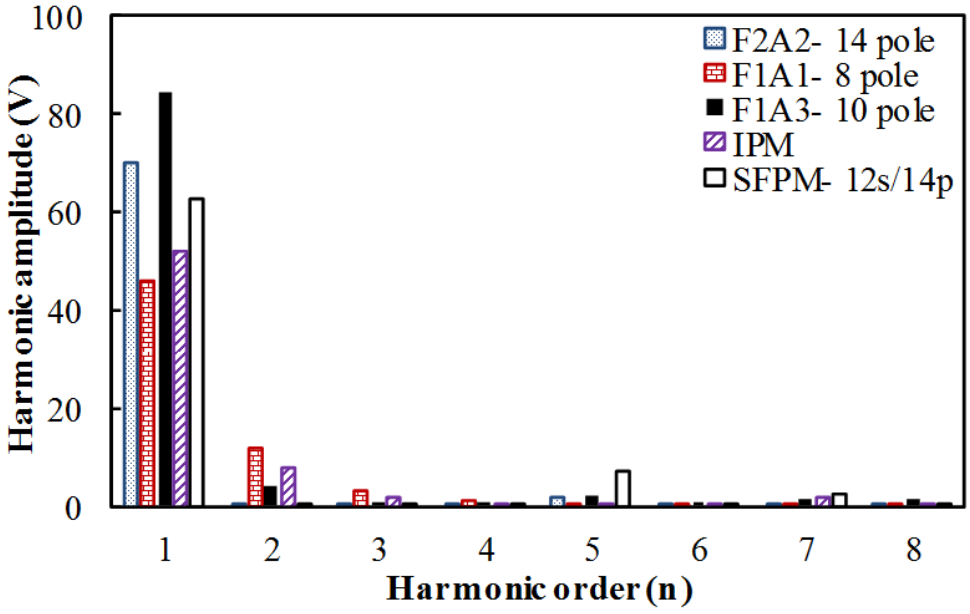

(b)

Fig. 4.9. Armature phase back-EMF waveforms, 1000rpm, for WFSF machines, field slot current density= 26.8A/mm^2. (a) Waveforms. (b) Harmonics.

By avoiding the usage of rare-earth magnets, the ferrite magnet SFPM machine and the WFSF machine show much lower material costs than the rare-earth PM machines, Table 4.2. Fig. 4.10 is the comparison of average torques of these relatively low-cost machines. As can the seen, the F2A2-14 pole and the F1A3-10 pole WFSF machines show higher average

torques than the 12-slot/14-pole ferrite magnet SFPM machine when the current densities are over 10A/mm^2. When the current density is 25A/mm^2, the average torque of the F1A1-8 pole WFSF machine is similar to that of the SFPM machine. In a SFPM machine or a WFSF machine the electromagnetic torque is the major component of the output torque [ZHU11], [ZHO14a]. The electromagnetic torque of a SFPM machine or a WFSF machine can be expressed as:

$$\mathrm{T} = \frac{3}{2} p \Psi_{pm} I_q \tag{4.1}$$

where p is the pole number of a machine, Ψ_{pm} is the PM excited flux-linkage in the SFPM machine or the wound field excited flux-linkage in the WFSF machine. I_q is the q-axis current.

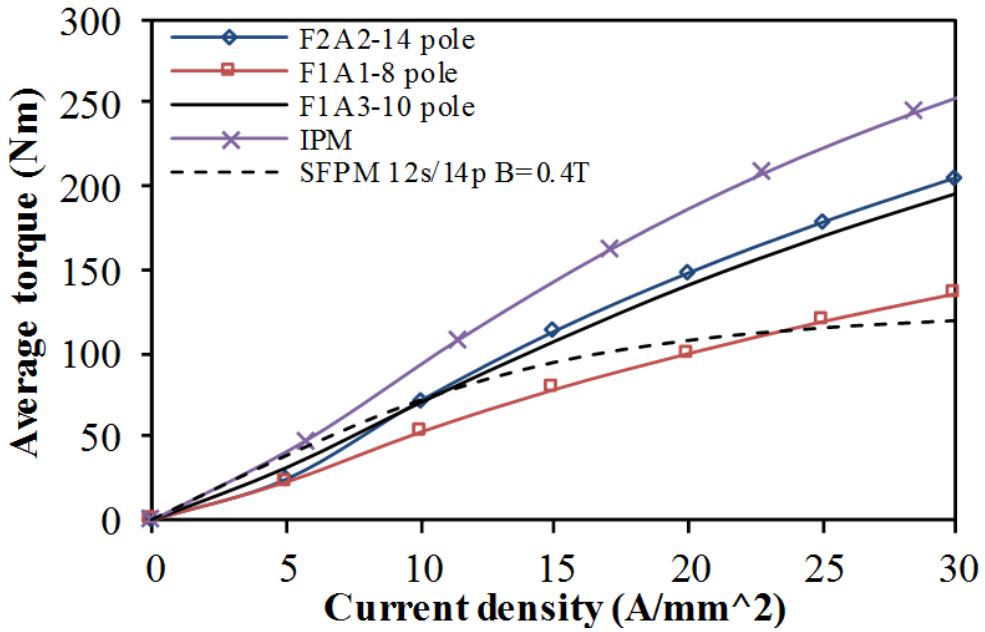

Fig. 4.10. Comparison of average torque with various current densities, BLAC operation.

In the SFPM machine, only I_q increases with the increase of current density. Meanwhile, in the WFSF machine, not only I_q but Ψ increases with the increase of current density. Moreover, at high current density, the armature reaction is strong in the ferrite magnet SFPM machine. Therefore, as can be seen from Fig. 4.10, unlike the SFPM machine, the average torque of a WFSF machine is still incremental over torque density when the current density is high. When the current density is 26.8A/mm^2, the average torques of the F2A2-14 pole machine, the F1A1-8 pole machine and the F1A3-10 pole machine can be 80%, 52% and 78% as much as that of the IPM machine, respectively, as shown in Fig. 4.11. The torque ripples

of the IPM machine, the SFPM machine and the F2A2-14 pole machine are all around 10%. The torque ripples in the F1A1-8 pole machine and the F1A3-10 pole machine are 55% and 44%, respectively, which are relatively high. Fortunately, the easily implemented two-stepped rotor skewing can introduce a specified shift to reduce the torque ripple significantly. This will be investigated in the future.

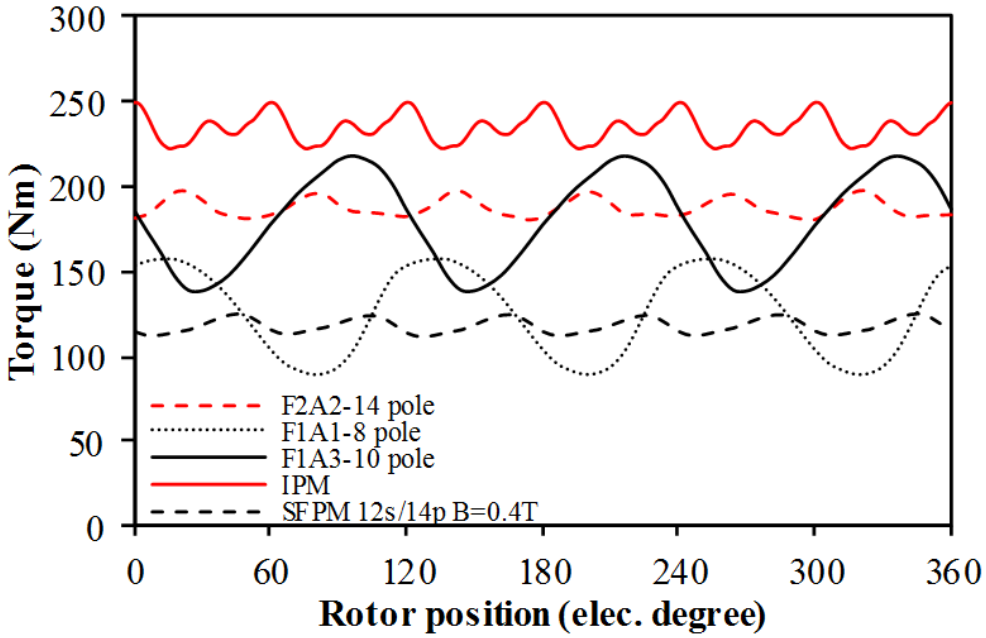

Fig. 4.11. Comparison of torque waveforms, current density= 26.8A/mm^2, BLAC operation.

Among three WFSF machines, the F1A1-8 pole machine shows the lowest copper and silicon steel usages due to its shortest end-winding and segmented rotor lamination, as shown in Table 4.2. Since 2/3 stator slots of the F1A3-10 pole machine contain short pitched coils, its copper usage is lower than the F2A2-14 pole machine whose coils are all fully pitched. Due to the factor that the ferrite magnet is cheap, the material cost of ferrite magnet SFPM machine, whose coils are all short pitched, is even lower than some WFSF machines.

The material usage efficiencies (average torque/material cost) of the IPM machine, the 12-slot/14-pole ferrite/NdFeB magnet SFPM machine and three WFSF machines are compared in Fig. 4.12. For the 12-slot/14-pole NdFeB magnet SFPM machine, its highest material cost results in the lowest material usage efficiency. All WFSF and ferrite magnet SFPM machines show much better material usage efficiencies than the IPM machine. When the current density is high, all WFSF machines show better material usage efficiencies than the SFPM machines.

Overall, the WFSF machine is competitive in cost-sensitive applications due to its relatively high torque density, low material cost and high material usage efficiency.

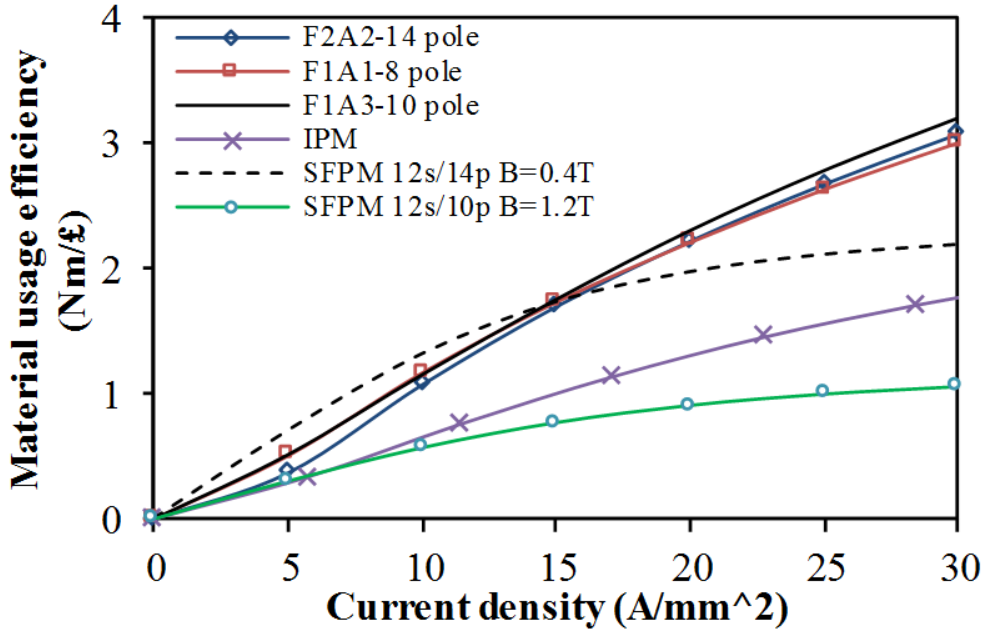

Fig. 4.12. Comparison of material usage efficiencies with various current densities.

Although this chapter mainly focuses on the torque density of machines engaged in cost-sensitive applications. The efficiency, which is a widely concerned performance for wound field machines, of WFSF machine should be taken into consideration to ensure a fair comparison.

The efficiency maps of aforementioned three WFSF machines under fully loaded field current (167Arms, approximately 26.8A/mm^2 current density) and half loaded field current (84Arms, approximately 13.4A/mm^2 current density) are compared in Fig. 4.13 (a)-(f). It is worth mentioning that the mechanical losses of the machines are neglected, and the copper losses and iron losses of the machines under different d- and q-axis currents have been taken into the consideration during the calculations. The iron losses of these machines will be compared with other machines in Chapter VII. Overall, the F1A3-10 pole machine shows the highest efficiency among three WFSF machines. It can be seen that for each WFSF machine, the high efficiency region will move to low rotor speed and low output torque area with the reduction of field current. The reason is that the copper loss is dominated in the total loss when a WFSF machine is operated at low rotor speed, and high field current will not contribute to a significant increase of output torque at low output torque area. Therefore, in order to increase the operation efficiency under different rotor speed, the control of the field

current in a WFSF machine is needed to match the specific armature current and current angle. It can also be seen from the comparison that, under the same limitations of armature current and armature DC bus voltage, the maximum output torque of a WFSF machine will be lower with the decrease of field current. This means that the maximum field current is needed during the flux weakening region in terms of output power. The efficiency maps of the WFSF machines shown in this thesis have a limitation that the field currents are fixed in both constant torque and field weakening regions, which means for each case the optimal efficiency and torque-speed characteristic may not be achieved with the limited total current. Ideally, the amplitudes and the split ratio of field to armature currents needs to be controlled during the operation. However, this will result in increased price and reduced reliability due to the introduction of extra power devices for field windings, which can be a demerit of WFSF machine.

The efficiency map of the Prius IPM machine is shown in Fig. 4.13 (g). Compared with the PM machines such as Prius IPM machine, the output powers and efficiencies of three WFSF machines are relatively low. Relatively high loss in the WFSF machine may lead to severe thermal condition, and the machines may not survive thermally. This means the candidate WFSF machine may not be feasible to EV/HEV applications without temperature controlling system. Therefore, increasing the output torque and reducing the losses in the WFSF machine will be the priority for future work.

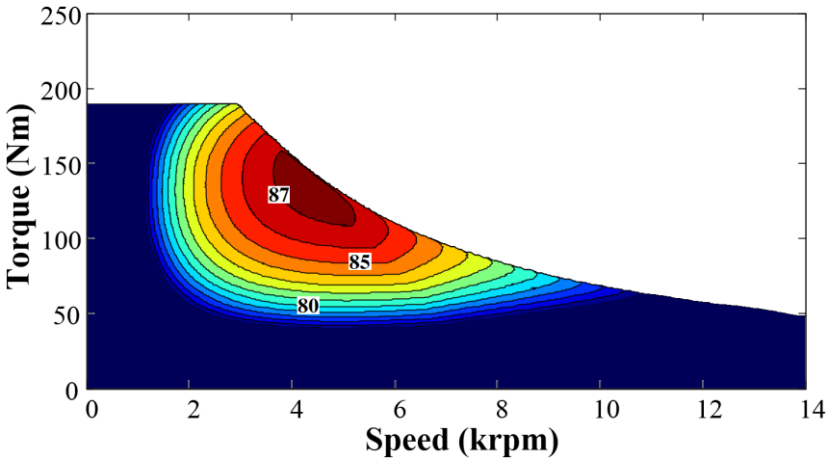

(a)

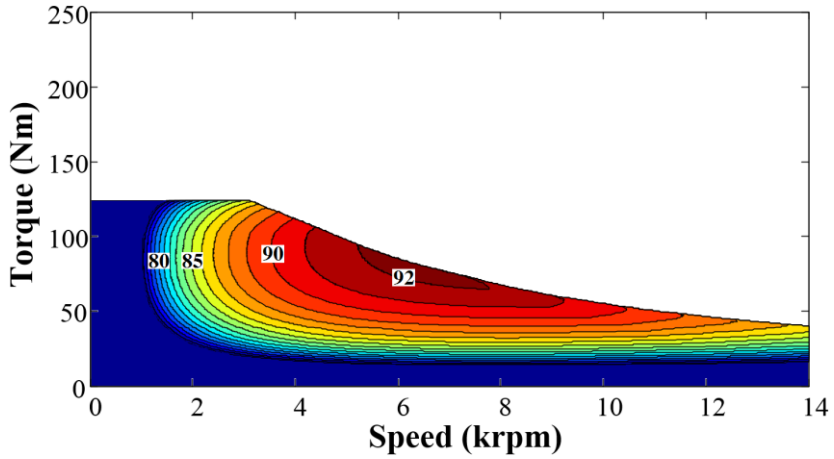
Torque (Nm)
Speed (krpm)
80
85
90
92

(b)

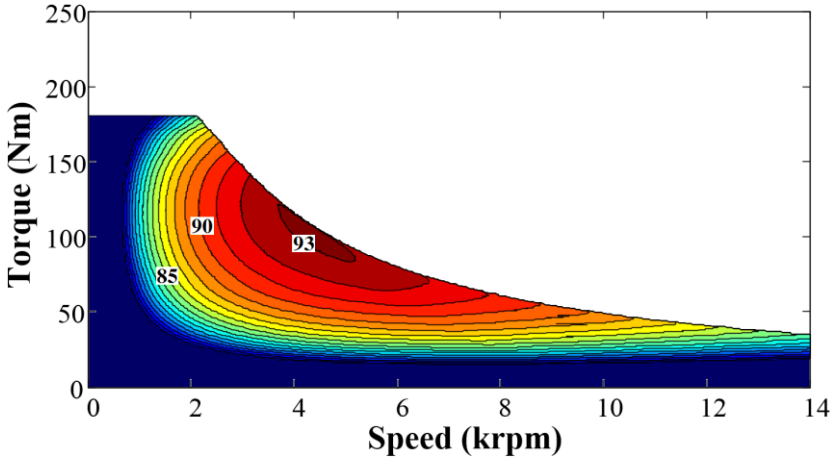
Torque (Nm)
Speed (krpm)
85
90
93

(c)

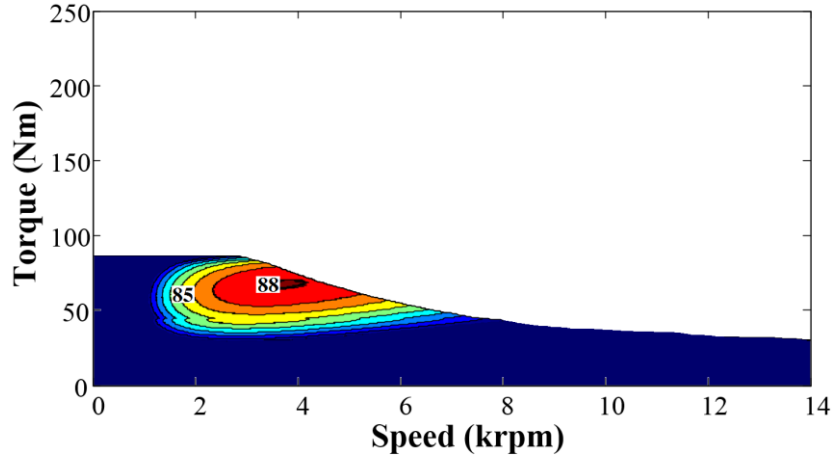
Torque (Nm)
Speed (krpm)
85
88

(d)

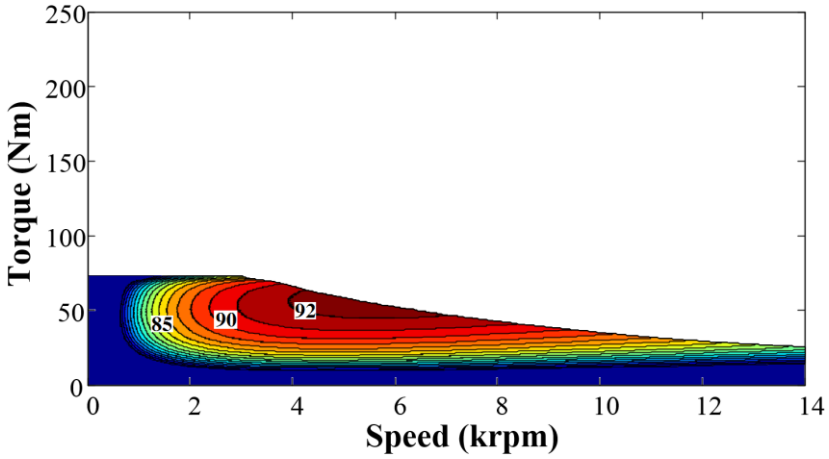

(e)

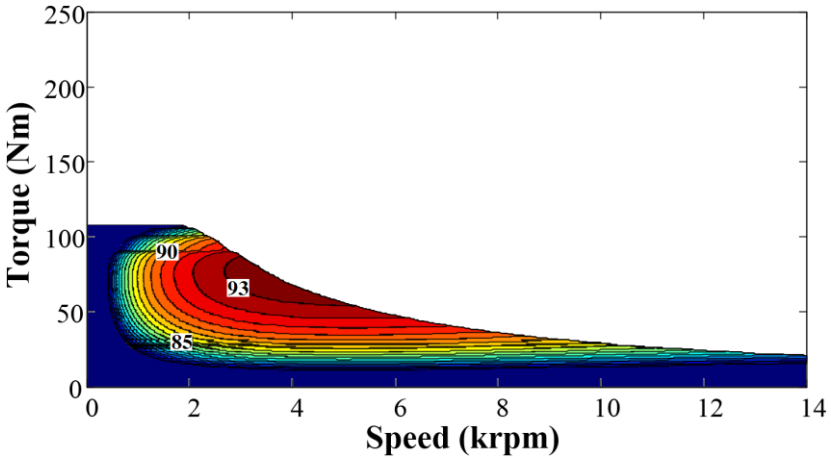

(f)

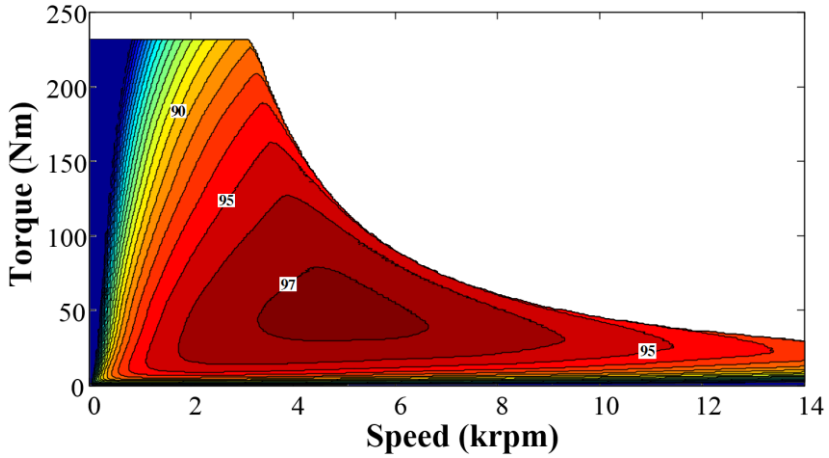

(g)

Fig. 4.13. Efficiency maps of machines, armature current limitation=167Arms, armature DC bus voltage =650V. (a) F2A2-14 pole, Field current=167A. (b) F1A1-8 pole, Field current=167A. (c) F1A3-10 pole, Field current=167A. (d) F2A2-14 pole, Field current=84A. (e) F1A1-8 pole, Field current=84A. (f) F1A3-10 pole, Field current=84A. (g) Prius IPM.

4.4.Summary

Three types of wound field switched flux machines with DC field and AC armature windings having the same coil-pitches of 1 slot-pitch or 2 slot-pitches and having different coil-pitches of 1 slot-pitch and 3 slot-pitches, respectively, are compared with the switched flux permanent magnet machines using ferrite magnets as well as the Toyota Prius 2010 interior permanent magnet machine of the same size in this chapter.

According to two-dimensional finite element analysis, the torque density of the improved F1A3-10 pole WFSF machine with unequal slots is 78% as much as that of the IPM machine, when the current density is 26.8A/mm^2. This machine also shows much higher material usage efficiency than the IPM machine and the SFPM machine.

The efficiency maps of WFSF machines have been plotted in this chapter. It is found that reduce the field current in the WFSF machine will decrease the maximum output power during the operation but will increase the efficiency when the machine operated at low speed.

As mentioned before, the main focus of this comparison is torque density, which means other performances including flux weakening capability has not been taken into consideration during the optimization. The torque-speed curves of the WFSF machines will be investigated in depth for future work.

CHAPTER V. SINGLE-PHASE WOUND FIELD SWITCHED FLUX MACHINES

This chapter presents a comparative study of two types of low-cost single-phase wound field switched flux machines with DC field and AC armature windings having the same coil-pitch of 2 slot-pitches and having different coil-pitches of 1 and 3 slot-pitches, respectively. Both can share the same stator lamination but the later can have shorter end-windings and lower iron loss for the 12-slot/6-pole configuration. The performance, including back-EMF, cogging torque, and static torque, of both machines are analysed and compared by two-dimensional (2-D) finite element analysis (FEA) and validated by experiments on the prototype machines.

5.1.Introduction

Since the switched flux (SF) principle was firstly introduced in 1955, various SF machine topologies have been proposed and investigated [RAU55], [HOA97], [ZHU10], and [ZHU11]. The SF machine possesses two major advantages: simple rotor structure and easy temperature rise management, since all excitation sources are on the stator. Recently, the research on the SF machines is dominated by using permanent magnet (PM) for primary excitation, because of its relatively high torque density and high efficiency. However, the price of rare earth material is high, it is desirable to reduce the usage of magnets or even replace magnets with field windings. For this reason some wound field switched flux (WFSF) machines are proposed for low-cost applications [POL99], [CHE10], [ZUL10], [POL03], [POL03b], [POL06], [SUL11], [SUL12], [WAN12], and [GAU12]. The working temperature of WFSF machines will not be limited by the maximum working temperature of PMs, and potential irreversible demagnetization of PMs no longer exists. Consequently, the power density of WFSF machine can be higher. Moreover, due to the variable flux wound field excitation, the flux weakening operation at high speed of WFSF machine is much easier than PM machines. No brushes/slip rings are required in WFSF machine, thus the service life and reliability of WFSF machine have the potential to be better than that of machines having rotor DC field windings.

A single-phase WFSF machine was proposed in [RAU55] and extensively investigated [POL03], [POL03b], and [POL06] by Pollock, as shown in Fig. 5.1, it has eight stator slots

and four rotor poles. Both armature and field windings are fully pitched and hence the end-winding is long. In this chapter, a 12-slot/6-pole machine is firstly investigated. This machine shares the same operating principle as Pollock's machine in which DC field and AC armature windings have the same coil-pitch of 2 slot-pitches. As will be shown in this chapter, when the axial length and stator outer diameter are 25mm and 90mm, respectively, the foregoing mentioned two machines show similar average torque when the copper loss is fixed, but the 12-slot/6-pole machine has much shorter end-windings, and consequently, much better copper usage efficiency. The field winding and armature winding of 12-slot/6-pole machine can be rearranged to make the DC field and AC armature windings have different coil-pitches of 1 slot-pitch and 3 slot-pitches, respectively. It is found that this winding-rearranged machine has even shorter end-windings. Like the single-phase PM machine introduced in [CHE06], the asymmetric rotor is employed in this proposed machine to enable it to self-start. The number of slots and poles of proposed 12-slot/6-pole machine can be halved, resulting in a 6-slot/3-pole machine. FEA analysis shows that this machine has significantly reduced iron-loss compared with other WFSF machines when their copper losses and rotor speeds are fixed. The FEA predicted back-EMF, cogging torque, torque-current characteristic are validated by experiments on two 12-slot/6-pole prototype machines.

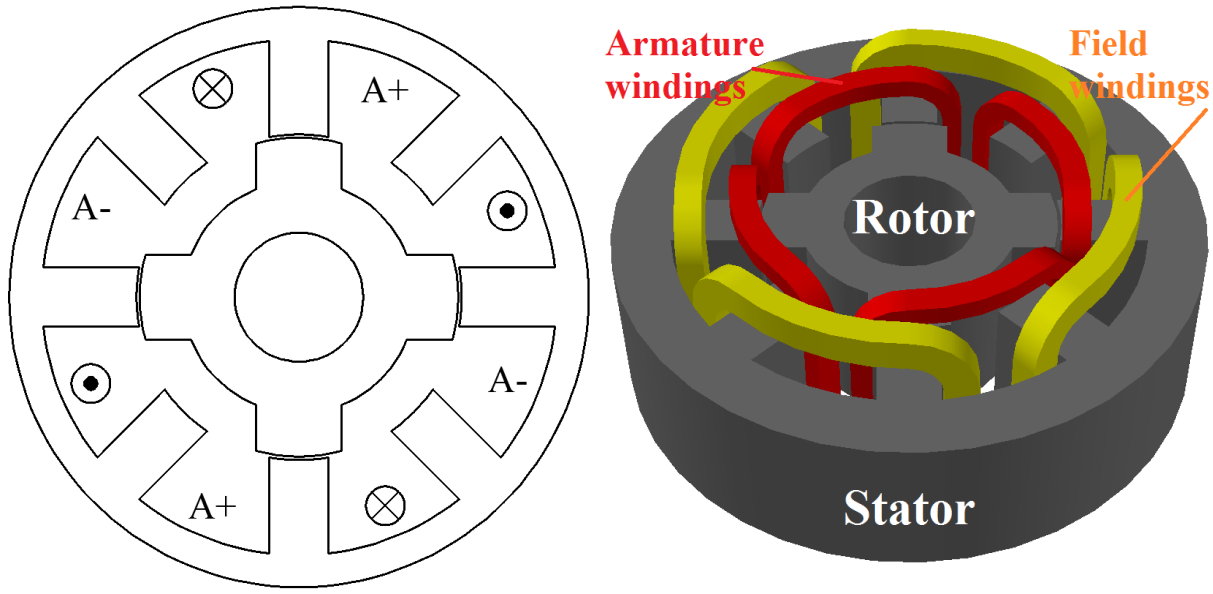

(a) (b)

Fig. 5.1 Conventional 8-slot/4-pole WFSF machine (F2A2-4 pole). (a) Cross-section. (b) 3D model.

5.2.Topologies of machines

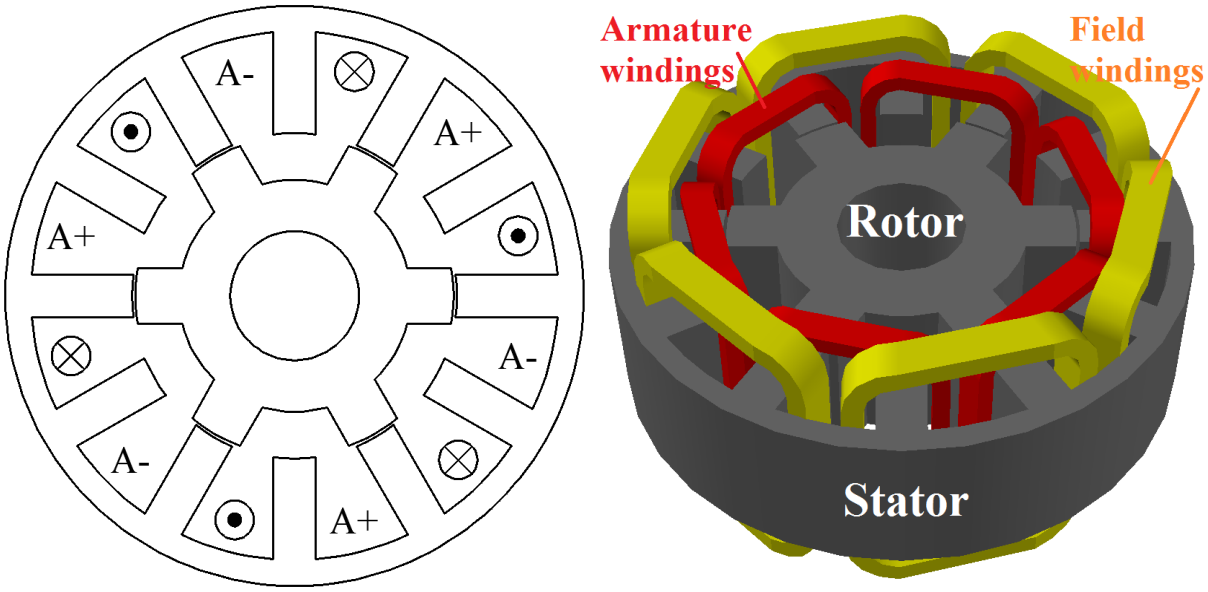

(a) (b)

Fig. 5.2 12-slot/6-pole WFSF machine (F2A2-6 pole). (a) Cross-section. (b) 3D model.

It can be seen from Fig. 5.2 that the 12-slot/6-pole machine that is derived from the conventional 8-slot/4-pole machine is equipped with salient-pole stator and rotor. DC field and AC armature windings have the same coil-pitch of 2 slot-pitches. Correspondingly, 6 armature coils and 6 field coils (or 3 armature coils and 3 field coils when consequent pole windings are employed) are fully pitched. The winding-rearranged 12-slot/6-pole machine, as shown in Fig. 5.3, employs the similar stator and rotor laminations. 4 short pitched field coils having 1 slot-pitch but only 4 (or 2, for consequent pole windings) long pitched field coils having 3 slot-pitches are disposed on the stator, which means its end-windings have the potential to be short. Fig. 5.4 shows the topology of a 6-slot/3-pole machine derived from the winding-rearranged 12-slot/6-pole machine.

In order to easily differentiate the foregoing mentioned machines, four WFSF machines will be named after their field and armature winding pitches and rotor pole numbers. For instance, the field winding pitch, armature winding pitch and rotor pole number of the winding-rearranged 12-slot/6-pole machine are 1, 3, and 6, respectively. Thus, this machine will be designated as “F1A3-6 pole”.

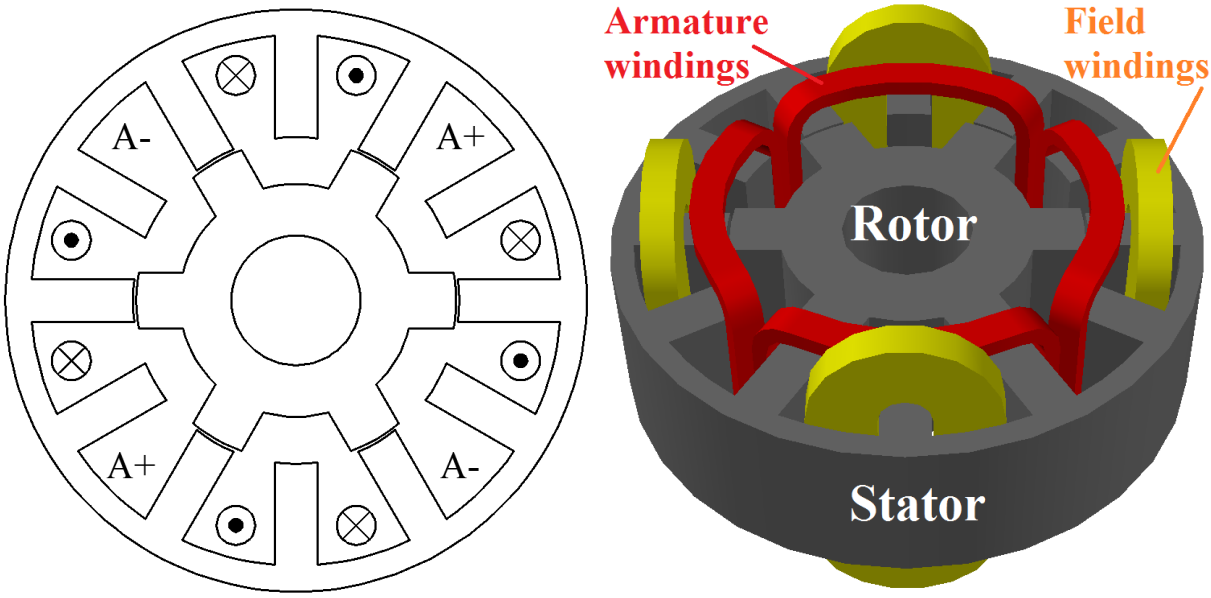

(a) (b)

Fig. 5.3 Winding rearranged 12-slot/6-pole WFSF machine (F1A3-6 pole). (a) Cross-section. (b) 3D model.

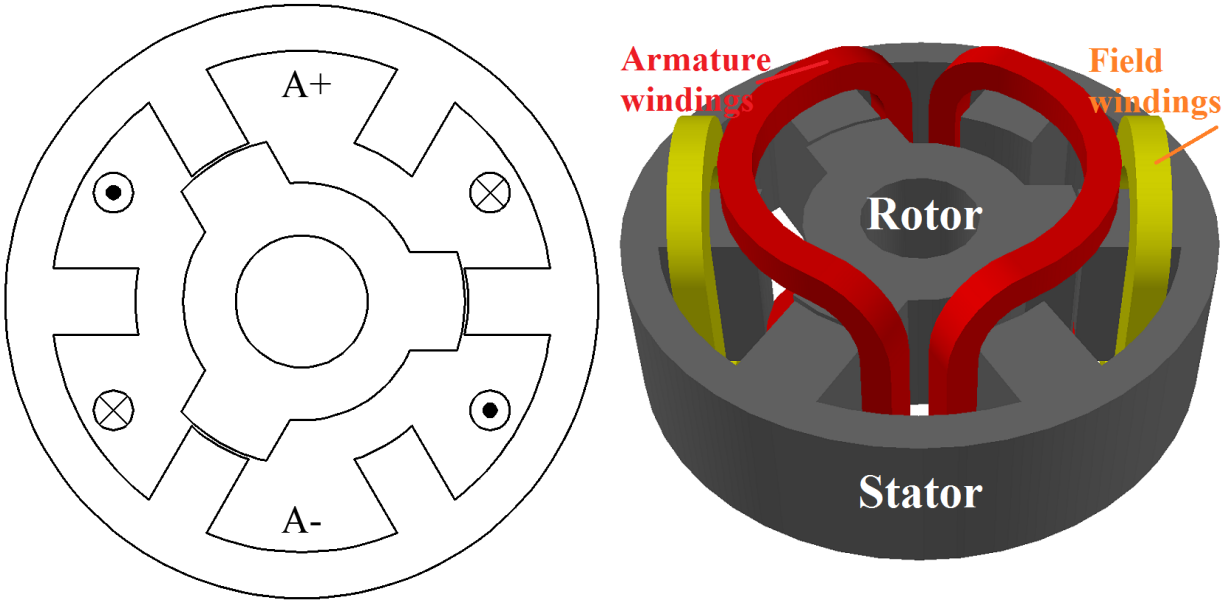

(a) (b)

Fig. 5.4 6-slot/3-pole WFSF machine (F1A3-3 pole). (a) Cross-section. (b) 3D model.

5.3.Operation principle

The operation principle of F2A2-4 pole machine has been introduced in [POL03b], and as mentioned above, the F2A2-6 pole machine shares the same operation principle and therefore

will not be described here. In terms of the F1A3 machines, its operation principle is similar to that of F2A2-4 pole machine, as shown in Fig. 5.5. It can be seen from Fig. 5.5 (a) when the rotor pole aligns with the centre of a field coil (and also the centre of armature coil), the flux-linkage in coil A1 is maximum, while in Fig. 5.5 (c), when the rotor slot aligns with the centre of the field coil (and also the centre of armature coil), the flux-linkage in coil A1 is also maximum but the direction is reversed, i.e. negative maximum. When the rotor pole is approximately aligned with either one of the stator slots which accommodate the field coils, the flux-linkage in coil A1 is zero, Fig. 5.5 (b) and (d). The periodical variation of bipolar flux-linkage with rotor position will induce back-EMF in the coils, which interacts with the applied armature current will produce the electromagnetic torque.

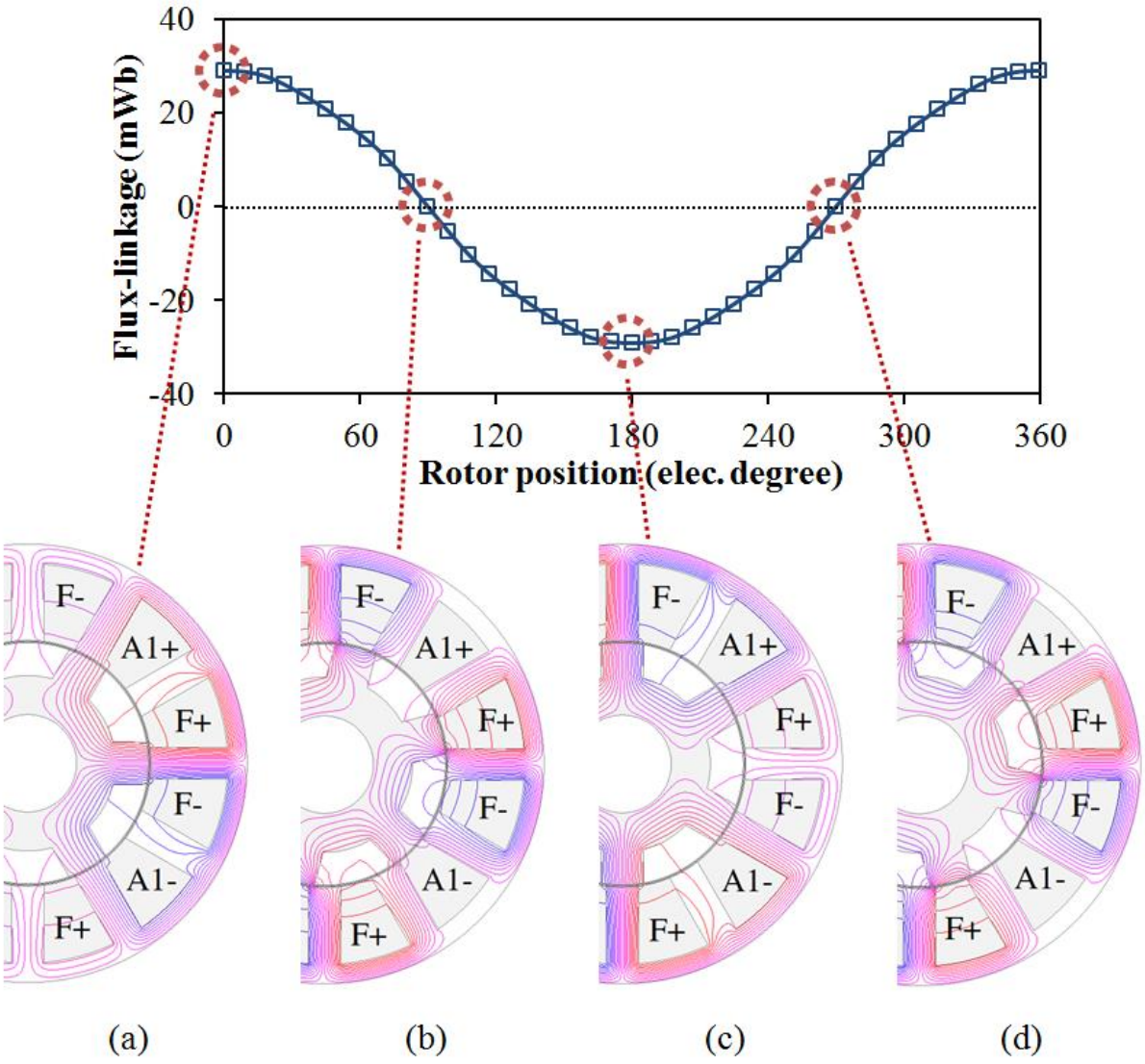

Fig. 5.5 Field distributions (armature current=0A, field current=10A) and typical flux-linkage waveform of single coil in F1A3-6 pole WFSF machine.

5.4.Comparison with low-cost machines

Switched flux permanent magnet (SFPM) machine using ferrite magnets could also be a choice in low-cost applications, Fig. 5.6 (a). The average torque-current density curves of the machines shown in Fig. 5.1 and Fig. 5.6 (a) are compared in Fig. 5.7. It can be seen that, F2A2-4 pole machine shows much higher average torque than SFPM-4-pole machine when the current density is larger than 8 A/mm^2. For this reason, WFSF machine is more suitable for low-cost high-torque required applications. The manufacturing cost of SFPM machine can be higher than WFSF machine since its stator is segmented and needs to be assembled carefully.

Switched reluctance (SR) machines are widely used in low-cost applications due to their low material costs. Fig. 5.6 (b) shows the topology of a conventional single-phase 4-rotor-pole SR machine. Under brushless DC (BLDC) operation, the winding of a single-phase SR machine can only be energized for half of the cycle (unipolar excitation). Therefore, the 4-rotor-pole SR machine will show a lower average torque compared with the F2A2-4 pole machine working under the same RMS current density, as shown in Fig. 5.7.

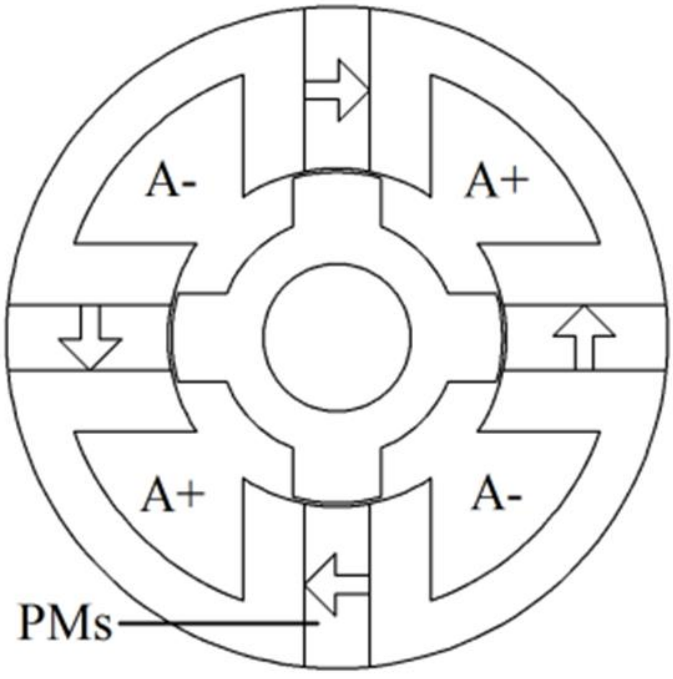

(a)

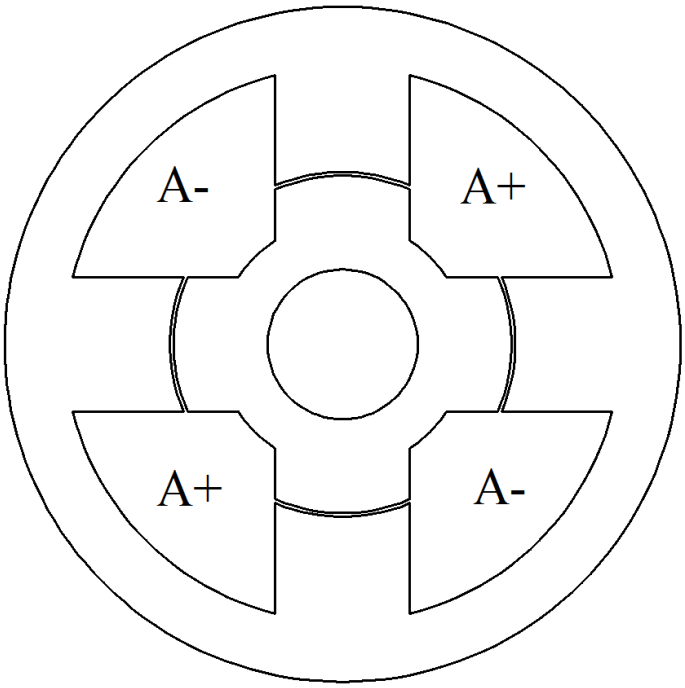

(b)

Fig. 5.6 Cross-section of two low-cost machines (a) Single-phase 4-rotor-pole SFPM machine. (b) Single-phase 4-rotor-pole SR machine.

As shown in Fig. 5.7, the average torques of foregoing mentioned SFPM machine, WFSF machine and SR machine at the current density of 20A/mm^2 will be 1.96Nm, 2.77Nm and 2.42Nm, respectively, which correspond to 30.49W, 76.60W and 66.32W copper losses of those machines, respectively. As can be seen from Fig. 5.8, the efficiency of the WFSF machine is similar to that of SR machine. It is worth mentioning that at 1000rpm, the FEA predicted iron losses of those machines are all less than 3W.

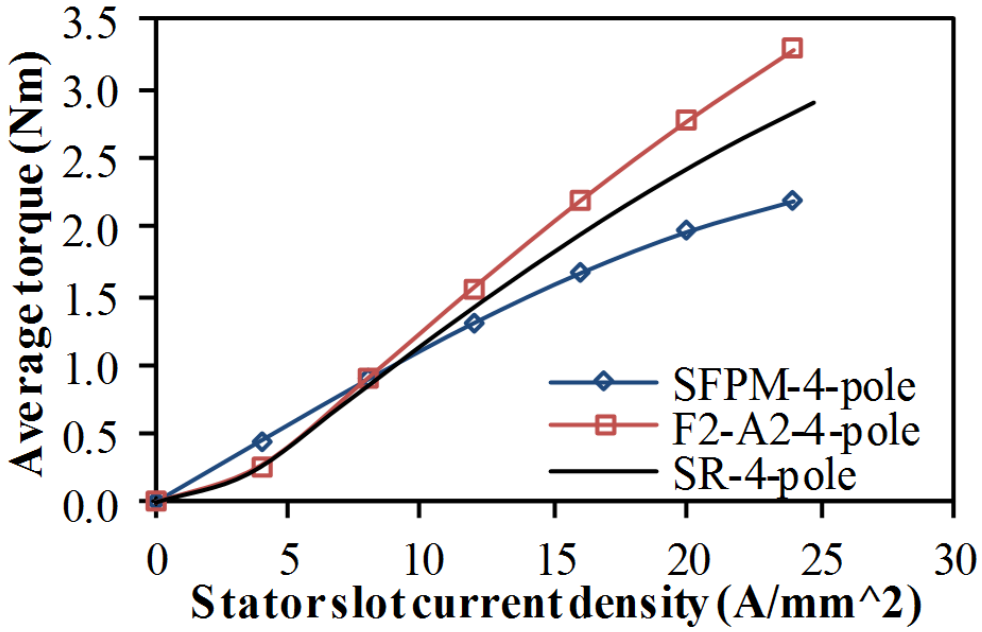

Fig. 5.7 Comparison of average torque with different stator slot current density, BLDC operation.

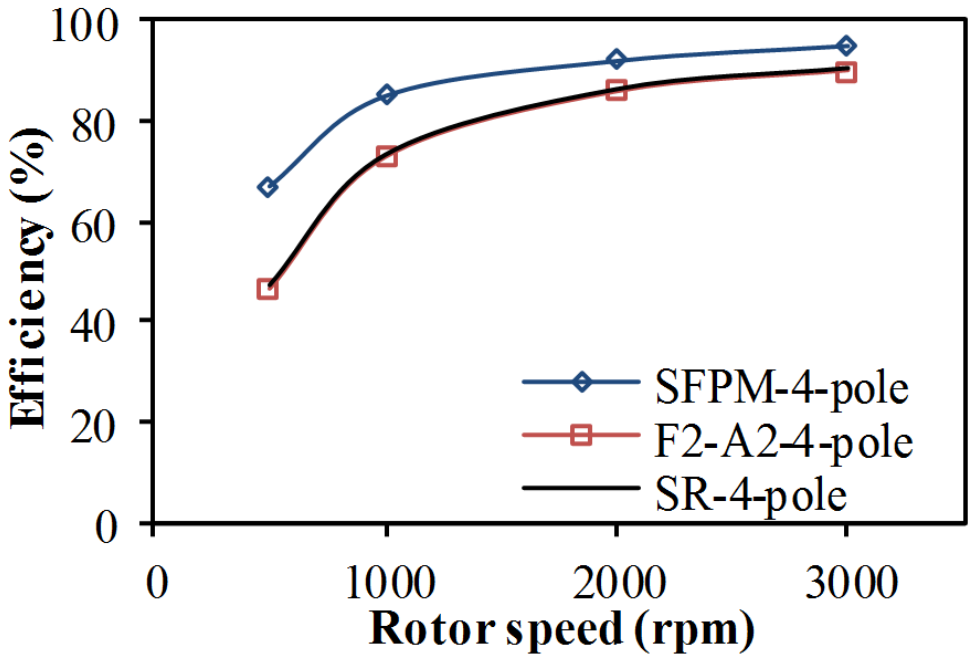

Fig. 5.8 Comparison of efficiency with different rotor speed, current density= 20A/mm^2, BLDC operation.

The KVA ratings and power factors of foregoing mentioned three machines reaching the maximum average torque at the current density=20A/mm^2, are shown in Table 5.1, of which

the total number of turns of armature windings is 180. It is obvious that the F2A2-4 pole WFSF machine shows much higher power factor and lower KVA rating than the SR machine.

Table 5.1 Comparison of machines

	SFPM	F2A2	SR
Total number of turns of armature windings	180	180	180
Total number of turns of field windings	--	180	--
Armature current (A)	22.32	24.67	54.89
Terminal voltage (V)	13.03	17.27	8.70
KVA rating (VA)	290.8	426.1	477.6
Copper loss (W)	30.49	76.60	66.32
Iron loss (W)	2.99	1.88	1.34
Output power (W)	205.59	282.74	253.59
Input power (W)	239.1	361.2	321.3
Power factor	0.82	0.85	0.68

(Current density=20A/mm^2, rotor speed=1000rpm)

5.5.Stator and rotor pole combination

Any rotor pole number from 1 to 11 can be employed except 4 and 8 for the F1A3 machine having 12 slots. It can be seen from Table 5.2 that the 2-, 6-, and 10-pole-rotor machines have the unity winding factor, and among them the 6-rotor-pole one has the largest main flux according to its operation principle. For this reason, the F1A3-6 pole machine appears to give the best performance. Likewise, the 3-pole rotor can be the most appropriate for F1A3 6-slot machine. It can be seen from Fig. 5.9 that, the 3-rotor-pole machine shows the highest peak torque among F1A3-6 stator-slot machines. Meanwhile, for F1A3-12-stator-slot machines, 6-rotor-pole machine shows the highest peak torque.

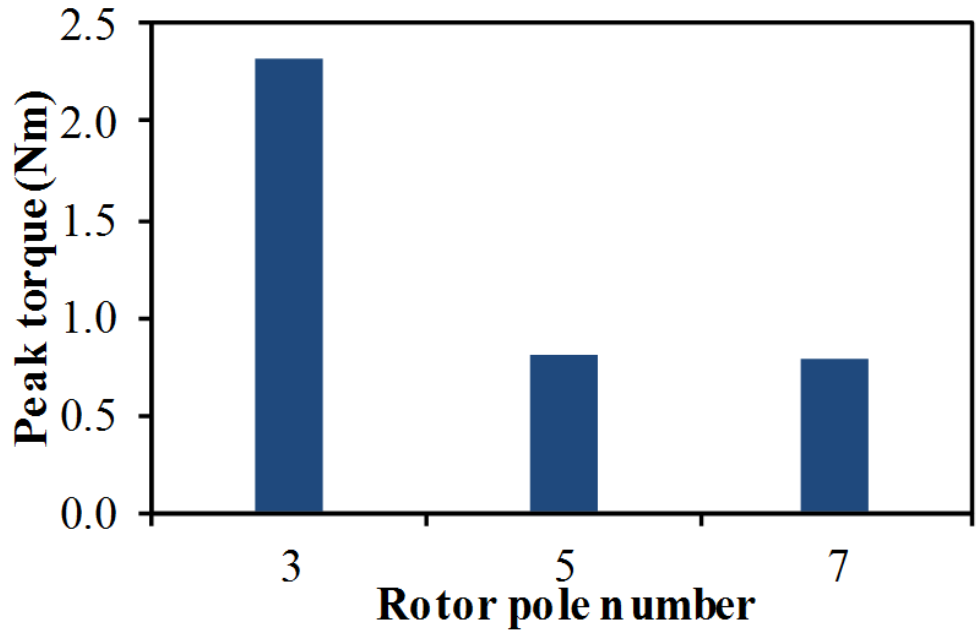

(a)

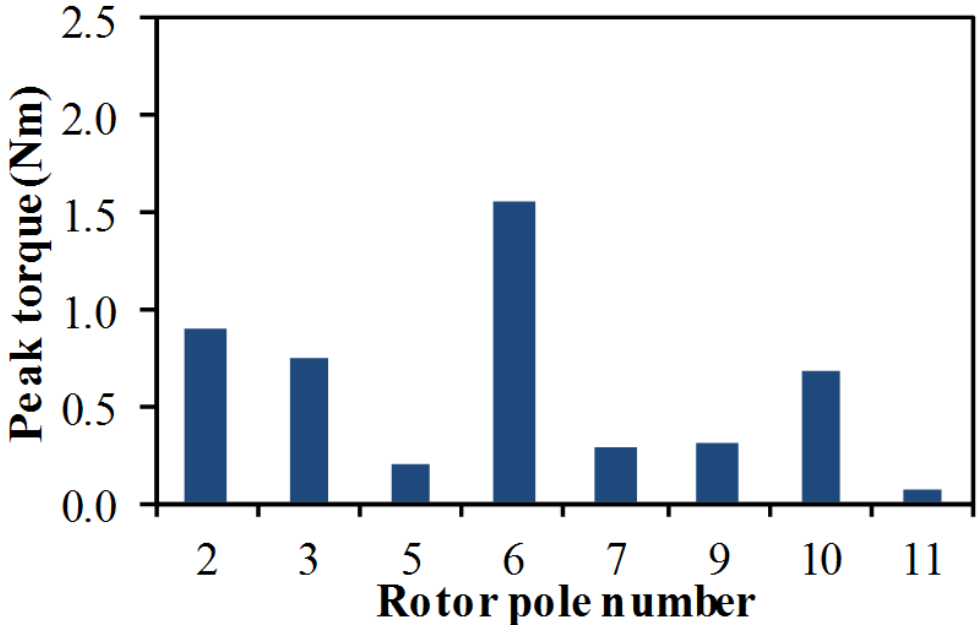

(b)

Fig. 5.9 Comparison of peak torque with different rotor pole numbers in F1A3 machines, armature current= field current= 10A. (a) 6-stator-slot. (b) 12-stator-slot.

Table 5.2 Winding Factors of Different Rotor Pole Number in F1A3-12-Slot Machine

Rotor pole number		Distribution factor	Pitch factor	Winding factor
4n	4	0	0	0
	8	0	0	0
4n+1	1	0.707	0.707	0.5
	5	0.707	0.707	0.5
	9	0.707	0.707	0.5
4n+2	2	1	1	1
	6	1	1	1
	10	1	1	1
4n+3	3	0.707	0.707	0.5
	7	0.707	0.707	0.5
	11	0.707	0.707	0.5

where n is an integer number.

5.6.Parameter optimization

For comparison, all the stator and rotor parameters in the foregoing mentioned WFSF machines have been optimized to achieve the maximum average output torque under the constraint of same copper loss (60W). It is worth mentioning that, the rotor pole width, stator pole width, stator slot opening and stator back-iron thickness are initially set to be the same in each machine before optimization, which is usually employed in the 3-phase switched flux permanent magnet machines [HOA97], [ZHU10], and [ZHU11]. The copper loss P_{Cu} of a single-phase WFSF machine can be expressed as:

$$P_{Cu} = I_a^2 R_{at} + I_f^2 R_{ft} \tag{5.1}$$

where I_a is the RMS armature current, R_{at} is the total armature winding resistance, I_f is the field current, R_{ft} is the total field winding resistance. The end-windings have been taken into consideration during the optimization. The optimized parameters of the investigated machines are given in Table 5.3. It can be seen that for the machine having less stator slot number, after optimization, larger stator pole width, stator back-iron thickness and rotor pole

width are achieved, since more flux has to pass through the stator pole, stator back-iron and rotor pole. According to optimization, F1A3-6 pole machine shows larger stator pole width and stator back-iron thickness than those of F2A2-6 pole machine. It is because the stator poles with field coils in F1A3 machine can be more saturated when the flux goes from the stator side to the rotor side. With the purpose of reducing the flux leakage between the stator poles with field coils (this stator pole contains the flux produced by two field slots in F1A3 machines) and its neighbouring stator poles, the rotor pole width in F1A3-6 pole machine is smaller than that of F2A2-6 pole machine. The stator parameters of two 6-pole machines (F2A2-6 pole and F1A3-6 pole) are nearly the same, which means in actual fabrication, the common stator may be employed for different applications by changing the winding arrangements only.

Table 5.3 Main parameters of machines

Items	F2A2-4 pole	F2A2-6 pole	F1A3-6 pole	F1A3-3 pole
Rated speed (rpm)	1000	1000	1000	1000
Stator outer radius (mm)	45	45	45	45
Axial length (mm)	25	25	25	25
Split ratio	0.5	0.55	0.55	0.55
Stator slot number	8	12	12	6
Rotor pole number	4	6	6	3
Air-gap length (mm)	0.5	0.5	0.5	0.5
Stator pole arc (degree)	21	14	15	23
Rotor pole arc (degree)	31	23	20	35
Stator back-iron thickness (mm)	5	3.5	4	7
Total armature slot area (mm^2)	1110.2	1014.9	676.6	586.5
Total field slot area (mm^2)	1110.2	1014.9	1353.2	1173.0
Total number of turns of armature windings	180	180	180	180
Total number of turns of field windings	180	180	180	180
Packing factor (effective copper area/slot area)	0.4	0.4	0.4	0.4

In order to share the stator lamination structure between F2A2-6 pole machine and F1A3-6 pole machine, all slots are of the same area in the stator. For this reason, the ratio of field and armature current can be adjusted by changing the field and armature currents directly. It can be seen from Fig. 5.10 that, for the F2A2 machines, the highest average torque is achieved when the armature slot current density is equal to the field slot current density. Meanwhile, for the F1A3 machines, the highest average torque is achieved when the field slot current density is 0.9 times as the armature slot current density. Since all optimal ratios of field to armature current density are approximately 1, the field windings and armature windings can be connected in series in power-electronic controllers to reduce the cost.

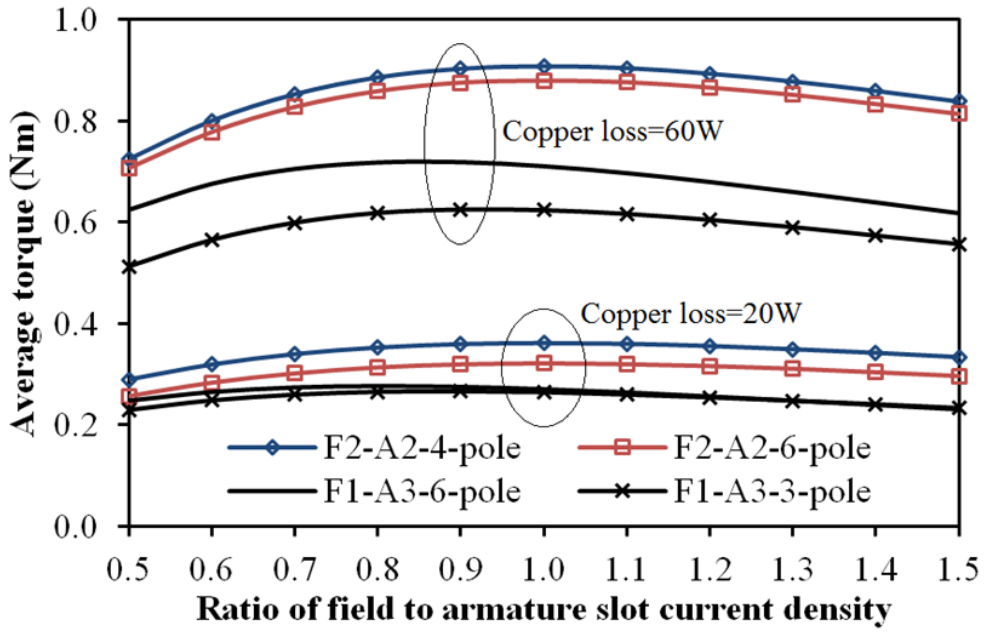

Fig. 5.10 Comparison of ratio of field to armature slot current density with different copper loss, BLDC operation.

The end-windings cannot be ignored in short axial length applications. When the copper loss is fixed to 60W and the cross-section of each machine remains the same, the variation of average torque with axial length is shown in Fig. 5.11. Obviously, the longer the axial length of a machine is, the smaller the end-windings will influence the machine performance. Since the copper loss is fixed, the increase of average torque of each machine will not be proportional to the increase of axial length. Instead, the electric loading will be decreased with the increase of axial length. Consequently, the growth rate of average torque will be decreased with the increase of axial length. It can be seen from Fig. 5.11 that, when the axial length of F2A2 machines is less than 25mm, the 4-pole and the 6-pole machines have similar

average torque, however, the 4-pole machine shows higher average torque when the axial length is long. Similarly, the F1A3-3 pole machine exhibits higher average torque than F1A3-6 pole machine when the axial length is longer than 60mm. This can be explained as follows. When the end-winding is ignored, compared with the machine having more slots and poles, the same type of machine having less slots and poles has larger main flux under the same field current, and consequently, larger average torque under the same armature current.

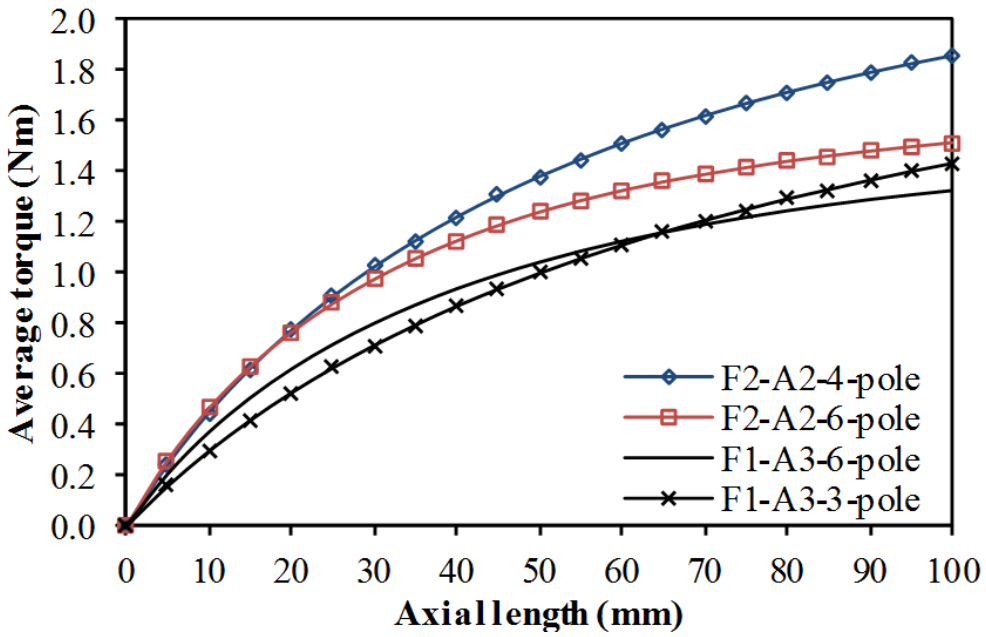

Fig. 5.11 Comparison of torque variation with different axial length, BLDC operation, copper loss=60W.

It is worth mentioning that although the envelop sizes of the compared four machines are the same, the difference of the thermal dissipation performance will lead to different thermal condition of this machines even under the constraint of the same copper loss. Obviously, for the F1A3-3 pole and F2A2-4 pole machines, relatively large slot areas result in severe thermal condition at the centre parts of the coils. For F2A2-6 pole and F1A3-6 pole machines, their thermal dissipation performances have potential to be better than the F1A3-3 pole and F2A2-4 pole machines due to reduced slot areas. Although two 6-pole machines have the same stator slot number, their thermal dissipation performances may not be the same due to the different slot areas based on the optimization. Even the common stator is employed for these two machines, the difference between the optimal ratios of the field currents to the armature currents will result in the different thermal dissipation performances. Obviously, comparison of the machines under the same copper loss has some limitations when the effect

of thermal dissipation is accounted. Therefore, the machines can be compared under the constraint of the same maximum operating temperature in view of thermal condition in further investigations.

In low-cost applications, the copper usage is a key factor affecting the total cost of a wound field motor since copper is much more expensive than other materials in a wound field motor. When the axial length is 25mm, the copper usage of four WFSF machine is shown in Table 5.4. As predicted before, the F2A2-6 pole machine has smaller copper usage than the 4-pole one and the F1A3-6 pole machine has even smaller usage than the F2A2-6 pole machine.

Table 5.4 Comparison of copper usage

	F2A2-4 pole	F2A2-6 pole	F1A3-6 pole	F1A3-3 pole
Field winding volume (mm^3)	25850.7	21496.0	24772.9	26671.7
Armature winding volume (mm^3)	25850.7	21496.0	15958.8	20097.7
Total winding volume (mm^3)	51701.5	42991.9	40731.8	46769.4

When the copper loss is fixed to 60W and the cross-section of each machine remains the same, the variation of copper usage efficiency (average torque/total copper usage) with axial length is shown in Fig. 5.12. In this figure, the variation of average torque with axial length follows the same trend shown Fig. 5.11. The copper usage of effective length increases proportional to the axial length, and the total copper usage is the sum of the copper usages of effective length and end-winding. Similar to Fig. 5.11, the shorter the axial length of a machine is, the larger proportion of the end-windings in the total copper usage will be.

As can be seen, when the axial length is shorter than 25mm, both the F1A3-6 pole and the F2A2-6 pole machines show better copper usage than the conventional F2A2-4 pole machine due to their significantly reduced end-windings. This means for short axial length and low-cost applications, the F1A3-6 pole and the F2A2-6 pole machines are more competitive.

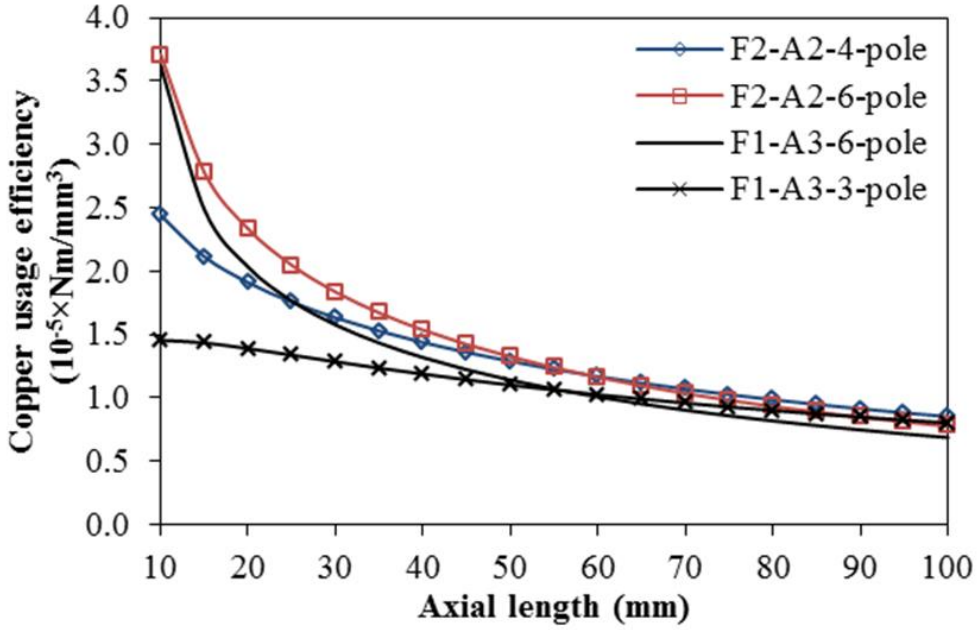

Fig. 5.12 Comparison of copper usage efficiency with different axial length, BLDC operation, copper loss=60W.

5.7.Drive circuit for machines

As mentioned before, since all optimal ratios of field to armature current density in WFSF machines are approximately 1, the field winding and armature winding can be connected in series. One possible topology of motor drive circuit, which is developed from [POL06], is shown in Fig. 5.13 (a). For F1A3 machines, in order to ensure the current densities in each slot are the same, the armature windings are connected in two parallel strands.

When the rotor speed is 1000rpm, the armature and field current waveforms of four optimized WFSF machines under 36V terminal voltages are shown in Fig. 5.14. The waveforms are achieved from Ansoft Maxwell. Fig. 5.13 (b) shows a drive circuit associated with 2-D FEA during the simulation. The armature and field current waveforms are obtained from the ampere meters marked on this figure.

As can be seen, the armature current waveforms are very close to ideal 180 °square current waveforms. Ignoring the fluctuations caused by the reverse of armature current, the field current shows good stability. It is worth mentioning that the output torque of WFSF machine is tiny during the reverse of armature current, which means the fluctuations in field current will not influence the output torque dramatically. Therefore, in order to compare four WFSF machines under the same electric loadings, ideal brushless DC (BLDC) operation and constant field current are engaged in further analysis.

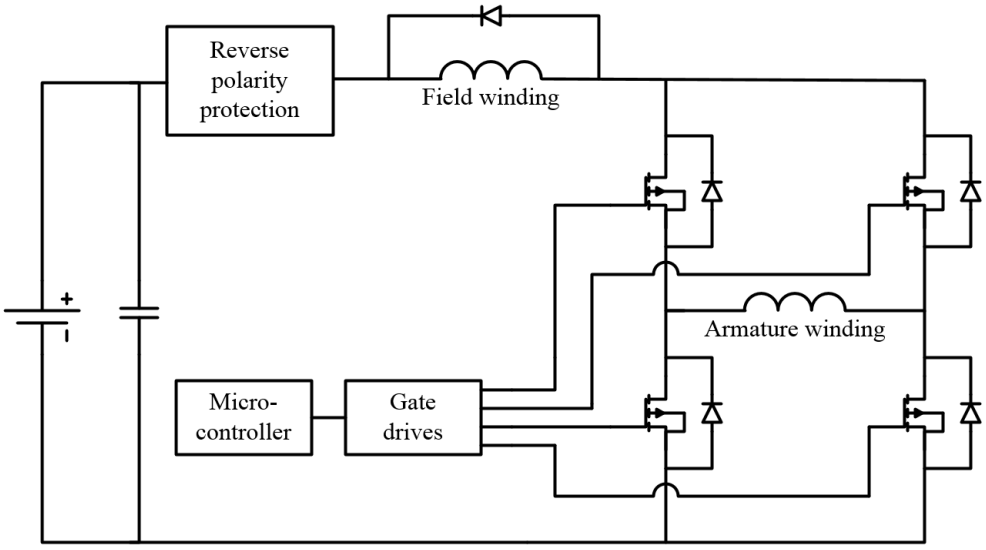

(a)

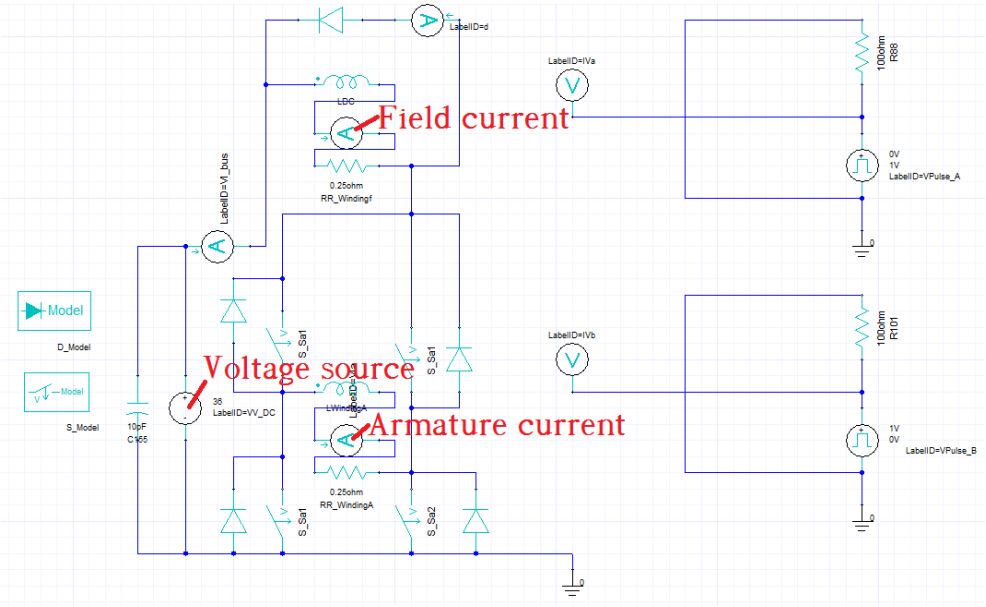

(b)

Fig. 5.13 Drive circuit for WFSF machines. (a) Topology of the drive circuit. (b) One drive circuit associated with 2-D FEA.

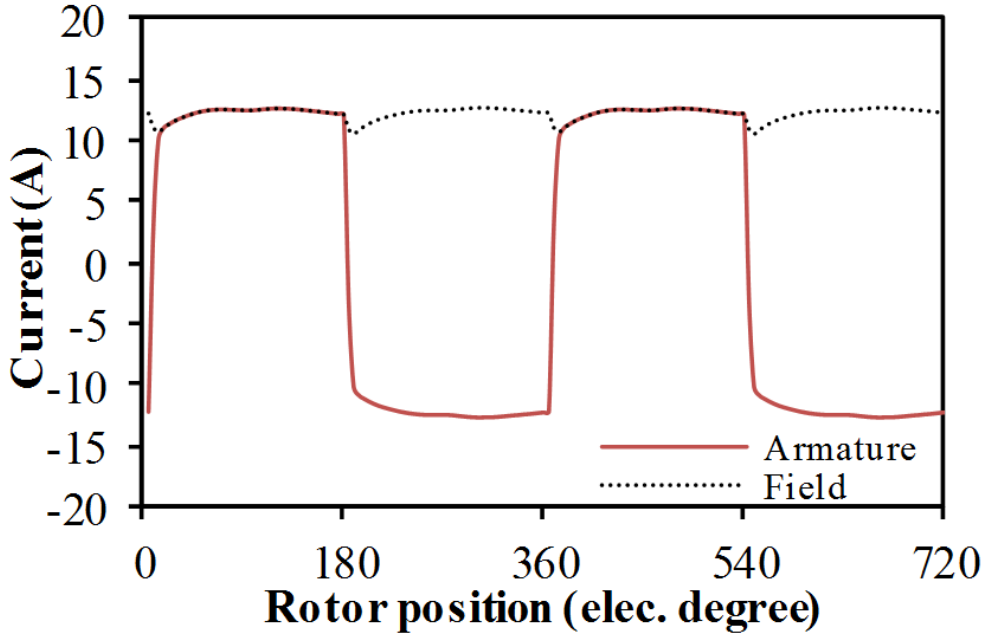
20
15
10
5
0
-5
-10
-15
-20
Current (A)
0
180
360
540
720
Rotor position (elec. degree)
Armature
Field

(a)

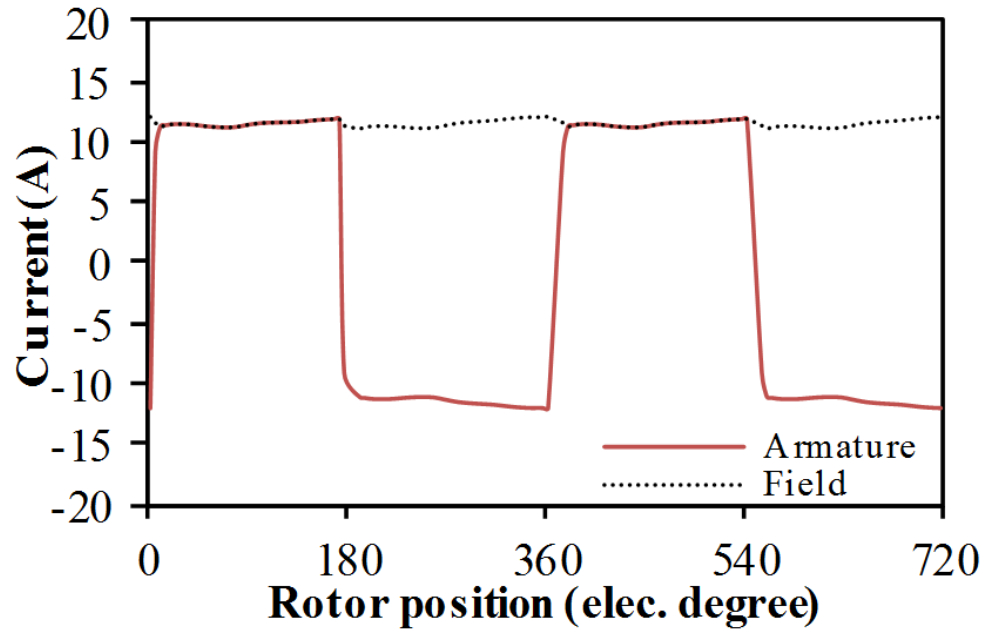
20
15
10
5
0
-5
-10
-15
-20
Current (A)
0
180
360
540
720
Rotor position (elec. degree)
Armature
Field

(b)

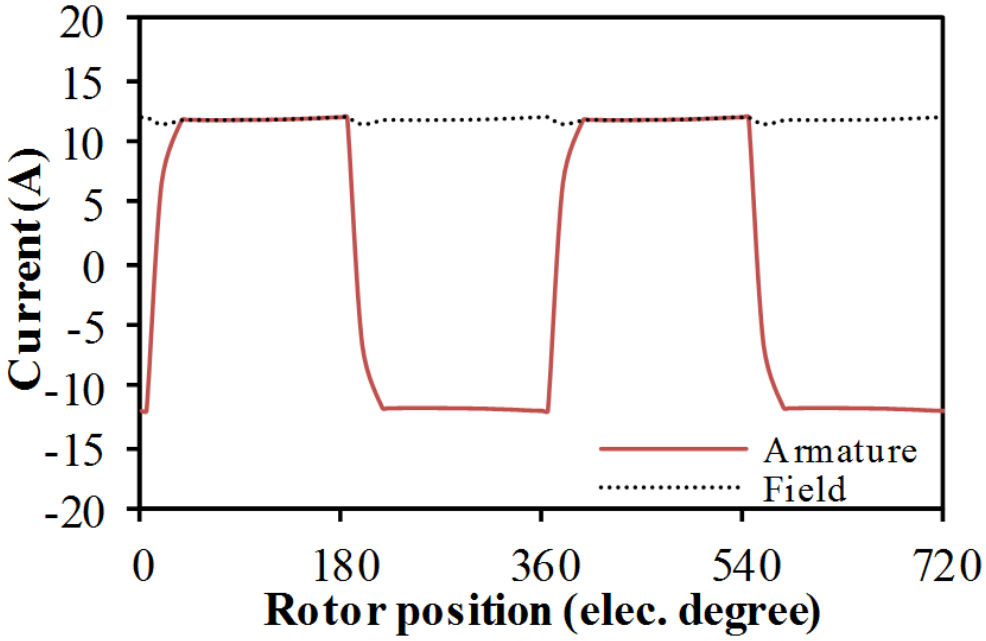

(c)

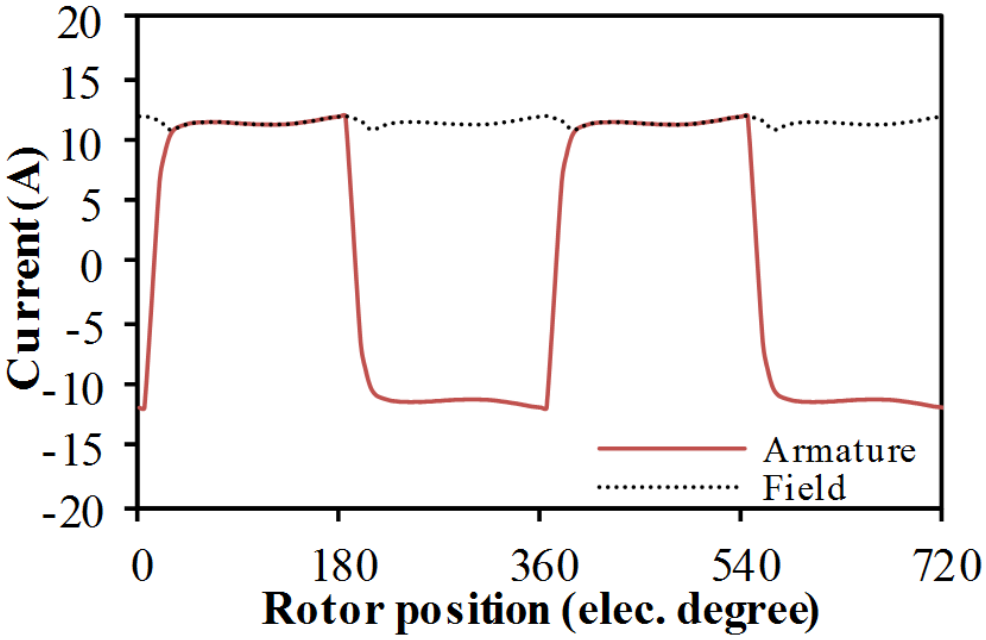

(d)

Fig. 5.14 Armature current waveforms under 36V terminal voltages, 1000rpm. (a) F2A2-4 pole. (b) F2A2-6 pole. (c) F1A3-6 pole. (d) F1A3-3 pole.

5.8.Comparison of machines

The performance of foregoing mentioned four optimized single-phase WFSF machines are compared in this section. It should be noticed that the end-windings have been taken into consideration in the copper loss calculation, but the end effects are ignored in 2-D FEA.

5.8.1. Open-circuit field distribution

Fig. 5.15 shows the open-circuit field distributions of four WFSF machines when the coil A1 has the maximum flux-linkage. It can be seen that for both F2A2 and F1A3 machines, the flux linking coil A1 varies from a positive maximum to negative maximum as the rotor rotates by half of a rotor tooth-pitch.

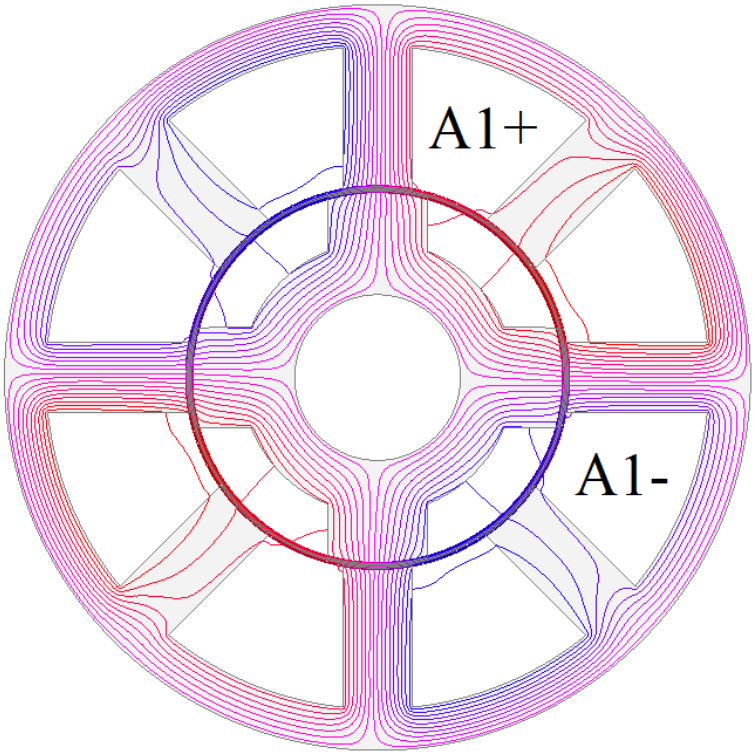

(a)

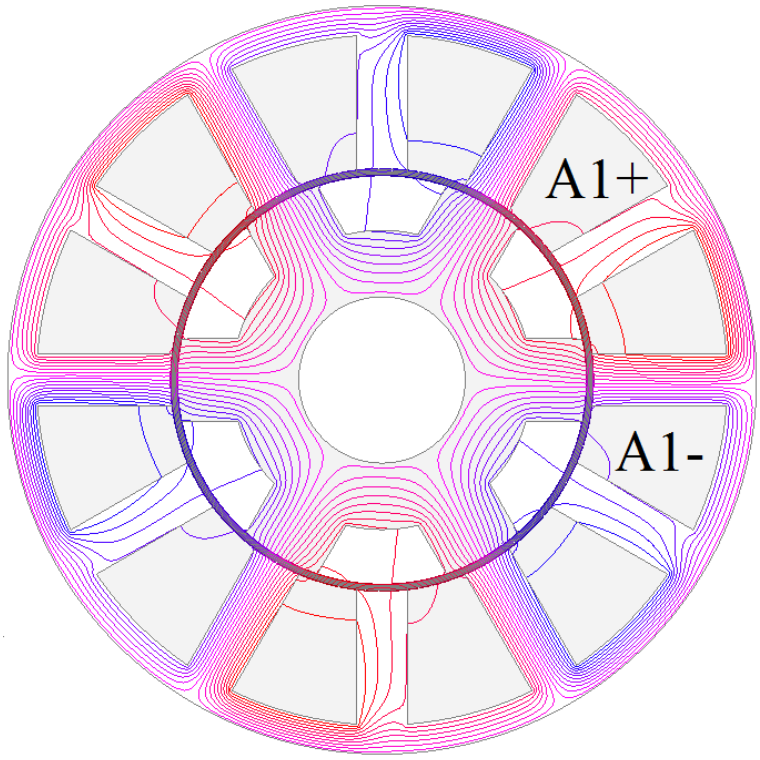

(b)

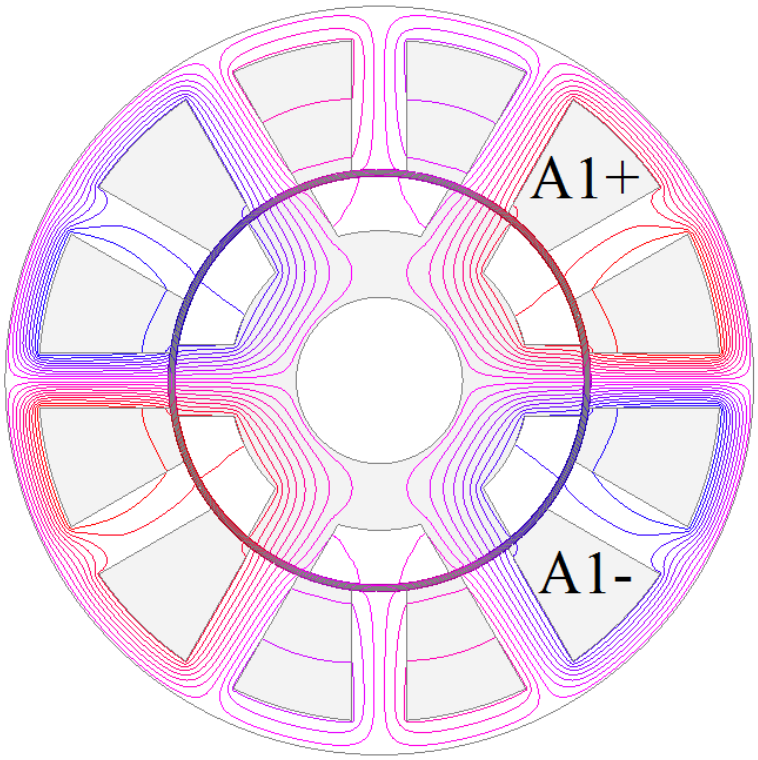

(c)

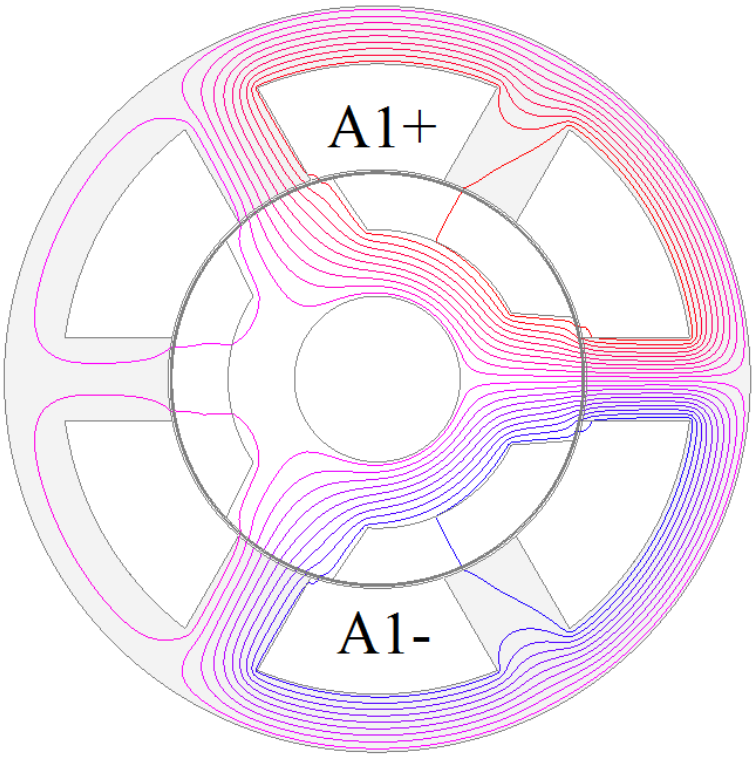

(d)

Fig. 5.15 Flux distributions with field excitation only, maximum flux-linkage with coil A1 (field current=6A). (a) F2A2-4 pole. (b) F2A2-6 pole. (c) F1A3-6 pole. (d) F1A3-3 pole.

5.8.2. Back-EMF

Fig. 5.16 is the 2-D FEA predicted back-EMFs of four WFSF machines with various field currents and different rotor positions at a fixed rotor speed (1000rpm). For the amplitude of back-EMF waveforms under the same rotor speed, the F2A2-6 pole machine is similar to the F1A3-6 pole one, Fig. 5.16 (b) and (c). It can also be seen that for F2A2 machines, the 4-pole machine has larger EMF peak to peak value than the 6-pole one under the same field current. The reason for this is that smaller slot number leads to larger stator pitch and results in less flux leakage, and consequently, larger main flux and larger back-EMF. Similarly, the back-EMF amplitude of F1A3-3 pole machine is larger than that of F1A3-6 pole one. Since all of machines are designed for low-cost applications, BLDC operation, i.e. 180 electric degrees rectangular current waveform, is employed in each machine to reduce the cost in power devices.

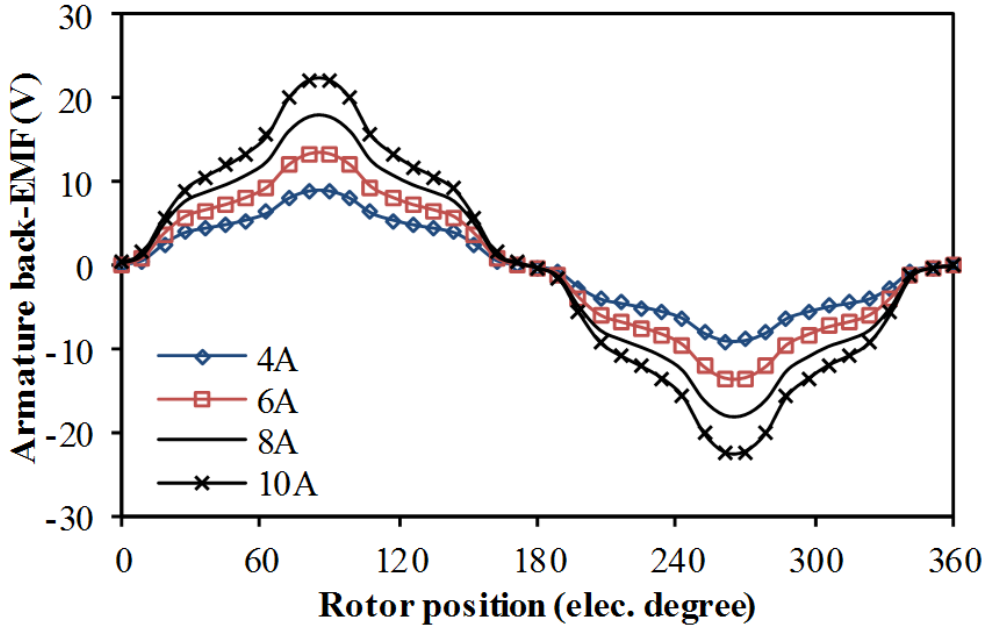
Armature back-EMF (V)
30
20
10
0
-10
-20
-30
0
60
120
180
240
300
360
Rotor position (elec. degree)
4A
6A
8A
10A

(a)

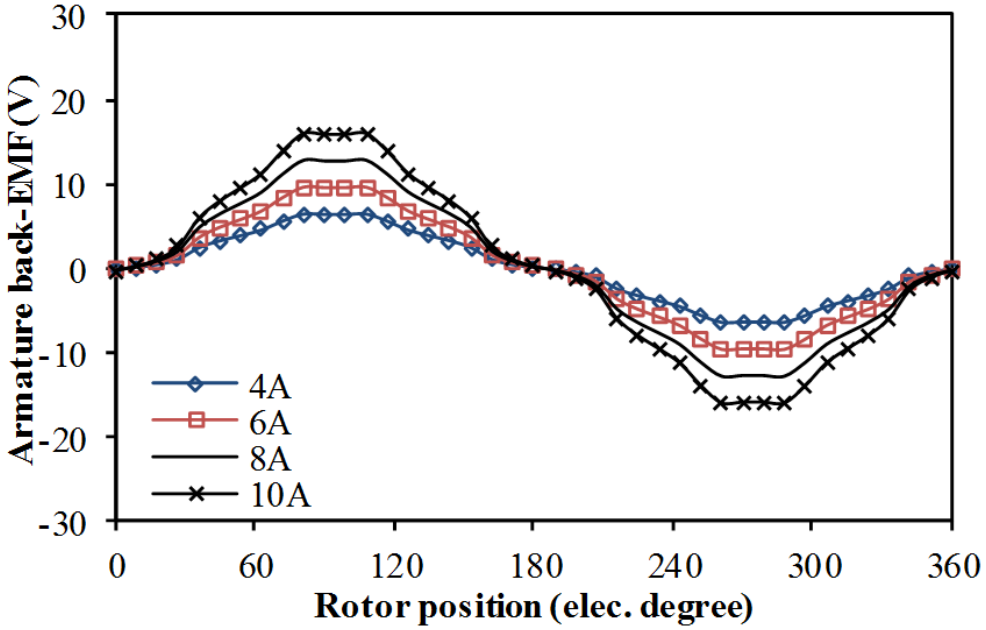
Armature back-EMF (V)
30
20
10
0
-10
-20
-30
0
60
120
180
240
300
360
Rotor position (elec. degree)
4A
6A
8A
10A

(b)

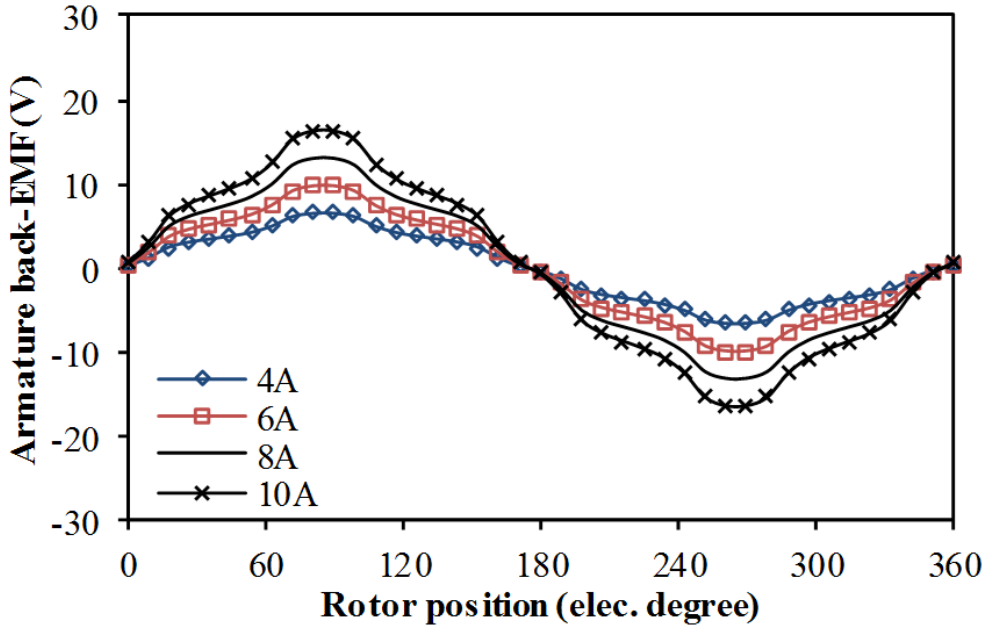

(c)

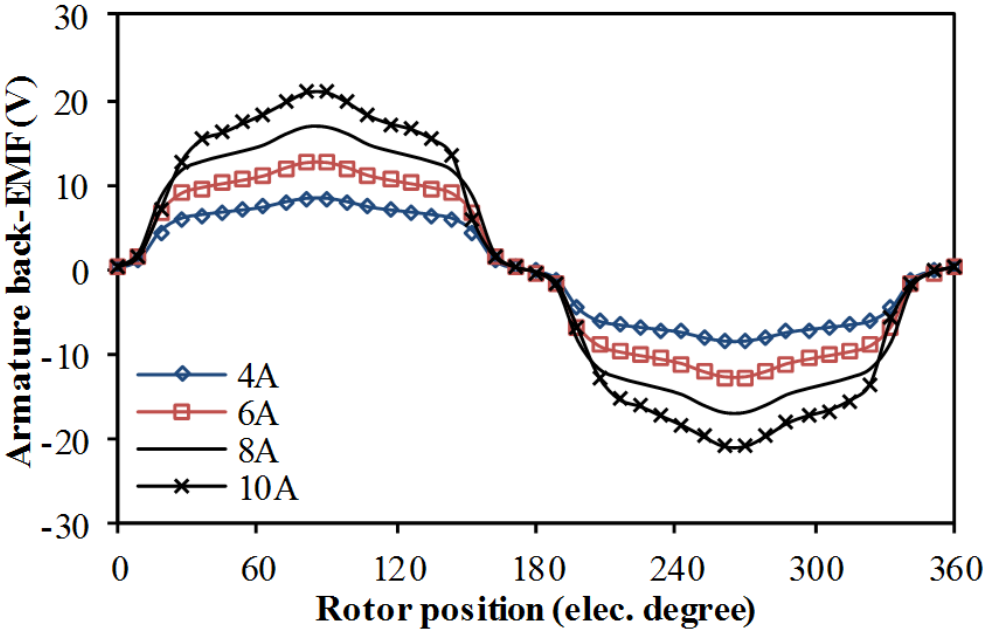

(d)

Fig. 5.16 Armature back-EMF waveforms at various field excitations, 1000rpm. (a) F2A2-4 pole. (b) F2A2-6 pole. (c) F1A3-6 pole. (d) F1A3-3 pole.

5.8.3. Torque Characteristics

When the field currents are fixed to 6A, the static torques of four WFSF machines with various armature currents are shown in Fig. 5.17. When the armature currents are 0A, the curves in the figure represent the cogging torques in those machines. In spite of the fact that

the F1A3-3 pole machine has the highest peak torque compared with other WFSF machines under the same armature current, the flat-tops of its torque waveforms are much narrower than those of the others. This may lead to a significant reduction in the average torque.

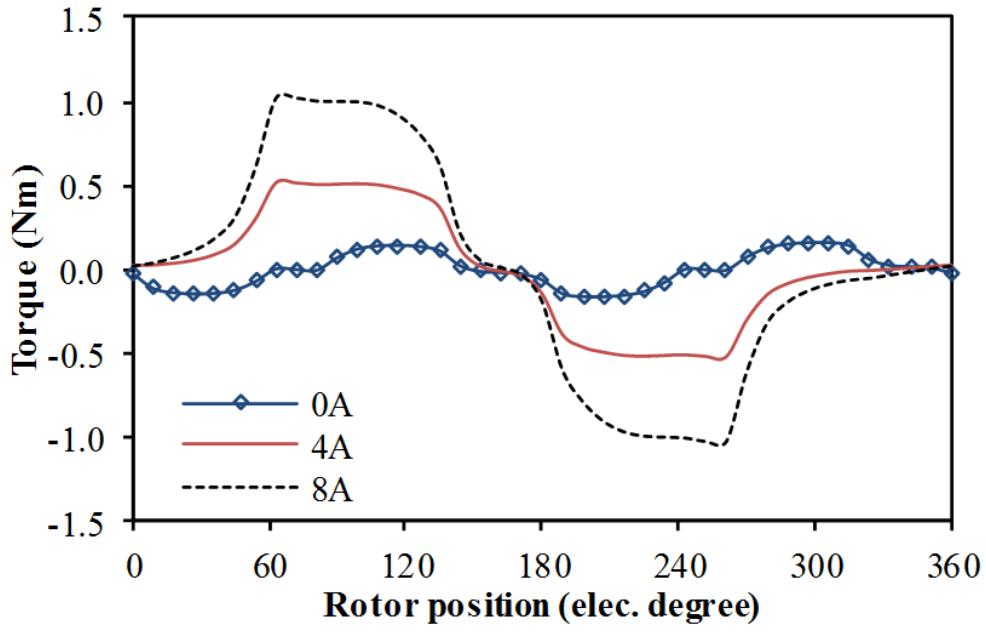

(a)

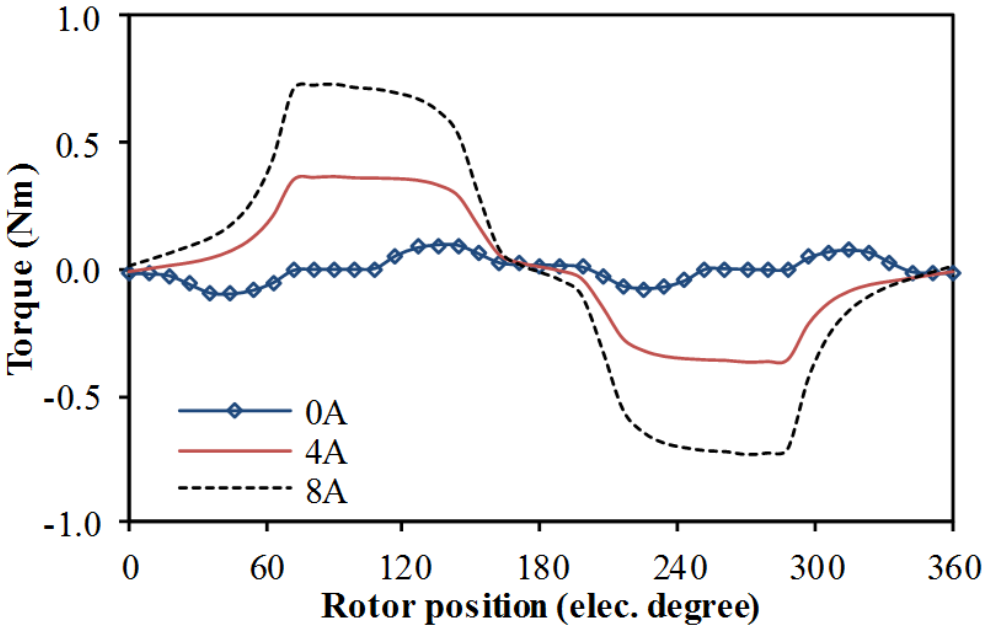

(b)

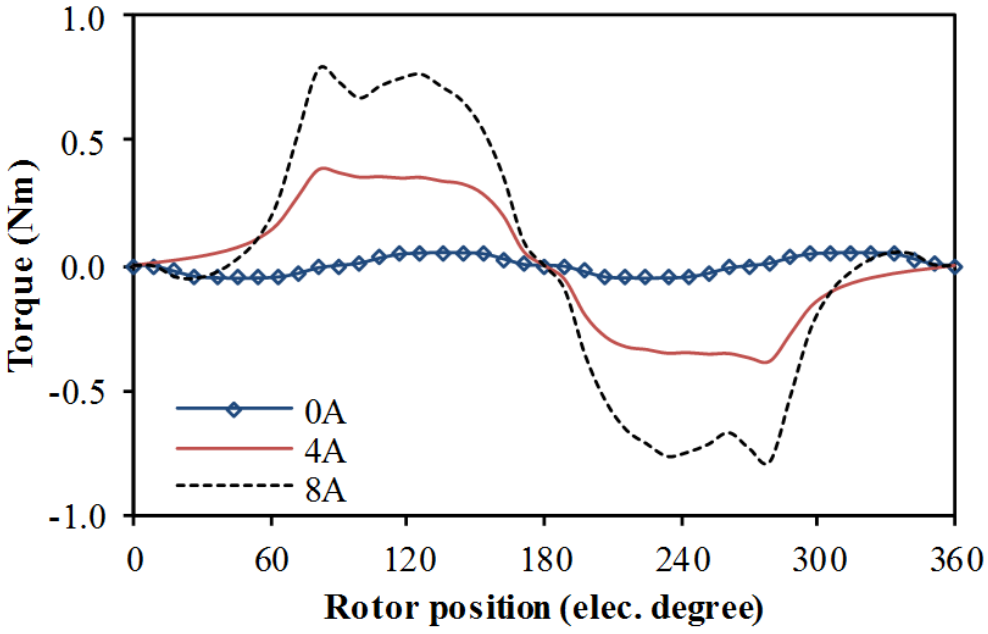

(c)

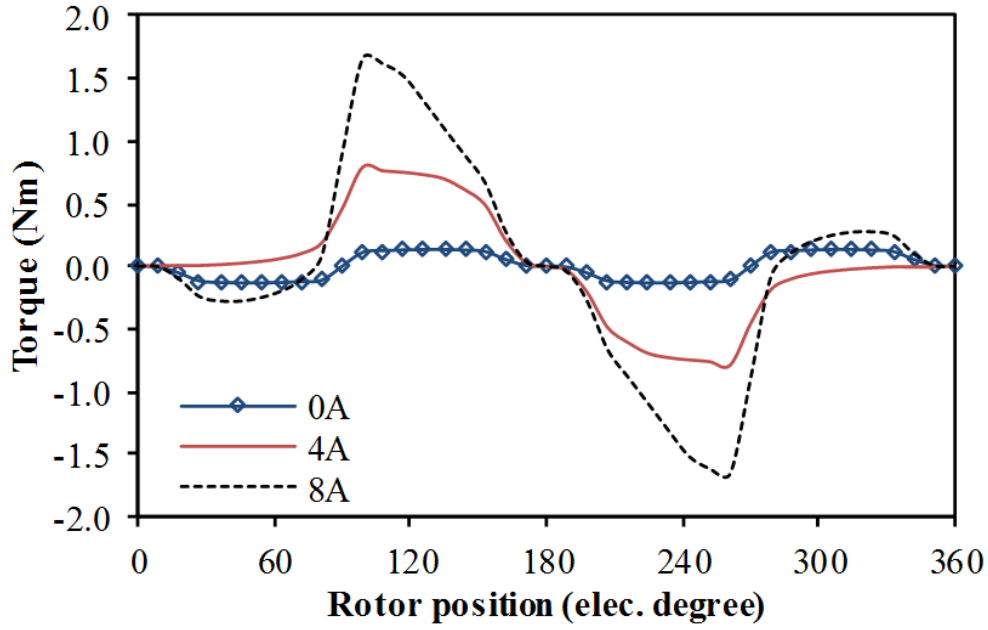

(d)

Fig. 5.17 Torque-rotor position curves for different armature currents with a 6A field current. (a) F2A2-4 pole. (b) F2A2-6 pole. (c) F1A3-6 pole. (d) F1A3-3 pole.

Fig. 5.18 shows the average torque of four WFSF machines for a range of armature and field currents (4A-10A). It can be seen, compared with F2A2 machines, the average torques of F1A3 machines at higher currents are lower since their stators are easily saturated.

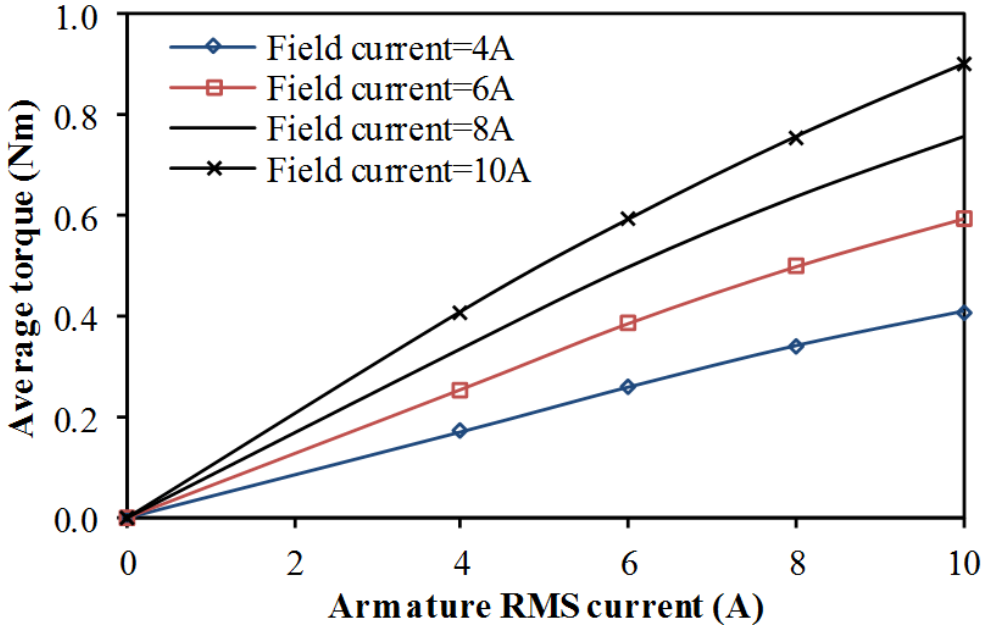
Field current=4A
Field current=6A
Field current=8A
Field current=10A
Average torque (Nm)
Armature RMS current (A)
0.0
0.2
0.4
0.6
0.8
1.0
0
2
4
6
8
10

(a)

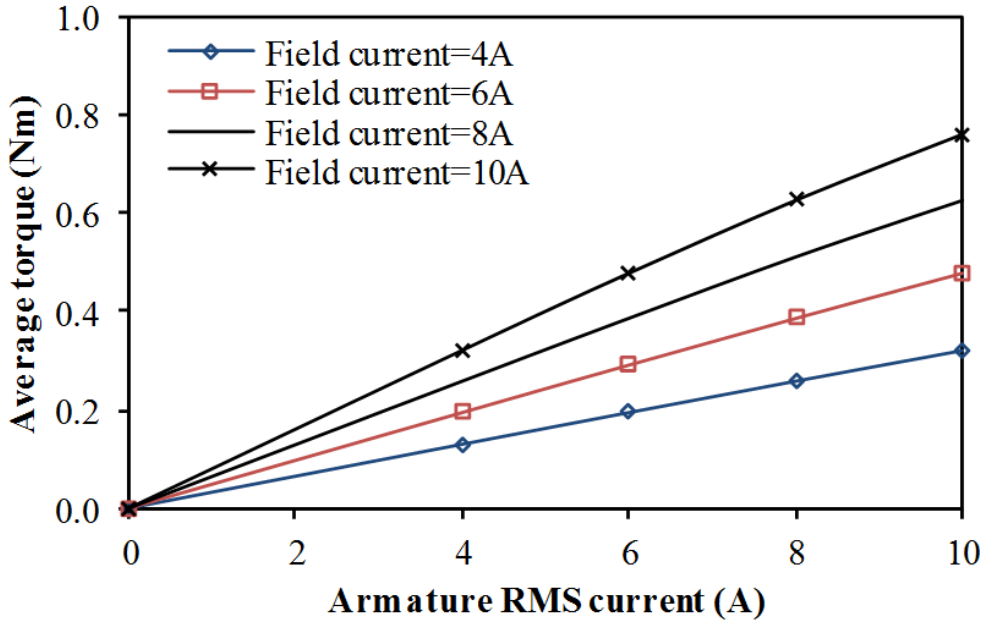
Field current=4A
Field current=6A
Field current=8A
Field current=10A
Average torque (Nm)
Armature RMS current (A)
0.0
0.2
0.4
0.6
0.8
1.0
0
2
4
6
8
10

(b)

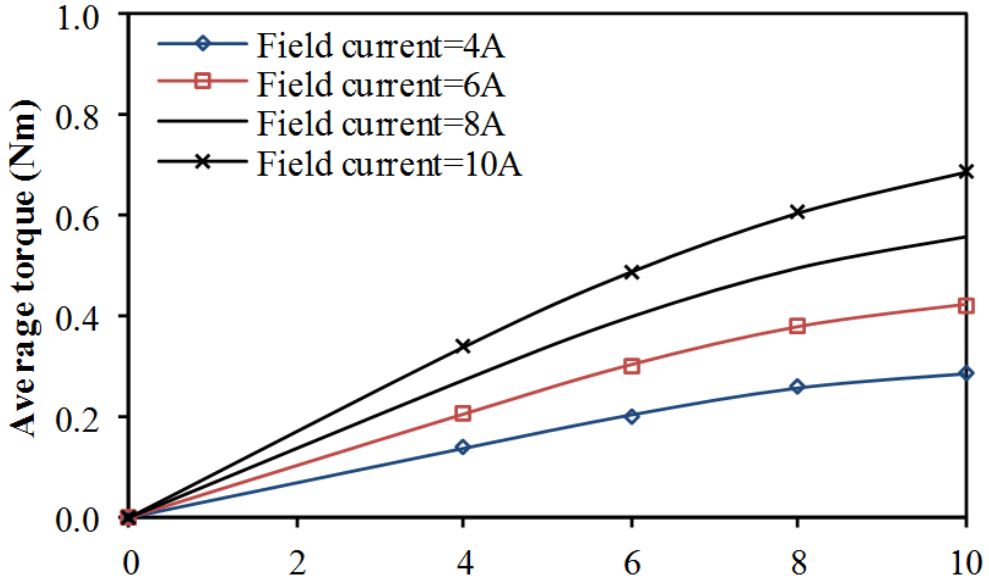

(c)

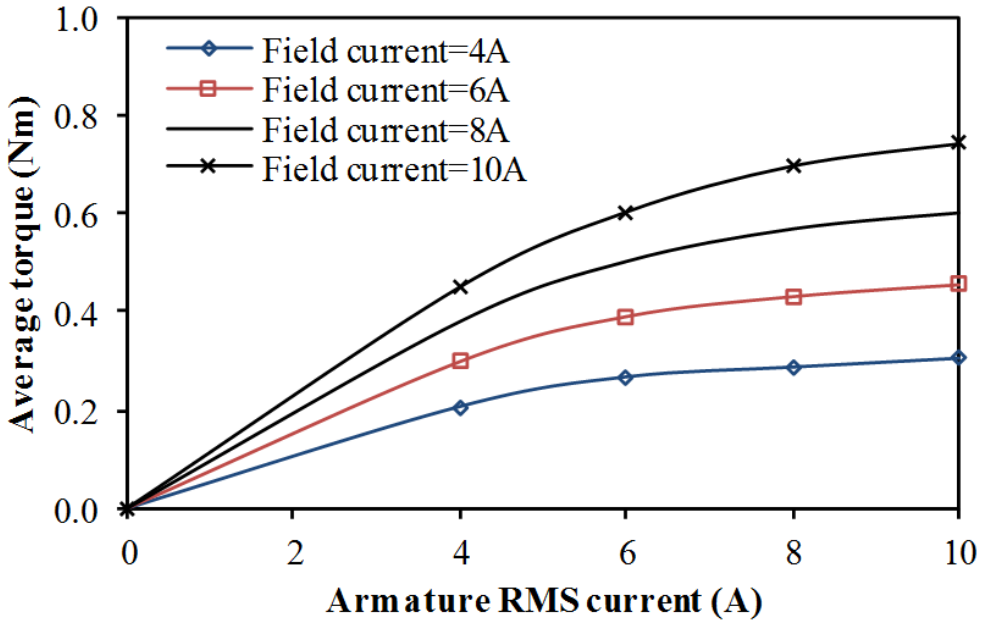

(d)

Fig. 5.18 Torque-current curves for different armature currents with different field current, BLDC operation. (a) F2A2-4 pole. (b) F2A2-6 pole. (c) F1A3-6 pole. (d) F1A3-3 pole.

The comparison of four WFSF machines with various copper losses is shown in Fig. 5.19. Due to its relatively longer end-windings, the F1A3-3 pole machine has the lowest average torque compared with other machines under the same copper loss. It can also be seen that the average torque of two F2A2 machines are similar and higher than that of the F1A3 machines.

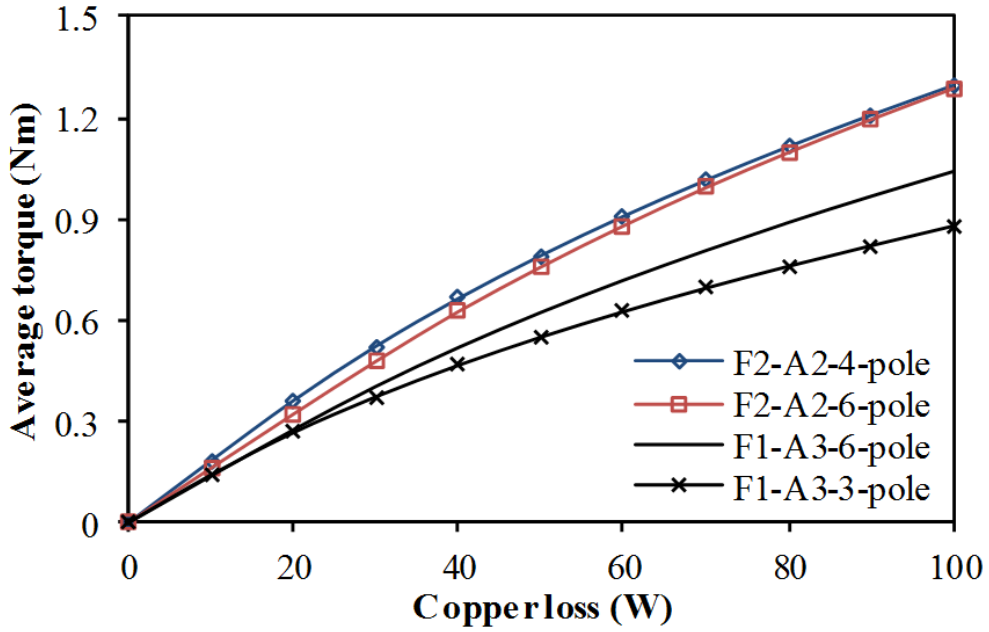

Fig. 5.19 Comparison of torque-copper loss curves, BLDC operation.

According to above investigation, it can be noticed that compared with the F2A2 machines, the F1A3 machines have relatively lower average torque but higher peak torque.

5.8.4. Iron loss

When the rotor speed is the same, the WFSF machine having more rotor poles shows higher frequency and shorter cycle time of flux density variation, consequently, larger iron loss in the lamination [PAN08]. Fig. 5.20 compares the total iron loss of four WFSF machines when the armature current and the field current are fixed. It can be seen that the F1A3-3 pole machine has smallest iron loss among those machines. Compared between two 6-pole machines, the F1A3-6 pole machine has a significantly reduced iron loss. This is benefited from the unchanged flux directions in the stator poles with field coils in F1A3 machines.

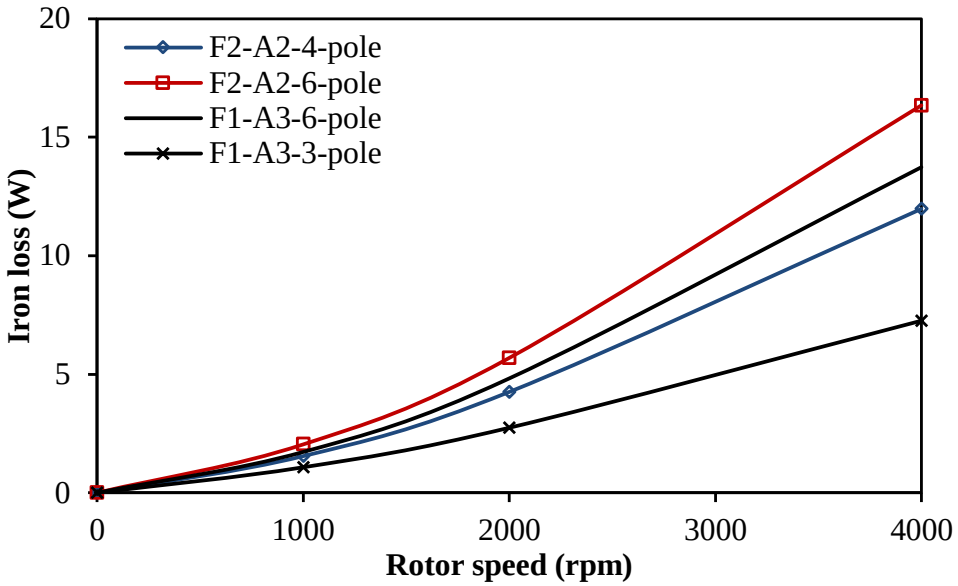

Fig. 5.20 Comparison of stator and rotor iron losses, BLDC operation, armature current=field current=15A.

5.9.Starting torque of machines

The self-starting capability of aforementioned WFSF machines is not taken into consideration. In this section, the self-starting capability of two 6-pole machines will be investigated.

Unlike the rotor with tips that are employed in the conventional F2A2-4 pole machine, the chamfered rotor can be employed in both the F2A2-6 pole and F1A3-6 pole machines to enable machines to avoid the null point in torque waveforms. In order to use the same rotor for these two machines, the rotor pole arc, chamfer angle and chamfer depth are optimized and the optimized topology is shown in Fig. 5.21. It can be seen from Fig. 5.22 that by employing this chamfered rotor, two investigated 6-pole machines have achieved unidirectional torque. For the F2A2-6 pole and F1A3-6 pole machines, their minimum torques are about 12% (0.15Nm) and 15% (0.18Nm) of their peak torques, respectively.

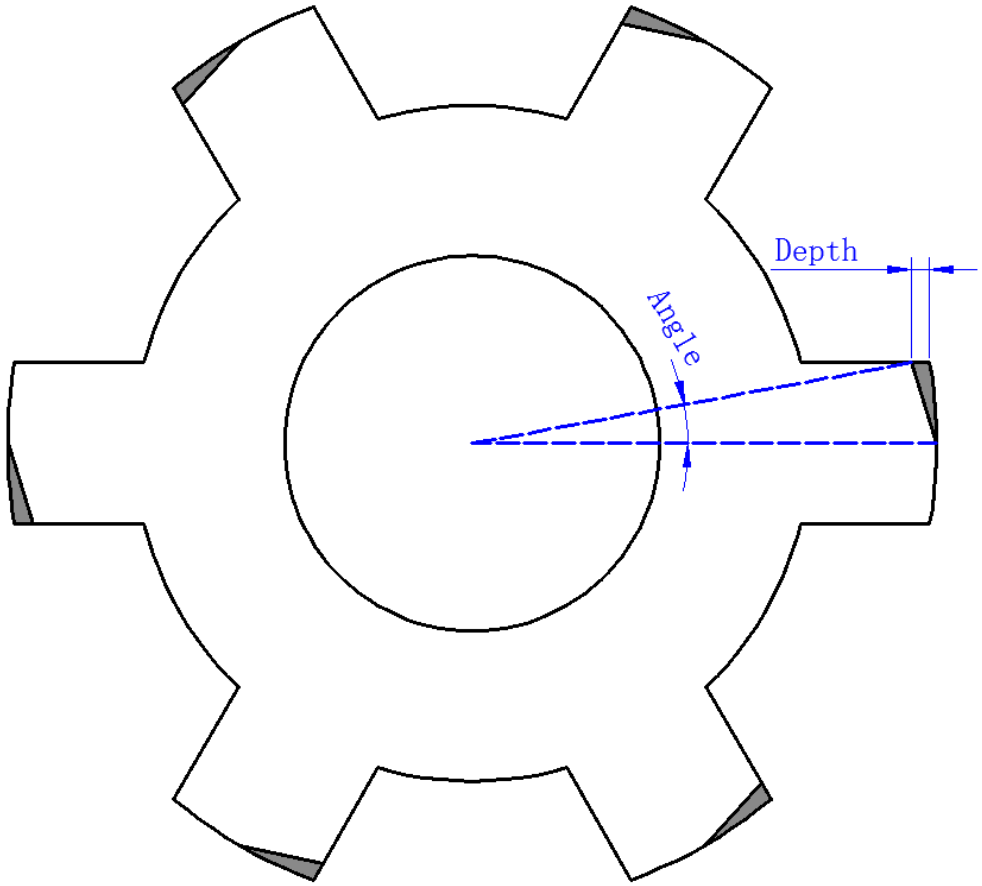

Fig. 5.21 Asymmetric rotor, with pole-arc=24°, and chamfer angle/depth= 12°/1.2mm.

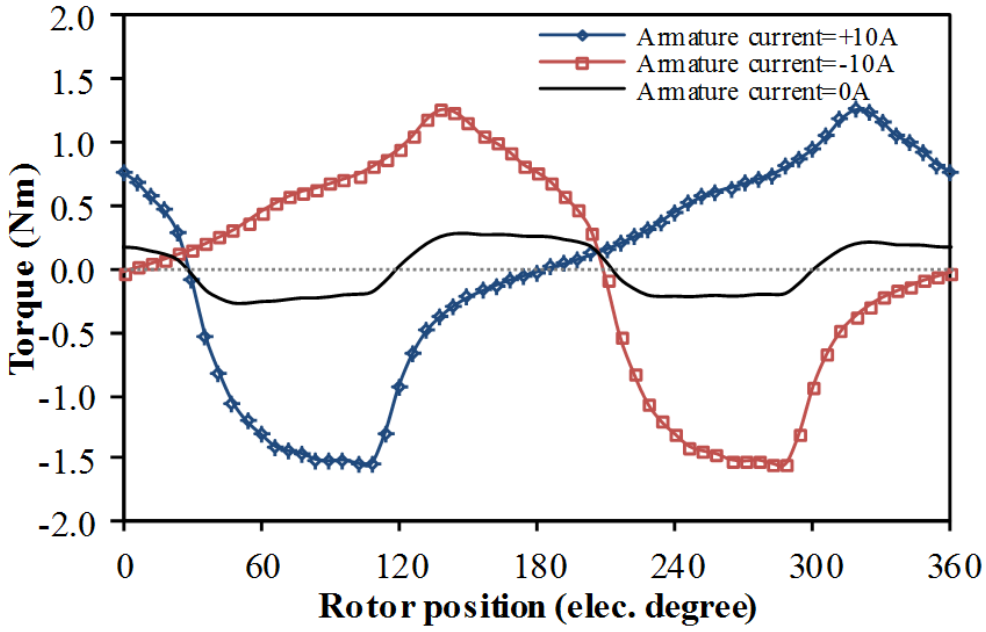

(a)

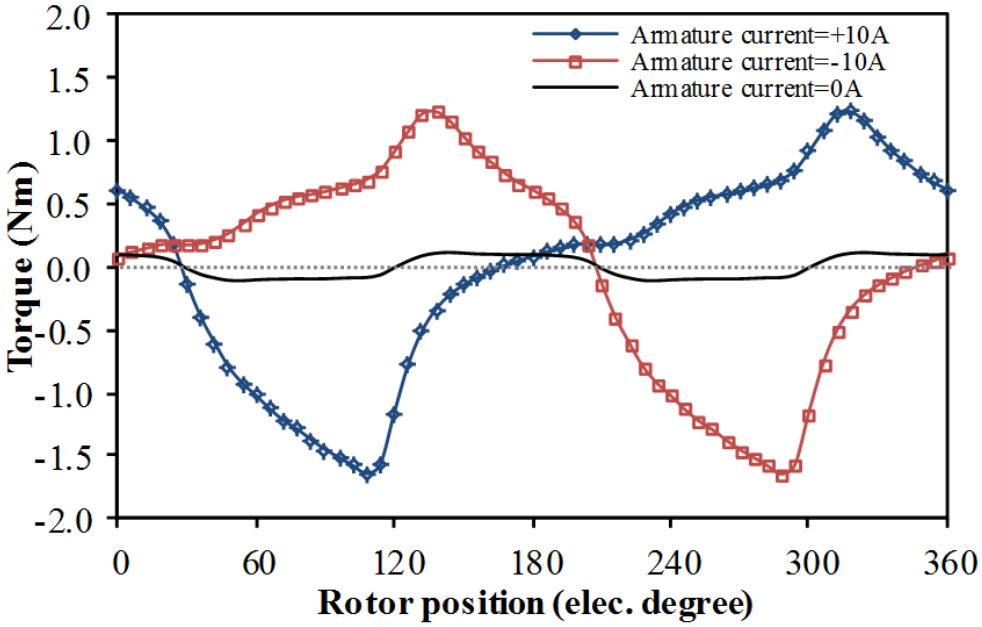

(b)

Fig. 5.22 Static torque-rotor position characteristics with asymmetric rotor, field current=10A. (a) F2A2-6 pole. (b) F1A3-6 pole.

5.10. Experimental validation

For the validation of the FEA predictions, the stators of foregoing mentioned two 6-pole machines (F2A2-6 pole machine and F1A3-6 pole machine) and a common rotor have been prototyped, Fig. 5.23. It is worth mentioning that the laminations of two stators are exactly the same, and this means that both the time and cost of prototype manufacture can be saved.

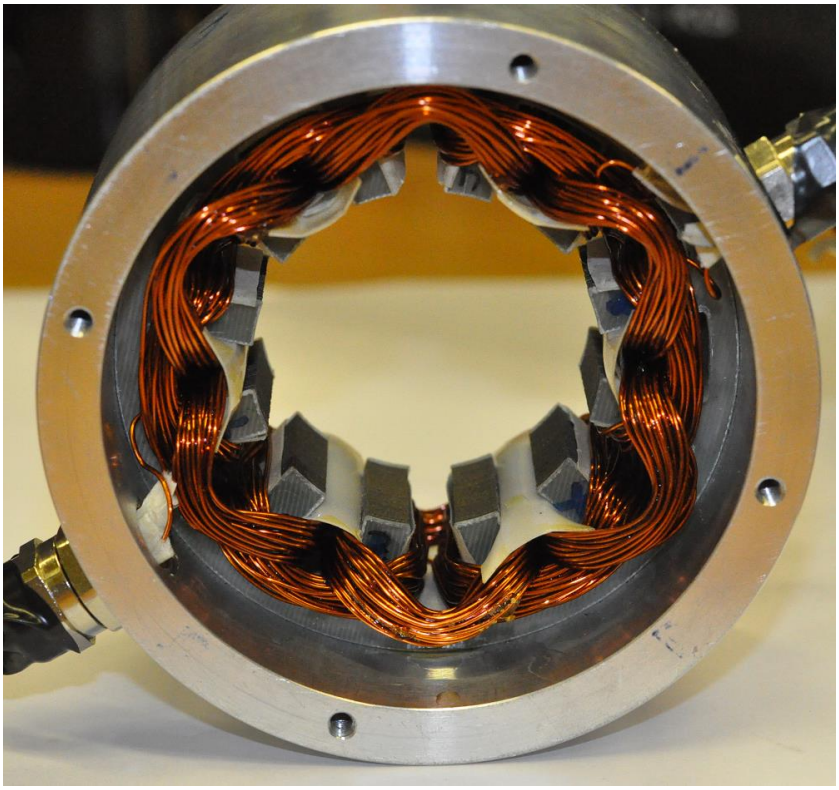

(a)

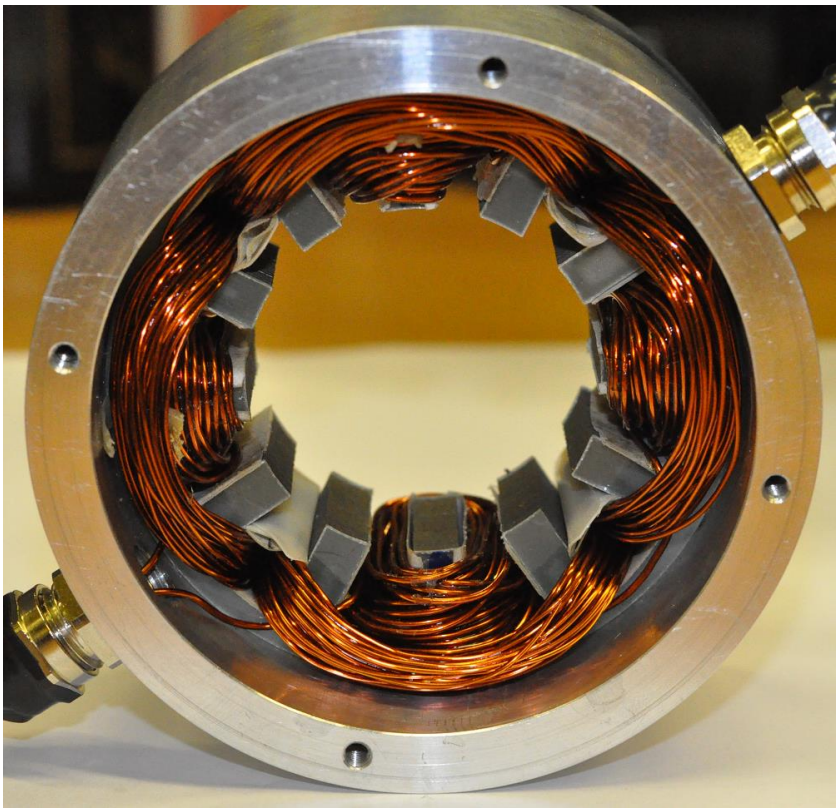

(b)

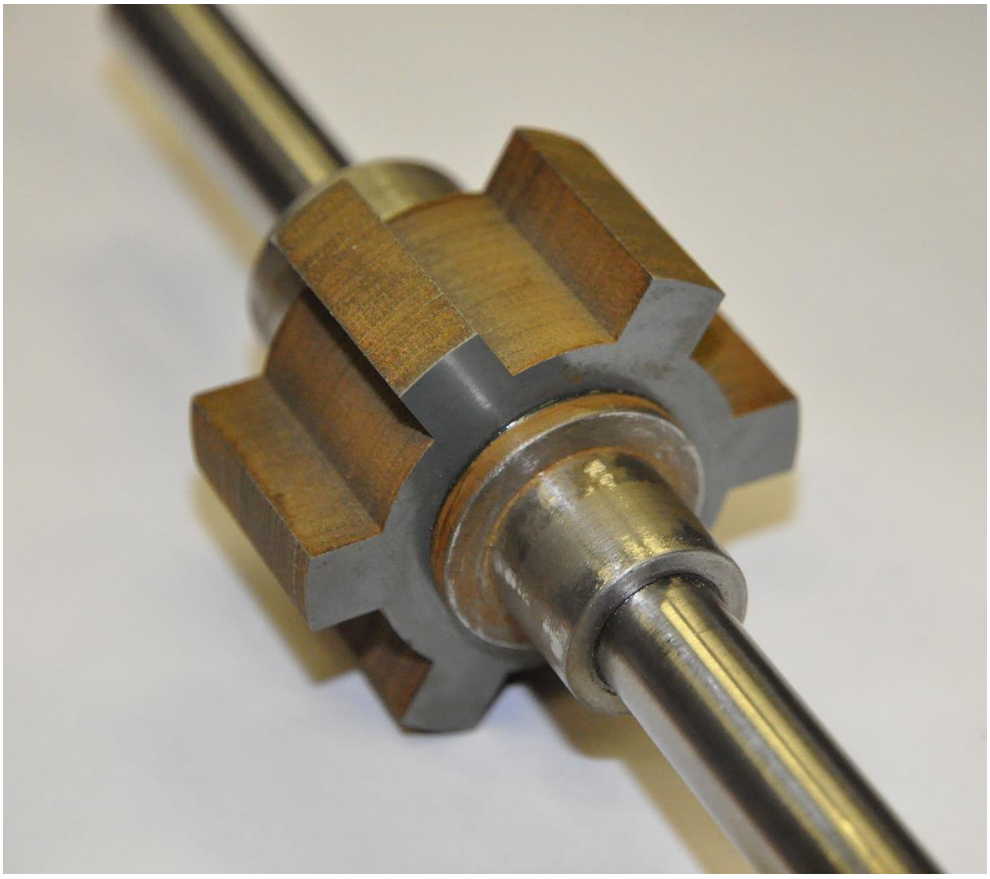

(c)

Fig. 5.23 Prototypes of WFSF machines. (a) stator of F2A2-6 pole machine, (b) stator of F1A3-6 pole machine, (c) common 6-pole rotor.

The screenshots of measured armature back-EMFs of two 6-pole machines are shown in Fig. 5.24. In two machines, the field currents (I-f) maintained 5A and were excited from a DC power supply.

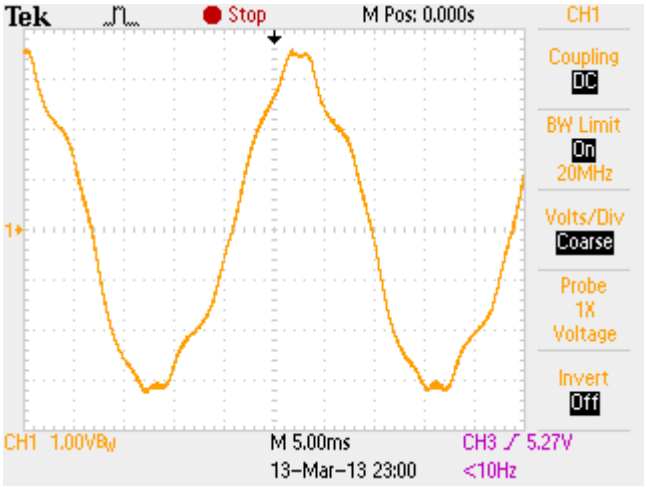

(a)

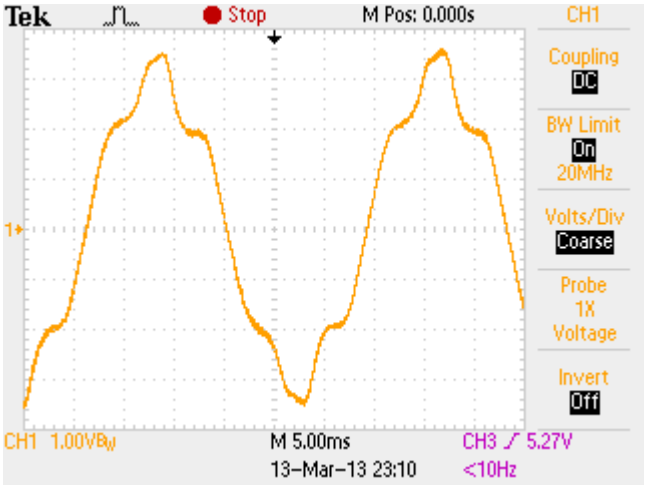

(b)

Fig. 5.24 Experimental back-EMF waveforms, field current= 5A. (a) F2A2-6 pole machine, 358.2rpm. (b) F1A3-6 pole machine, 356.6rpm.

The predicted and measured armature back-EMF waveforms of two 6-pole machines at two different field excitations (4A and 6A) are compared in Fig. 5.25. For both machines, there is good agreement between predicted and measured results except that the measured back-EMF peak value is slightly smaller than the predicted value. Such differences can be observed at different field excitations and ignoring the end-effects is mainly responsible for this [ZHU07].

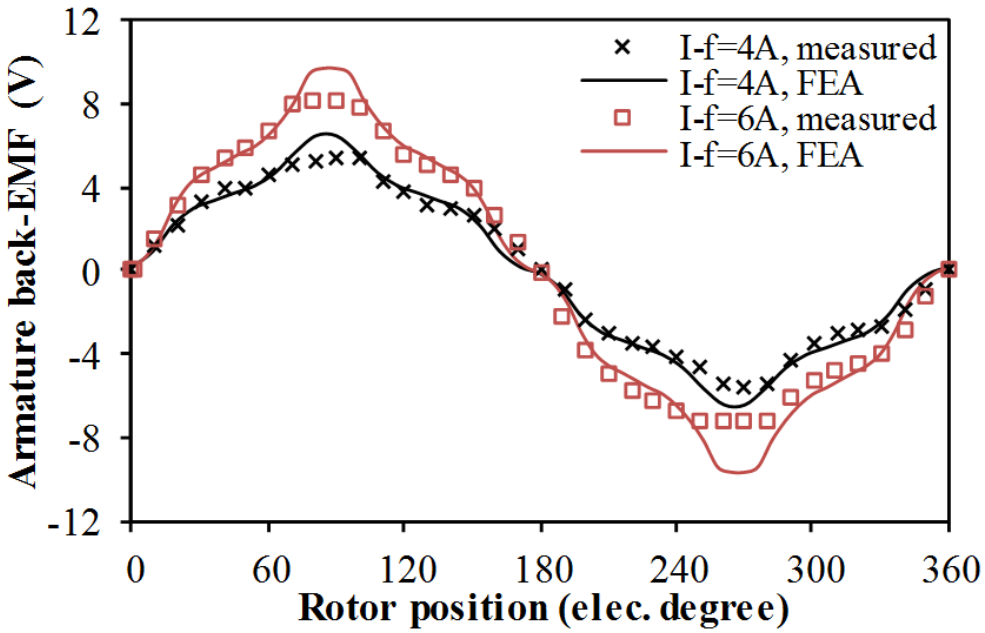

(a)

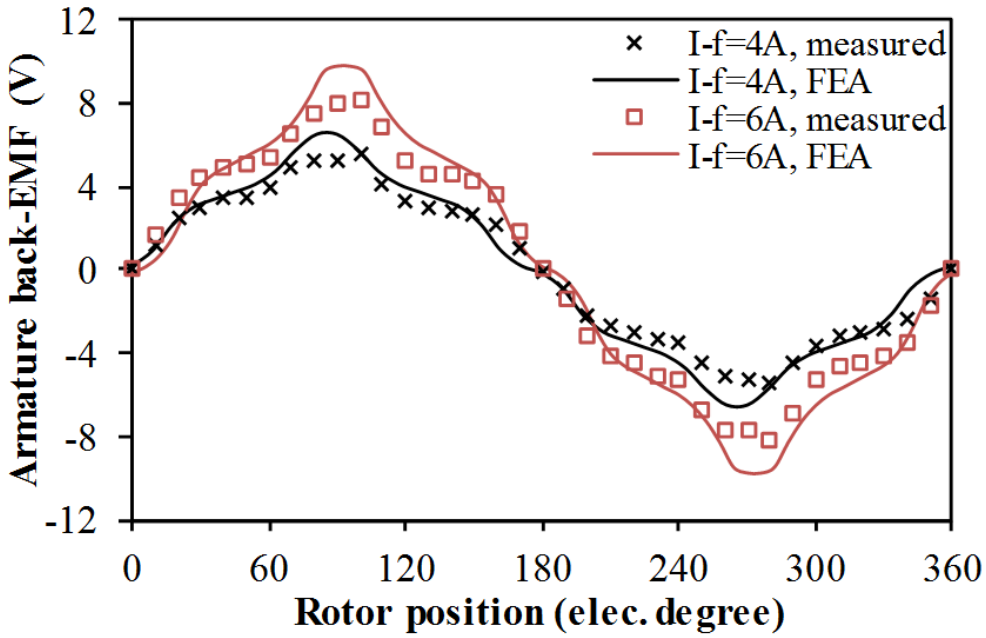

(b)

Fig. 5.25 Back-EMF waveforms, 1000rpm. (a) F2A2-6 pole machine, (b) F1A3-6 pole machine.

When the armature current (I-a) is 0A, the cogging torque waveforms under different field currents are measured and have been compared with the FEA predictions. Fig. 5.26 (a) and Fig. 5.26 (b) show the cogging torque waveforms of F2A2-6 pole machine and F1A3-6 pole machine, respectively. Due to the mechanical tolerance which usually increases the cogging torque, there is a slight difference between measured and FEA predicted cogging torque waveforms. But overall, good agreement has been achieved.

The static torque waveforms with various field currents and armature currents (4A and 6A) of F2A2-6 pole machine and F1A3-6 pole machine are shown in Fig. 5.26 (c) and Fig. 5.26 (d), respectively. It can be seen that under the same armature current, the F1A3-6 pole machine shows slightly higher peak to peak torque than the F2A2-6 pole machine. It should be noticed that when the armature currents and field currents of both machines are 6A, the field slot current density and armature slot current density of the F2A2-6 pole machine are all 5.3A/mm^2 (copper loss=19.6W). For the F1A3-6 pole machine, the field slot current density and armature slot current density are 4A/mm^2 and 8A/mm^2, respectively (copper loss=24.7W). The measured results show generally good agreement with the predicted results.

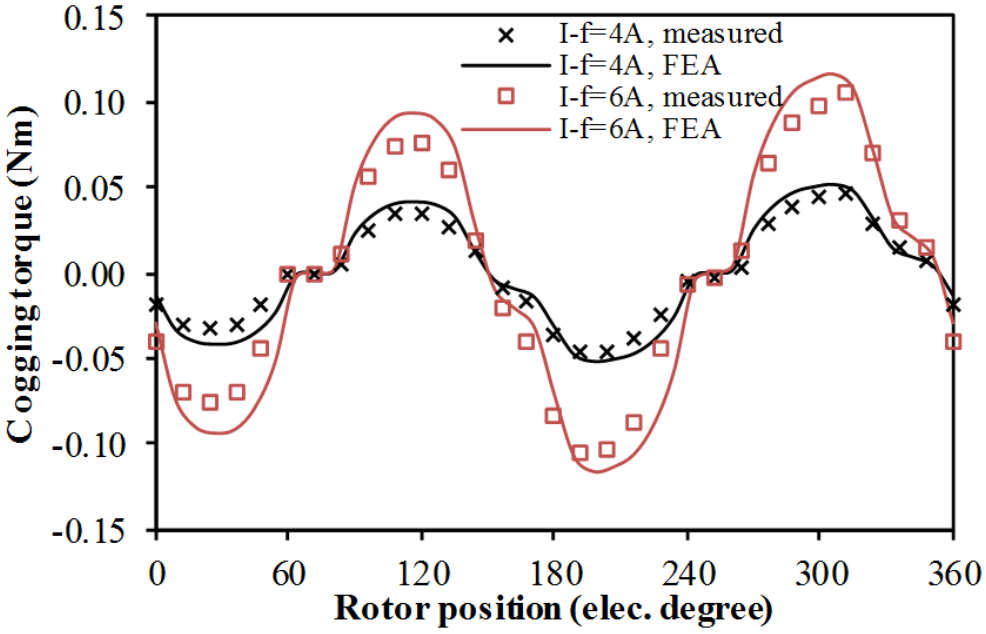
0.15
0.10
0.05
0.00
-0.05
-0.10
-0.15
Cogging torque (Nm)
0
60
120
180
240
300
360
Rotor position (elec. degree)
I-f=4A, measured
I-f=4A, FEA
I-f=6A, measured
I-f=6A, FEA

(a)

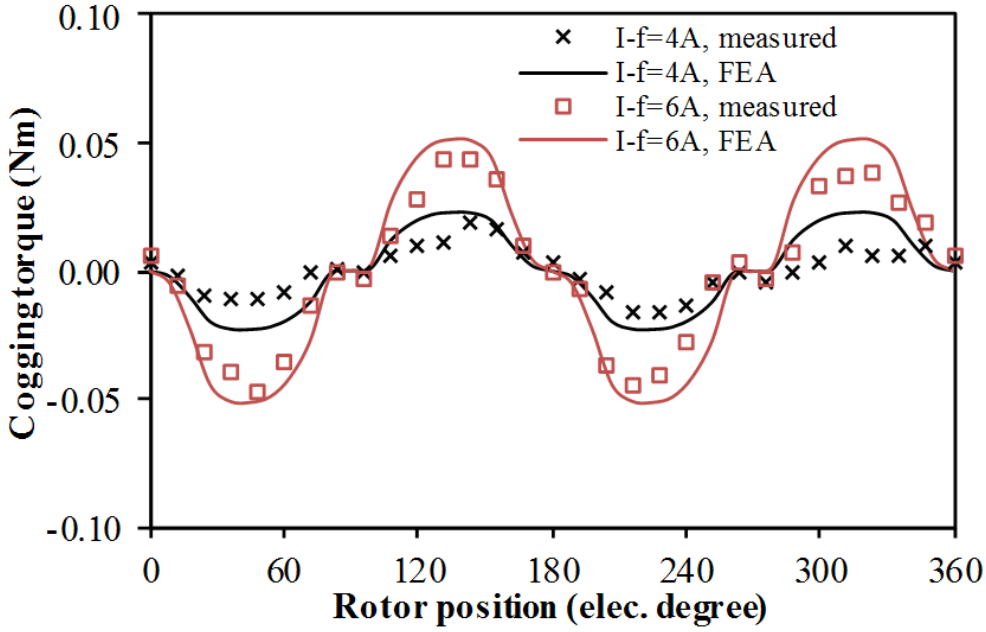
0.10
0.05
0.00
-0.05
-0.10
Cogging torque (Nm)
0
60
120
180
240
300
360
Rotor position (elec. degree)
I-f=4A, measured
I-f=4A, FEA
I-f=6A, measured
I-f=6A, FEA

(b)

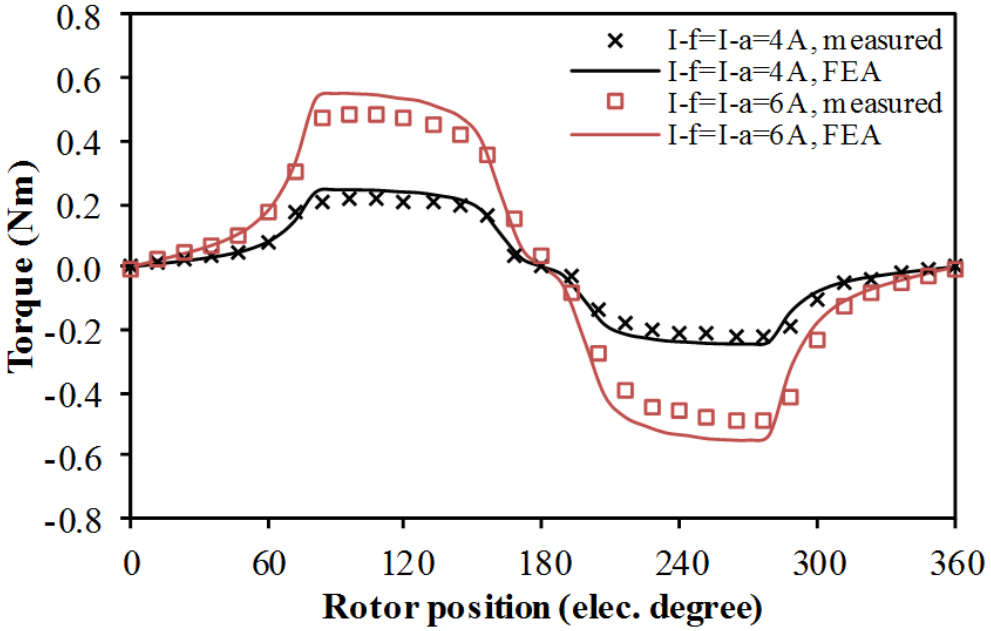

(c)

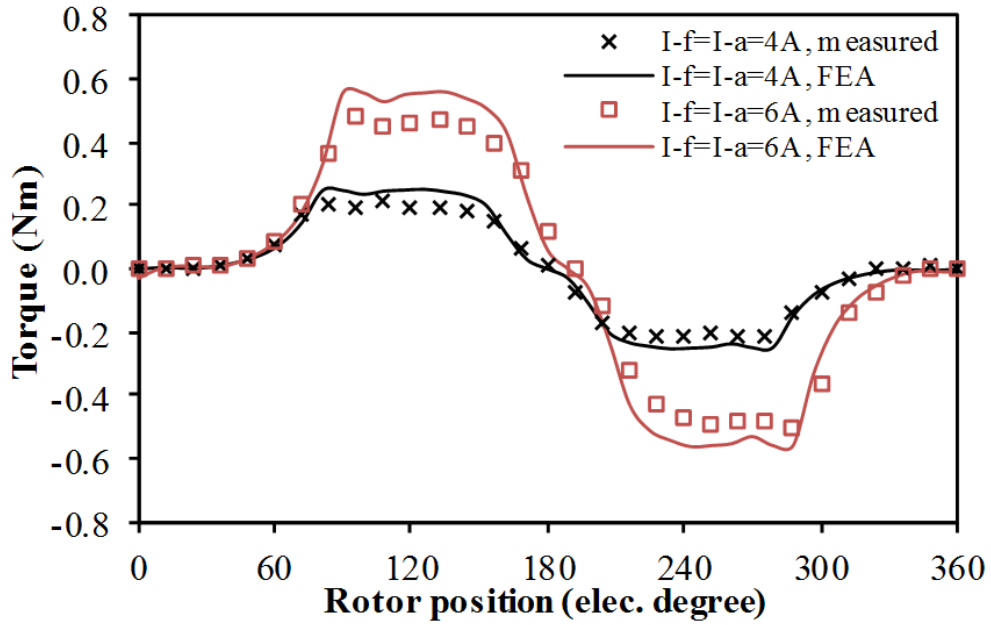

(d)

Fig. 5.26 Cogging torque and static torque waveforms with various field current and armature current. (a) cogging torque, F2A2-6 pole machine, (b) cogging torque, F1A3-6 pole machine, (c) static torque, F2A2-6 pole machine, (d) static torque, F1A3-6 pole machine.

5.11. Summary

Two types of low-cost single-phase wound field switched flux machines with DC field and AC armature windings having the same coil-pitch of 2 slot-pitches and having different coil-

pitches of 1 slot-pitch and 3 slot-pitches, respectively, are compared in this chapter. The back-EMF, cogging torque, static torque with different field and armature currents of two 6-pole machines have been validated by experiments on the prototype machines.

Compared with the F2A2-4 pole WFSF machine, the F2A2-6 pole WFSF machine shows the similar average torque when the copper loss is fixed but shorter end-windings, and consequently, better copper usage efficiency for applications requiring short axial length.

The F1A3-6 pole machine can share the same stator topology with F2A2-6 pole machine and has even shorter end-windings and smaller iron loss.

The slot number and pole number of F1A3-6 pole machine can be halved and result in a F1A3-3 pole machine. Compared with the F2A2-4 pole machine, this machine shows significantly reduced iron loss.

CHAPTER VI. NON-OVERLAPPING STATOR WOUND FIELD SYNCHRONOUS MACHINES

Three-phase non-overlapping stator wound field synchronous (NSWFS) machines having salient-pole rotors are systematically investigated in this chapter. The influence of stator slot and rotor pole number combinations of the NSWFS machines is investigated based on the optimised designs. According to two-dimensional (2-D) finite element analysis (FEA), it is found that the NSWFS machine exhibits higher torque density and lower torque ripple than the non-overlapping segmented rotor NSWFS (SNSWFS) machine. Additionally, the influences of unequal slot and step-skew angle on the torque density enhancement and torque ripple suppression are investigated in the NSWFS machines, respectively. The FEA predicted back-EMF, cogging torque, and static torque of NSWFS machines are validated by experiments on the prototype machines.

6.1.Introduction

Although rare-earth permanent magnet (PM) machines exhibit high torque density and high efficiency, the high price of rare-earth PMs may prevent them to be applied to some cost sensitive applications, such as domestic appliances. How to reduce/avoid the usage of PMs in the electrical machines without tremendous sacrifice of electromagnetic performance becomes a research hotspot recently. The stator wound field synchronous (SWFS) machines, which are PM-free, show the advantages of easy thermal management and simple rotor structure without employing the brushes/slip rings as in the conventional rotor wound field synchronous machines. Consequently, high torque density and high rotor speed may be achieved. Recently, most investigations on the SWFS machines focus on the wound field switched flux (WFSF) machines and variable flux reluctance (VFR) machines [POL99], [POL06], [CHE10b], [ZUL10], [SUL11], [SUL12], [TAN13], [GAU13], [ZHO14], [ZHO14b], [KHA14], [FUK12], and [LIU13]. The WFSF machines are based on switched flux principle which was firstly proposed in 1955 [RAU55]. Meanwhile, the VFR machines have been developed from a split-coil switched reluctance machine proposed in 1988 [PUL88].

In 1999, a single-phase WFSF machine with field and armature coil pitches of 2 slot-pitches is proposed for low-cost applications [POL99]. This machine shows higher efficiency

than an induction machine [POL06]. Further, the three-phase version of this machine has been proposed and widely investigated [CHE10b], [ZUL10], [SUL11], [SUL12], [TAN13], and [GAU13], as shown in Fig. 6.1. It is found that this machine can achieve higher material usage efficiency (torque/material cost) than a switched flux PM machine. However, the torque density of this machine is relatively low and limited by magnetic saturation. Therefore, in order to increase the torque density, a WFSF machine with field and armature coil pitches of 1 slot-pitch and 3 slot-pitches respectively has been proposed [ZHO14], [ZHO14b], as shown in Fig. 6.2. Compared with the switched reluctance machine, this machine exhibits higher torque density and higher power factor. Nevertheless, the aforementioned WFSF machines are all overlapping winding machines, which may lead to longer end-windings, larger axial machine length, increased copper usage and manufacturing cost.

The VFR machines exhibit relatively short end-windings with concentrated windings [FUK12], [LIU13], as shown in Fig. 6.3. However, the non-overlapping armature and field windings of this machine are wound on the same stator poles, which results in reduced slot areas for the armature winding and thus increased copper loss and reduced efficiency.

The segmented rotor WFSF machine, which is designated as a segmented rotor non-overlapping stator wound field synchronous (SNSWFS) machine, shows the advantages of easy manufacture and short end-windings since alternate armature and field coils are wound separately on the stator teeth, as shown in Fig. 6.4. However, the segmented rotor cannot be easily fabricated, whilst the torque density of this machine topology is low due to the special rotor structure since rotor segments restrict the flux paths in this machine and these segments are highly saturated during the loaded operation [ZUL10]. In order to increase the torque density of the SNSWFS machine, a conventional salient-pole rotor may be employed. In [KHA14], the segmented rotor is replaced by the salient-pole rotor in this machine topology having 24/10, 24/14, 24/16, 24/20 and 24/22 stator slot/rotor pole combinations, but there is no obvious torque increase due to inappropriate polarities of field excitations (the polarities of adjacent field coils are of opposite direction), Fig. 6.5.

In this chapter, novel non-overlapping stator wound field synchronous (NSWSF) machines employing salient-pole rotors, as shown in Fig. 6.6, will be systematically investigated. As can be seen, unlike the SNSWFS machine, the polarities of the field coils in this machine are all of the same direction. The stator slot and rotor pole number combinations of the NSWFS machine are investigated in this chapter. It is found by the two-dimensional (2-D) finite element analysis (FEA) that this machine topology shows much higher torque density than

the SNSWFS machine and also that in [KHA14], whilst small torque ripple can be achieved by selecting the appropriate stator slot/rotor pole number combinations.

In this chapter, the 6-slot NSWFS machines will be investigated firstly, followed by a comparison with an optimized SNSWFS machine. Then, the comparisons will be made between 12-slot NSWFS machines having different poles. Finally, easy manufactured 2-step skewing rotors will be employed in the 12-slot NSWFS machines to reduce the torque ripples. The back-EMFs, cogging torques, and static torques of the 6- and 12-slot NSWFS machines predicted by FEA will be validated by experiments.

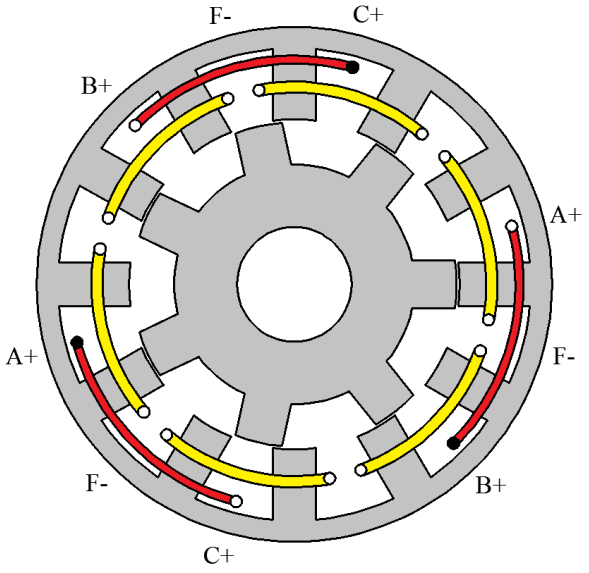

Fig. 6.1. Cross-section of 3-phase WFSF machine field coil=armature coil=2 slot-pitches, 12-slot/7-pole.

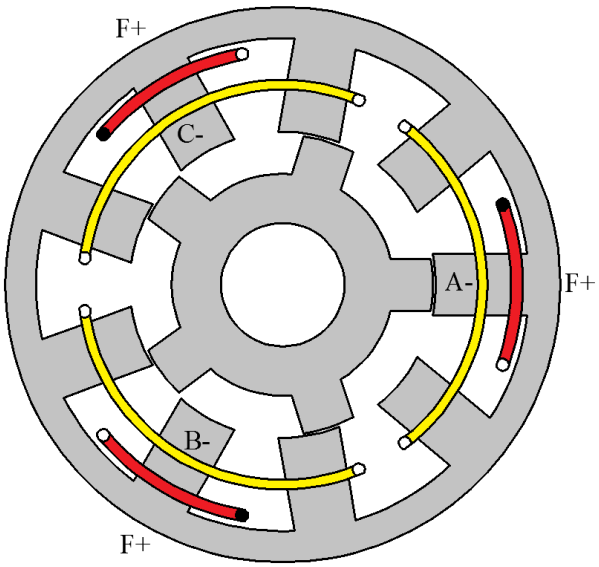

Fig. 6.2. Cross-section of 3-phase WFSF machine, field coil=1 slot-pitch, armature coil=3 slot-pitches, 9-slot/5-pole.

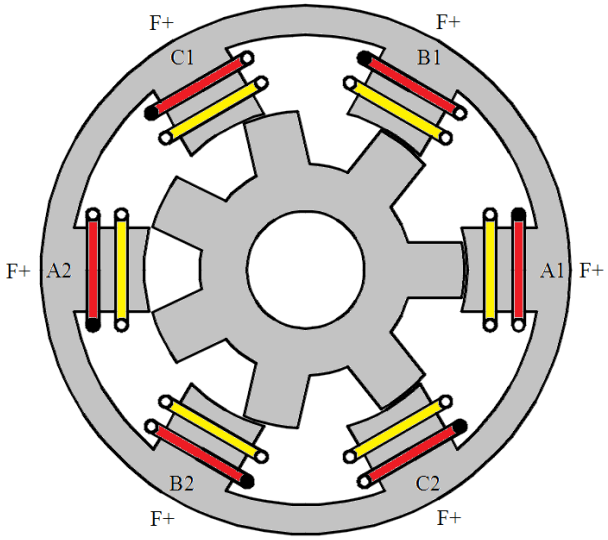

Fig. 6.3. Cross-section of 3-phase VFR machine, 6-slot/7-pole.

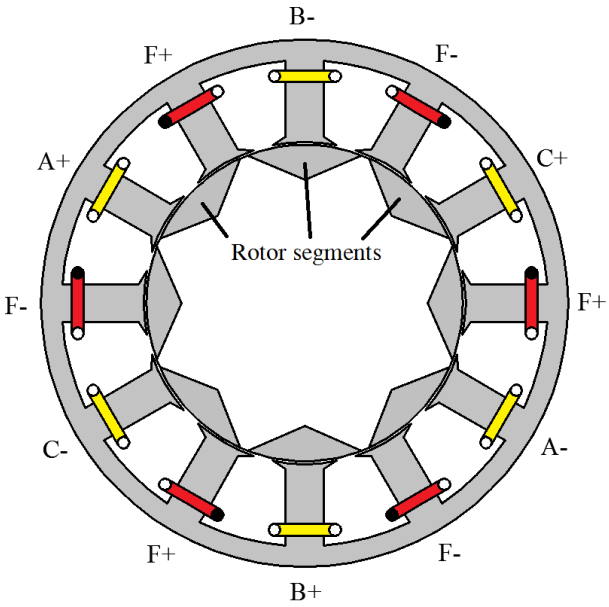

Fig. 6.4. Cross-section of 3-phase SNSWFS machine with segmented rotor, 12-slot/8-pole.

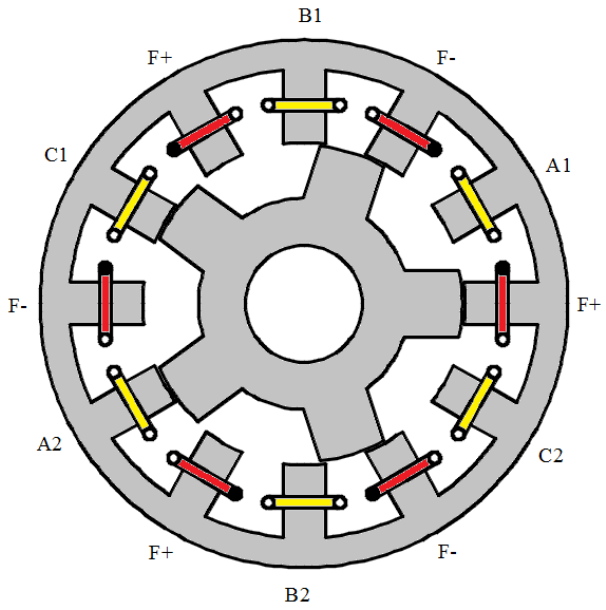

Fig. 6.5. Cross-section of 3-phase NSWFS-AP machine, 12-slot/5-pole.

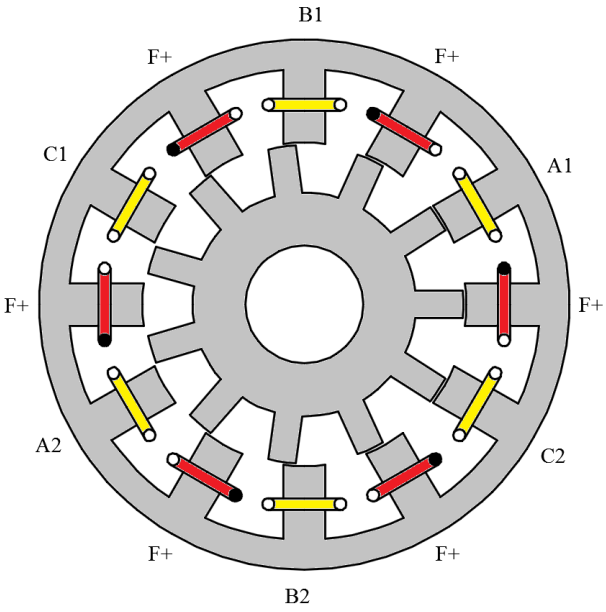

Fig. 6.6. Cross-section of proposed 3-phase NSWFS machine, 12-slot/11-pole.

A comparison is made between the torque capabilities of machine topology which has alternate field coil polarities (NSWFS-AP) as shown in Fig. 6.5 and the proposed NSWFS in which all field coils have the same polarities, shown in Fig. 6.6. According to the investigation in [KHA14], the 12-slot/5-pole NSWFS-AP machine should have the highest torque density among the 12-slot NSWFS machine-AP machines. Thus, the comparison will be made between a 12-slot/5-pole NSWFS-AP machine and a proposed 12-slot/11-pole NSWFS machine of the same size (stator outer radius=45mm, axial length=25mm, air-gap

length=0.5mm). These two machines have been optimized to achieve the maximum average torques under the constraint of 60W copper loss. As can been seen in Fig. 6.7, the torque density of the NSWFS-AP machine is much lower than that of the proposed NSWFS machine. The reason is that inappropriate polarities of field excitations in the NSWFS-AP machine lead to much higher flux leakage than that of the proposed NSWFS machine, as shown in Fig. 6.8. Moreover, the 6-slot topologies are invalid to the NSWFS-AP machines. Therefore, more benefits will be obtained by employing field coils with identical polarities in the NSWFS machine with salient-pole rotor. The investigations in this chapter are focused on the proposed NSWFS machines.

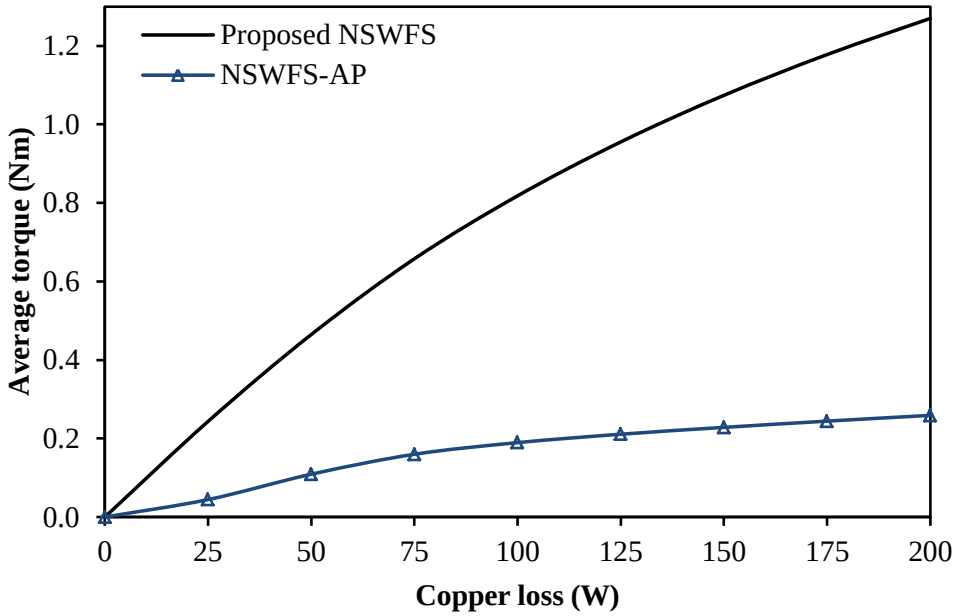

Fig. 6.7. Comparison of average torque-copper loss curves of the proposed NSWFS and NSWFS-AP machines.

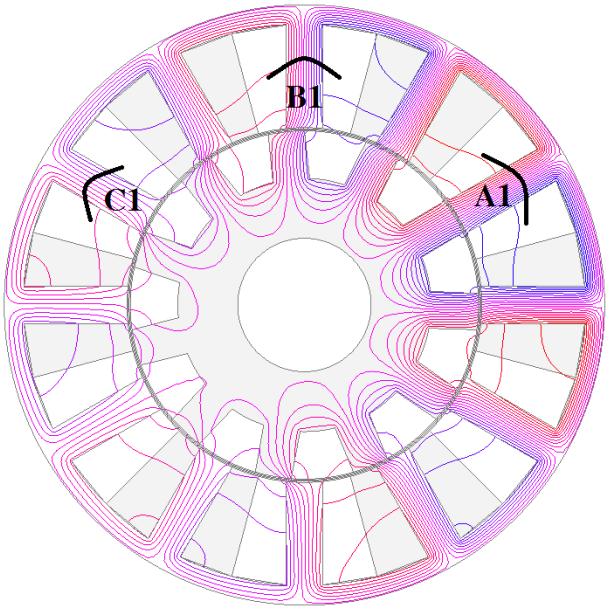

(a)

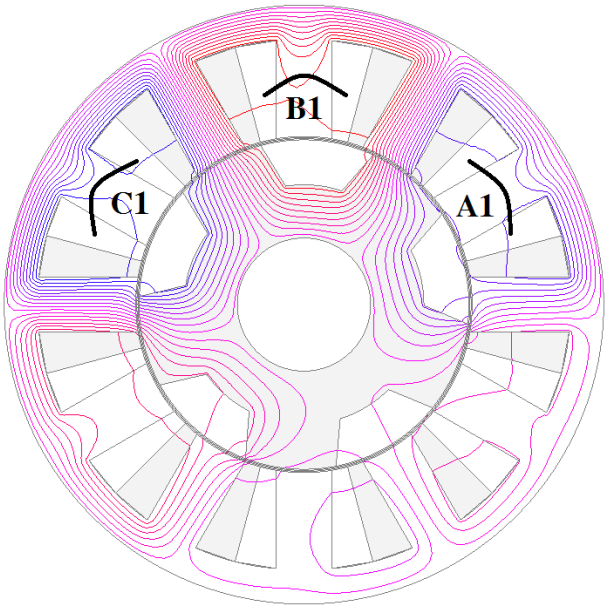

(b)

Fig. 6.8. Flux distributions, field current=20A, armature current=0A. (a) Proposed NSWFS machine. (b) NSWFS-AP machine.

6.2.Topologies and winding configurations of NSWFS machines

As can be seen in Fig. 6.9, 3 field coils and 3 armature coils are disposed alternately on the stator in a 6-slot NSWFS machine. Any rotor pole number except 3, 6, and 9 are feasible to the 6-slot NSWFS machine. Both field coils and armature coils are alternatively tooth-wound and non-overlapping. The winding factors of machines are shown in Table I. As can be seen,

the 5- and 7-pole machines show the largest winding factors among 6-slot machines. In the 6-slot NSWFS machine, the phase winding, which is consisted by one coil, has unipolar flux-linkage. However, as will be shown later, it is expected that the 12-slot NSWFS machine, whose phase winding is consisted of two coils, may achieve bipolar flux-linkage. For the 12-slot NSWFS machine, any rotor pole number except 3, 6, 9 and 12 can be employed. The winding factors of machines are shown in Table 6.1. As can be seen, the 11- and 13-pole machines show the largest winding factor among 12-slot machines.

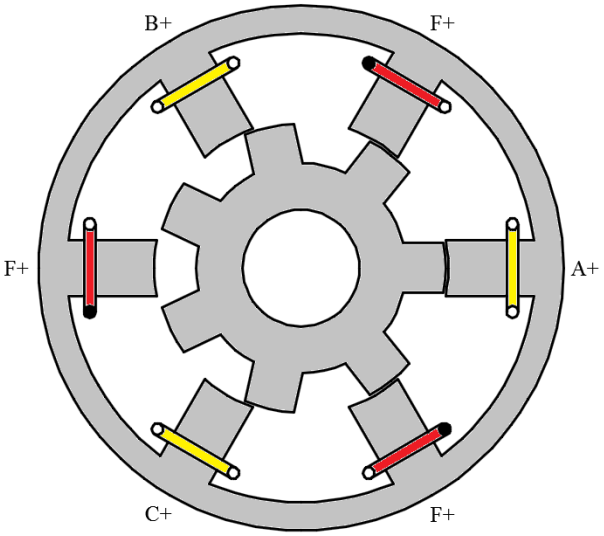

Fig. 6.9. Cross-section of proposed 3-phase NSWFS machine, 6-slot/7-pole.

Table 6.1. Winding factors of NSWFS machines

Stator slot/rotor pole number	Distribution factor	Pitch factor	Winding factor
6-slot/4-pole	1	0.5	0.5
6-slot/5-pole	1	0.866	0.866
6-slot/7-pole	1	0.866	0.866
6-slot/8-pole	1	0.5	0.5
12-slot/10-pole	1	0.866	0.866
12-slot/11-pole	1	0.966	0.966
12-slot/13-pole	1	0.966	0.966
12-slot/14-pole	1	0.866	0.866

The armature winding polarities of the 6-slot NSWFS machine are defined in Fig. 6.10. As can be seen in Fig. 6.11, the winding configurations and coil EMF vectors of the 6-slot/4- and 7-pole machines are the same. Meanwhile, the 6-slot/5- and 8-pole machines have the same winding configurations and coil EMF phasors.

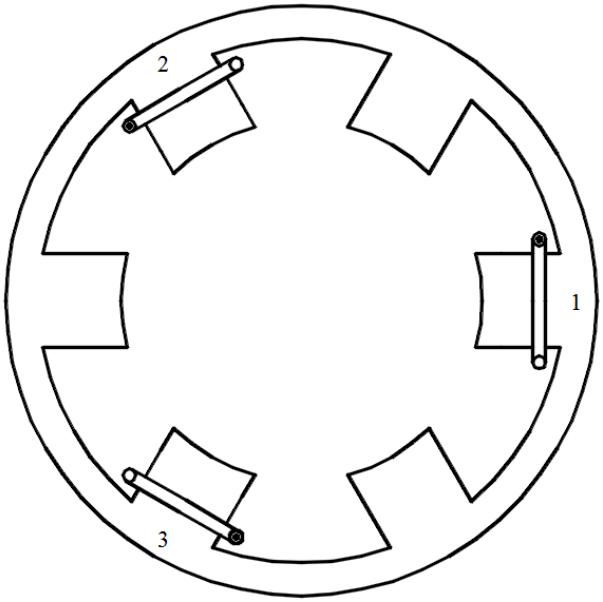

Fig. 6.10. Polarity of armature windings, 6-slot NSWFS machine.

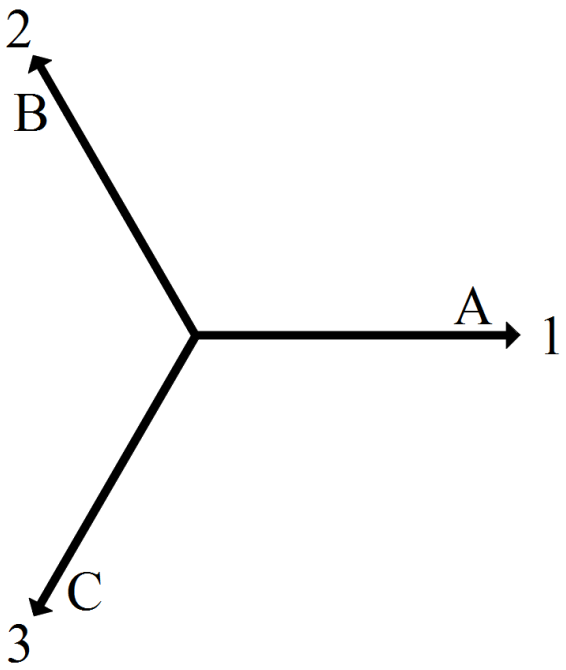

(a)

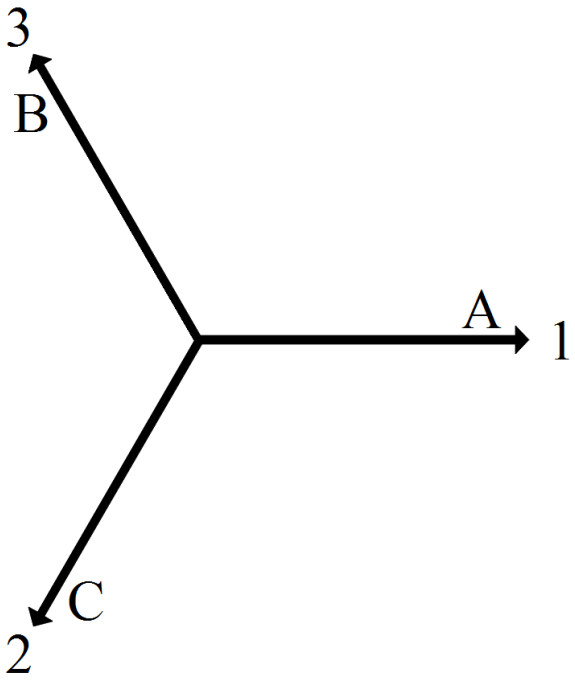

(b)

Fig. 6.11. Winding configurations and coil EMF phasors of 6-slot NSWFS machines. (a) 4- and 7-pole. (b) 5- and 8-pole.

The armature winding polarities of the 12-slot NSWFS machine are defined in Fig. 6.12. The winding configurations and coil EMF phasors of 12-slot/10-, 11-, 13- and 14-pole machines are shown in Fig. 6.13.

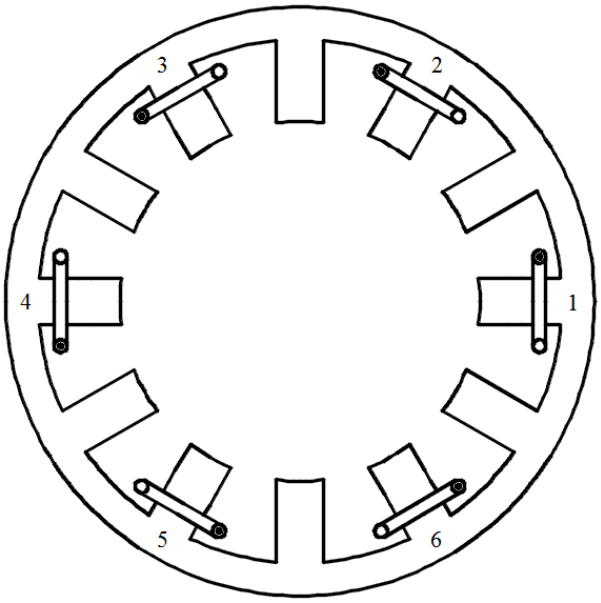

Fig. 6.12. Polarity of armature windings, 12-slot NSWFS machine.

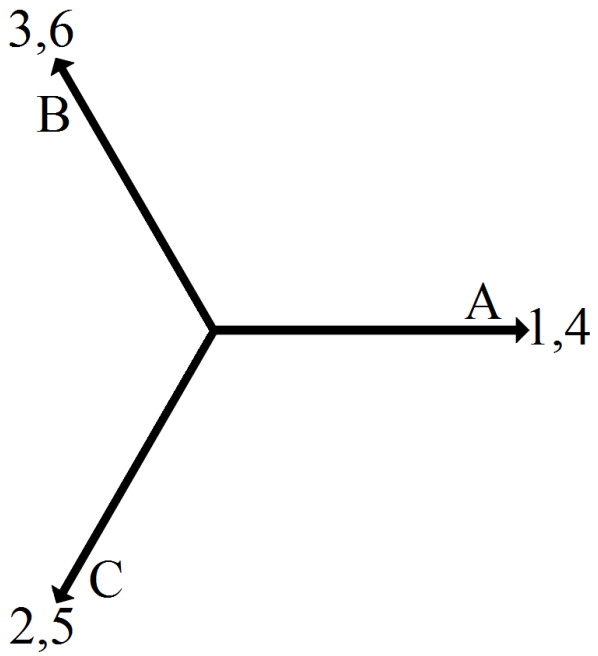

(a)

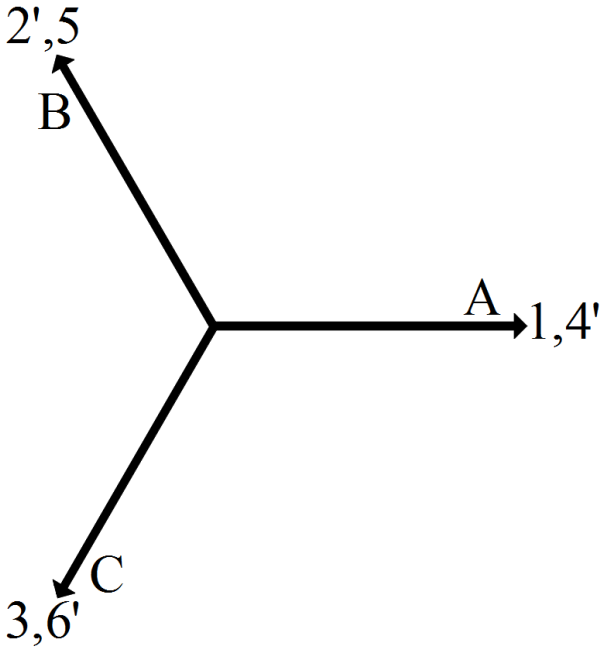

(b)

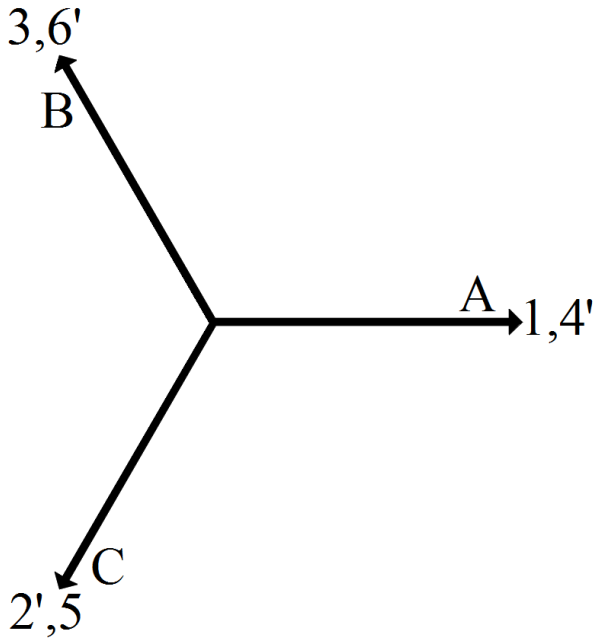

(c)

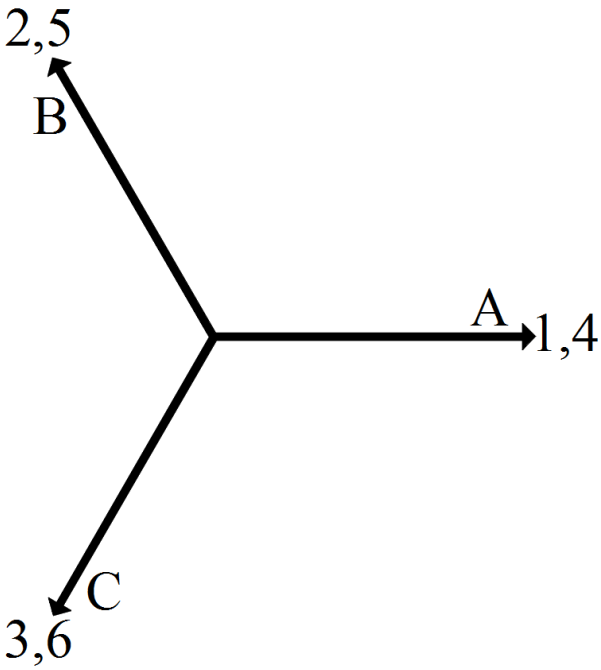

(d)

Fig. 6.13. Winding configurations and coil EMF phasors of 12-slot NSWFS machines. (a) 10-pole. (b) 11-pole. (c) 13-pole. (d) 14-pole.

Fig. 6.14 shows the operation principle of 6-slot NSWFS machine. As shown in Fig. 6.14 (a), when the rotor slot aligns with the centre of the armature coil, the flux-linkage in coil A is minimum, while in Fig. 6.14 (c), when the rotor pole aligns with the centre of the armature

coil, the flux-linkage in coil A is maximum. The periodical variation of unipolar flux-linkage with rotor position will induce back-EMF in the coils.

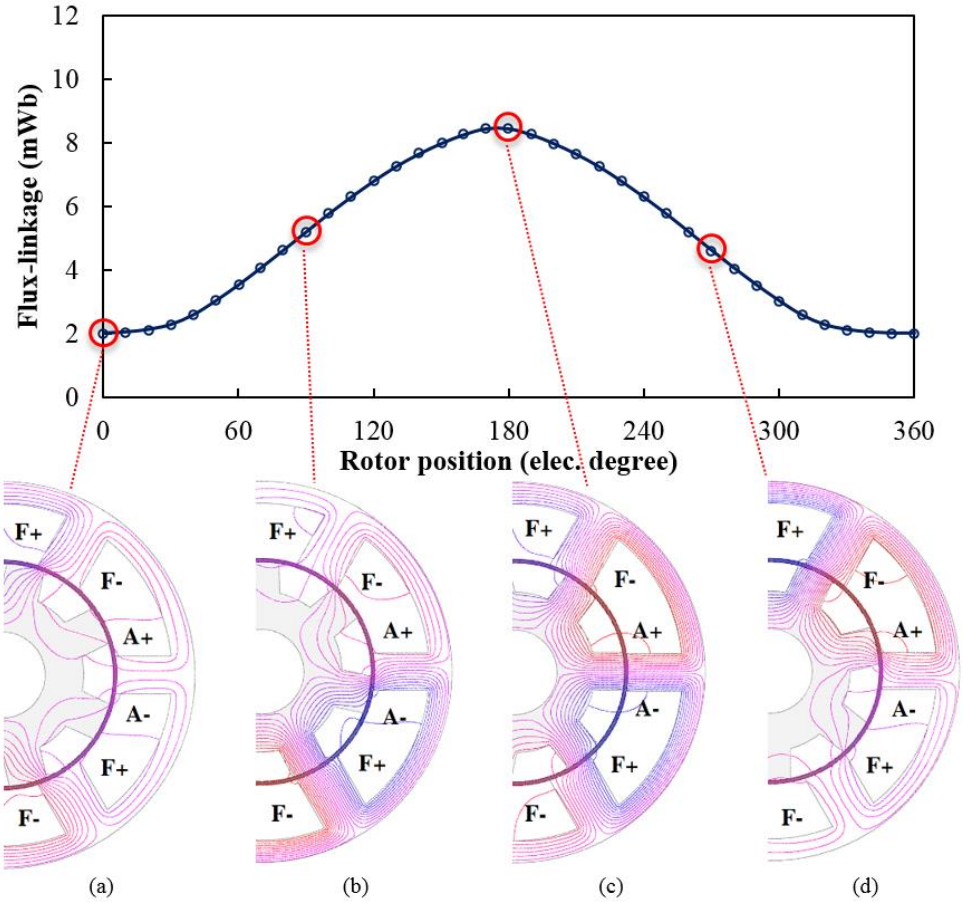

Fig. 6.14. Operation principle of 6-slot NSWFS machine. (a) 0 elec. degree. (b) 90 elec. degrees. (c) 180 elec. degrees. (d) 270 elec. degrees.

In the 12-slot NSWFS machine, two coils consist a phase winding. For the machines having even-number-pole rotors, the flux-linkages in the coils and windings are both unipolar, and they have the same operation principles as the 6-slot machines, as shown in Fig. 6.15 (a). Meanwhile, for the machines having odd-number-pole rotors, the flux-linkages in the coils are unipolar but the flux-linkages in the windings are bipolar, as shown in Fig. 6.15 (b).

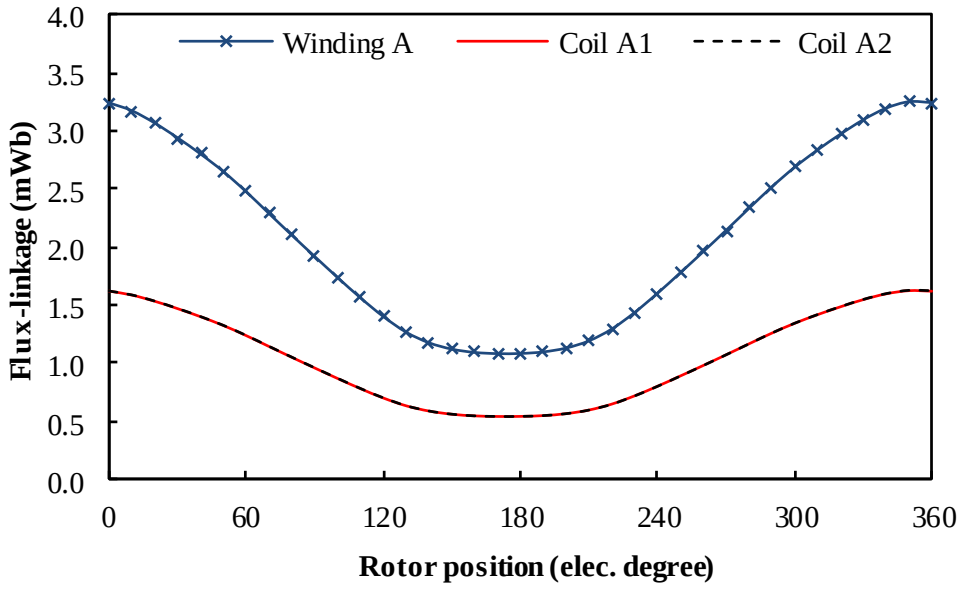

(a)

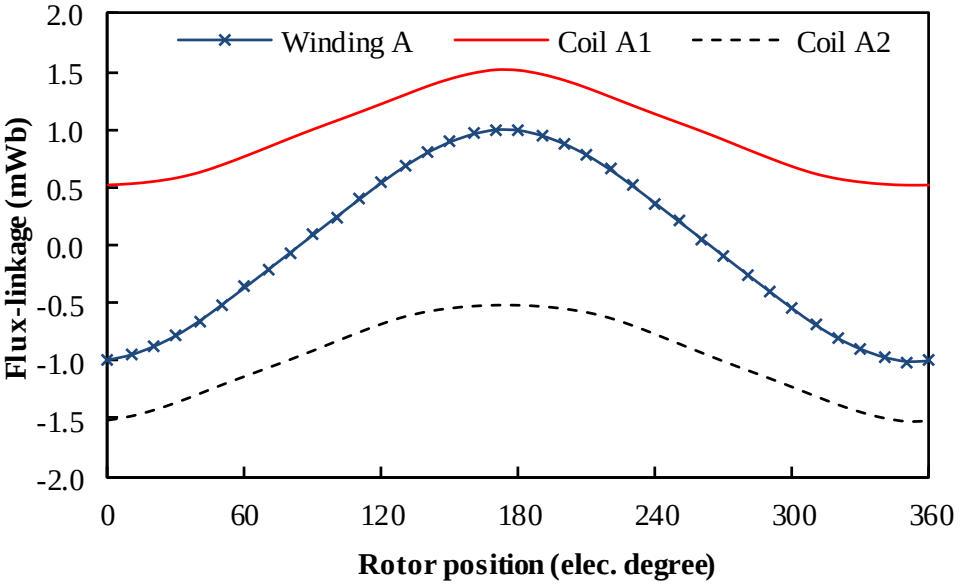

(b)

Fig. 6.15. Flux-linkage of 12-slot NSWFS machines. (a) 10-pole. (b) 11-pole.

The operation principle of 12-slot NSWFS machine having odd-number-pole rotor is shown in Fig. 6.16. As can be seen in Fig. 6.16 (a), when the rotor pole aligns with the centre of coil A1 (rotor slot aligns with the centre of coil A2), the unipolar flux-linkages in coils A1 and A2 are maximum and minimum, respectively. Meanwhile, as shown in Fig. 6.16 (b), when the rotor pole aligns with the centre of coil A2 (rotor slot aligns with the centre of coil A1), the unipolar flux-linkages in coils A1 and A2 are minimum and maximum, respectively. The unipolar flux-linkages in both coils result in bipolar flux-linkages in the phase winding.

The back-EMF will be induced by periodical variation of bipolar flux-linkage with rotor position.

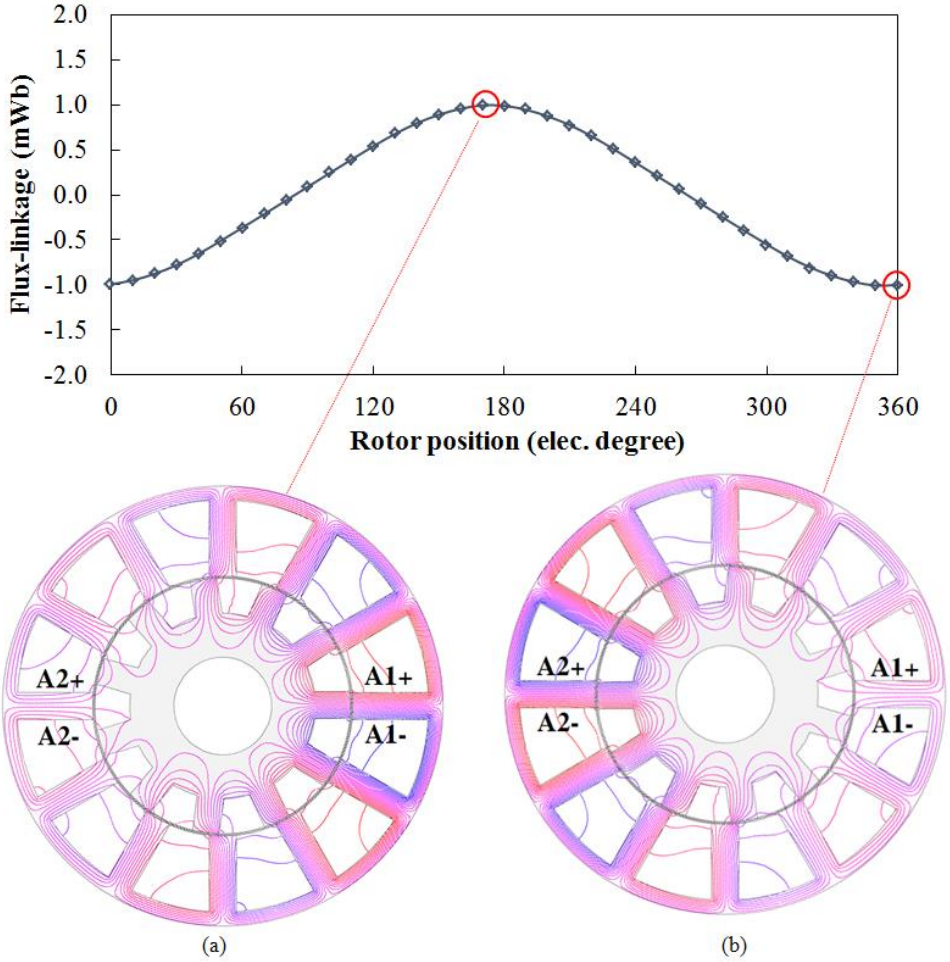

Fig. 6.16. Operation principle of 12-slot NSWFS machine having odd-number-pole rotor. (a) 180 elec. degrees. (b) 360 elec. degrees.

In this chapter, the 6-slot NSWFS machines will be investigated first and then the 12-slot machines will be compared in order to avoid the complication of comparison. In order to compare the performances of 6-slot machines fairly, the machines having different rotor pole numbers have been globally optimized using ANSYS Maxwell to achieve the maximum average torque under the constraint of 60W copper loss. It is worth mentioning that for simplicity the end-windings are not taken into consideration during the optimization. The optimized parameters are shown in Table 6.2. Under the same objective and constraint, a SNSWFS machine of the same air-gap length, stack length and outer stator diameter with the 6-slot NSWFS machines have also been globally optimized. The optimized parameters are also shown in Table 6.2. It is worth mentioning that the percentages of field winding areas of

these machines have been optimized when the copper loss is 60W, as shown in Fig. 6.17 (a). Fig. 6.17 (b) shows the optimized percentages of field winding areas of the 6-slot/7-pole machine under different copper losses. As can be seen, the optimized percentage of this machine is close to 50% when the electric loading is low, and this means that the saturation of the machine leads the shift of the optimal field winding percentage in the slots.

Table 6.2. Main parameters of machines

Items	NSWFS, 4-pole	NSWFS, 5-pole	NSWFS, 7-pole	NSWFS, 8-pole	SNSWFS
Stator slot number	6	6	6	6	12
Rotor pole number	4	5	7	8	8
Rated speed (rpm)	400	400	400	400	400
Stator outer radius (mm)	45	45	45	45	45
Axial length (mm)	25	25	25	25	25
Air-gap length (mm)	0.5	0.5	0.5	0.5	0.5
Split ratio	0.52	0.53	0.56	0.57	0.6
Stator tooth width (mm)	12.4	11.1	9.4	9.1	6.2
Stator back-iron thickness (mm)	7.0	6.1	5.4	5.2	4.5
Rotor pole width (mm)	12.7	10.9	8.8	7.6	40deg
Percentage of field winding area in slot	55%	57%	59%	59%	50%
Total stator slot area (mm^2)	1652.2	1909.1	2066.5	2081.0	1804.3
Total number of turns of armature windings	180	180	180	180	180
Total number of turns of field windings	180	180	180	180	180
Packing factor (effective copper area/slot area)	0.4	0.4	0.4	0.4	0.4

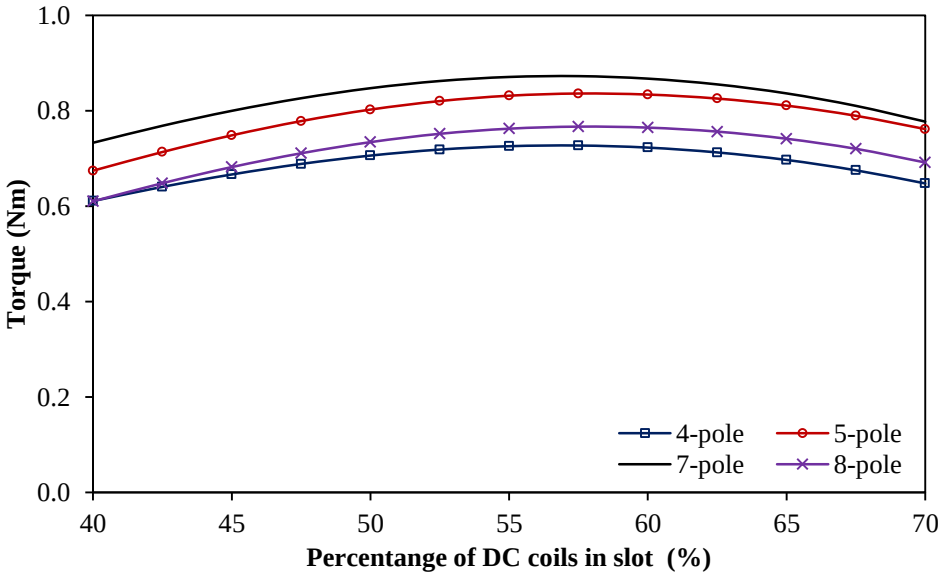

(a)

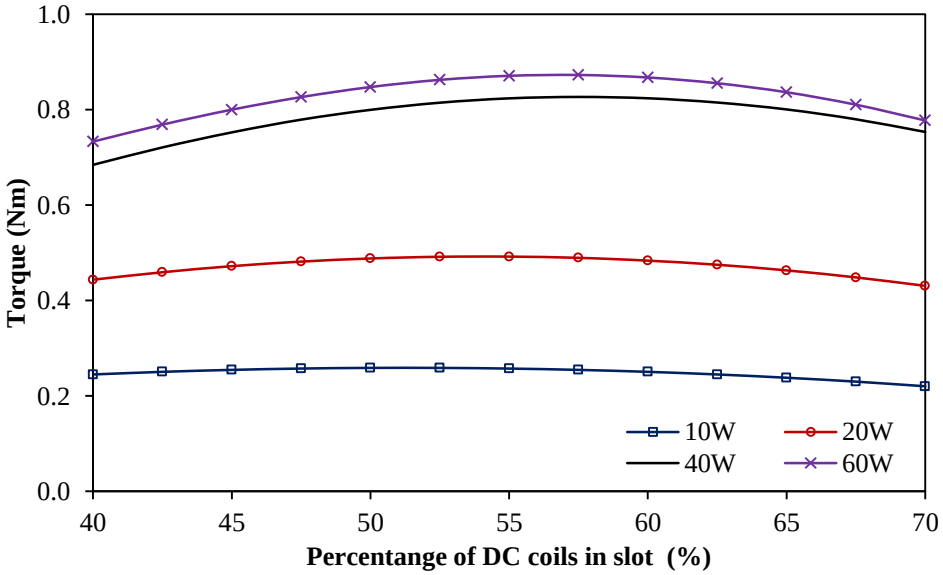

(b)

Fig. 6.17. Comparison of percentages of DC coils in slots, BLAC operation. (a) 6-slot NSWFS machines. (b) 6-slot/7-pole NSWFS machines.

6.3.Comparison of 6-slot NSWFS machines

6.3.1. Open-Circuit Field Distribution

Fig. 6.18 shows the flux distributions of the optimized 6-slot NSWFS machines. The field and armature currents are 30A and 0A, respectively.

When the field current is 30A, the radial air-gap flux densities of the NSWFS machines and the SNSWFS machine are shown in Fig. 6.19. As can be seen, the peak-to-peak values of the flux densities in four NSWFS machines are similar to each other but larger than that of the SNSWFS machine. As mentioned before, the reason is that the rotor segments restrict the flux paths in the SNSWFS machine.

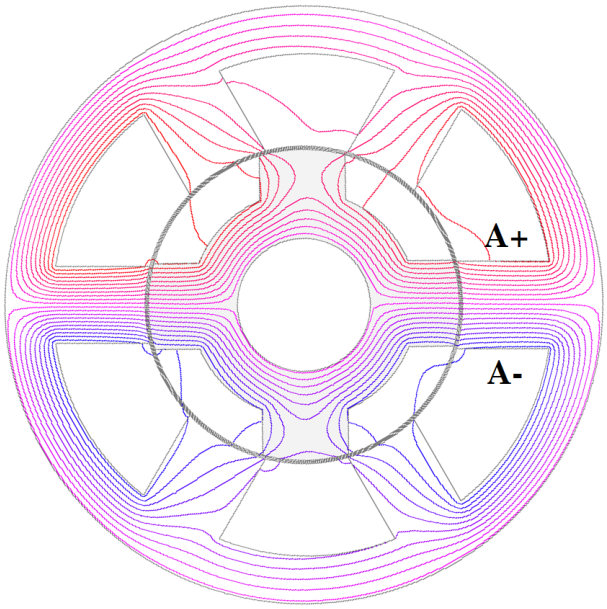

(a)

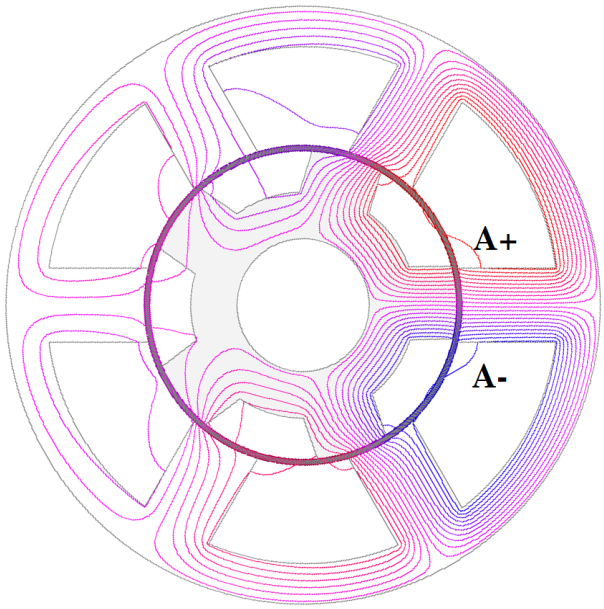

(b)

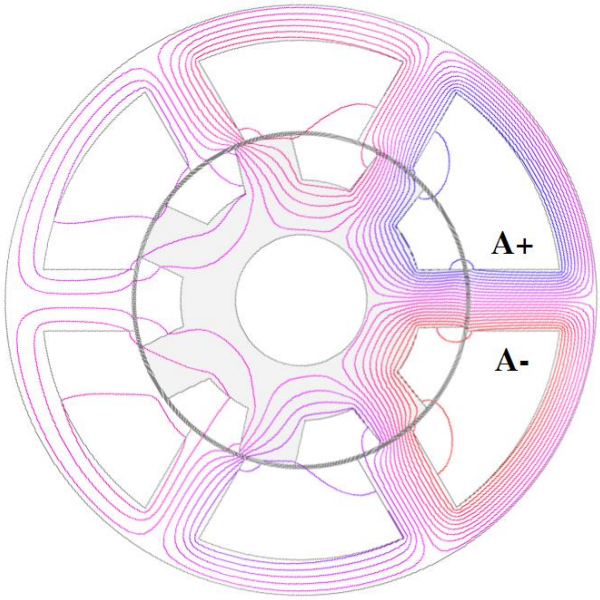

(c)

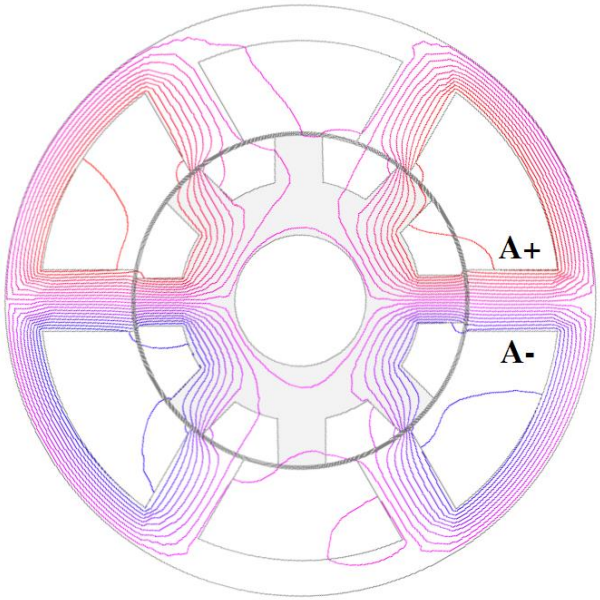

(d)

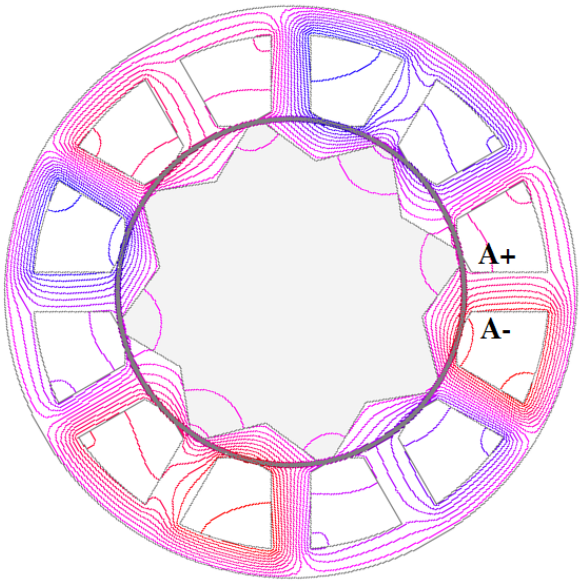

(e)

Fig. 6.18. Open-circuit flux distributions of 6-slot NSWFS machines, field current=30A. (a) 4-pole. (b) 5-pole. (c) 7-pole. (d) 8-pole. (e) SNSWFS

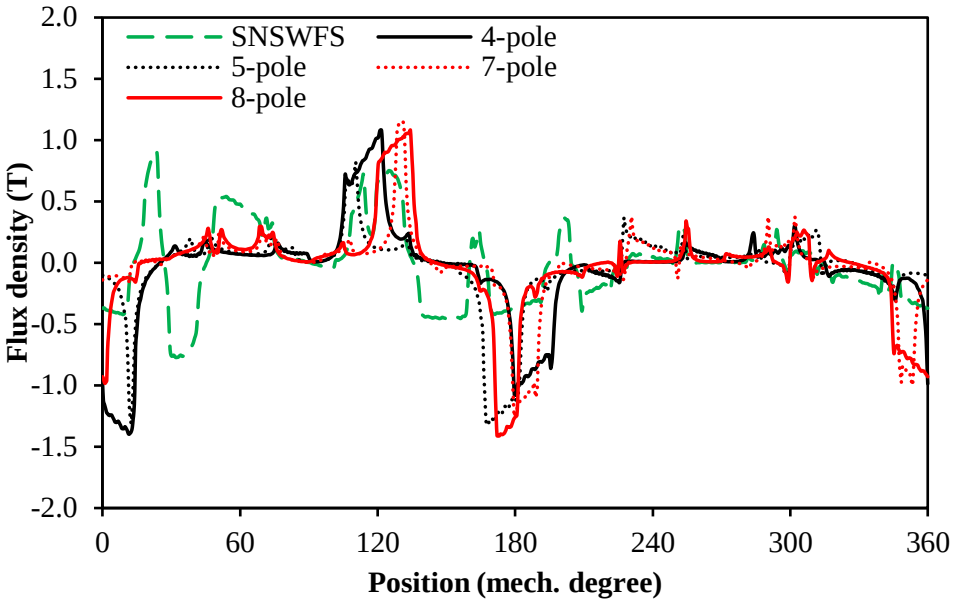

Fig. 6.19. Comparison of radial air-gap flux density distributions of 6-slot NSWFS machines having different number of rotor poles, field current=30A.

6.3.2. Open-Circuit Flux-Linkage and Back-EMF

When the field current is 30A, the open-circuit flux-linkage waveforms and harmonics of the 6-slot NSWFS machines are shown in Fig. 6.20.

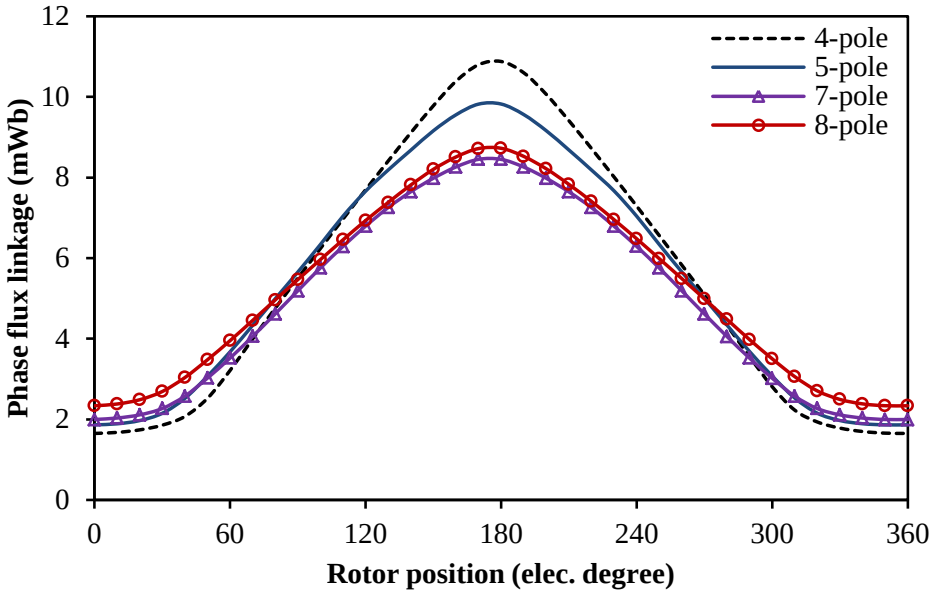

(a)

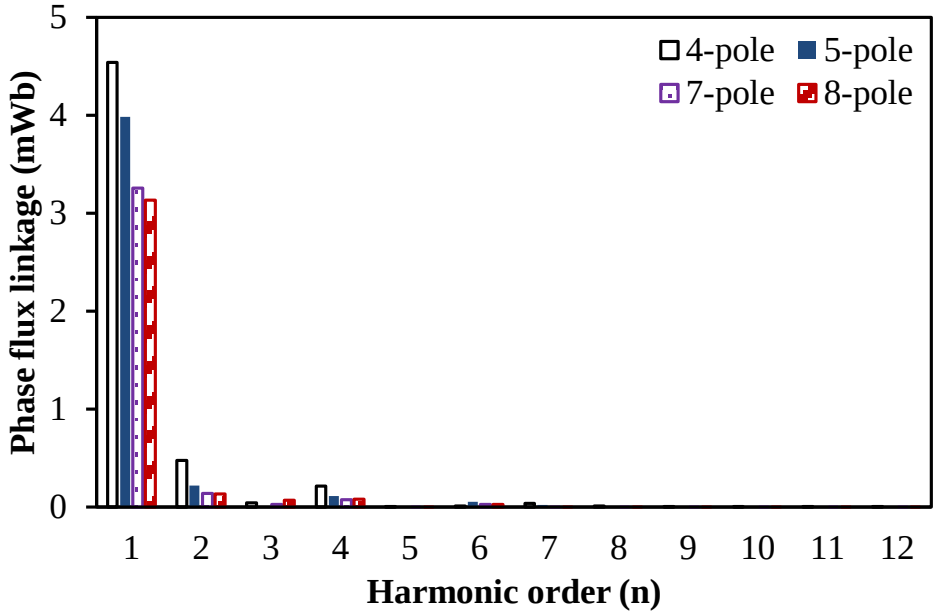

(b)

Fig. 6.20. Comparison of phase flux-linkages of machines. (a) Waveforms. (b) Harmonics.

When the field current is 30A, the back-EMF waveforms and harmonics of the NSWFS machines and the SNSWFS machine at 400rpm are shown in Fig. 6.21. As can be seen, the 7-pole NSWFS machine shows the highest fundamental amplitude. Therefore, the torque of this machine has potential to be high. The 4-pole NSWFS machine shows relatively high harmonic amplitudes and the low-cost brushless DC (BLDC) operation may be considered. However, in terms of other machines, the back-EMFs are more close to sinusoidal waveforms,

which make them suitable for brushless AC (BLAC) operation. Therefore, for fair comparison, BLAC operation is adopted in further comparison. For the SNSWFS machine, its back-EMF fundamental amplitude is relatively small, but the harmonics are lower than the 6-slot NSWFS machines. Therefore, the SNSWFS machine is expected to have lower torque density but lower torque ripple than those of the NSWFS machine.

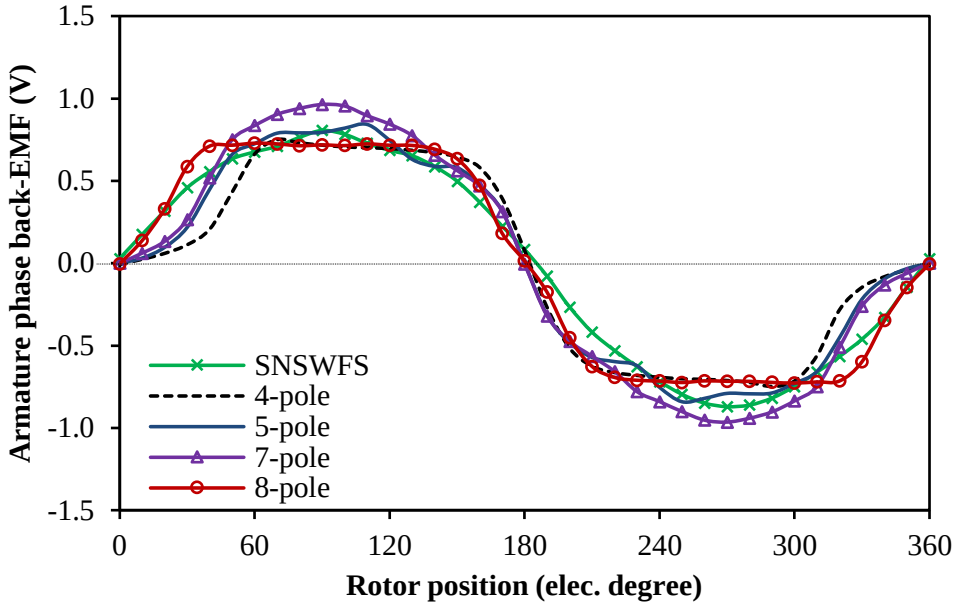

(a)

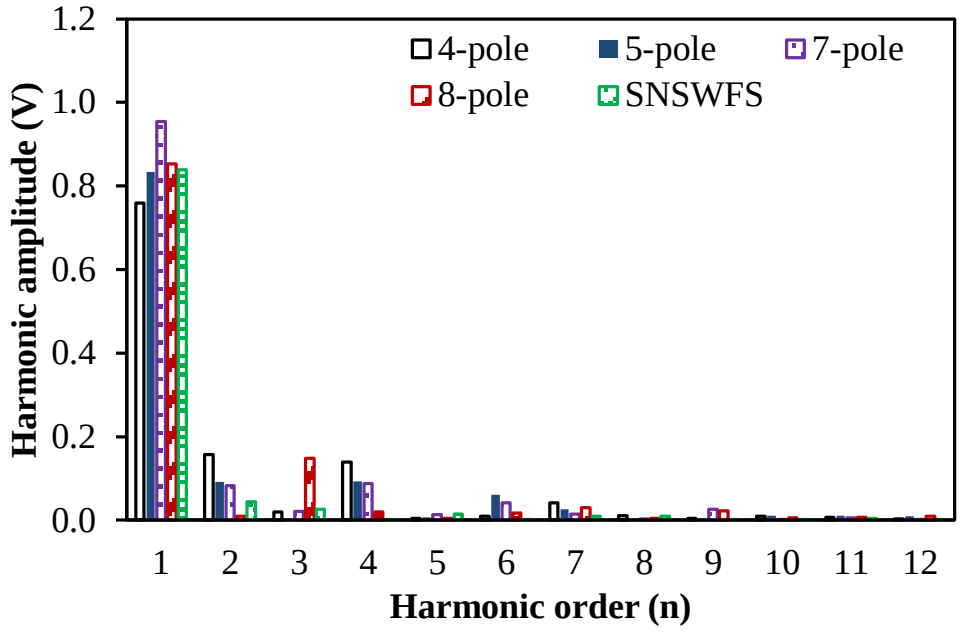

(b)

Fig. 6.21. Comparison of phase back-EMFs of 6-slot NSWFS machines having different number of rotor poles, 400rpm, field current=30A. (a) Waveforms. (b) Harmonics.

6.3.3. Torque Characteristics

When the field and armature currents are 30A and 0A, respectively, the cogging torque waveforms and harmonics of four NSWFS machines and the SNSWFS machine are compared in Fig. 6.22. As can be seen, all of the cogging torque peak-to-peak values are smaller than 0.23Nm. However, the torque ripples of the 6-slot NSWFS machines are not expected to be low since the harmonics in the back-EMFs are relatively high. As can be seen from Fig. 6.22 (b), during one electric cycle, the 3rd cogging harmonic amplitude is higher than the other orders in the SNSWFS machine, 4- and 8-pole NSWFS machines. Meanwhile, for the 5- and 7-pole NSWFS machines, the amplitude of the 6th cogging harmonics is the highest. It is worth noticing that the cogging torque orders are based on one electric cycle to allow for comparison between the machines having different pole numbers.

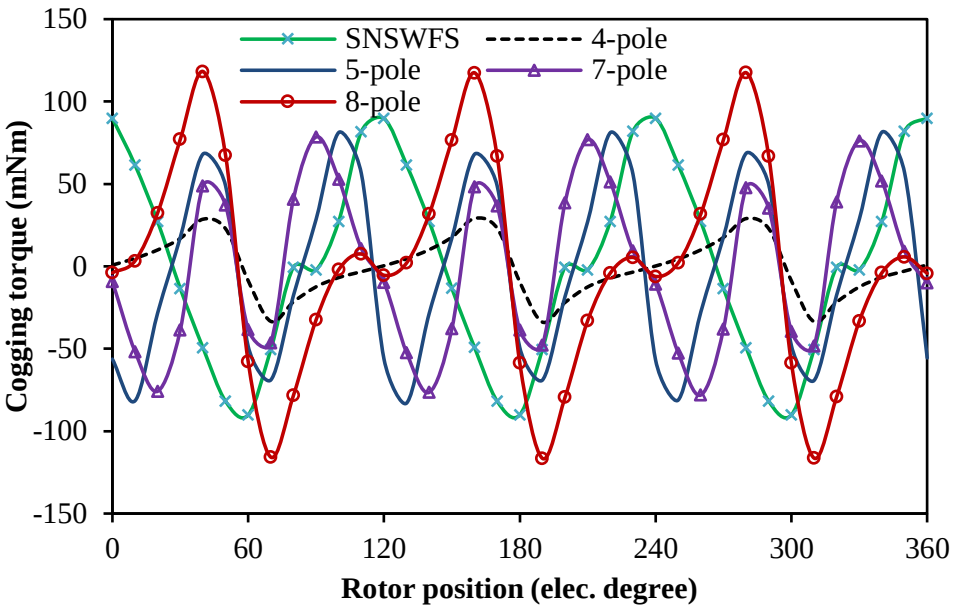

(a)

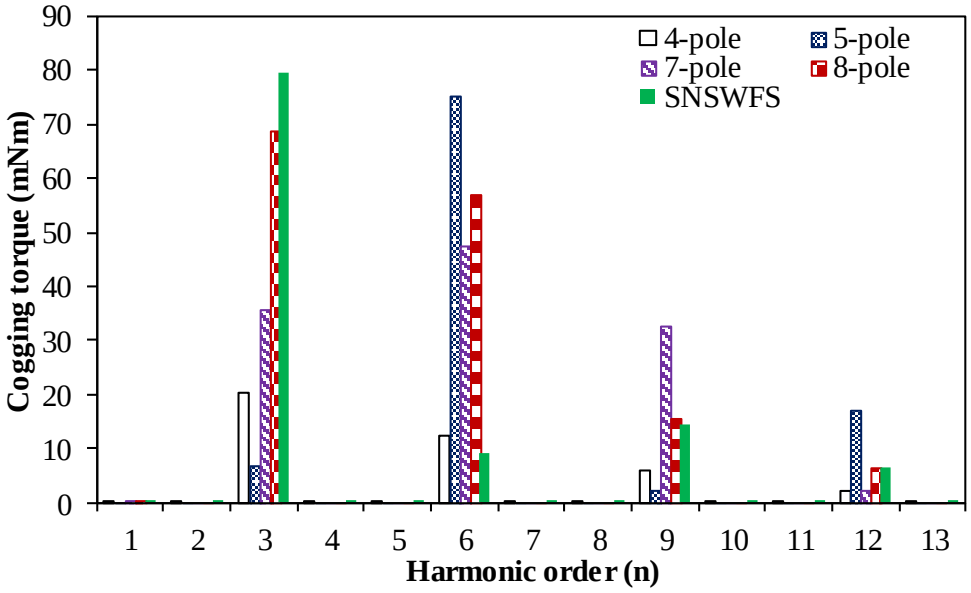

(b)

Fig. 6.22. Comparison of cogging torques of 6-slot NSWFS machines having different number of rotor poles, field current=30A. (a) Waveforms. (b) Harmonics.

Fig. 6.23 shows the torque waveforms of the NSWFS machines and the SNSWFS machine when the armature and field currents are both 30A under brushless AC (BLAC) operation. As can be seen, the torque ripples of the 4-, 5-, 7- and 8-pole machines are 79%, 56%, 55% and 46%, respectively. Meanwhile, the torque ripple in the SNSWFS machine is 35%.

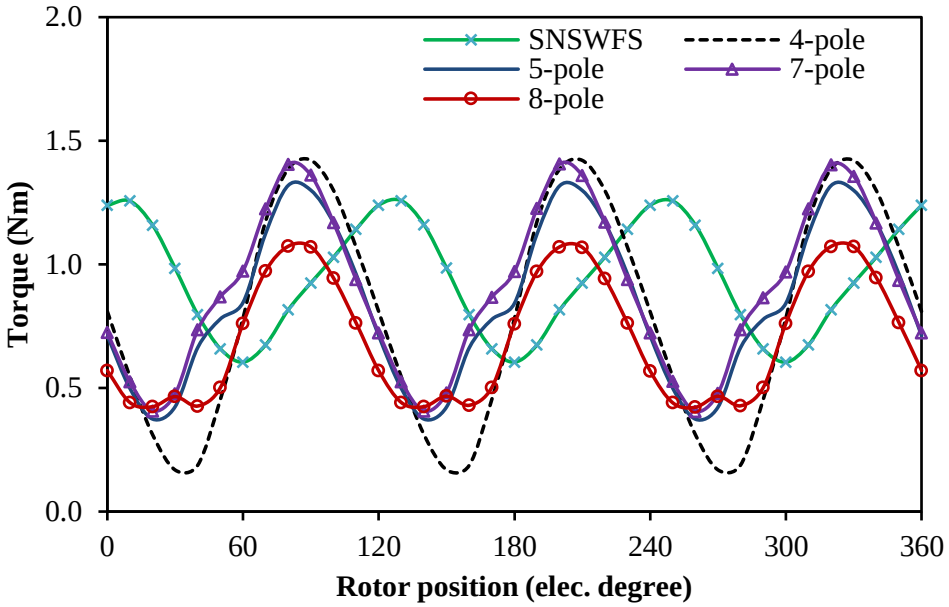

Fig. 6.23. Comparison of torque waveforms, field current=armature current=30A, BLAC operation.

Fig. 6.24 is the comparison of the average torque-copper loss curves. It is worth mentioning that the percentages of the field winding areas in slots of these machines follow the optimized results shown in Table 6.2. As can be seen, the 7-pole and 8-pole machines show the highest average torque when the copper loss is low. However, the 8-pole NSWFS machine is easily saturated, and the 5-pole and 7-pole machines have higher average torque than other machine under high electric loadings. Overall, all NSWFS machines show higher torque density than an optimized SNSWFS machine at low electric loadings. When the copper loss is 60W, the average torque of the 7-pole machine is 72% higher than that of the SNSWFS machine.

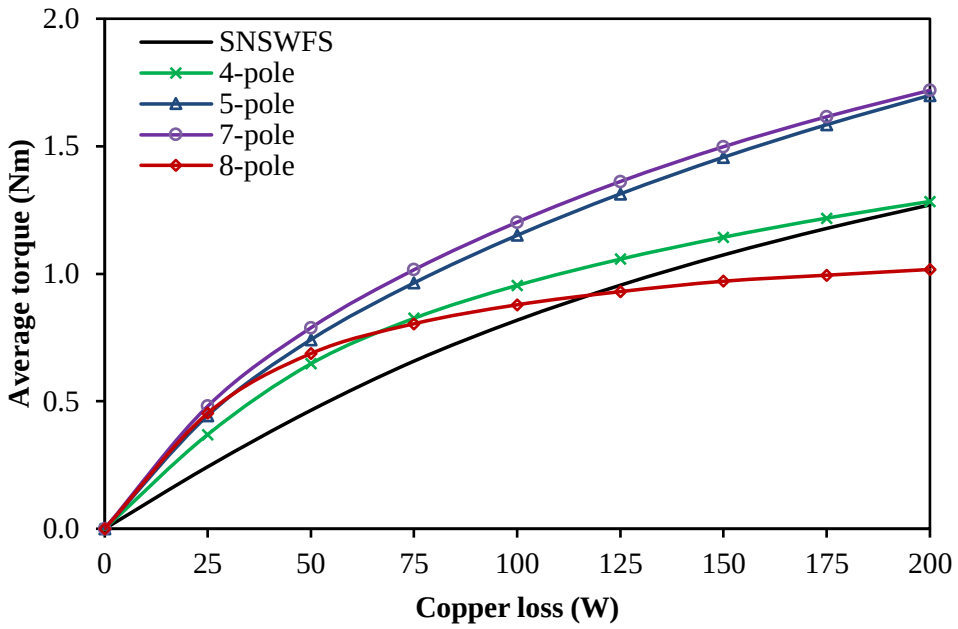

Fig. 6.24. Comparison of average torque-copper loss curves of 6 slot NSWFS machines having different number of rotor poles, BLAC operation.

Since the optimized percentage of field winding area in the slot of a NSWFS machine is not 50%, the electric loadings of the field and armature current are not the same, and consequently, the saturation situations of the teeth having field coil and armature coil are not the same with equal teeth. The torque density of the NSWSF machine may have potential to be increased by employing unequal teeth to reduce the saturation. Therefore, the aforementioned four 6-slot machines with unequal teeth have been globally optimized again to achieve the maximum average torque under the constraint of 60W copper loss. The optimized parameters are shown in Table 6.3. As can be seen, the difference between re-

optimized and original parameters is not significant. Fig. 6.25 compares the average torque-copper loss curves of the NSWFS machine with equal and unequal teeth. For all machines, the torques are increased by less than 3%. This means that there is no significant torque increases by employing unequal teeth for the NSWFS machine. Therefore, equal teeth NSWFS machines will be chosen for further investigations.

Table 6.3. Dimensions of machines with unequal teeth

Items	4-pole	5-pole	7-pole	8-pole
Split ratio	0.52	0.52	0.58	0.59
Width of stator tooth having armature coil, W_1 (mm)	13.2	11.2	8.8	8.2
Width of stator tooth having field coil, W_2 (mm)	11.6	11.0	10.1	14.0
Stator back-iron thickness (mm)	7.2	6.1	5.2	5.5
Rotor pole width (mm)	12.9	10.9	8.9	7.8
Percentage of field winding area in slot	56%	58%	58%	59%
Total stator slot area (mm^2)	1686.5	1947.0	1917.8	1656.7

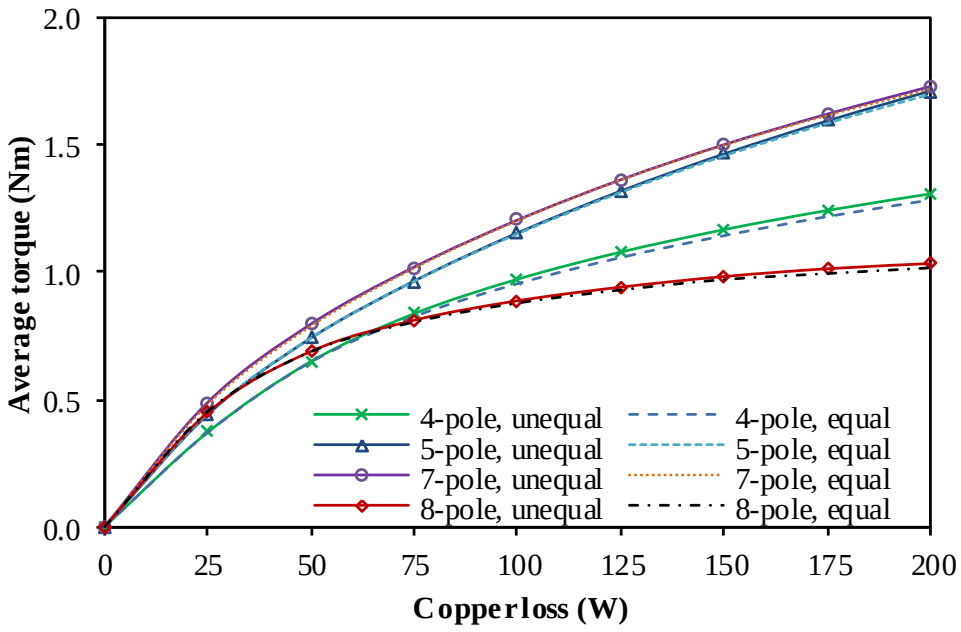

Fig. 6.25. Comparison of average torque-copper loss curves of NSWFS machines with equal and unequal teeth in 6-slot NSWFS machines having different number of rotor poles.

6.4.Comparison of 12-slot NSWFS machines

Based on the investigation in the previous section, it is found that compared with the SNSWFS machine of the same size, the 6-slot NSWFS machines have larger average torques but also much larger torque ripples. In this section, 12-slot NSWFS machines will be investigated and compared. It is found that by employing the rotor having specific pole numbers will lead to small torque ripple. As can be seen in Fig. 6.6, the two coils of a phase winding are disposed on the stator every 180 mechanical degrees in a 12-slot NSWFS machine. Similar to the 6-slot machines, the optimal percentages of field winding areas in the slots are compared in Fig. 6.26.

Table 6.4. Main parameters of 12-slot NSWFS machines

Items	10-pole	11-pole	13-pole	14-pole
Stator slot number	12	12	12	12
Rotor pole number	10	11	13	14
Rated speed (rpm)	400	400	400	400
Stator outer radius (mm)	45	45	45	45
Axial length (mm)	25	25	25	25
Air-gap length (mm)	0.5	0.5	0.5	0.5
Split ratio	0.57	0.58	0.6	0.62
Stator tooth width (mm)	6.2	5.6	5.3	5.2
Stator back-iron thickness (mm)	3.4	2.9	2.6	2.4
Rotor pole width (mm)	5.8	5.5	4.5	4.1
Percentage of field winding area in slot	54%	55%	56%	58%
Total stator slot area (mm^2)	2146.4	2309.3	2328.2	2280.6
Total number of turns of armature windings	180	180	180	180
Total number of turns of field windings	180	180	180	180
Packing factor (effective copper area/slot area)	0.4	0.4	0.4	0.4

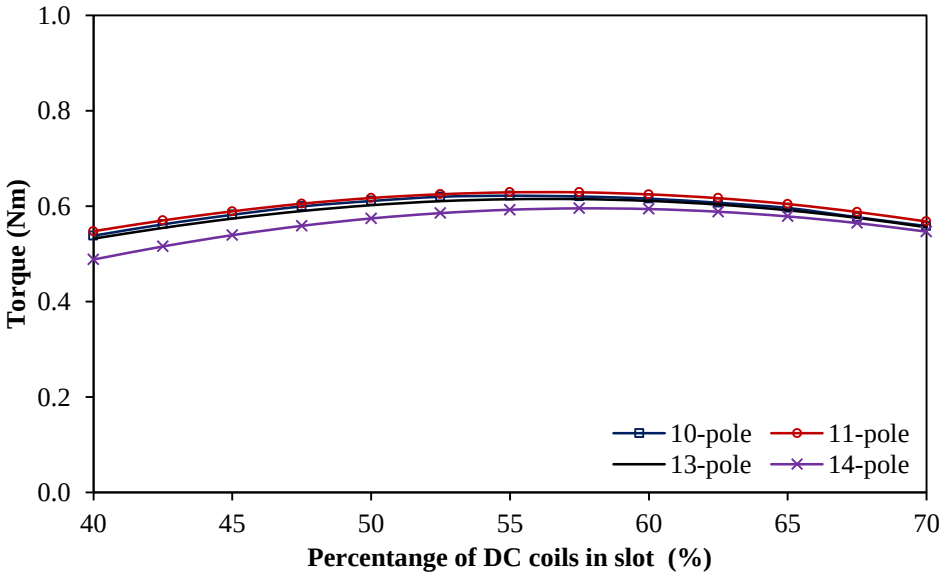

(a)

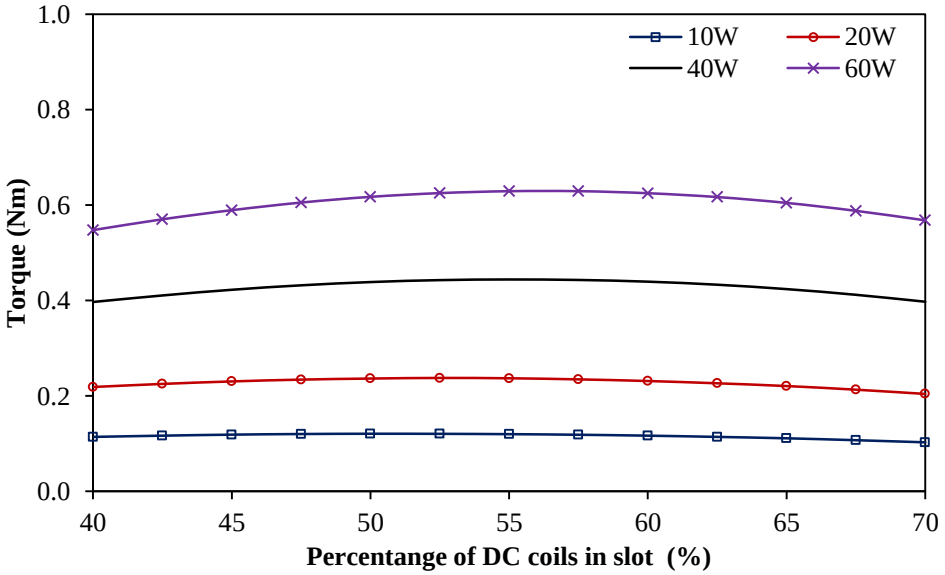

(b)

Fig. 6.26. Comparison of percentages of DC coils in slots, BLAC operation. (a) 12-slot NSWFS machines. (b) 12-slot/11-pole NSWFS machines.

6.4.1. Open-Circuit Field Distribution

When the field current is 30A, the flux distributions of aforementioned four 12-slot NSWFS machines are shown in Fig. 6.27. In this figure, coil A1 of each machine has the largest flux-linkage.

As predicted before, for the machines having even-number-pole rotors, namely 10- and 14-pole rotors, two unipolar coils of one phase achieve the largest flux-linkage at the same

time, as shown in Fig. 6.27 (a) and (d). Meanwhile, as shown in Fig. 6.27 (b) and (c), for the machines having odd-number-pole rotors, namely 11- and 13-pole rotors, when one coil of a phase has the largest flux-linkage, the other coil in this phase has the smallest flux-linkage. Therefore, the phase flux-linkage can be bipolar.

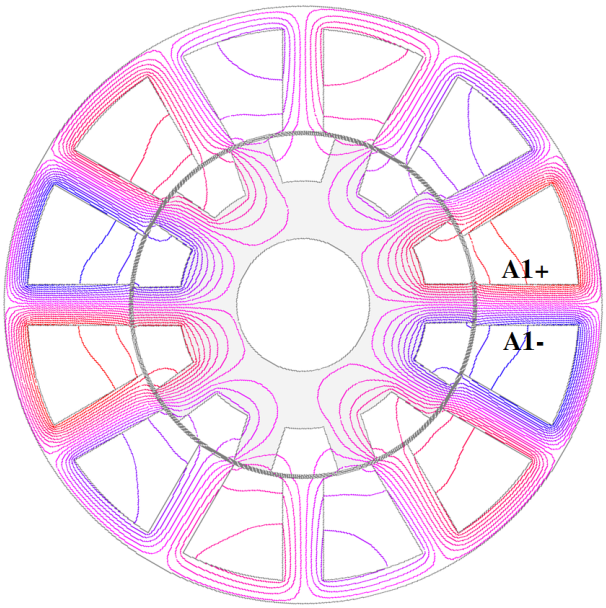

(a)

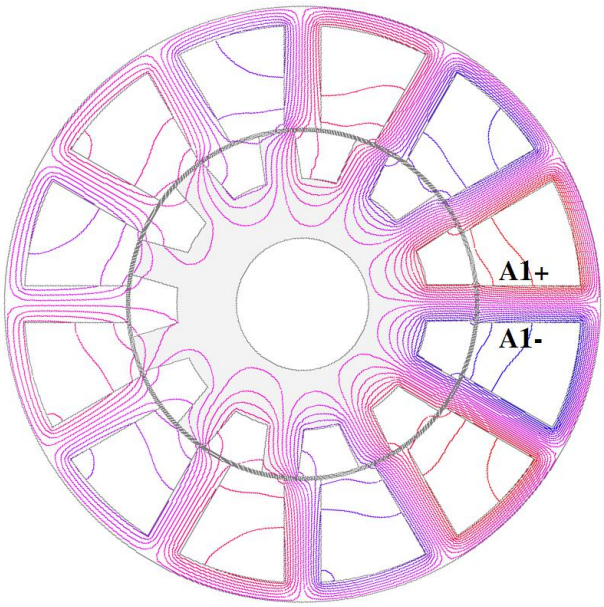

(b)

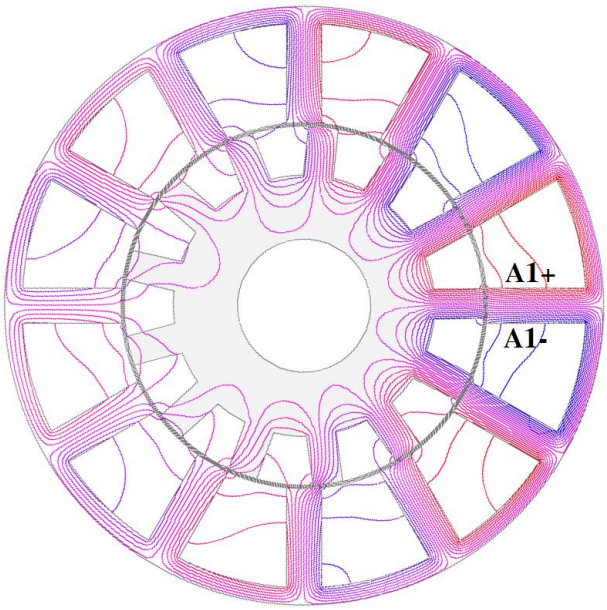

(c)

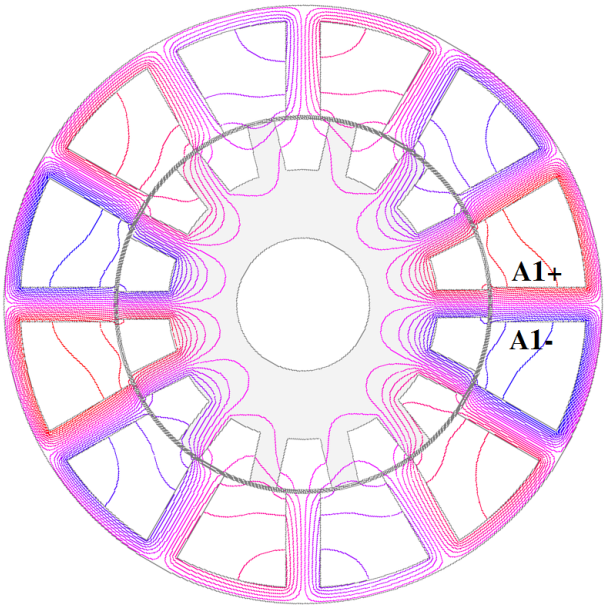

(d)

Fig. 6.27. Flux distribution of 12-slot NSWFS machine, field current =30A. (a) 10-pole. (b) 11-pole. (c) 13-pole. (d) 14-pole.

6.4.2. Open-Circuit Flux-Linkage and Back-EMF

When the field current is 30A, the open-circuit flux-linkage waveforms and harmonics of the 12-slot NSWFS machines are shown in Fig. 6.28.

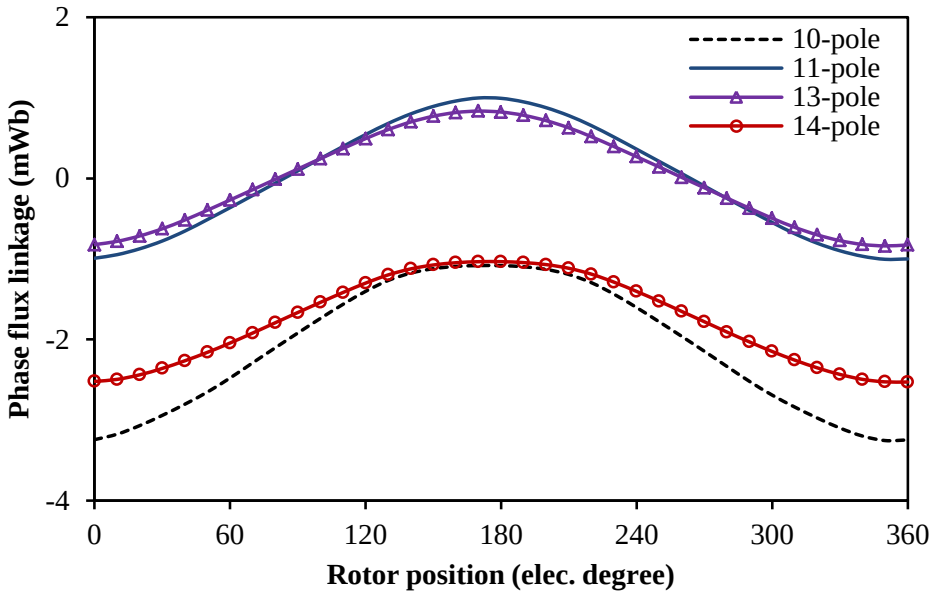

(a)

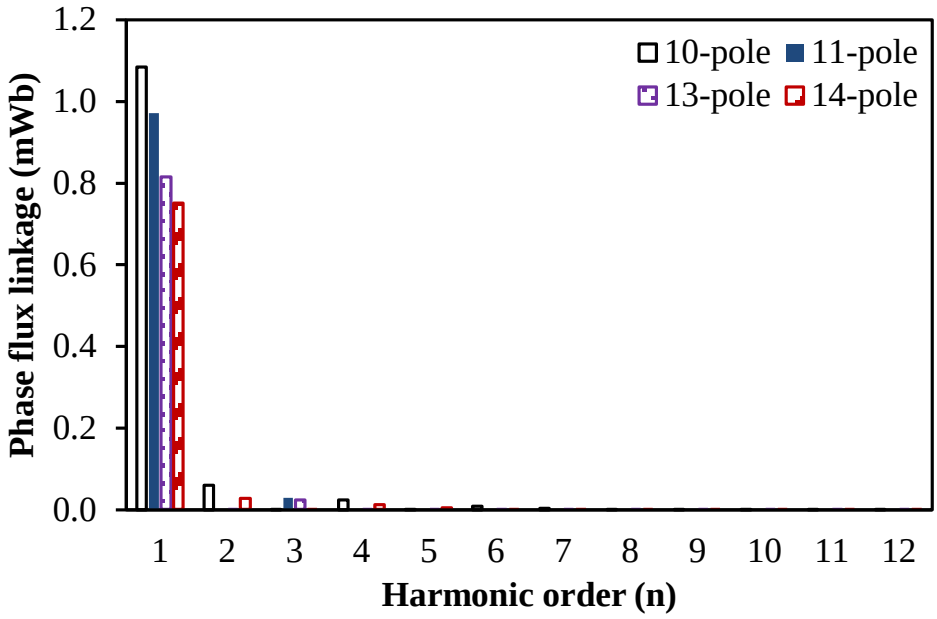

(b)

Fig. 6.28. Comparison of phase flux-linkages of machines. (a) Waveforms. (b) Harmonics.

When the field current is 30A and the rotor speed is 400rpm, the back-EMF waveforms and harmonics of the 12-slot NSWFS machines are shown in Fig. 6.29. Similar to the 6-slot/5-pole and 7-pole machines, the 12-slot/10-pole and 14-pole machines show high harmonics in the back-EMF waveforms. Obviously, this will lead to high torque ripples in the machines, and will restrict the promotion of the NSWFS machines in practical applications. Encouragingly, as can be seen in Fig. 6.29, the harmonics in the 12-slot/11- and 13-pole machines are much lower than the other machines, and their even order harmonic amplitudes

are even close to zero. Consequently, the torque ripples of the 12-slot/11- and 13-pole NSWFS machines are likely to be low.

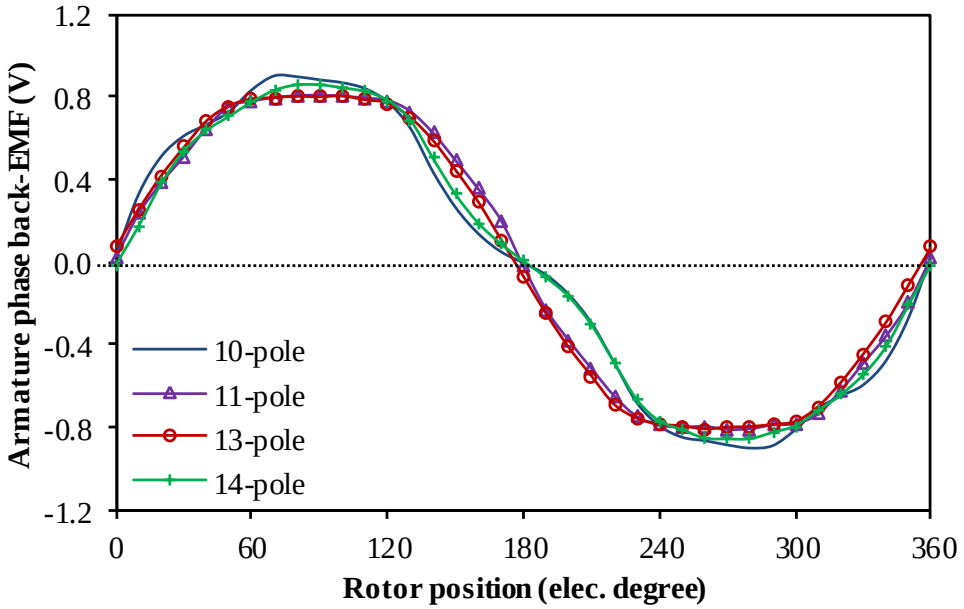

(a)

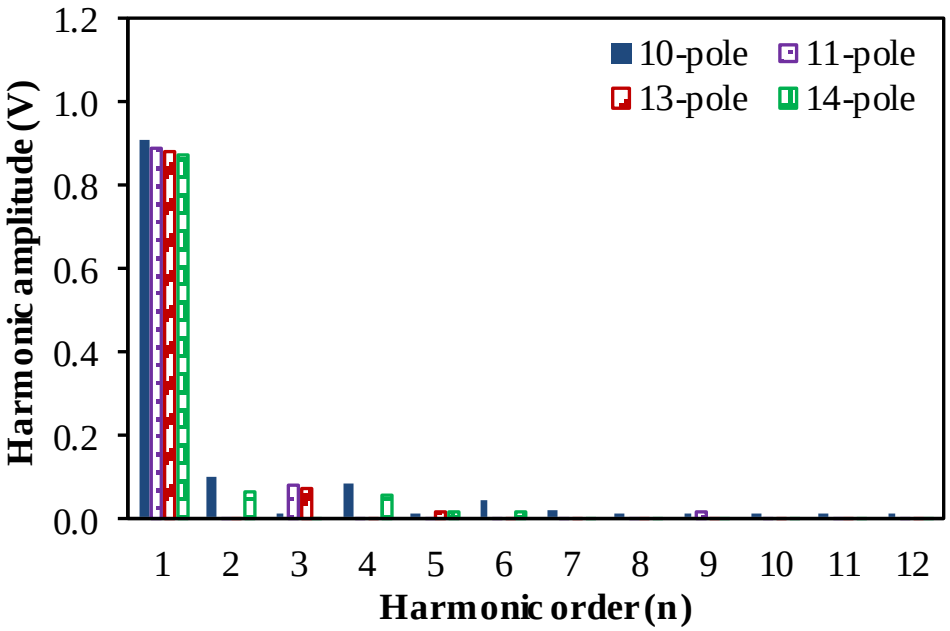

(b)

Fig. 6.29. Comparison of phase back-EMFs of 12-slot NSWFS machines having different number of rotor poles, 400rpm, field current =30A. (a) Waveforms. (b) Harmonics.

Fig. 6.30 shows the coil back-EMF waveforms and harmonics of the 12-slot/11- and 13-pole machines. As can be seen, the back-EMF harmonics of each coil are high. But the

difference between two coils results in the offset of even order harmonics in the phase back-EMF. Therefore, it can be expected that the torque ripples of the odd-number-rotor NSWFS machines are smaller than those of the even-number-rotor NSWFS machines.

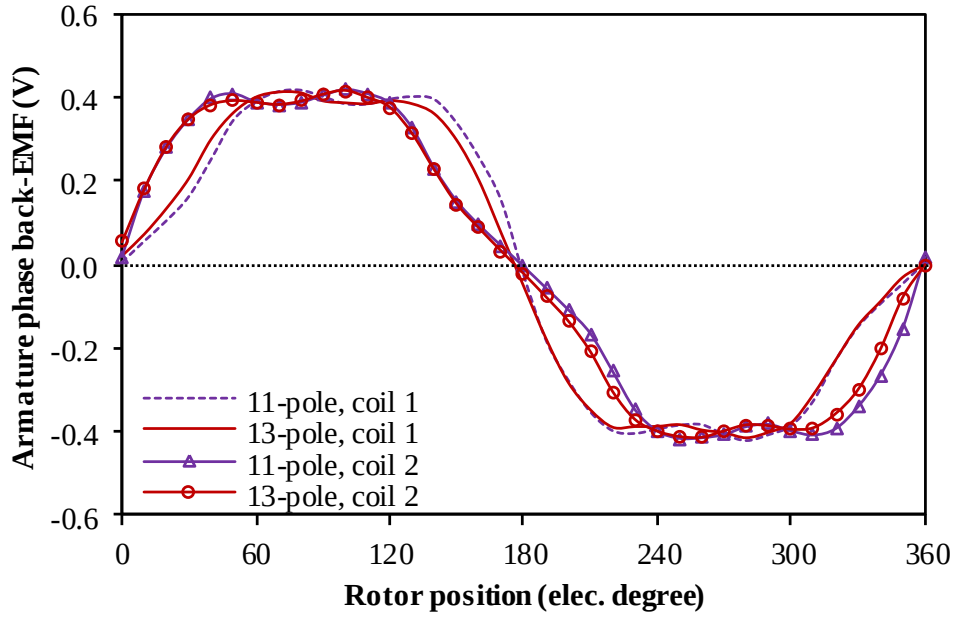

(a)

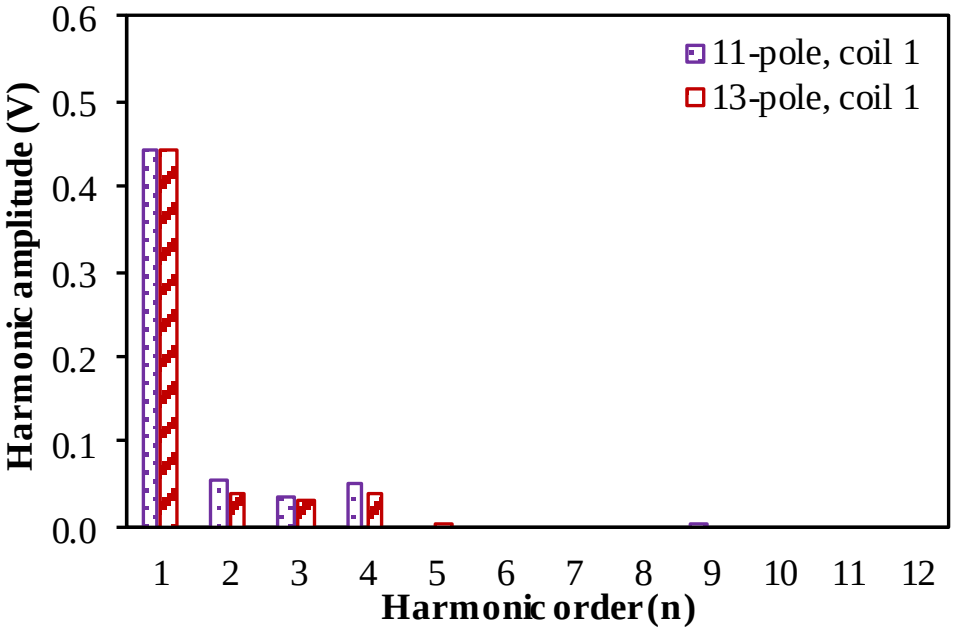

(b)

Fig. 6.30. Coil back-EMFs of the 11- and 13-pole NSWFS machine, 400rpm, field current =30A. (a) Waveforms. (b) Harmonics.

6.4.3. Torque Characteristics

When the field current is 30A and the armature current is 0A, the cogging torque waveforms and harmonics of the 12-slot NSWFS machines are shown in Fig. 6.31. As can be seen, the cogging torque peak-to-peak values of the 12-slot/11- and 13-pole machines are much smaller than the other machines since the least common multiples between stator slot and rotor pole numbers of these two machines are much higher than other machines. Therefore, the torque ripples of the 11- and 13-pole machines should be the lowest among all 12-slot NSWFS machines due to the lowest harmonic amplitudes and cogging torque peak-to-peak values. For the 10- and 14-pole machines, amplitudes of the 6^{th} and the 12^{th} cogging harmonics are high during one electric cycle, as shown in Fig. 6.31 (b), and in following investigation, rotor skewing will be employed to reduce the torque ripples.

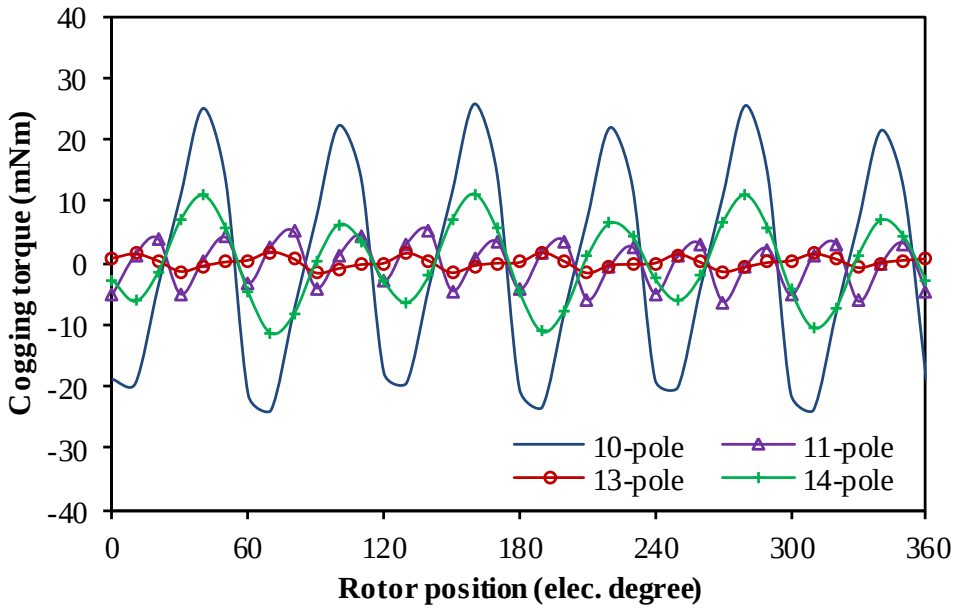

(a)

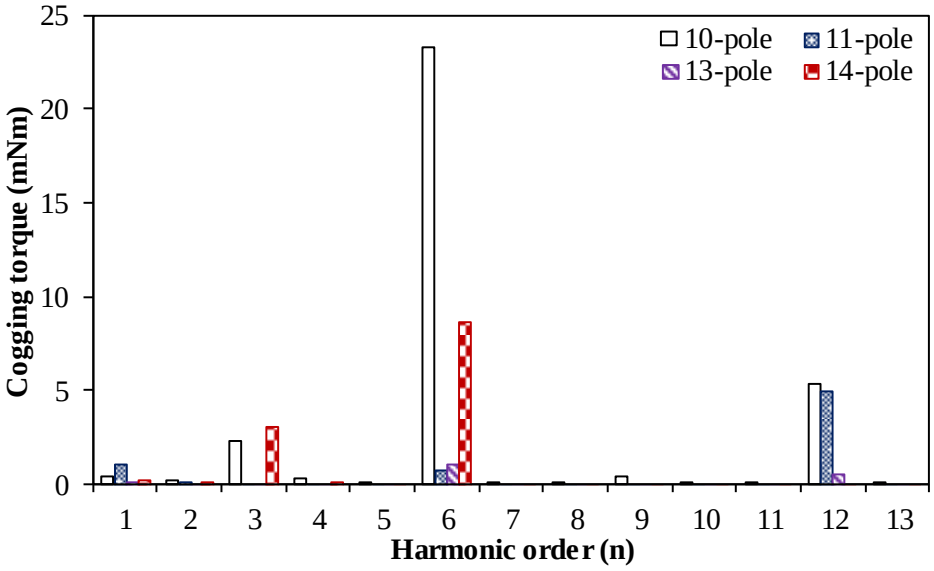

(b)

Fig. 6.31. Comparison of cogging torques of 12-slot NSWFS machines having different number of rotor poles, field current=30A. (a) Waveforms. (b) Harmonics.

Fig. 6.32 shows the torque waveforms of the 12-slot NSWFS machines when the field and armature currents are both 30A. And their average torques and torque ripples are compared in Fig. 6.33. As predicted before, the 11- and 13-pole machines show the lowest torque ripple, which are 3.8% and 2.5%, respectively. Meanwhile, high torque ripples are presented in the other machines. The torque ripples in the 10- and 14-pole machines are 57.6% and 56.0%, respectively.

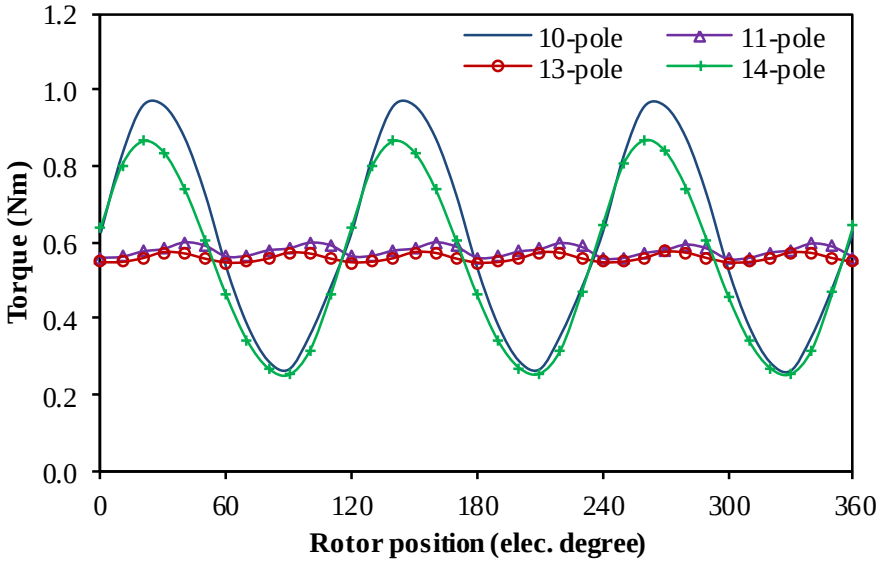

Fig. 6.32. Comparison of torque waveforms, field current density=armature current density=30A, BLAC operation.

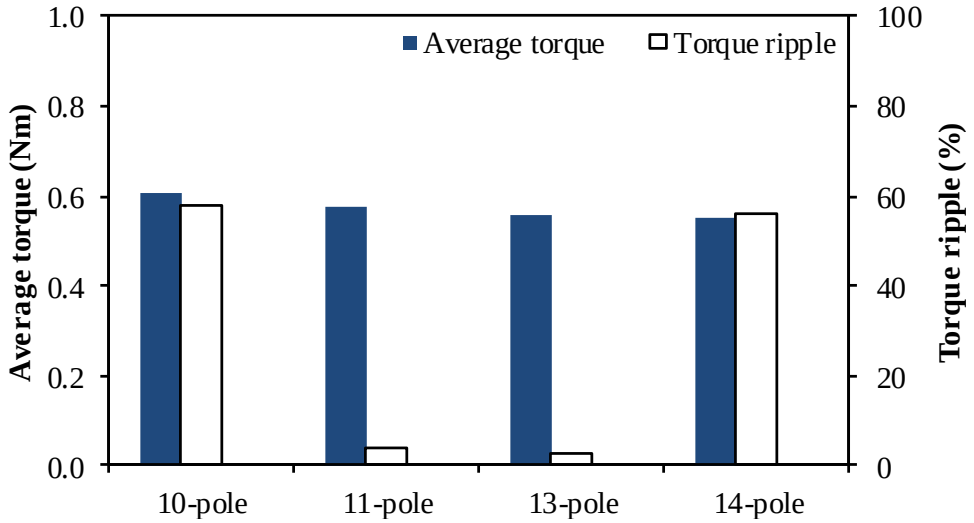

Fig. 6.33. Comparison of average torque and torque ripple, field current density=armature current density=30A, BLAC operation.

High torque ripples in 12-slot/10- and 14-pole machines can be reduced by employing two-step-skewing rotor, as shown in Fig. 6.34.

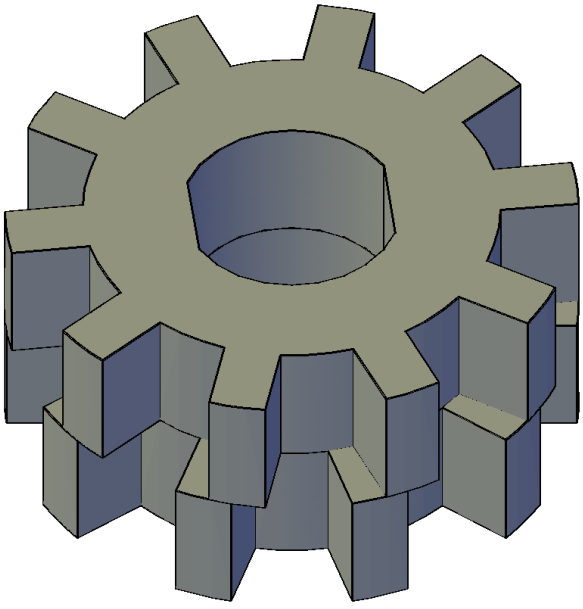

Fig. 6.34. Rotor with two-step skewing.

The torque ripple of the 12-slot/10-pole machine can be decreased to 27% with rotor skewed by 9 degrees (copper loss=60W). However, the average torque will be also decreased by 34%, as shown in Fig. 6.35. In terms of the 12-slot/14-pole machine, when the rotor

skewing angle is 7 degrees, the torque ripple can be decreased to 18% with the average torque decreased by 38%, Fig. 6.36.

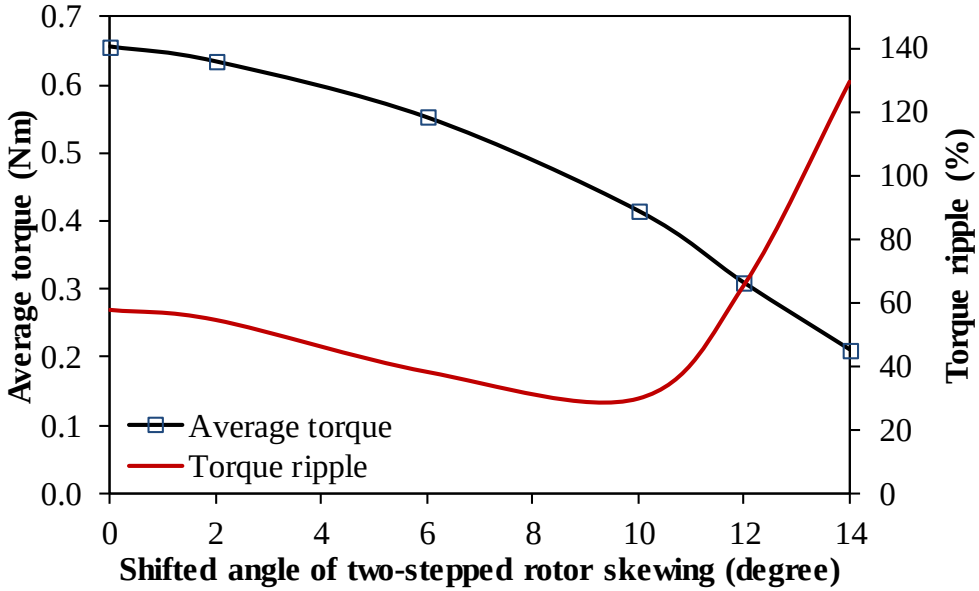

Fig. 6.35. Variation of average torque and torque ripple with rotor skewing angle of 12-slot/10-pole NSWFS machine, copper loss=60W.

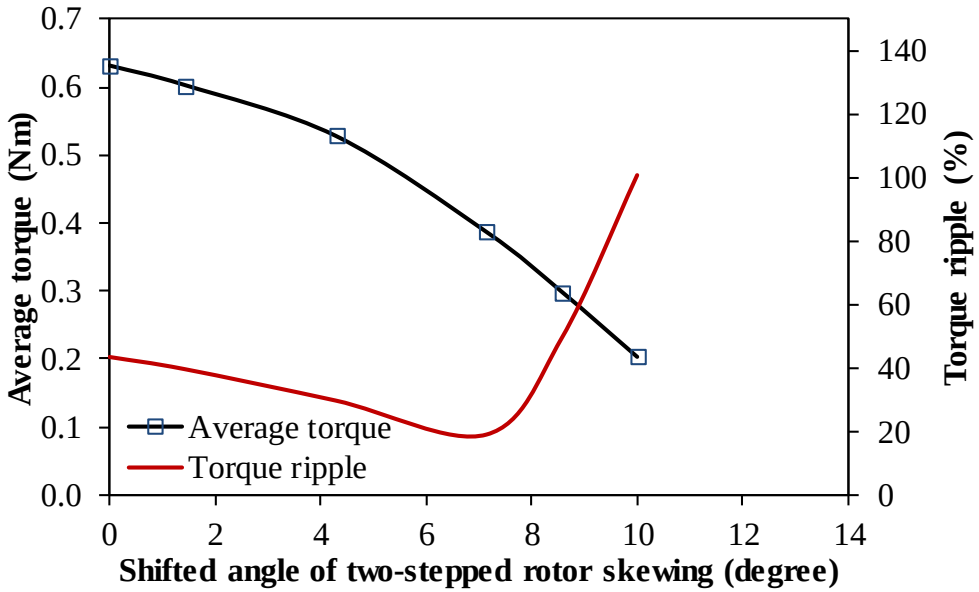

Fig. 6.36. Variation of average torque and torque ripple with rotor skewing angle of 12-slot/14-pole NSWFS machine, copper loss=60W.

The average torque-copper loss curves of four 12-slot NSWFS machines without rotor skewing, the 6-slot/7-pole NSWFS machine and the SNSWFS machine are compared in Fig. 6.37. The percentages of the field winding areas in slots of these machines follow the

optimized results shown in Table 6.2 and Table 6.4. As can be seen, among all 12-slot machines, the 11-pole machine shows the highest average torque. All NSWFS machines show higher average torque than the SNSWFS machine when the copper loss is less than 100W. Compared with the 6-slot/7-pole NSWFS machine, which has the highest average torque among 6-slot machines, the average torques of the 12-slot machines are relatively low.

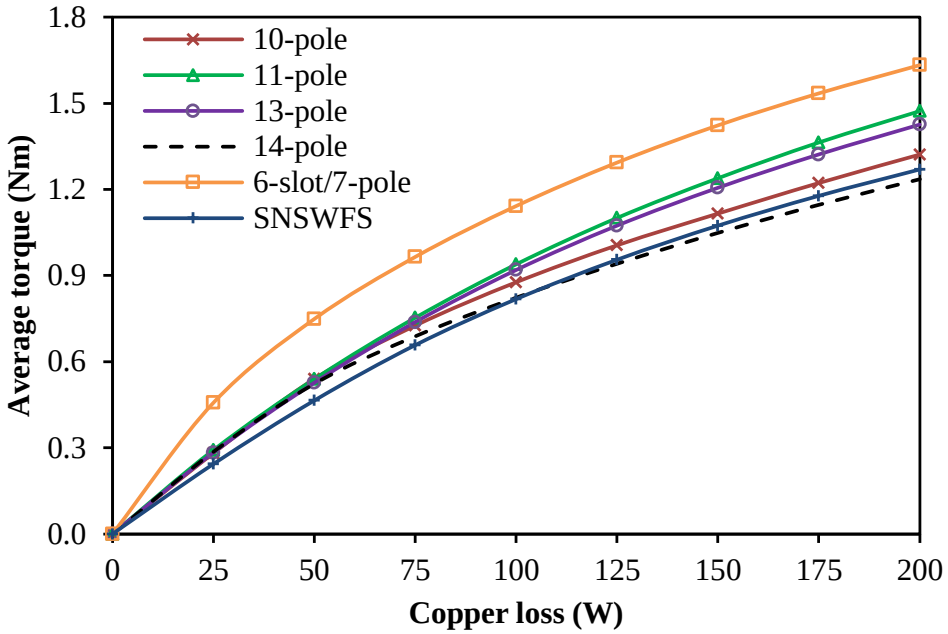

Fig. 6.37. Comparison of average torque-copper loss curves, BLAC operation.

For the WFSF machine, larger stator slot and rotor pole numbers will lead to significantly increased flux leakage, and consequently, reduced torque density [SUL12]. Similarly, as shown in Fig. 6.38 when the electric loadings are the same, the NSWFS machine having more stator slots and rotor poles shows increased flux leakage (Note: The number of divisions of flux lines is the same in Fig. 6.36.). Therefore, as mentioned before, the torque densities of 12-slot NSWFS machines are relatively low compared with those of 6-slot NSWFS machines.

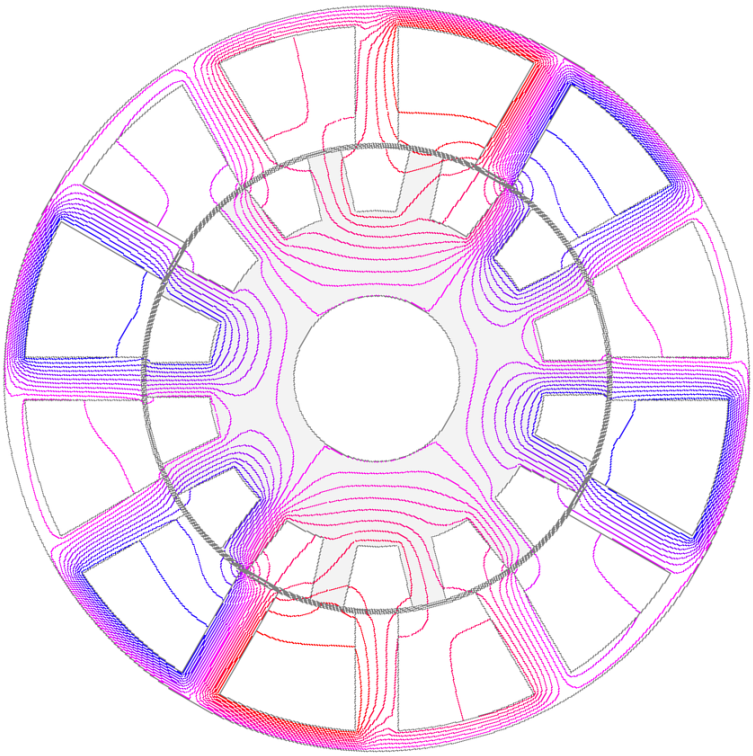

(a)

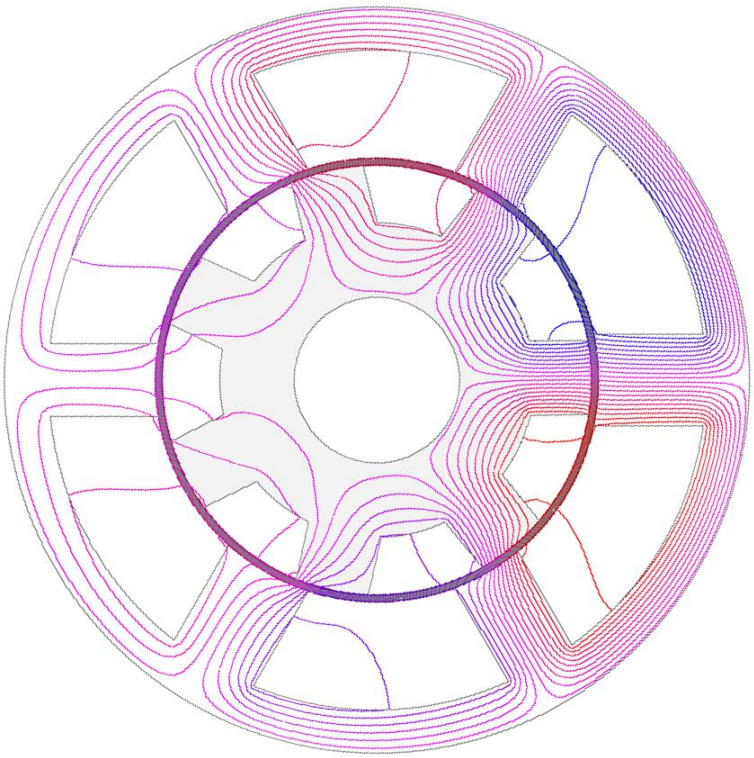

(b)

Fig. 6.38. Flux distributions, field current=armature current=30A. (a) 12-slot/14-pole. (b) 6-slot/7-pole.

When the copper loss is 60W, the torque ripple of the 6-slot/7-pole NSWFS machine is 42.9%, which is 31.4% higher than that of the SNSWFS machine, as can be seen in Fig. 6.39. For the 12-slot/11-pole machine, its average torque is 15.2% higher than the SNSWFS machines and its torque ripple is only 3.5%, which is just 10.8% and 8.2% as high as those of the SNSWFS machine and the 6-slot/7-pole NSWFS machine, respectively. The 12-slot/13-pole machine has even smaller torque ripple which is only 3.3%.

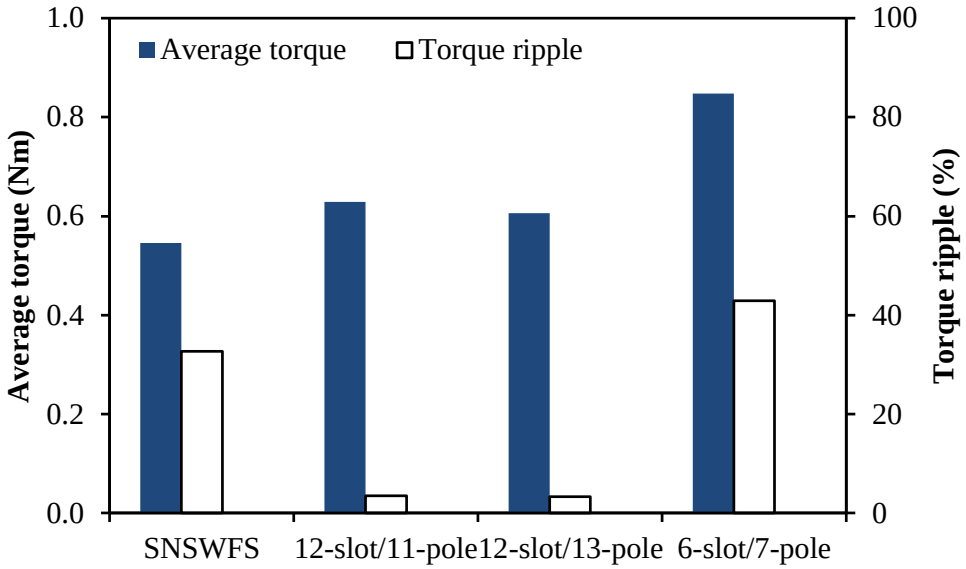

Fig. 6.39. Comparison of average torques and torque ripples of machines, copper loss=60W, BLAC operation.

6.4.4. Unbalanced magnetic force

Fig. 6.40 and Fig. 6.41 show the UMFs of the 6-slot and 12-slot NSWFS machines, respectively. As can be seen, the machines having odd-pole-number rotors show the highest UMFs. UMFs exist in the 6-slot/4- and 8-pole machines, although the numbers of slot and pole are both even. In these machines, each armature winding is consisted of only one coil, and there are no aligned armature coils to offset the UMFs.

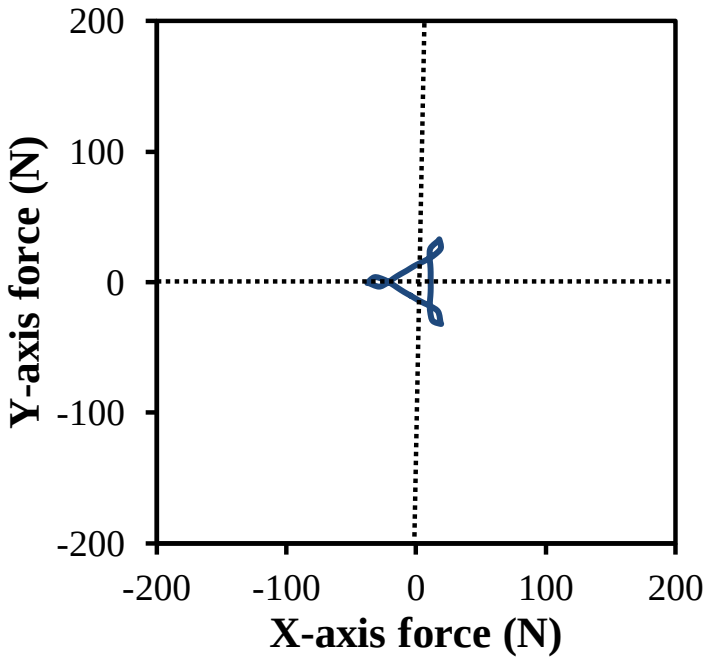
200
100
0
-100
-200
Y-axis force (N)
-200
-100
0
100
200
X-axis force (N)

(a)

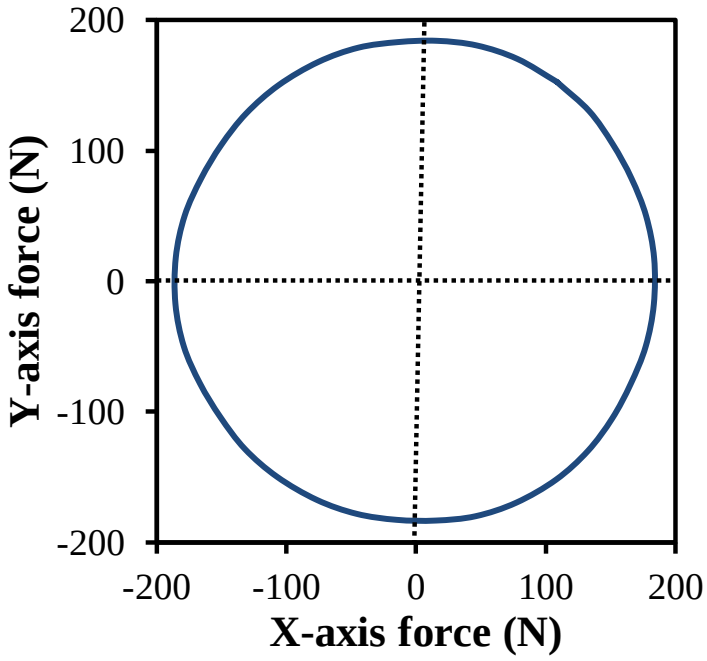
200
100
0
-100
-200
Y-axis force (N)
-200
-100
0
100
200
X-axis force (N)

(b)

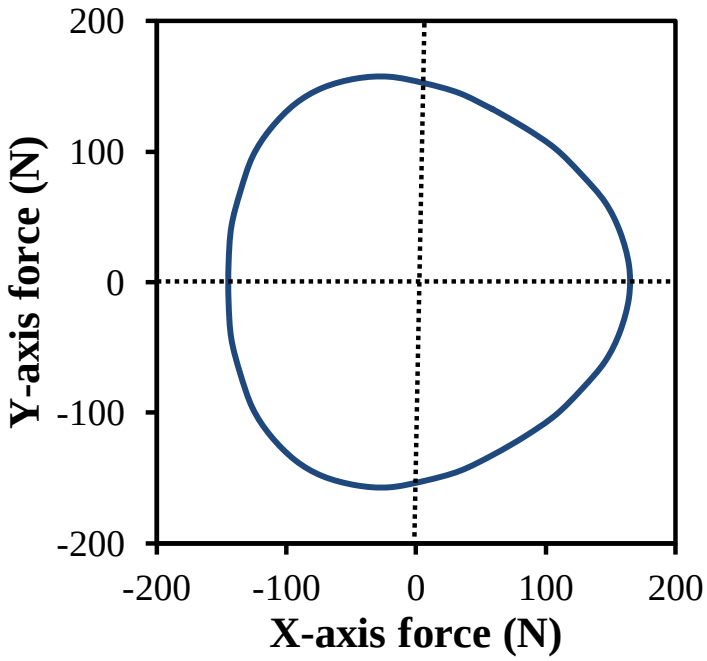

(c)

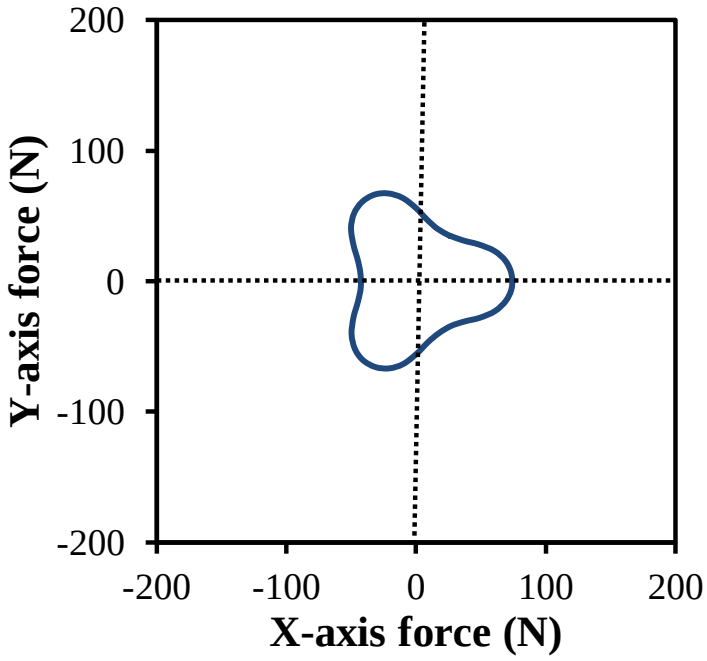

(d)

Fig. 6.40. Comparison of UMFs, Field current = Armature current = 30A, BLAC operation. (a) 6-slot/4-pole. (b) 6-slot/5-pole. (c) 6-slot/7-pole. (d) 6-slot/8-pole.

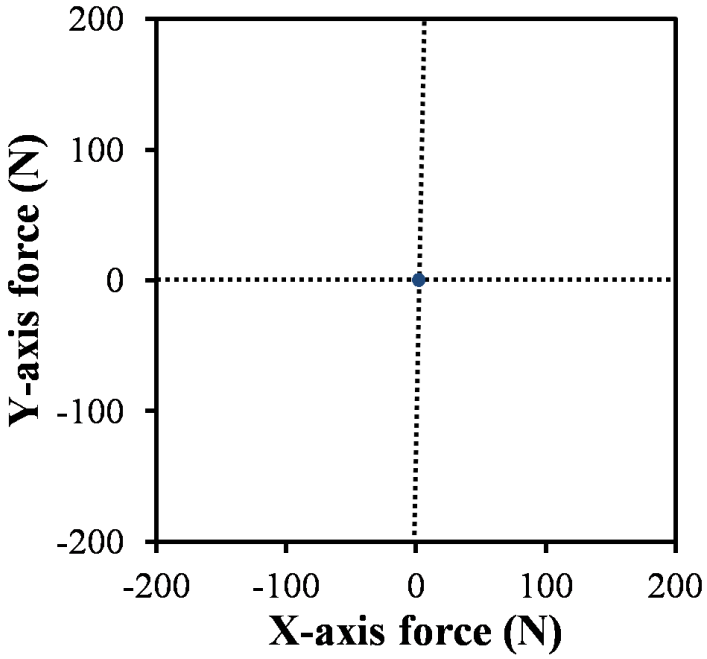
200
100
0
-100
-200
Y-axis force (N)
-200
-100
0
100
200
X-axis force (N)

(a)

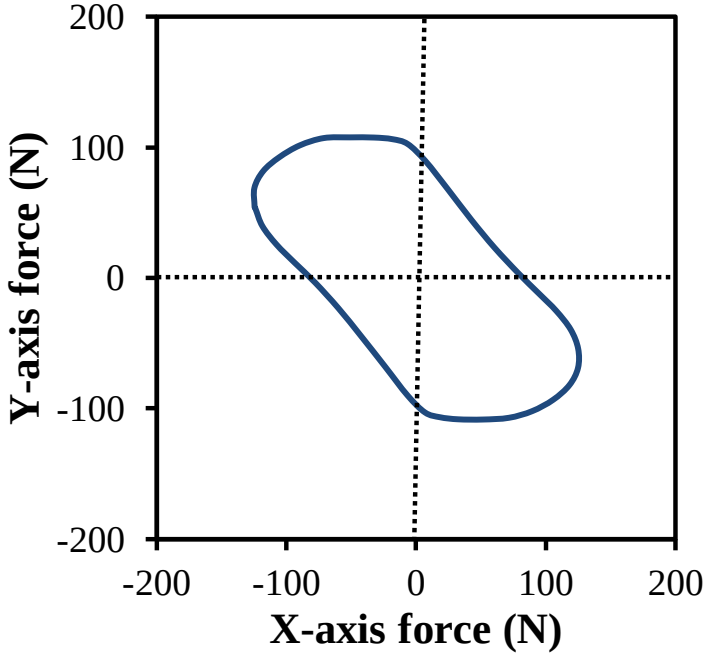
200
100
0
-100
-200
Y-axis force (N)
-200
-100
0
100
200
X-axis force (N)

(b)

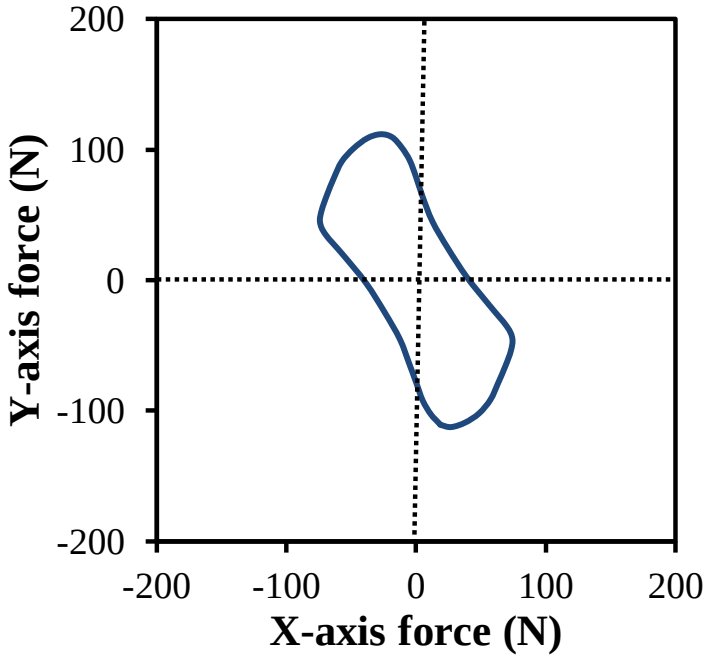

(c)

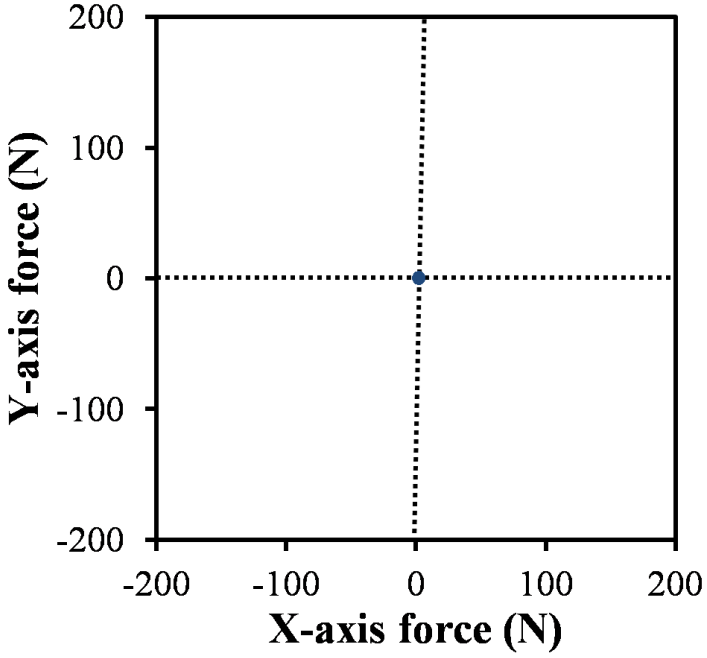

(d)

Fig. 6.41. Comparison of UMFs, Field current = Armature current = 30A, BLAC operation. (a) 12-slot/10-pole. (b) 12-slot/11-pole. (c) 12-slot/13-pole. (d) 12-slot/14-pole.

6.5.Experimental validation

For validating the FEA predictions, aforementioned four 6-slot NSWFS and four 12-slot NSWFS machines have been prototyped, as shown in Fig. 6.42.

It is worth mentioning that only one 6-slot common stator and one 12-slot common stator were built for the sake of reducing the cost. The dimensions of two stators are based on the 6-slot/7-pole and the 12-slot/11-pole machines, respectively, since these two machines show the best performances.

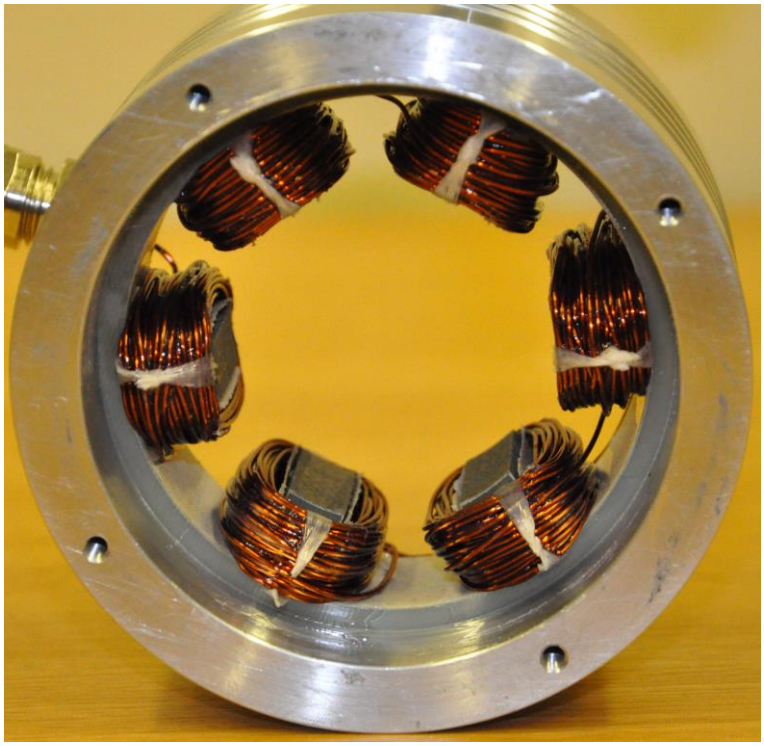

(a)

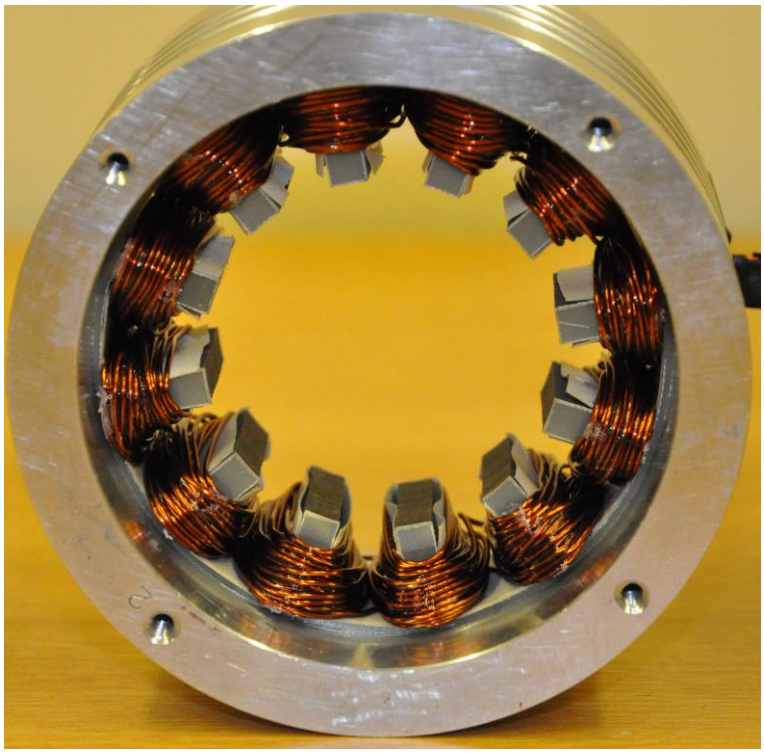

(b)

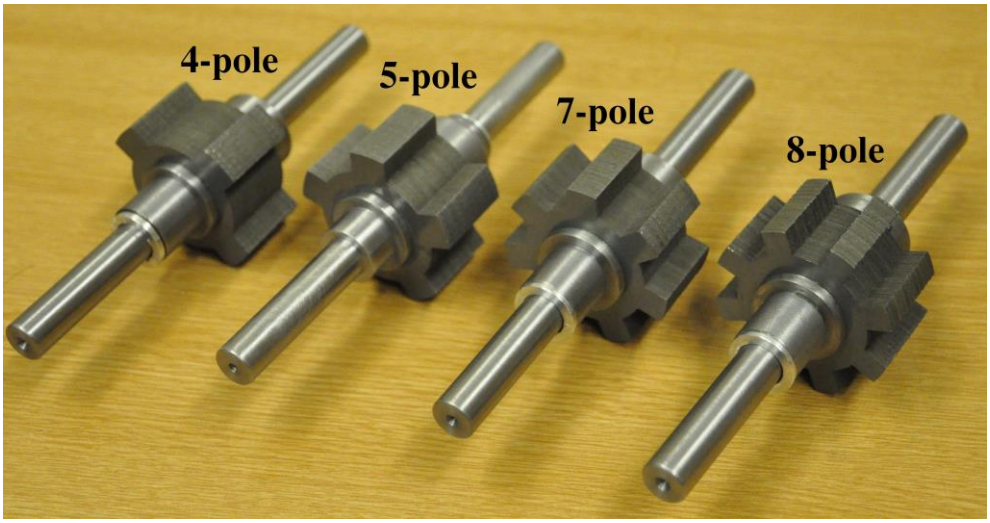

(c)

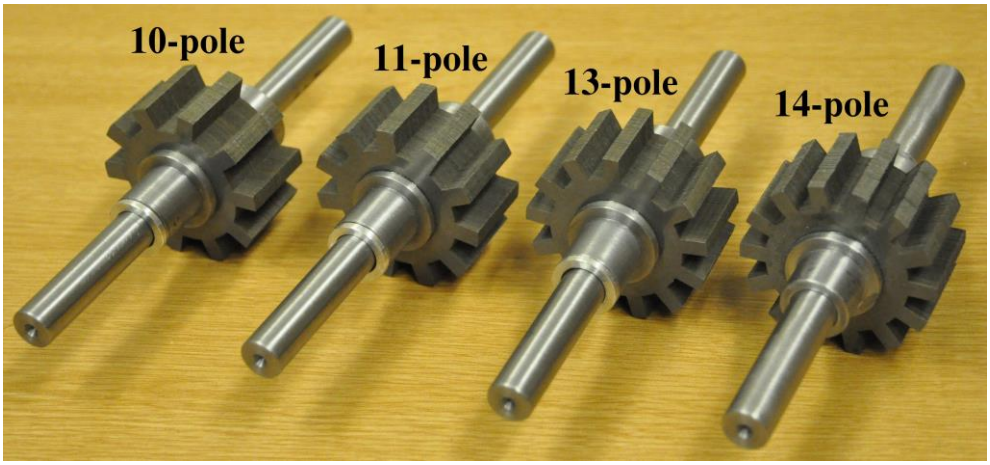

(d)

Fig. 6.42. Prototypes of NSWFS machines. (a) Common stator of 6-slot machines. (b) Common stator of 12-slot machines. (c) Rotors of 6-slot machines. (d) Rotors of 12-slot machines.

When the field current is 20A (current density is ~10A/mm^2), the predicted and measured back-EMF waveforms of NSWFS machines are compared in Fig. 6.43. As can be seen, good agreements between predicted and measured results are achieved. It is worth noticing that the measured back-EMF is slightly smaller than the predicted back-EMF due to ignoring of end-effects.

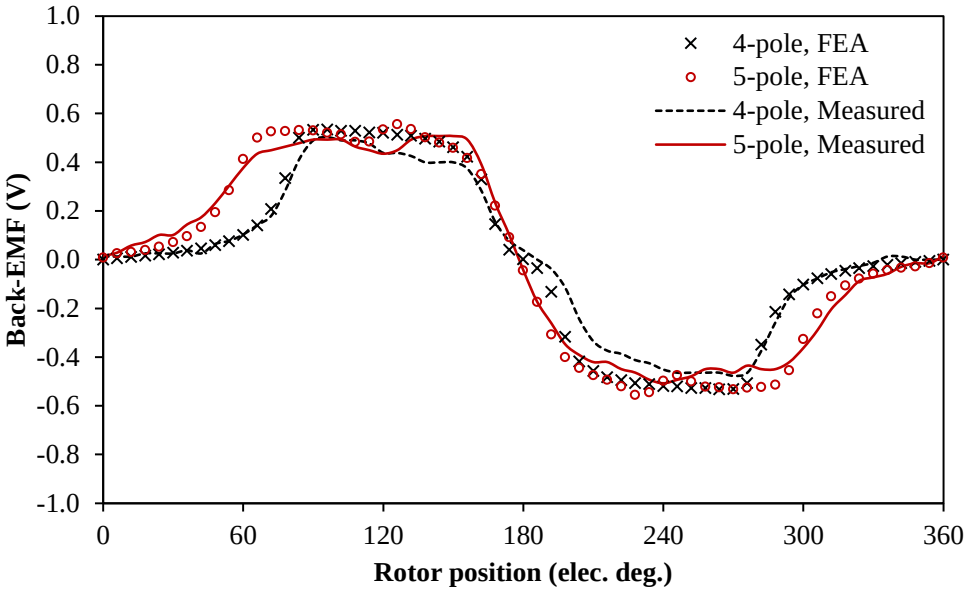
1.0
0.8
0.6
0.4
0.2
0.0
-0.2
-0.4
-0.6
-0.8
-1.0
Back-EMF (V)
0
60
120
180
240
300
360
Rotor position (elec. deg.)
4-pole, FEA
5-pole, FEA
4-pole, Measured
5-pole, Measured

(a)

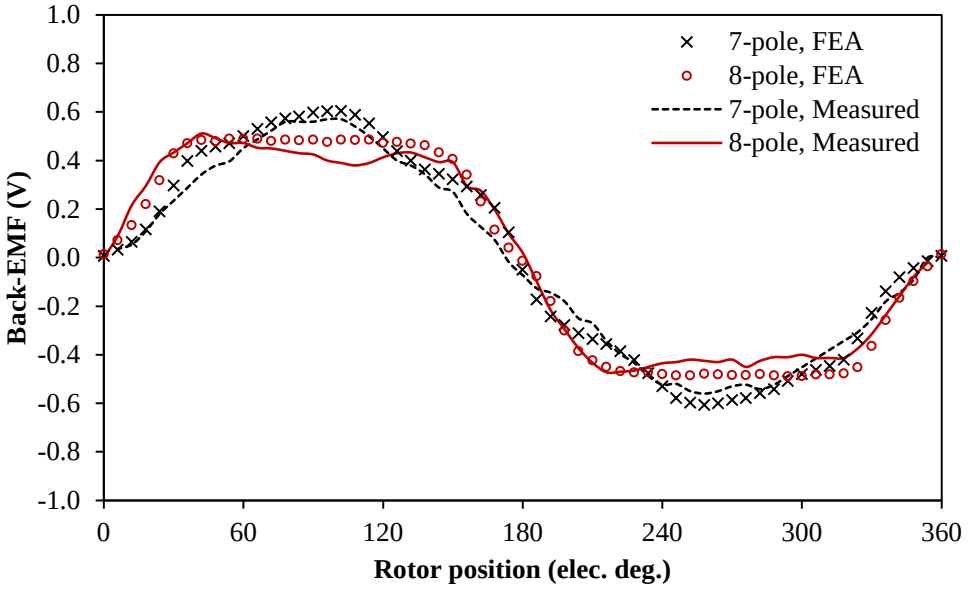
1.0
0.8
0.6
0.4
0.2
0.0
-0.2
-0.4
-0.6
-0.8
-1.0
Back-EMF (V)
0
60
120
180
240
300
360
Rotor position (elec. deg.)
7-pole, FEA
8-pole, FEA
7-pole, Measured
8-pole, Measured

(b)

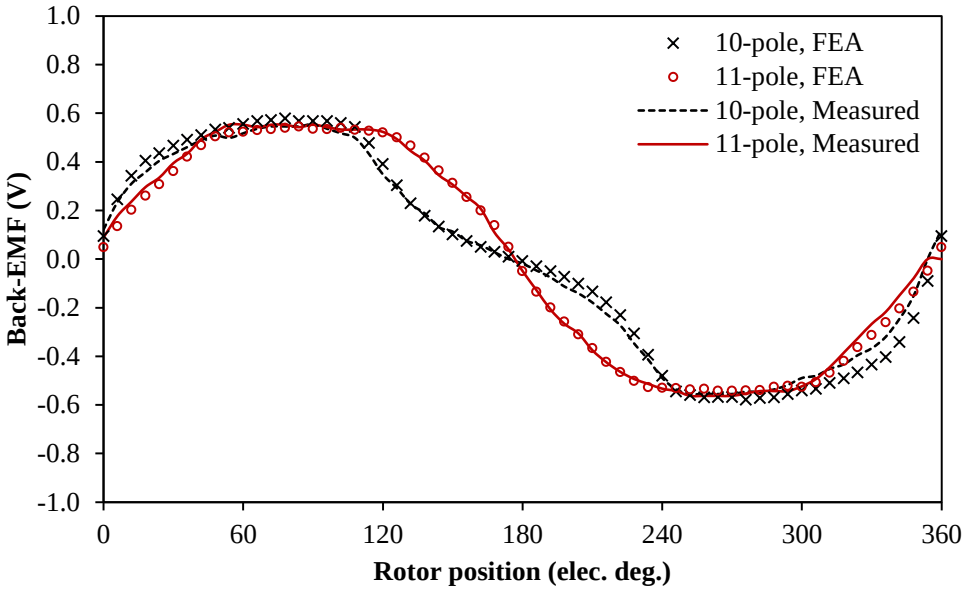

(c)

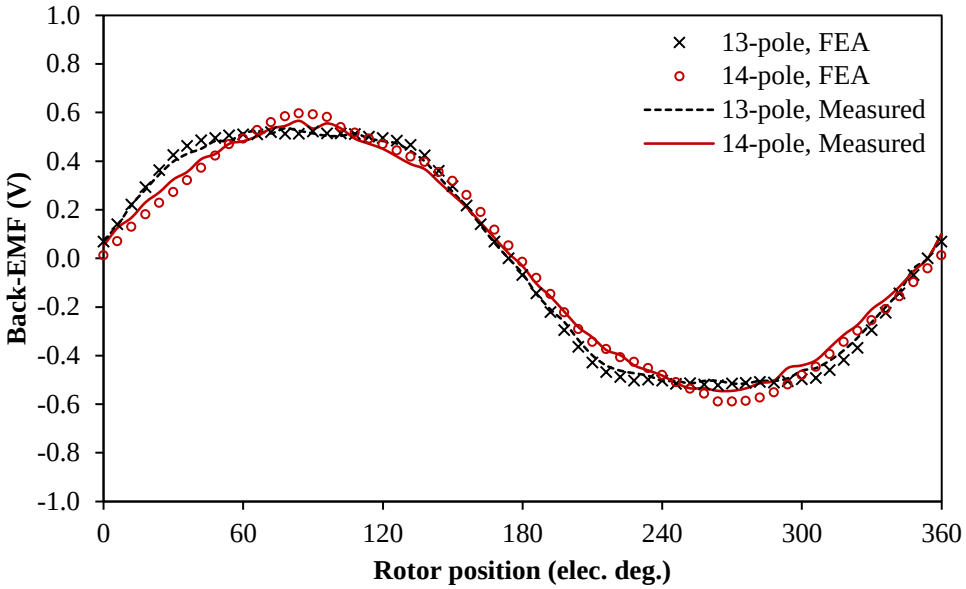

(d)

Fig. 6.43. Back-EMF waveforms, 400 r/min. (a) 6-slot/4- and 5-pole. (b) 6-slot/7- and 8-pole. (c) 12-slot/10- and 11-pole. (d) 12-slot/13- and 14-pole.

When the armature and field currents are 0A and 20A, respectively, the predicted and measured cogging torque waveforms of NSWFS machines are compared in Fig. 6.44. For the 6-slot and 12-slot/10-pole machines, there are good agreements between predicted and measured results. Meanwhile, the FEA predicted cogging torques of the 12-slot/11-, 13- and 14-pole machines are relatively small, and the measured results are higher than the predicted results due to assembly and mechanical tolerances.

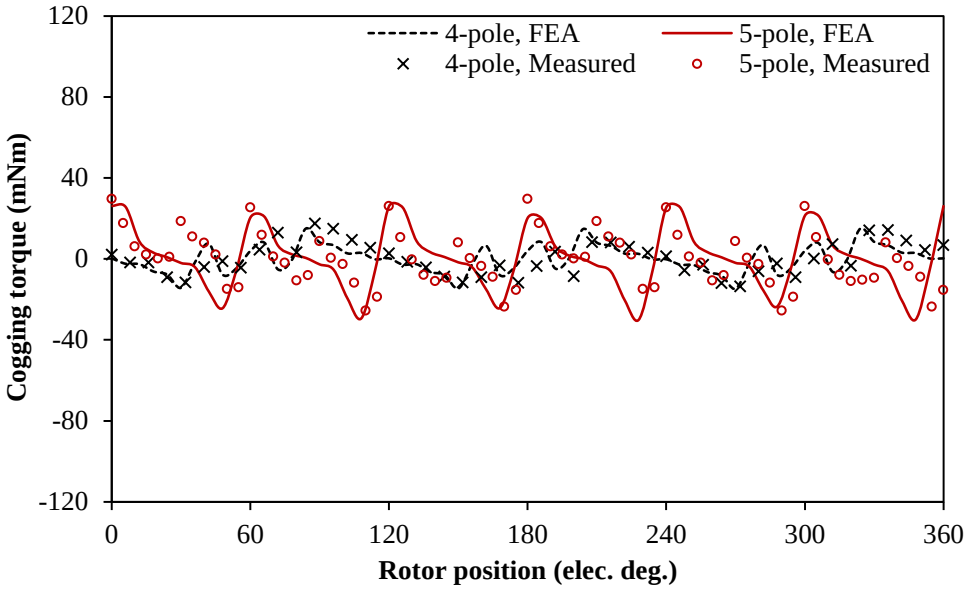
4-pole, FEA
5-pole, FEA
4-pole, Measured
5-pole, Measured
Cogging torque (mNm)
120
80
40
0
-40
-80
-120
0
60
120
180
240
300
360
Rotor position (elec. deg.)

(a)

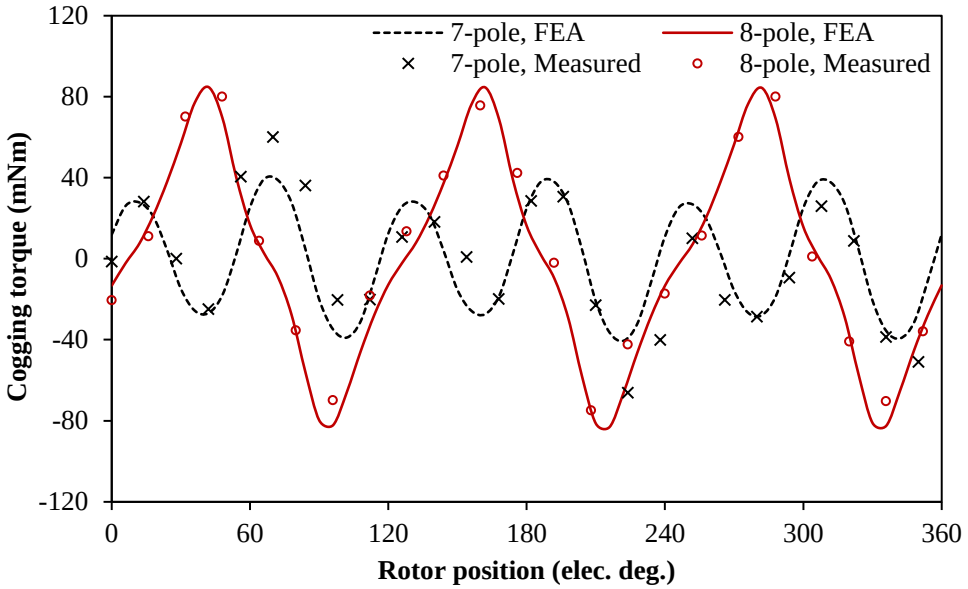
7-pole, FEA
8-pole, FEA
7-pole, Measured
8-pole, Measured
Cogging torque (mNm)
120
80
40
0
-40
-80
-120
0
60
120
180
240
300
360
Rotor position (elec. deg.)

(b)

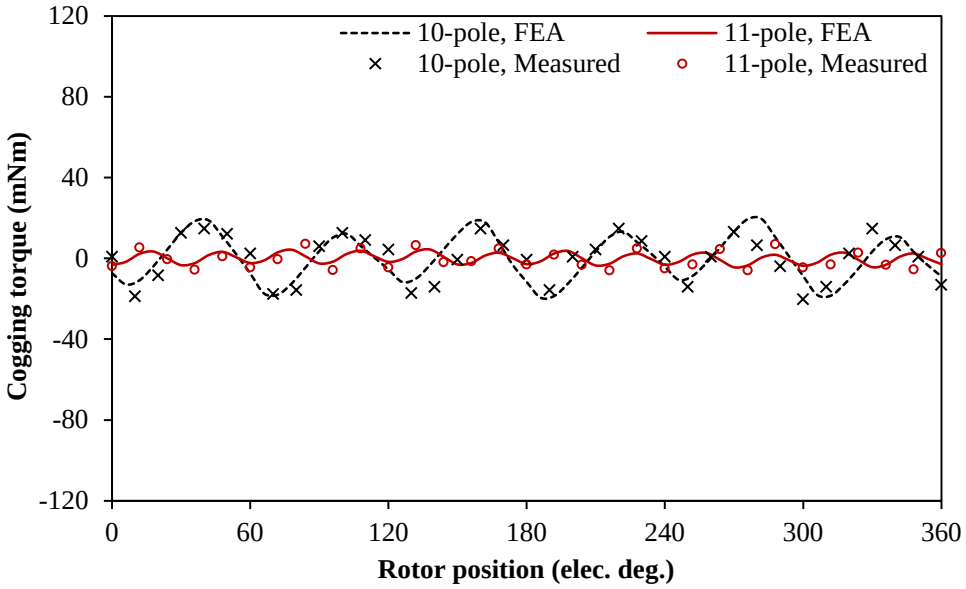

(c)

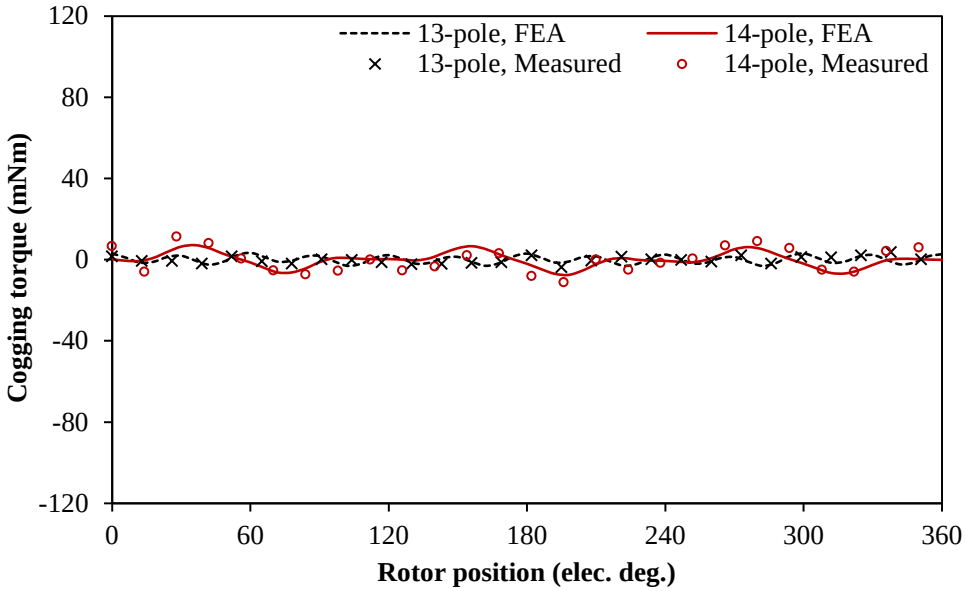

(d)

Fig. 6.44. Cogging torque waveforms, field current=20 A. (a) 6-slot/4- and 5-pole. (b) 6-slot/7- and 8-pole. (c) 12-slot/10- and 11-pole. (d) 12-slot/13- and 14-pole.

Fig. 6.45 compares the predicted and measured torques of NSWFS machines with different q-axis currents when the field currents are 20A. It can be seen that the measured torques are slightly smaller than the predicted torques due to end-effects. Overall, good agreements are achieved.

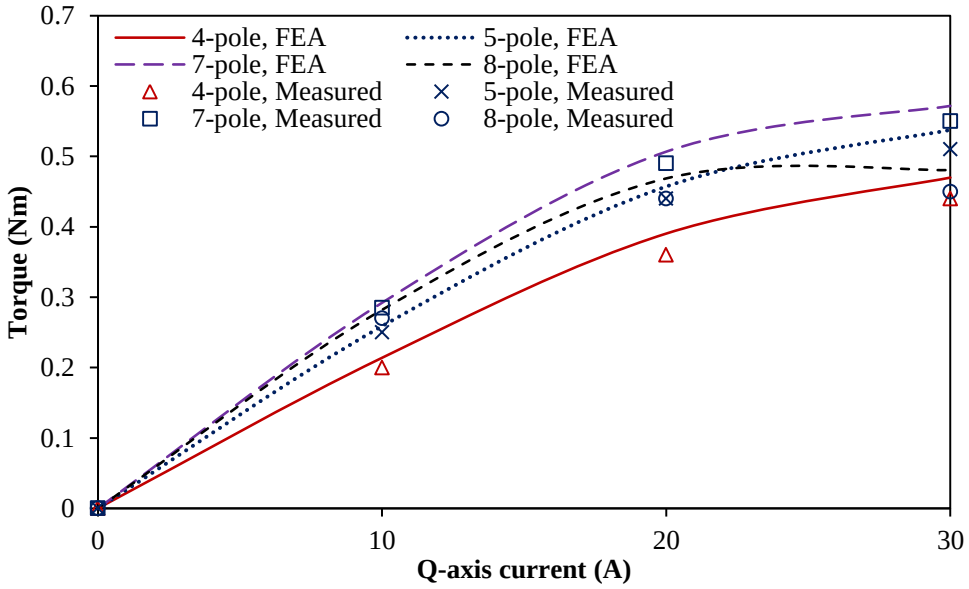

(a)

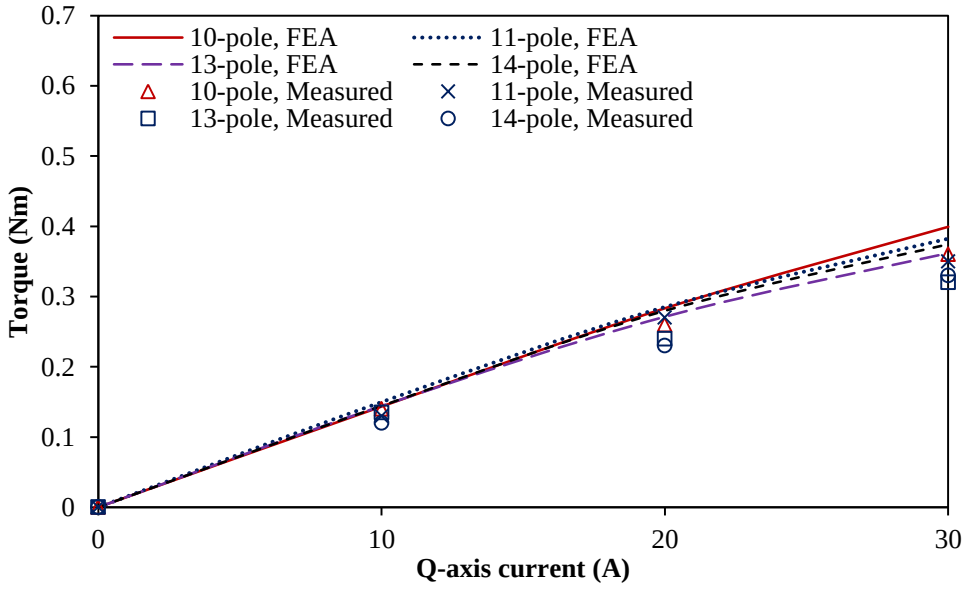

(b)

Fig. 6.45. Torque-current curves, field current=20 A. (a) 6-slot. (b) 12-slot.

6.6.Summary

Three-phase non-overlapping stator wound field synchronous machines employing salient-pole rotors have been investigated in this chapter. The influence of stator slot and rotor pole number combinations of the NSWFS machines is investigated based on the optimised designs. The electromagnetic performances, including back-EMF, cogging torque, and static torque,

of NSWFS machines are analysed and compared by 2-D FEA and validated by experiments on the prototype machines.

It is found that under the same copper loss, the torque density of the 6-slot/7-pole non-overlapping stator wound field synchronous machine can be 72% higher than that of an optimized segmented rotor non-overlapping stator wound field synchronous machine. For the 12-slot non-overlapping stator wound field synchronous machines, the 12-slot/11- and 13-pole machines show higher torque densities and much lower torque ripples than an optimized segmented rotor non-overlapping stator wound field synchronous machine under the same copper loss.

CHAPTER VII. GENERAL CONCLUSIONS

7.1.Conclusions

Several new topologies of stator-WF machines have been proposed and investigated in this thesis. The comparisons have been made between various stator-WF machines. Besides, the topology of a sandwiched SFPM machine, which can be regarded as the origin of a proposed stator-WF machine, has been improved. Most investigations on these novel machines have been examined by experiments. They are summarized as follows.

7.1.1. Sandwiched SFPM machine using V-shaped magnets

The sandwiched SFPM machine, which shows high torque density among all radial-field SFPM machine, can be enhanced further by employing V-shaped magnets. Additionally, the magnet usage is also reduced in this improved machine. Essentially, employing V-shaped magnets allows the sandwiched SFPM to enlarge the slot area by reducing the stator lamination area and magnet thickness without sacrificing the performance.

It is found that the optimal skewing angle for the lowest torque ripple is different from the optimal skewing angle for the lowest cogging torque/amplitude of EMF harmonic in the V-shaped sandwiched SFPM machine. The explanation of this is that the asymmetry in the magnetic circuits caused by saturation result in the phase shift of on-load cogging torque.

7.1.2. Three-phase stator-WF machines

Most investigations on the three-phase WFSF machines were focused on the conventional F2A2 WFSF and segmented rotor F1A1 WFSF machines. In this thesis, a novel three-phase F1A3 WFSF machine has been proposed. Compared with the segmented rotor F1A1 WFSF machine, this machine exhibits much higher torque density since the flux paths will not be restricted by rotor segments. Moreover, compared with conventional F2A2 WFSF machine, this machine shows higher torque density and better copper usage efficiency due to its relatively short end-windings.

According to the investigation, it is found that employing unequal slots will lead to the torque density enhancements in WFSF machines since the bottoms of the stator tooth are usually more saturated. When the electric loading is high, the torque density of a WFSF

machine is not sensitive to the air-gap length, since shorter air-gap length will not lead to significant increase of air-gap flux density.

The efficiency maps of some WFSF machines have been plotted in this thesis. It is found that when the WFSF machine operated at low speed and low loading region, reducing the field current will increase the machine efficiency since the copper loss is dominated at this region.

Compared with the SFPM machines using low-cost ferrite magnets, WFSF machines exhibit higher torque densities under higher electric loading. Moreover, compared with the SFPM and IPM machines using rare-earth magnets, the WFSF machines show much higher material usage efficiencies.

To increase the torque density and reduce the difficulty of manufacture, the salient-pole rotor has replaced the segmented rotor in the segmented rotor F1A1 WFSF machine and results in a non-overlapping stator-WF synchronous machine. By selecting appropriate slot/pole combination, the salient-pole machine can achieve higher torque density and lower torque ripple than the segmented rotor machine.

It is also found that halving the slot and pole numbers of the stator-WF machines will reduce the flux leakages and consequently increase the torque densities of the machines.

7.1.3. General comparison of three-phase machines

With respect to high torque density and low torque ripple, five stator-WF machines (12s/8p segmented rotor F1A1, 12s/11p salient-pole rotor F1A1, 24s/14p F2A2, 18s/10p F1A3, 12s/8p F3A1) and two ferrite magnet SFPM machines (12s/10p SFPM, 6s/10p v-shaped magnets sandwiched SFPM machine) investigated in this thesis are chosen and compared with Toyota Prius IPM 2010 machine of the same size (stator outer diameter=264mm, axial length=50.8mm, air-gap length=0.73mm, packing factor=0.47, all armature and field currents are the same under the same current density), as shown in Fig. 7.1. All stator-WF and SFPM machines have been optimized to achieve the maximum average torque when the current density is 26.8A/mm^2. The optimized parameters are shown in Table 7.1.

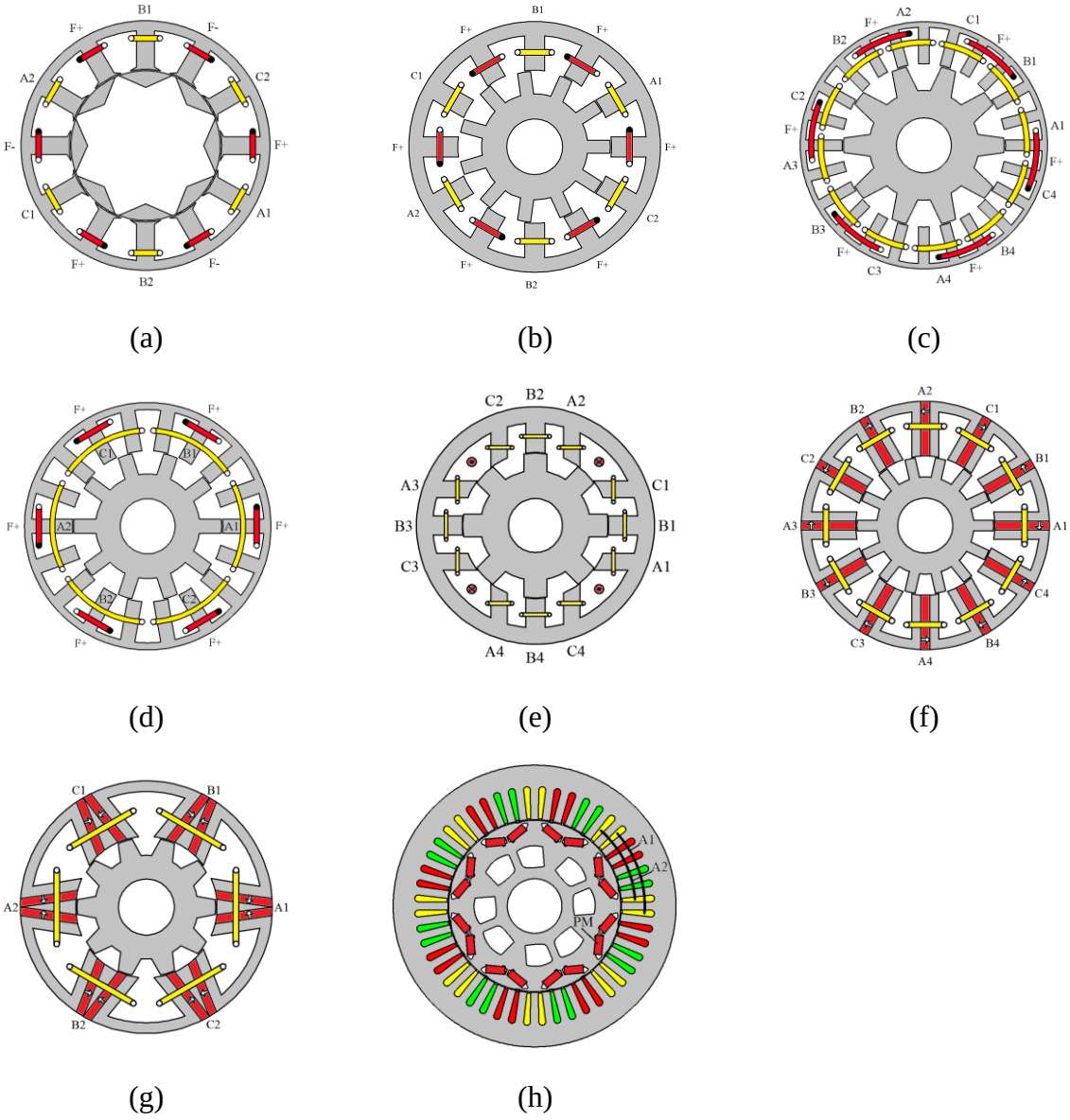

Fig. 7.1. Topologies of machines. (a) Segmented rotor F1A1-8 pole. (b) F1A1-11 pole. (c) F2A2-14 pole. (d) F1A3-10 pole. (e) F3A1-8 pole. (f) SFPM, 12s/10p, ferrite magnets. (g) V-shaped magnet sandwiched SFPM, 6s/10p, ferrite magnets. (h) Toyota Prius IPM.

Table 7.1. Main parameters of machines

Items	WFSF F1A1-8 pole	NSWFS F1A1-11 pole	WFSF F2A2-14 pole	WFSF F1A3-10 pole	F3A1-8 pole	V-shaped SSFPM 6s/10p B=0.4T	SFPM 12s/14p B=0.4T	IPM
Stator slot number	12	12	24	18	12	6	12	48
Rotor pole number	8	11	14	10	8	10	14	8
Stator outer radius (mm)	132	132	132	132	132	132	132	132
Axial length (mm)	50.8	50.8	50.8	50.8	50.8	50.8	50.8	50.8
Air-gap length (mm)	0.73	0.73	0.73	0.73	0.73	0.73	0.73	0.73
Split ratio	0.59	0.70	0.72	0.67	0.61	0.67	0.73	0.61
Stator tooth width at the top, W_1 (mm)	21.2	21.1	11.5	18.6	19.8	15.1	11.2	7.3
Stator tooth width at the bottom, W_2 (mm)	18.2	21.1	16.9	24.8	19.8	15.1	11.2	7.3
Stator back-iron thickness of field slot, L_1 (mm)	20	11	8.6	12.2	18	--	--	--
Stator back-iron thickness of armature slot, L_2 (mm)	20	11	9	8.6	18	15	9.8	20.2
Rotor pole arc (degree)	36.5	12	8.5	12.5	18	12.7	7.7	--
Total armature slot area (mm^2)	5928.7	5772.0	4549.0	4870.8	4152.2	5809.3	5368.3	7156.8
Total field slot area (mm^2)	5928.7	5772.0	4960.8	6943.2	3744.6	--	--	--
Total number of turns of armature windings	444	432	336	372	312	444	408	528
Total number of turns of field windings	444	432	372	528	280	--	--	--
Packing factor (effective copper area/slot area)	0.47	0.47	0.47	0.47	0.47	0.47	0.47	0.47
Magnet material	--	--	--	--	--	Ferrite	Ferrite	NdFeB
Number of PM pieces	--	--	--	--	--	12	12	16
PM thickness (mm)	--	--	--	--	--	13.3	16.9	7.2
PM length (mm)	--	--	--	--	--	42.1	35.0	17.9

A. Torque waveforms and torque ripples

When the current density is 26.8A/mm^2, the torque waveforms of machines are shown in Fig. 7.2. As can be seen in Fig. 7.3, F1A1-11 pole and F2A2-14 pole machines show the lowest torque ripples among these machines.

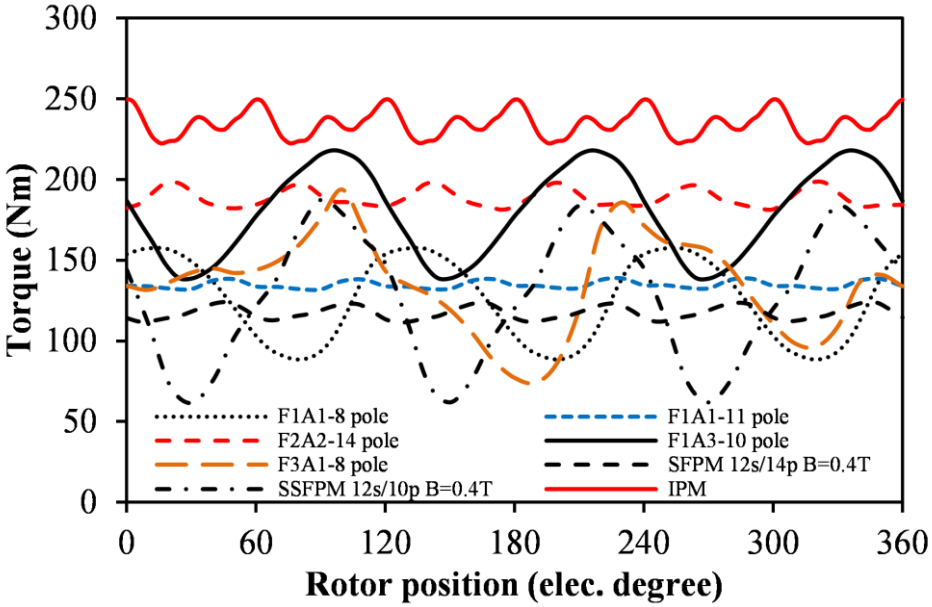

Fig. 7.2. Comparison of torque waveforms, current density=26.8A/mm^2, BLAC operation.

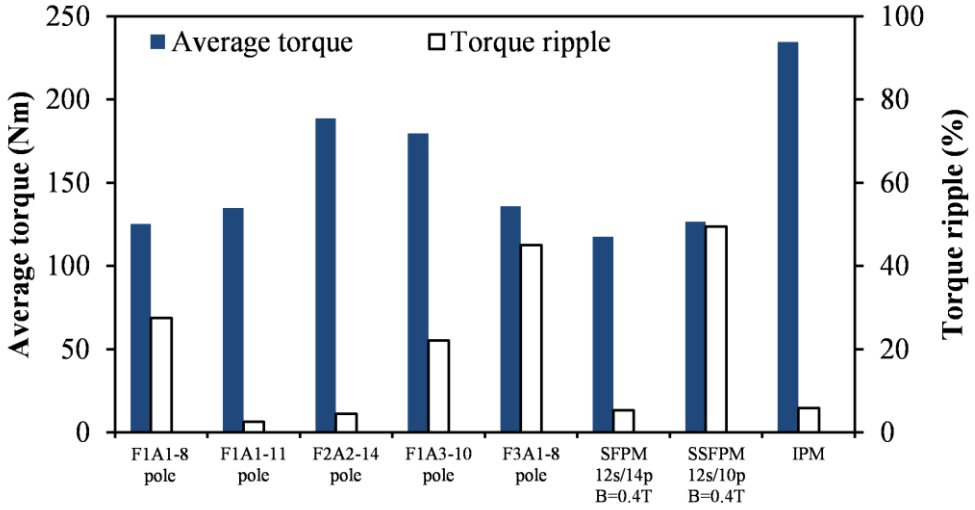

Fig. 7.3. Comparison of average torque and torque ripple, current density=26.8A/mm^2, BLAC operation.

B. Torque-current density curves and material usage efficiency

Fig. 7.4 and Fig. 7.5 compare the average torques and material usage efficiencies (based on the purchase prices of materials in late 2013) under different current densities. Stator-WF machines show higher average torques than the SFPM machine under high electric loading. As can be seen in Fig. 7.5, all stator-WF machines show the similar material usage efficiency since the torque densities of short-pitched machines are low. Sandwiched SFPM machine can achieve very high material usage efficiency, and this is benefited from its low material cost and high torque density.

Overall, the stator-WF machines, of which sums of field and armature winding pitches are even integers, exhibit good torque capabilities. Among these stator-WF machines, the torque capabilities of non-overlapping stator-WF machines are smaller than other stator-WF machines.

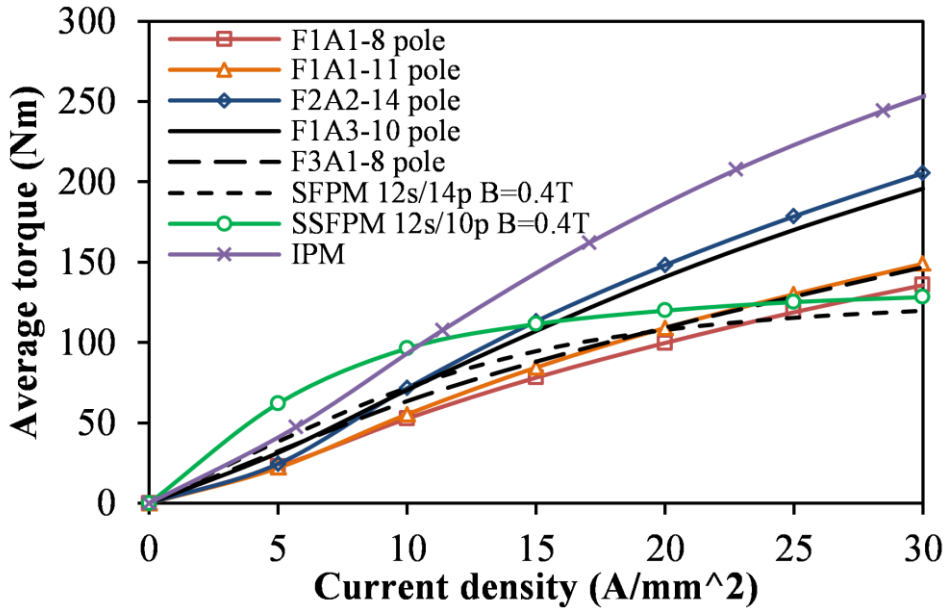

Fig. 7.4. Comparison of average torque-current density curves.

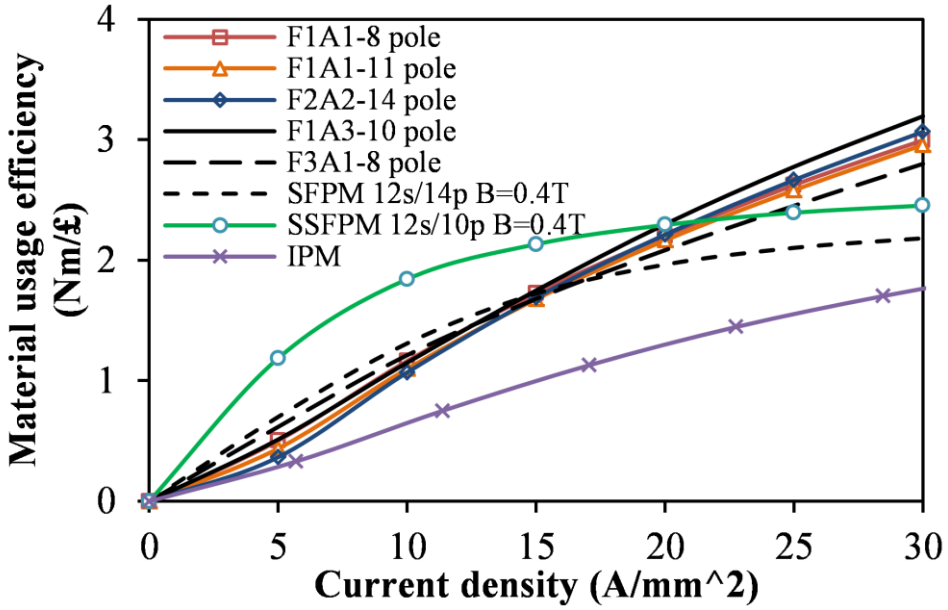

Fig. 7.5. Comparison of material usage efficiency.

C. Iron losses, efficiency maps and power factors

The iron losses, efficiency maps and power factors of machines are compared in Fig. 7.6, Fig. 7.7, and Fig. 7.8, respectively. In terms of the stator-WF machines, the machines having 1 slot-pitch field windings (F1 machines) exhibit much lower iron losses than the F2A2 machine. In Fig. 7.7, the efficiency maps of machines are compared. As can be seen, the SFPM machines have much larger high-efficiency areas than the stator-WF machines due to

no field winding copper losses. It is worth noticing that the F3A1-8 pole machine will produce negative average torque under some negative d- and positive q-axis currents, and the efficiency map of this machine is not plotted.

The power factor of machines is given by $\cos\varphi$, where φ is the angle between current and voltage vectors. The d- and q-axis voltages are given by (7.1) and (7.2), respectively.

$$U_d = -\omega\Psi_q + R_a I_d \tag{7.1}$$

$$U_q = \omega\Psi_d + R_a I_q \tag{7.2}$$

where U_d and U_q are the d- and q- axis voltages, ω is the electrical angular velocity, Ψ_d and Ψ_q are the d- and q-axis flux-linkages, R_a is the phase resistance, I_d and I_q are the d- and q-axis currents.

As shown in Fig. 7.8, the power factors of all stator-WF and SFPM machines are relatively low. In future, the power factor will be taken into consideration during the machine optimization.

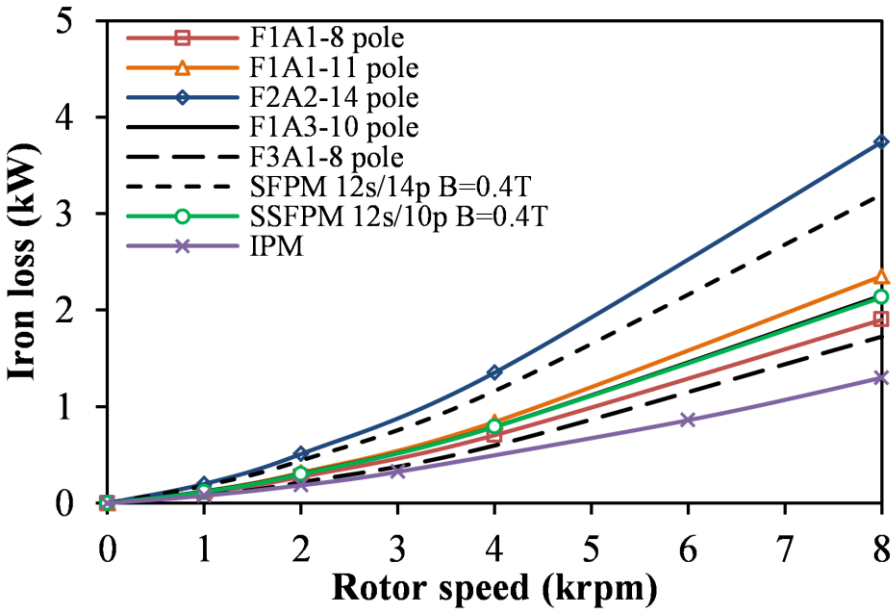

Fig. 7.6. Comparison of iron losses, current density=26.8A/mm^2, BLAC operation.

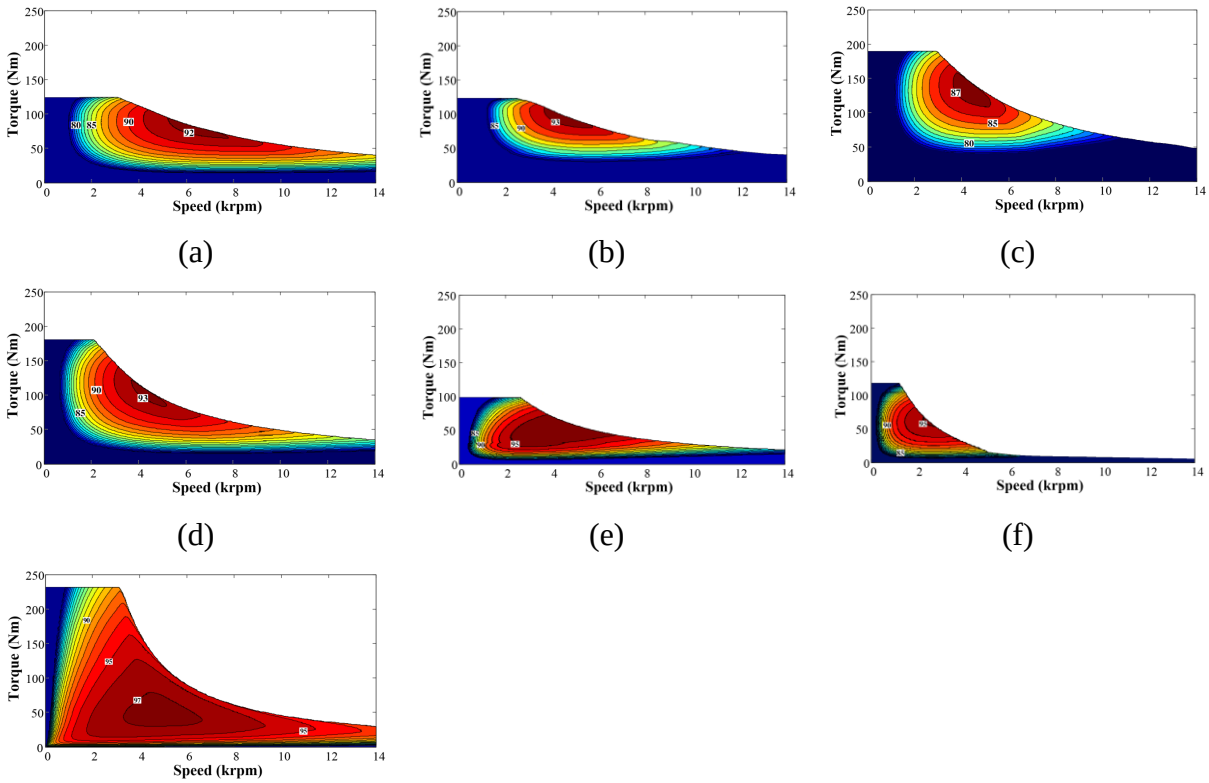

Fig. 7.7. Comparison of efficiency maps, for stator-WF machines, field current = 167A. (a) Segmented rotor, F1A1-8 pole. (b) F1A1-11 pole. (c) F2A2-14 pole. (d) F1A3-10 pole. (e) SFPM, 12s/14p. (f) SSFPM, 6s/10p. (g) IPM.

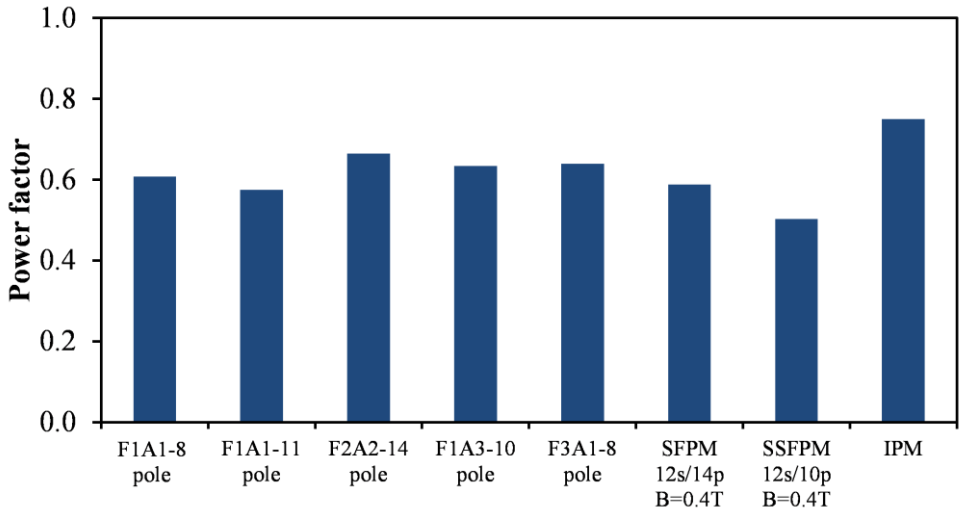

Fig. 7.8. Comparison of power factors, current density=26.8A/mm^2, 1000 rpm.

7.1.4. Single-phase WFSF machines

Based on the topology and operation principle of the successfully commercialized F2A2-4 pole single-phase WFSF machine, a F2A2-6 pole single-phase WFSF machine has been proposed in this thesis. Compared with the F2A2-4 pole machine under the same copper loss, this machine shows similar torque density but shorter end-windings. Thus, better copper usage efficiency has been achieved.

A F1A3-6 pole machine has been proposed as well. This single-phase WFSF machine, which can share the same stator lamination topology with F2A2-6 pole machine, has even shorter end-windings and smaller iron loss compared with the F2A2-6 pole machine. The slot number and pole number of F1A3-6 pole machine can be halved and result in a F1A3-3 pole machine. Compared with the F2A2-4 pole machine, this machine shows significantly reduced iron loss.

It is also found in this thesis that compared with a single-phase switched reluctance machine of the same size, a single-phase WFSF machine exhibit similar efficiency but higher torque density and power factor under the same current density.

7.2.Future work

Following the research work in this thesis, future research includes:

(a) Investigations of the F2A1 stator-WF, F1A3 and F2A3 WFSF machines.

(b) Development of drive circuit topologies of WFSF machines for cost-sensitive applications.

(c) Improvement of efficiencies and power factors of WFSF machines.

(d) New topologies of hybrid excited stator-PM machines.

REFERENCES

[BAS11] M. L. Bash and S. D. Pekarek, "Modeling of salient-pole wound-rotor synchronous machines for population-based design," *IEEE Trans. Energy Convers.*, vol. 26, no. 2, pp. 381-392, 2011.

[BAS12] M. L. Bash and S. Pekarek, "Analysis and validation of a population-based design of a wound-rotor synchronous machine," *IEEE Trans. Energy Convers.*, vol. 27, no. 3, pp. 603-614, 2012.

[BIA02] N. Bianchi and S. Bolognani, "Design techniques for reducing the cogging torque in surface-mounted PM motors," *IEEE Trans. Ind. Appl.*, vol. 38, no. 5, pp. 1259–1265, 2002.

[CHE06] Y. Chen, Y.S. Chen, Z.Q. Zhu, and D. Howe, and Y.Y. Ye, "Starting torque of single-phase flux-switching permanent magnet motors," *IEEE Trans. Magn.*, vol. 42, no. 10, pp. 3416-3418, 2006.

[CHE08] J. T. Chen, Z.Q. Zhu, and D. Howe, "Stator and rotor pole combination and optimal design of multi-tooth flux-switching PM brushless AC machines," *IEEE Trans. Magn.*, vol. 44, no. 12, pp. 4659-4667, 2008.

[CHE08b] J. Chen, R. Chen, C.Y. Gong, and Z.H. Chen, "Study on variable speed direct drive wind energy conversion system with doubly salient electro- magnetic generator," *ICEMS2008,* 2008, vol. 5, no. 2, pp. 2401-2407.

[CHE10] J. T. Chen and Z. Q. Zhu, "Comparison of all- and alternate-poles wound flux-switching PM machines having different stator and rotor pole numbers," *IEEE Trans. Ind. Appl.*, vol. 46, no. 4. pp. 1406–1415, 2010.

[CHE10b] J. T. Chen, Z. Q. Zhu, S. Iwasaki, and R. Deodhar, "Low-cost flux-switching brushless AC machines," *IEEE Vehicle Power and Propulsion Conf.,* 1-3 Sept., 2010, Lille, France, VPPC 2010, Paper RT6/95-13475.

[CHE11] J. T. Chen, Z. Q. Zhu, S. Iwasaki, R. Deodhar, "A novel E-core flux-switching PM brushless AC machine for direct-drive applications," *IEEE Trans. Ind. Appl.*, vol.47, no.3, pp. 1273-1282, 2011.

[CHE11b] J. T. Chen, Z. Q. Zhu, S. Iwasaki, R. Deodhar, "Influence of slot opening on optimal stator and rotor pole combination and electromagnetic performance of flux-switching PM brushless AC machines," *IEEE Trans. Ind. Appl.*, vol. 47, no. 4, pp. 1681-1691, 2011.

[DEO97] R. P. Deodhar, S. Andersson, I. Boldea and T. J. E. Miller, "The flux-reversal machine: a new brushless doubly-salient permanent-magnet machine," *IEEE Trans. Ind. Appl.*, vol. 33, no. 4, pp. 925-934, 1997.

[DOR11] D. G. Dorrell and M. Popescu, "Effect of winding asymmetries and winding connection on small synchronous machines," *IEEE Trans. Ind. Appl.*, vol. 47,

no. 6, pp. 2453-2459, 2011.

[ELR08] A. M. EL-Refaie, Z. Q. Zhu, T. M. Jahns, and D. Howe, "Winding inductances of fractional slot surface-mounted permanent magnet brushless machines," *in Conf. Rec. IEEE IAS Annu. Meeting*, Edmonton, AB, Canada, Oct. 2–5, 2008, pp. 1–8.

[FAS14] A. Fasolo, L. Alberti, and N. Bianchi, "Performance comparison between switching-flux and IPM machine with rare earth and ferrite PMs," *IEEE Trans. Ind. Appl.*, in Press.

[FEI06] W. Z. Fei and J. X. Shen, "Novel permanent magnet switching flux Motors," *Proc. 41st Int.Universities Power Eng. Conf.*, 2006, pp. 729-733.

[FEI12] W. Z. Fei, P. Luk, and J. X. Shen, "Torque analysis of permanent magnet flux switching machines with rotor step skewing," *IEEE Trans. Magn.*, vol. 48, no. 10, pp. 2644-2673, 2012.

[FEI12b] W.Z. Fei, P. C. K. Luk, J. X. Shen, Y. Wang, and M.J. Jin, "A novel permanent-magnet flux switching machine with an outer-rotor configuration for in-wheel light traction applications," *IEEE Trans. Ind. Appl.*, vol. 48, no. 5. pp. 1496–1506, 2012.

[FRI10] G. Friedrich, "Experimental comparison between wound rotor and permanent magnet synchronous machine for integrated starter generator applications," in *IEEE Energy Conv. Congr. Expo (ECCE2010)*, Atlanta, USA, 2010, pp. 1731-1736.

[FUK12] T. Fukami, Y. Matsuura, K. Shima, M. Momiyama, and M. Kawamura, "A multipole synchronous machine with nonoverlapping concentrated armature and field windings on the stator," *IEEE Trans. Ind. Electron.*, vol. 59, no. 6, pp. 2583-2590, 2012.

[FUK12] T. Fukami, Y. Matsuura, K. Shima, M. Momiyama, and M. Kawamura, "A multipole synchronous machine with nonoverlapping concentrated armature and field windings on the stator," *IEEE Trans. Ind. Electron.*, vol. 59, no. 6, pp. 2583-2590, Jun. 2012.

[GAU12] B. Gaussens, E. Hoang, O. de la Barriere, J. Saint-Michel, M. Lecrivain and M. Gabsi, "Analytical approach for air-gap modeling of field-excited flux-switching machine: no-load operation," *IEEE Trans. Magn.*, vol. 48, no. 9, pp. 2505-2517, 2012.

[GAU13] B. Gaussens, O. de la Barriere, E. Hoang, J. Saint-Michel, P. Manfe, M. Lecrivain and M. Gabsi, "Magnetic field solution in doubly slotted airgap of conventional and alternate field-excited switched flux topologies," *IEEE Trans. Magn.*, vol. 49, no. 9, pp. 5083-5096, 2013.

[GRI12] A. Griffo, D. Drury, T. Sawata, and P. H. Mellor, "Sensorless starting of a wound field synchronous starter/generator for aerospace applications," *IEEE Trans. Ind. Electron.*, vol. 59, no. 9, pp. 3579-3587, 2012.

[HOA97] E. Hoang, A. H. Ben-Ahmed and J. Lucidarme, “Switching flux permanent magnet polyphased synchronous machines,” *7th European Conf. on Power Electronics and Applications*, pp.903-908, 1997.

[HWA14] Y.J. Hwang, M.C. Ahn, Y.S. Yoon, and H.M. Kim, “Electromagnetic design of a 15 MW-class HTS flux switching synchronous generator considering mechanical stress of the rotor core,” *IEEE Trans. on Appl. Supercond.,* vol. 24, no. 3, pp. 5202305-5202305, Jun. 2013.

[ISH05] D. Ishak, Z.Q. Zhu, and D. Howe, “eddy-current loss in the rotor magnets of permanent-magnet brushless machines having a fractional number of slots per pole,” *IEEE Trans. Magn.,* vol. 41, no. 9, pp. 2462-2469, 2005.

[KHA14] F. Khan, E. Sulaiman, and M.Z. Ahmad, “Coil test analysis of wound field three-phase flux switching machine with non-overlapping winding and salient rotor,” *2014 IEEE International Power Engineering and Optimization Conference (PEOCO2014),* 2014, pp. 243-247.

[LI08] H. Li and Z. Chen, “Overview of different wind generator systems and their comparisons,” *IET Renew. Power Generat.,* vol. 2, no. 2, pp. 123-138, 2008.

[LI95] S.H. Li, F. Liang, Y. Zhao and T.A. Lipo, "A doubly salient doubly excited variable reluctance motor, " *IEEE Trans. Ind. Appl.,* vol.31, no.1, pp.99-106, 1995.

[LIA95] Y. Liao, F. Liang and T. A. Lipo, “A novel permanent magnet machine with doubly saliency structure,” *IEEE Trans. Ind. Appl.,* vol.3, no.5, pp.1069-1078, 1995.

[LIU12] H. Liu, L. Xu, M. Shangguan, and W. N. Fu, “Finite element analysis of 1 MW high speed wound-rotor synchronous machine,” *IEEE Trans. Magn.,* vol. 48, no. 11, pp. 4650-4653, Nov. 2012.

[LIU13] X. Liu and Z. Q. Zhu, “Electromagnetic performance of novel variable flux reluctance machines with DC-field coil in stator,” *IEEE Trans. Magn.,* vol. 49, no. 6, pp. 3020-3028, Jun. 2013.

[LU11] K. Lu, P.O. Rasmussen, S. J. Watkins, and F. Blaabjerg, “A new low-cost hybrid switched reluctance motor for adjustable-speed pump applications,” *IEEE Trans. Ind. Appl.,* vol. 47, no. 1, pp. 314-321, 2011.

[LUO09] C. A. Luongo, P. J. Masson, T. Nam, D. Mavris, H. D. Kim, G. V. Brown, M. Waters, and D. Hall, “Next generation more-electric aircraft: a potential application for HTS superconductors,” *IEEE Trans. on Appl. Supercond.,* vol. 19, no. 3, pp. 1055-1068, Jun. 2009.

[MI09] C. C. Mi, L. Yongbin, and H. Karmaker, “Modeling of the starting performance of large solid-pole synchronous motors using equivalent circuit approach,” *IEEE Trans. Magn.,* vol. 45, no. 12, pp. 5399-5404, Dec. 2009.

[OJE12] J. Ojeda, M. Simoes, G. Li, and M. Gabsi, “Design of a flux-switching electrical generator for wind turbine systems,” *IEEE Trans. Ind. Appl.,* vol. 48, no. 6, pp.

1808–1816, 2012.

[OWE10] R. L. Owen, Z. Q. Zhu, A. S. Thomas, G. W. Jewell, and D. Howe, "Alternate poles wound flux-switching permanent-magnet brushless AC machines," *IEEE Trans. Ind. Appl.*, vol. 46, no. 2, pp. 790–797, 2010.

[PAN08] Y. Pang, Z. Q. Zhu, D. Howe, S. Iwasaki, R. Deodhar, and A. Pride, "Investigation of iron loss in flux-switching permanent magnet machines," *IET, Power Electronics, Machines and Drives,* 2-4 April, 2008, York, UK, pp.460-464.

[POL03] H. Pollock, C. Pollock, R. T. Walter, and B. V. Gorti, "Low-cost, high power density, flux switching machines and drives for power tools," *in Conf. Rec. IEEE IAS Annu. Meeting*, 2003, pp. 1451–1457.

[POL03b] C. Pollock, H. Pollock, and M. Brackley, "Electronically controlled flux switching motors: A comparison with an induction motor driving an axial fan," *in Conf. Rec. IEEE IAS Annu. Meeting*, 2003, pp. 2465–2470.

[POL06] H. Polinder, F. F. A. van der Pijl, G. J. de Vilder, and P. J. Tavner, "Comparison of direct-drive and geared generator concepts for wind turbines," *IEEE Trans. Energy Convers.*, vol. 21, no. 3, pp. 725-733, 2006.

[POL06b] C. Pollock, H. Pollock, R. Barron, J. R. Coles, D. Moule, A. Court, and R. Sutton, "Flux-switching motors for automotive applications," *IEEE Trans. Ind. Appl.*, vol. 42, no. 5, pp. 1177–1184, 2006.

[POL99] C. Pollock and M. Wallace, "The flux switching motor, a DC motor without magnets or brushes," *in Conf. Rec. IEEE IAS Annu. Meeting*, 1999, vol. 3, pp. 1980–1987.

[PUL88] D. W. J. Pulle, "Performance of split-coil switched reluctance drive," *IEE Proc. B Electric Power Appl.*, vol. 135, no. 6, pp. 318-323, 1988.

[QI09] G. Qi, J.T. Chen, Z.Q. Zhu, D. Howe, L.B. Zhou, and C.L. Gu, "influence of skew and cross-coupling on flux-weakening performance of permanent-magnet brushless AC machines," *IEEE Trans. Magn.*, vol. 45, no. 5 pp. 2110-2117, 2009.

[QU13] R. Qu, Y. Liu, and J. Wang, "Review of superconducting generator topologies for direct-drive wind turbines," *IEEE Trans. on Appl. Supercond.*, vol. 23, no. 3, pp. 5201108-5201108, 2013.

[RAU55] S. E. Rauch and L. J. Johnson, "Design principles of flux-switching alternators," *AIEE Trans*. 74III, pp. 1261-1268, 1955.

[RIB07] J. Ribrant, and L. M. Bertling, "Survey of failures in wind power systems with focus on Swedish wind power plants during 1997–2005," *IEEE Trans. Energy Convers.*, vol. 22, no. 1, pp. 167-173, 2007.

[ROS06] C. Rossi, D. Casadei, A. Pilati, and M. Marano, "Wound rotor salient pole synchronous machine drive for electric traction," *in Conf. Rec. IEEE Industry*

Appl., Tampa, Florida, 2006, pp. 1235-1241.

[SAR94] B. Sarlioglu, Y. F. Zhao and T. A. Lipo. "A novel doubly saliency single-phase permanent magnet generator," *Proc. IEEE Industry Applications Society Annual Meeting*, pp.9-15, 1994.

[SCH08] R. Schiferl, A. Flory, W. C. Livoti, and S. D. Umans, "High-temperature superconducting synchronous motors: economic issues for industrial applications," *IEEE Trans. Ind. Appl.*, vol. 44, no. 5, pp. 1376-1384, 2008.

[SHI14] J.T. Shi, Z.Q. Zhu, D. Wu, and X. Liu, "Comparative study of novel synchronous machines having permanent magnets in stator poles," *Proc. Int. Conf. Elec. Machines, (ICEM2014),* 2014.

[SUL11] E. Sulaiman, T. Kosaka and N. Matsui, "A new structure of 12slot-10pole field-excitation flux switching synchronous machine for hybrid electric vehicles", *Proc. of 14th European Conference on Power Electronics and Applications,* No.245, 2011.

[SUL12] E. Sulaiman, T. Kosaka and N. Matsui, "Design study and experimental analysis of wound field flux switching motor for HEV applications," *Proc. Int. Conf. Elec. Machines, (ICEM2012),* pp. 1269-1275, 2012.

[TAN13] Y. Tang, E. Ilhan, J. J. H. Paulides and E. A. Lomonova, "Design considerations of flux-switching machines with permanent magnet or dc excitation," *in Conf. Power Electronics and Applications (EPE), 2013.* pp. 1-10.

[THO12] A. S. Thomas, Z. Q. Zhu, and L. J. Wu, "Novel modular-rotor switched flux permanent magnet machines," *IEEE Trans. Ind. Appl.*, vol. 48, no. 6. pp. 2249–2258, 2012.

[TRA12] G. Traxler-Samek, T. Lugand, and M. Uemori, "Vibrational forces in salient pole synchronous machines considering tooth ripple effects," *IEEE Trans. Ind. Electron.*, vol. 59, no. 5, pp. 2258-2266, 2012.

[WAN12] Y. Wang and Z. Deng, "Comparison of hybrid excitation topologies for flux-switching machines," *IEEE Trans. Magn.*, vol. 48, pp. 2518-2527, 2012.

[WAN99] C. Wang, S. A. Nasar and I. Boldea, "Three-phase flux reversal machine," *IEE Proc.-Electric Power Applications*, vol. 146, no. 2, pp. 139-146, 1999.

[WU14] D. Wu, J.T. Shi, Z.Q. Zhu, and X. Liu, "Electromagnetic performance of novel synchronous machines with permanent magnets in stator yoke," *IEEE Trans. Magn.*, vol. 50, no. 9, 2014.

[YAM11] K. Yamazaki, S. Tamiya, K. Shima, and T. Fukami, "Reduction of magnetic saturation by using additional permanent magnets in synchronous machines," in *IEEE Energy Conv. Congr. Expo.*, Phoenix, USA, 2011, pp. 141-145.

[YU13] L. Yu, Z. Zhang, and Y. Yan, "Development and analysis of doubly salient brushless dc generators for automobile auxiliary power unit application," *IEEE*

Vehicle Power and Propulsion Conf., 2013, VPPC 2013, pp. 1-6, 2013.

[ZHA09] J. Zhang, M. Cheng, and Y. Zhang, "Single-phase doubly salient permanent magnet generator with full-pitched winding," *Inter. Electric Machines and Drives Conf. (IEMDC2009), 2009 International Conference on*, Miami Florida, pp. 311-316, 2009.

[ZHA11] J. Zhang; M. Cheng; and X. Feng "Design and comparison of wind power permanent magnet generator with doubly salient structure and full pitched windings", *Electric Utility Deregulation and Restructuring and Power Technologies (DRPT), 2011 4th International Conference on,* On page(s): 1329 - 1334

[ZHA12] Z.R. Zhang, Y.G. Yan, and Y.Y. Tao, "A new topology of low speed doubly salient brushless DC generator for wind power generation," *IEEE Trans. Magn.*, vol. 48, no. 3, pp. 1227-1233, 2012.

[ZHO13] Y. J. Zhou and Z. Q. Zhu, "Torque density and magnet usage efficiency enhancement of sandwiched switched flux permanent magnet machines using V-shaped magnets," *IEEE Trans. Magn.*, vol. 49, no 7, pp. 3834-3838, 2013.

[ZHO14] Y. J. Zhou and Z. Q. Zhu, "Comparison of low-cost single-phase wound field switched flux machines," *IEEE Trans. Ind. Appl.*, vol. 50, no. 5, pp 3314-3324, 2014

[ZHO14b] Y. J. Zhou and Z. Q. Zhu, "Comparison of wound field switched flux machines," *IEEE Trans. Ind. Appl.*, vol. 50, no. 5, pp 3335-3345, 2014

[ZHU00] Z. Q. Zhu, and D. Howe, "Influence of design parameters on cogging torque in permanent magnet motors," *IEEE Trans. Energy Convers*., vol. 15, no. 4, pp. 407–412, 2000.

[ZHU07] Z. Q. Zhu, J. T. Chen, Y. Pang, D. Howe, S. Iwasaki, and R. Deodhar, "Analytical modeling of end-effect on electromagnetic torque in flux-switching permanent magnet machine," *Proc. Int. Conf. Elect. Mach. Syst.*, Seoul, Korea, 2007, pp. 943–948.

[ZHU07b] Z. Q. Zhu, D. Ishak, D. Howe, and J. Chen, "Unbalanced magnetic forces in permanent-magnet brushless machines with diametrically asymmetric phase windings," *IEEE Trans. Ind. Appl.*, vol. 43, no. 6, pp 1544-1552, 2007.

[ZHU08] Z. Q. Zhu, J. T. Chen, D. Howe, S. Iwasaki, and R. Deodhar, "Analysis of a novel multi-tooth flux-switching permanent magnet brushless ac machines for high torque direct drives," *IEEE Trans. Magn.*, vol. 44, no. 11, pp. 4313-4316, 2008.

[ZHU09] Z. Q. Zhu, "A simple method for measuring cogging torque in permanent magnet machines," in *IEEE Power & Energy Society General Meeting, PES'09*, 2009, pp. 1–4.

[ZHU10] Z.Q. Zhu, and J.T. Chen, "Advanced flux-switching permanent magnet brushless machines,", *IEEE Trans. on Magn.*, vol. 46, no. 6, pp. 1447-1453,

2010.

[ZHU11] Z.Q. Zhu, “Switched flux permanent magnet machines – innovation continues”, *Proc. Int. Conf. on Electrical Machines and Systems*, 20-23 August 2011, Beijing, paper Keynote Speech-06.

[ZUL10] A. Zulu, B. Mecrow, and A. Armstrong, “A wound field three-phase flux-switching synchronous motor with all excitation sources on the stator,” *IEEE Trans. Ind. Appl.*, vol. 46, no. 6. pp. 2363-2371, 2010.

[ZUL12] A. Zulu, B. Mecrow, and A. Armstrong, “Permanent-magnet flux-switching synchronous motor employing a segmental rotor,” *IEEE Trans. Ind. Appl.*, vol. 48, no. 6. pp. 2259–2267, 2012.

APPENDIX A. CALCULATION AND TESTING METHODS

A.1. Cogging torque and static torque testing methods

A method described in [ZHU09] was utilized to measure cogging torque and static torque in this thesis, as shown in Fig. A.1. The stator of tested machine was held on a lathe jaws, meanwhile, the rotor shaft was attached to a balanced beam whose one end was rested on the tray of a digital weight gauge. In order to ensure that the measured torque was unidirectional, a pre-load weight was added to the measured end of balanced beam. The torque acting on the rotor was measured by rotating the stator.

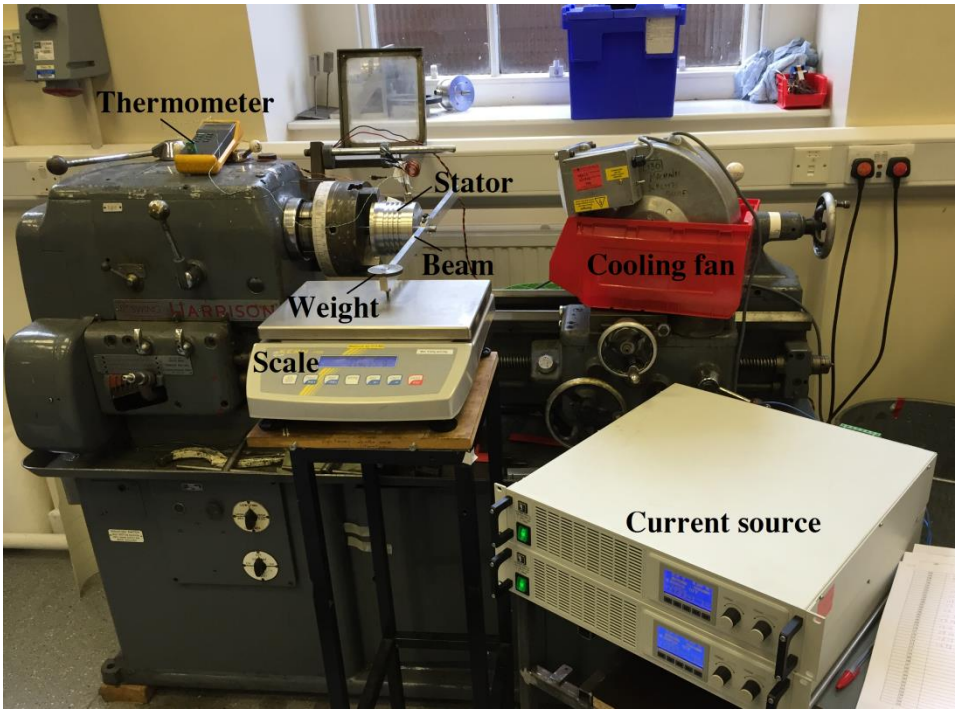

Fig. A.1. Experiment rig of measuring cogging torque and static torque [ZHU09]

A.2. Torque and iron loss calculation methods

All torque and iron loss in this thesis are calculated by Ansoft Maxwell. Based on the manufacturer-provided loss curves (steel grade: M330-35A), the eddy-current loss coefficient (k_c), the hysteresis loss coefficient (k_h), and the excessive loss coefficient (k_e) are derived as 0.0600, 152.618, and 13.6627, respectively. The iron-core loss is expressed as:

$$P_{iron} = k_c(fB_m)^2 + k_h f B_m^2 + k_e(fB_m)^{1.5} \quad \text{(A.1)}$$

where f is the operation frequency in an element, and B_m is the amplitude of the flux density in an element.

A.3. Torque-speed curve and efficiency map calculation methods

The influence of cross-coupling on the electromagnetic torque has been taken in to the consideration during the torque-speed curve calculation in this thesis. The electromagnetic torque is given by [QI09]:

$$T = \frac{3}{2}p[\Psi_{pm}(I_q)I_q + (L_d(I_d, I_q) - L_q(I_d, I_q))I_d I_q] \quad \text{(A.2)}$$

where

$$\Psi_{pm}(I_q) = \Psi_d(I_d = 0, I_q) \quad \text{(A.3)}$$

$$L_d(I_d, I_q) = \frac{\Psi_d(I_d, I_q) - \Psi_{pm}(I_q)}{I_d} \quad \text{(A.4)}$$

$$L_q(I_d, I_q) = \frac{\Psi_q(I_d, I_q)}{I_q} \quad \text{(A.5)}$$

The terminal voltage U_a can be calculated from:

$$U_a = \sqrt{(\omega\Psi_q(I_d, I_q) - R_a I_d)^2 + (\omega\Psi_d(I_d, I_q) - R_a I_q)^2} \quad \text{(A.6)}$$

In terms of the efficiency map calculations in this thesis, the mechanical losses of the machines are neglected, and the copper losses (includes end-windings) and iron losses of the machines under different *d*- and *q*-axis currents have been taken into the consideration during the calculations. For PM machines, the PM losses (P_{PM}) under different *d*- and *q*-axis currents have also been taken in the consideration, and can be expressed as [ISH05]:

$$P_{PM} = \int_{Vol} \rho_{PM} J_{PM}^2 \, dVol \quad \text{(A.7)}$$

where ρ_{PM} and J_{PM} are the resistivity and eddy current density of PMs, respectively.

APPENDIX B. PERFORMANCES OF F3A1 MACHINE

A F3A1 stator-WF machine has been introduced and compared with other machines in Chapter VII, as shown in Fig. B.1. Obviously, it is more appropriate to have unequal-slot stator for this machine since some stator slots contain both field and armature windings (named as field slots) and some slots contain armature windings only (named as armature slots). Therefore, in this thesis, the investigated F3A1 machine employs a popular 12-slot stator configuration, which has been introduced by [CHE08], [ZHA12], and [YU13]. As can be seen in Fig. B.1, the angle between two teeth of a field slot is 90 degrees allowing for increased field slot area. According to [CHE08], the 8-pole machine shows the best performance among three-phase 12-slot F3A1 stator-WF machines. Hence, 12-slot/8-pole F3A1 stator-WF is chosen for investigation and comparison in this thesis. As mentioned before, this machine has been optimized to achieve the maximum average torque when the current density is 26.8A/mm^2. In a field slot, the armature winding area is equal to that of an armature slot area. Meanwhile, the remaining area in this slot is field winding area. It is worth mentioning that the numbers of turns of field and armature coils have been determined to ensure that the armature and field currents are approximately 167Arms when the current densities are 26.8A/mm^2. The main parameters of this machine have been shown in Table 7.1.

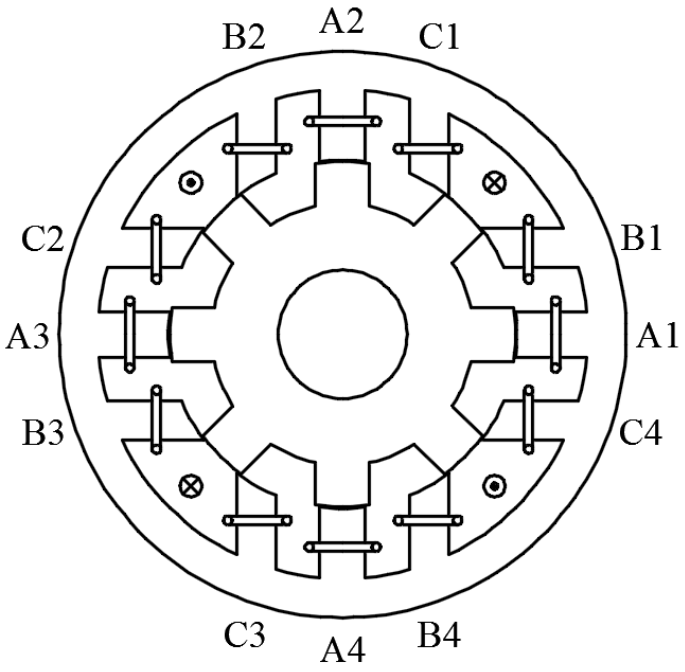

Fig. B.1. Topology of 12-slot/8-pole F3A1 stator-WF machine.

The performances, including torque waveform, torque ripple, average torque-current density curve, material usage efficiency, iron loss, and power factor, of the 12-slot/8-pole F3A1 stator-WF machine have been investigated and compared with other machines in Chapter VII. Other performances of this machine will be shown as follows.

B.1. Open-Circuit Field Distribution

When the field current (I_f) is 167A and the armature current (I_a) is 0A, the flux distributions of the F3A1 machine are shown in Fig. B.2. As can be seen in Fig. B.2 (a), when the rotor pole is aligned with coil A1, the coil A1 has the maximum flux-linkage. Meanwhile, when the rotor slot is aligned with coil A1, the coil A1 has the minimum flux-linkage, as shown in Fig. B.2 (b). Obviously, the flux path of phase A is different from the other two phases, and this will lead to unbalanced three-phase flux-linkages due to magnetic saturation and flux leakage.

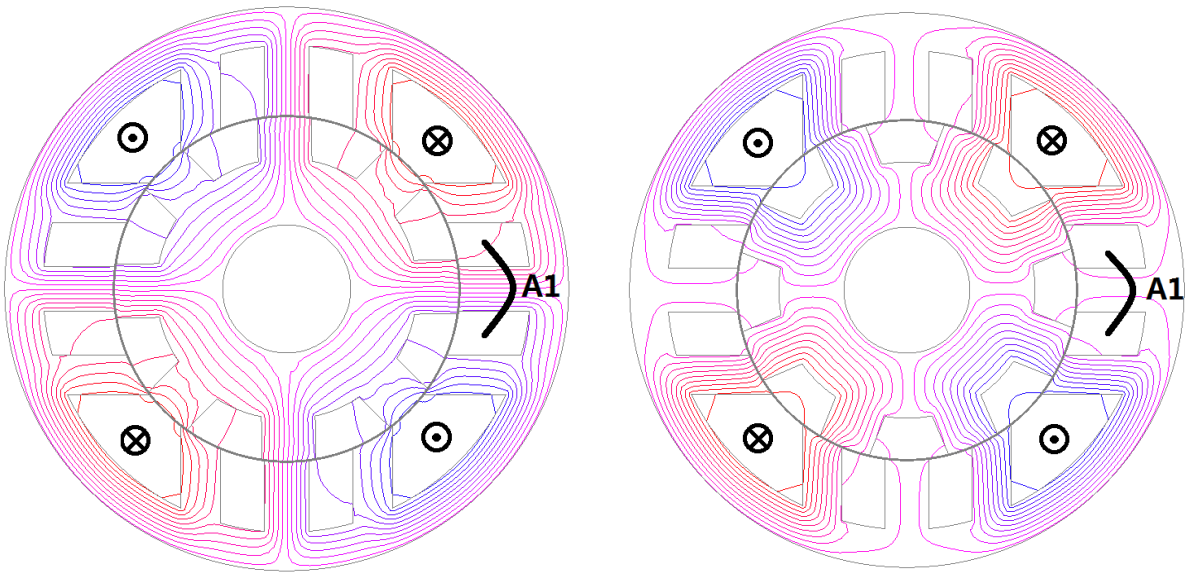

(a) (b)

Fig. B.2. Open-circuit flux distributions of F3A1 machine, field current=167A. (a) 0 elec. deg. (b) 180 elec. deg.

B.2. Open-Circuit Flux-Linkage and Back-EMF

When the field current is 84A/167A, the three-phase flux-linkages and back-EMFs of F3A1 machine are shown in Fig. B.3 and B.4, respectively. As mentioned before, the

waveforms and harmonics of flux-linkages in phase A are different from other two phases due to different flux paths, Fig. B.3. As can be seen, the phase flux-linkage of this machine is unipolar, and higher field current leads to larger flux-linkage bias. The phase back-EMFs are also unbalanced. As can be seen in Fig. B.4, the back-EMF waveforms are not sinusoidal and the harmonics are relatively high. Hence, the F3A1 machine will exhibit significant torque ripple for BLAC operation.

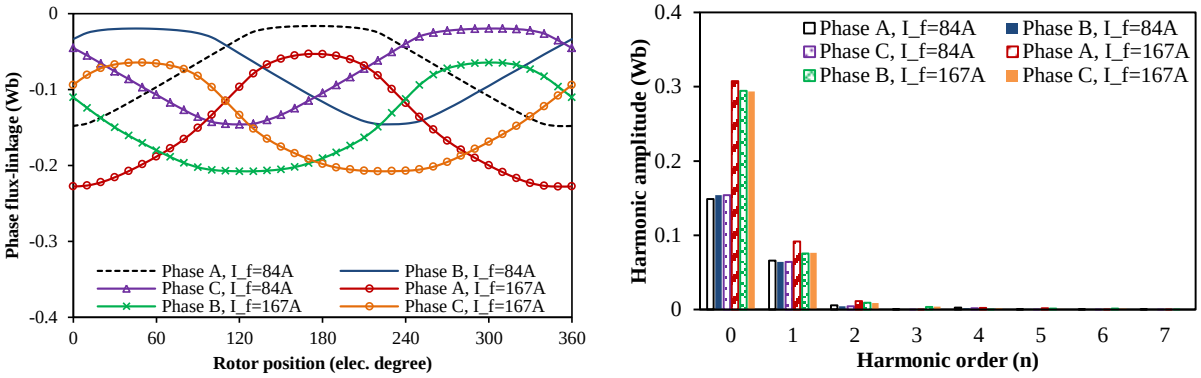

(a) (b)

Fig. B.3. Phase flux-linkages of F3A1 machine. (a) Waveforms. (b) Harmonics.

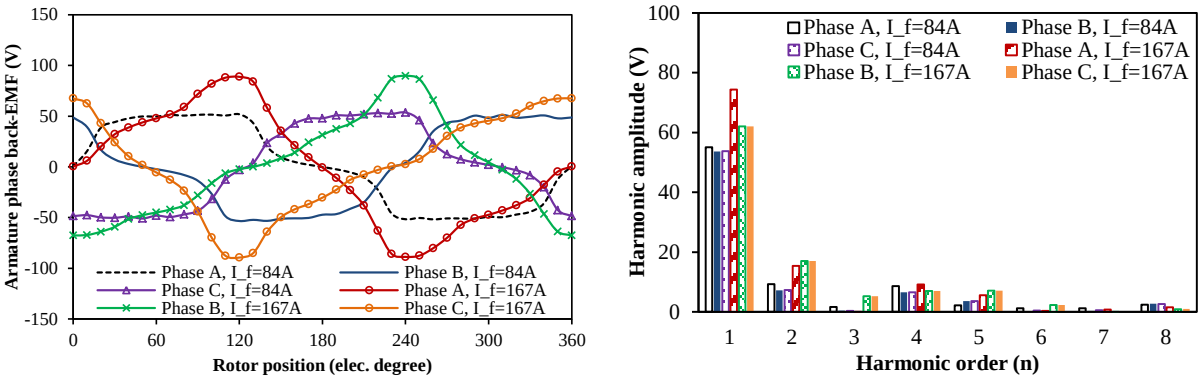

(a) (b)

Fig. B.4. Phase back-EMFs of F3A1 machine, 1000 rpm. (a) Waveforms. (b) Harmonics.

B.3. Torque Characteristics

When the armature current is 0A, the cogging torque waveforms of the F3A1 machine under different field currents are compared in Fig. B.5 (a). The average torque-current angle curves of this machine are shown in Fig. B.5 (b). As can be seen, the maximum torque is achieved when the current angle is almost equal to 0. Therefore, the d-axis current can be set to 0 in further analysis. Fig. B.5 (c) shows its torque-current curves. Under the fixed field

current, over high armature current will not result in high average torque in the F3A1 machine due to severe magnetic saturation.

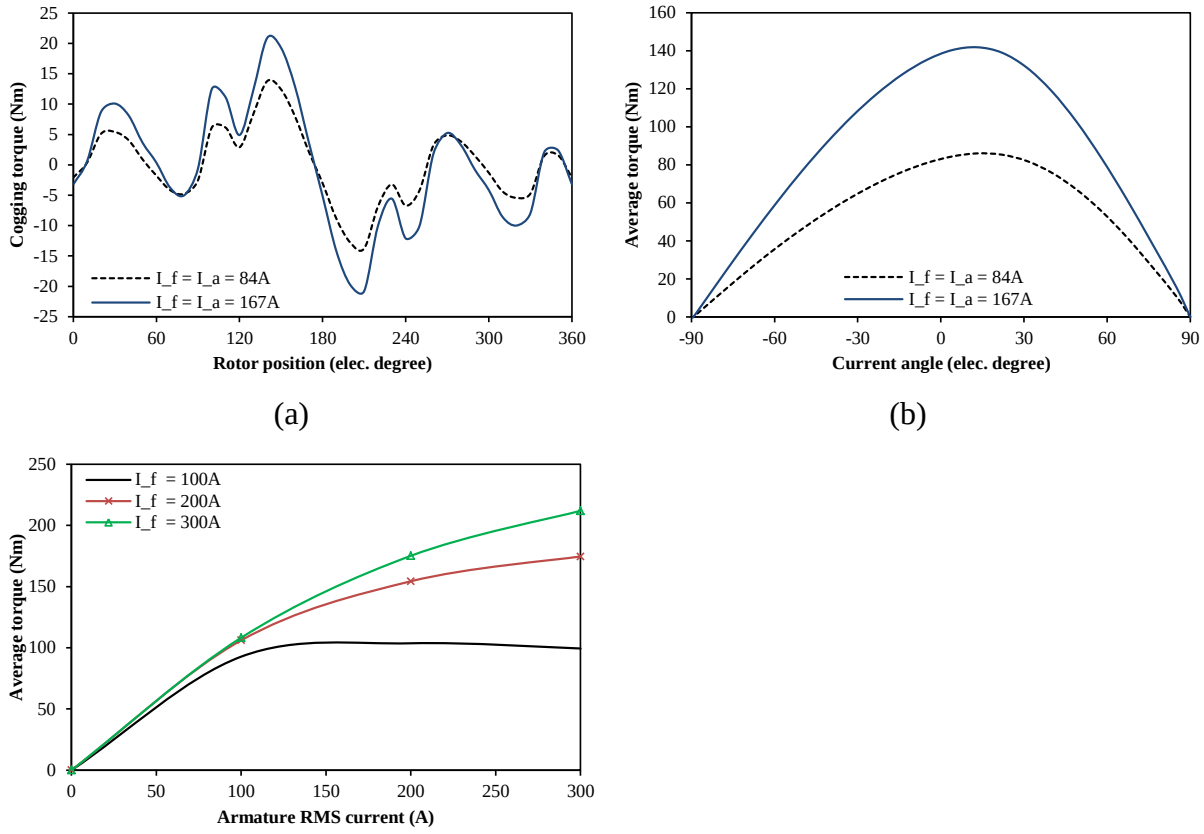

Fig. B.5. Torque characteristics. (a) Cogging torques. (b) Torque-current angle curves, BLAC operation. (c) Torque-current curves, BLAC operation, I_d=0A.

APPENDIX C. MECHANICAL DRAWINGS OF ANALYSED MACHINES

(Removed)

APPENDIX D. PUBLICATIONS RESULTED FROM PHD STUDY

Journal papers published or in press:

1. Y. J. Zhou and Z. Q. Zhu, "Torque density and magnet usage efficiency enhancement of sandwiched switched flux permanent magnet machines using V-shaped magnets," *IEEE Trans. Magn.*, vol. 49, no 7, pp. 3834-3838, 2013.

2. Y. J. Zhou, Z. Q. Zhu, and R. Nilssen, "Comparison of linear switched flux permanent magnet machines," *Applied Mechanics and Materials*, 416-417, pp. 121-126, 2013.

3. Y. J. Zhou and Z. Q. Zhu, "Comparison of low-cost single-phase wound field switched flux machines," *IEEE Trans. Ind. Appl.*, vol. 50, no 5, pp. 3335-3345, 2014.

4. Y. J. Zhou and Z. Q. Zhu, "Comparison of wound field switched flux machines," *IEEE Trans. Ind. Appl.*, vol. 50, no 5, pp. 3314-3324, 2014.

Journal paper submitted:

1. Z. Q. Zhu and Y. J. Zhou, "Investigation of non-overlapping stator wound field synchronous machines," Submitted to *IEEE Trans. Energy Conversion.*

2. Z. Q. Zhu and Y. J. Zhou, "Recent developments in stator wound field synchronous machines," to be published *Trans. on China Electrical Engineering.*

Conference papers:

1. Y. J. Zhou and Z. Q. Zhu, "Comparison of low-cost single-phase wound field switched flux machines," *Int. Electric Machines and Drives Conf. (IEMDC2013),* pp. 1275-1282, 2013.

2. Y.J. Zhou, Z.Q. Zhu, and R. Nilssen, "Comparison of linear switched flux permanent magnet machines," *2013 International Symposium on Linear Drives for Industry Applications (LDIA2013),* 2013.

3. Y. J. Zhou and Z. Q. Zhu, “Comparison of low-cost wound field switched flux machines,” *2013 Int. Conf. on Energy Conversion Congress and Exposition (ECCE2013),* pp. 904-911, 2013.

4. Y. J. Zhou, Z. Q. Zhu, and X. Ge, “Comparison of torque densities in alternate wound field switched flux machines,” *2014 Int. Conf. on Electrical Machines and System (ICEMS2014),* 2014.

5. Z. Q. Zhu, Y. J. Zhou, and J. T. Chen, “Investigation of partitioned stator axial field switched flux machines,” *Ecological Vehicles and Renewable Energies (EVER), 2015 Int. Conf. on.* 2015.

6. Z. Q. Zhu, Y. J. Zhou, and J. T. Chen, “Electromagnetic performance of non-overlapping stator wound field synchronous machine with salient pole rotor,” to be presented at *2015 Int. Conf. on IEEE International Magnetics Conference (Intermag),* 2015.